Beiträge zur Geologie der Schweiz, Geotechnische Serie
Materiaux pour la Géologie de la Suisse, Série Géotechnique

No. 95, 2008

Quantifying Late Quaternary Natural Hazards in Swiss Lakes

Subaquatic Landslides, Slope Stability Assessments, Paleoseismic Reconstructions and Lake Outbursts

Michael Strasser

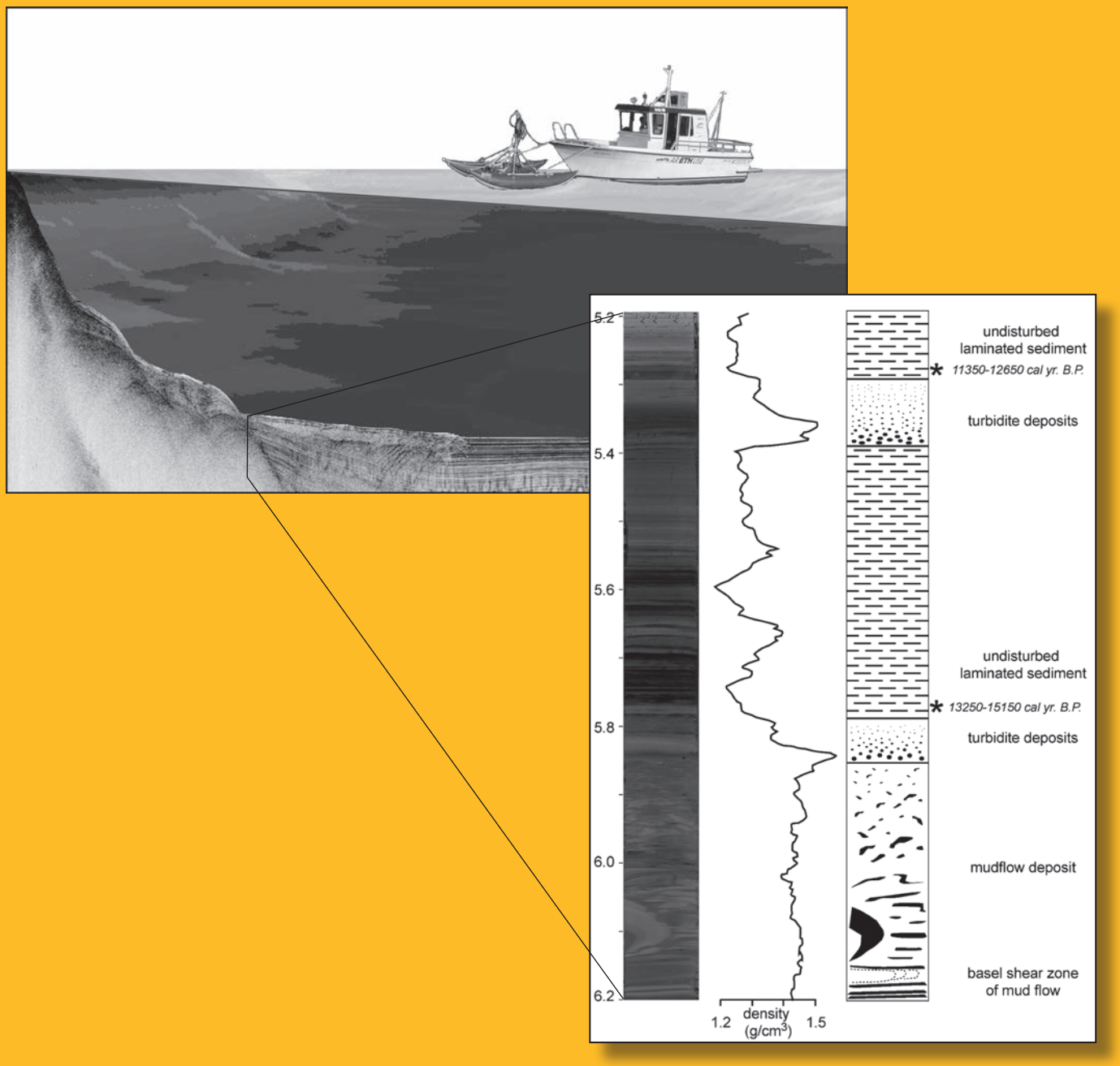

Herausgegeben von der Schweizerischen Geotechnischen Kommission (SGTK)
Publié par la Commission Géotechnique Suisse (SGTK)

ISBN 978-3-907997-30-7
ISSN 0582-1630

BEITRÄGE ZUR GEOLOGIE DER SCHWEIZ
GEOTECHNISCHE SERIE

herausgegeben von der

Schweizerischen Geotechnischen Kommission (SGTK)
(Organ der Akademie der Naturwissenschaften Schweiz SCNAT)

Lieferung 95

MATERIAUX POUR LA GEOLOGIE DE LA SUISSE
SERIE GEOTECHNIQUE

publiés par la

Commission Géotechnique Suisse (SGTK)
(Organe de l'Académie Suisse des Sciences Naturelles SCNAT)

Quantifying Late Quaternary Natural Hazards in Swiss Lakes

Subaquatic Landslides, Slope Stability Assessments, Paleoseismic Reconstructions and Lake Outbursts

Michael Strasser

2008

Vertrieb durch die Schweizerische Geotechnische Kommission, c/o ETH Zürich, 8092 Zürich
Publiziert mit Unterstützung der Akademie der Naturwissenschaften Schweiz SCNAT

Dissertation ETH, Nr. 17285
Eidgenössische Technische Hochschule Zürich, 2007
Referent: Prof. Dr. Flavio S. Anselmetti
Korreferenten: Prof. Dr. D. Giardini, Prof. Dr. A. J. Kopf, Prof. Dr. A. Solheim

This study was supported by Swiss National Science Foundation grant 620-066113

Der Druck dieser Arbeit wurde durch die Stiftung Dr. Joachim de Giacomi der Akademie der Naturwissenschaften Schweiz mitfinanziert.

Redaktion und DTP: Schweizerische Geotechnische Kommission (SGTK)
Lithographie und Druck: Fotorotar AG, 8132 Egg b. Zürich
Gedruckt auf chlorfrei gebleichtem Papier

ISBN-10 3-907997-30-1
ISBN-13 978-3-907997-30-7
ISSN 0582-1630

VORWORT DER SCHWEIZERISCHEN GEOTECHNISCHEN KOMMISSION

Im internationalen Vergleich gehört die Schweiz zu den Ländern mit mittlerer Erdbebenaktivität. In historischen Quellen wird von Erdbeben in der Schweiz berichtet, die teilweise enorme Schäden an Mensch und Umwelt angerichtet haben. So beispielsweise im Jahre 1356, als Basel von einem Erdbeben verwüstet wurde. Auch am 18. September 1601 führte ein Erdbeben in der Zentralschweiz zu massiven Schäden. Als interessantes Folgephänomen des Bebens wurde damals in Luzern ein Tsunami beobachtet, bei dem unter anderem das Wasser in der Reuss mehrmals versiegt und wieder über die Ufer getreten ist. Der kleine Rat von Luzern führte die Katastrophe damals auf die Sünden der Menschen zurück und interpretierte sie als Zorn Gottes. Er erliess als Busse ein aus heutiger Sichtweise fragliches Tanzverbot bis zur folgenden Fasnacht. Heute weiss man, dass solch starke Erdbeben vielmehr natürlichesse Ereignis sind, die sich in der Schweiz im Durschnitt nach mehreren Generationen wiederholen und bis in prähistorische Zeit nachweisbar sind.

Michael Strasser ist es in seiner Arbeit auf eindrückliche Art und Weise gelungen, in den Sedimenten des Vierwaldstätter- und Zürichsees subaquatische Massenbewegungen zu identifizieren und diese mit historischen und prähistorischen Erdbebenaktivitäten zu korrelieren. Mit Hilfe von reflektionsseismischen Profilen, Sedimentkernen und Radiokarbondatierungen konnte die räumliche und zeitliche Verbreitung von Massenbewegungen detailliert rekonstriert werden. Mittels rechnerischer Analysen konnte er zudem aufzeigen, welche kritische seismische Bodenbeschleunigung zu Massenbewegungen in ansonsten stabilen Hängen führt. Die zeitliche Übereinstimmung der Unterwasserrutschungen im Zürich- und Vierwaldstättersee lässt auf grosse Beben entlang des nördlichen Alpenrandes schliessen.

Die Schweizerische Geotechnische Kommission dankt dem Autor für die Möglichkeit, diese Arbeit in ihrer Publikationsreihe veröffentlichen zu dürfen.

Der vorliegende Band ergänzt die Publikationen in den Beiträgen zur Geologie der Schweiz, Geotechnische Serie Nr. 92 «Erdbebengefährdung in Abhängigkeit vom Geologischen Untergrund» (Ch. Beer, 1997) sowie Nr. 78 «Herkunft und Zusammensetzung von Silt in fliessenden Gewässern und Stauseen-Geotechnische Abtragsanalysen im Alpenraum» (M. Ammann, 1988).

Für den Inhalt von Text, Tabellen und Figuren ist der Autor allein verantwortlich.

Zürich, im März 2008

Der Präsident der Schweizerischen Geotechnischen Kommission

Prof. Max W. Schmidt

VERDANKUNGEN / ACKNOWLEDGMENTS

I am deeply grateful to my supervisor Flavio Anselmetti: «Merci viilmol, für alles was Du miar in da letscha viar Johr biibrocht häsch, siigs ufam See, im Labor, in dr Wüssaschafts-Welt oder im «reala» Läba. It was a great pleasure flying with you, you are the best pilot!»

I also thank my co-referents Domenico Giardini, Achim Kopf and Andres Sohlheim for their critical review of my thesis.

All co-authors of the individual chapters and publications are kindly acknowledged: Thank you Flavio Anselmetti, Felix Bussmann, Domenico Giardini, Donat Fäh, Achim Kopf, Beat Rick, Conrad Schindler, Michael Schnellmann and Sylvie Stegmann, for the great collaboration.

Special thanks are dedicated to Beni Dürr, Robert Hofmann, Matthias Lange and Marcel Mettler for their technical support during field work and in the lab. Urs Gerber is acknowledged for the excellent core photographs, Dr. Ruedi Baumann and Andy Müller for helping acquiring X-ray images and Irka Hajdas for guidance with ^{14}C-dating.

I am deeply grateful to the whole ETH Limno Team, friends and institutions for their assistance during the lake campaigns, support in the lab and office and for company during the last four years: Thank you Adi Gilli, Andy Müller, Andy Weller, Beat Louis, Chris Krugh, Christina Keller, Claudio Delle Piane, Clemens Augenstein, Dani Lutz, EAWAG Kastanienbaum, D-ERDW Library, Daniela Fanetti, Eduard Baca, Florian Kober, Florian Thevenon, Gaudenz Deplazes, Katrin Monecke, Manu Chapron, Mathias Camenzind, Mathias Papp, Michi Schnellmann, Miri Dühnforth, Nele Meckler, Nicolas Waldmann, Nina Stöckli, Pauline Rais, Regula Schälchli, Rolf, Ruth and Nic Strasser, Seepolizei Oberrieden, Stephanie Girardclos, Thomas Kocher, Thomas Löffler, Thomas Schmid, and Ulli Exner for all your indispensable support, motivation, company, sympathy and interest, without which this thesis never ever would have been able to completed.

Many of above mentioned peers, as well as Alexander Puzrin, Beat Keller, Brian McAdoo, Christian Schlüchter, Edi Kissling, Federico Giovanoli, Gabriela Schwarz-Zanetti, Hans Thierstein, Helmi Weissert, Homa Lee, Jiri Pika, Judy McKenzie, Michel Magny, Monika Gisler, Nicholas Deichmann, Peter Hochuli, Rob Kayen, Sarah Springman, Stefan Wiemer, Teddy Botton, Theo Kempf, Tobias Mörz and Wilfried Häberli are acknowledged for helpful discussions on data and interpretations, ideas, support and constructive criticism.

Thoughtful comments and suggestions by reviewers M. Bartholomew, A. Blass, M. De Batist, O. Korup, A. Pfiffner, G. St-Onge, M. Schnellmann, N. Sultan, and two anonymous reviewers considerably improved and completed initial versions of the individual manuscripts and are kindly acknowledged.

Many thanks also dedicated to geo-consulting company Geo Von Moos AG for their collaboration in Lake Lucerne and in the Zurich City area, as well as to geo-consulting companies Jäckli Geologie and Sieber & Cassina for providing unpublished data presented in chapter 5.

Christoph Bärtschi, Rainer Kündig and SGTK (Schweizerische Geotechnische Kommission) are kindly acknowleged for editing and publishing the thesis and sharing publication costs. Further co-financing of publication costs was kindly provided by Stiftung Dr. Joachim de Giacomi der Akademie der Naturwissenschaften Schweiz.

And last but not least I would like to thank Bettina: Danka viilmol für all Dini Unterstützig, Dis Verständnis und Dini Liabi.

TABLE OF CONTENTS

LIST OF TABLES AND FIGURES

List of Tables

List of Figures

ABSTRACT

Understanding geological processes that govern nature, evolution and consequences of geohazards, as well as quantitative information on their magnitudes and recurrence frequencies is a key requirement for natural hazard assessments in highly populated areas, such as central Switzerland. This thesis investigates and quantifies causes and effects of Late Quaternary seismic and environmental impacts in and around Lake Zurich and Lake Lucerne, by studying in detail subaquatic slope failure processes and their deposits with combined geophysical, sedimentological, in situ geotechnical and numerical modeling techniques.

Subaqueous mass movements are common features in both marine and lacustrine environments and can have severe impacts on offshore infrastructures and coastal areas. They can originate from various processes including rapid sedimentation and earthquakes. In this study, the fjord-type perialpine Lake Lucerne and Lake Zurich are used as model basins to investigate subaqueous slope stability under static and dynamic loading conditions and to decipher the role of seismic vs. aseismic trigger mechanisms. In the investigated lakes, lateral non-deltaic slopes generally are stable under static loading conditions but failed during past earthquakes along planar sliding surfaces that systematically developed at the glacial-to-postglacial lithological boundary. Coring and in situ geotechnical measurements in Lake Lucerne reveal this critical interface to be characterized by slightly underconsolidated, weak Late Glacial clay deposits above and overconsolidated, glacially-deformed, glacio-lacustrine deposits with excessive formation pore pressure below. In deltaic settings, however, sediment supply from local creeks and high sedimentation rates exhibit an important control on slope stability conditions, which may change over relative short geological time scales, and may facilitate aseismically-triggered delta slope failures.

The occurrence of historic and prehistoric earthquakes in the greater Lucerne area, as recorded by multiple coeval mass-movement deposits in the subsurface of Lake Lucerne, has already been documented in previous studies. New in situ geotechnical site characterization along failed and stable lateral slopes, combined with limit equilibrium calculations back-analyzing slope stability during past failure events allow for reconstruction of critical earthquake intensities. Results reveal seismic peak ground acceleration of ~0.08 g and ~0.14 g for the historic 1601 A.D. M_w ~6.2 earthquake and a prehistoric, ~2220 cal yr. B.P. earthquake, respectively. The value for the 1601 A.D. event lies in the range of calculated accelerations deduced from predictive ground motion models and suggests comparable macroseismic threshold intensities for basin-wide sliding (I=VII) as estimated from historical data. These findings thus pinpoint the potential of detailed subaqueous slope stability analysis as paleoseismological tool to quantitatively reconstruct prehistoric earthquake shaking intensities.

For the greater Zurich area, it was so far unknown whether or not strong seismic shaking occurred during prehistoric times. However, new Lake Zurich data comprising ~300 km of high-resolution seismic profiles, 6 gravity piston cores and 15 radiocarbon ages allow for establishing a complete Late Glacial-to-Holocene mass-movement catalogue that clearly reveals the occurrence of three events, during which multiple coeval landslides occurred throughout the lake. This clearly suggests a seismic trigger. Furthermore, the ages of these events match the ages of reconstructed prehistoric earthquakes recorded in Lake Lucerne. This correlation thus implies that three large earthquakes (at 2220, 11600 and 13770 cal. yr B.P.) shook central Switzerland, strong enough to trigger multiple mass movements in both lakes located ~40 km apart. Using calibrated macroseismic threshold intensities for lacustrine landsliding as input parameter for macroseismic reconstructions, empirical seismic attenuation models reveal minimal earthquake magnitudes of $M_w > 6.5$ and epicentres that potentially were located close to North-Alpine front. These findings indicate ongoing Alpine deformation that generated and could potentially again generate destructive earthquakes in heavily-populated regions that are unaccustomed to seismic activity during historic times.

In the subsurface of Lake Zurich, the oldest of these three events is associated with sediment waves that indicate formation under strong current conditions. This observation, combined with geomorphological and core data in downstream areas of Lake Zurich point towards a sudden collapse of the Zurich moraine and a subsequent lake outburst flood that lowered lake level by ~12 m. Fluid dynamic calculations reveal that averaged outburst discharge exceeded minimum values of ~2400 m^3s^{-1} and estimated peak discharge of ~20600 m^3s^{-1}. The moraine breakthrough could have been caused either by primary earthquake shaking and/or secondary effects, such as landslide-generated waves.

In summary, data and results presented in this thesis reveal occurrence and quantitative information on frequencies and intensities of varying seismic and environmental impacts that affected Lake Zurich and Lake Lucerne and their surroundings during the last ~17000 years. This study thus demonstrates the multi-disciplinary approach studying subaquatic mass movements in different basins to be a successful and promising strategy to assess the geo-hazard potential arising from such rare but potentially-destructive events.

ZUSAMMENFASSUNG

Die Abschätzung des Gefährdungspotentials natürlicher geologischer Ereignisse verlangt prozess-basierte Kenntnisse über die Entstehung und über mögliche Konsequenzen von Naturgefahren sowie quantitative Informationen über deren Intensitäten und Wiederkehrraten. Diese Studie befasst sich mit spätquartären Erdbeben und Umweltereignissen in und um den Zürich- und Vierwaldstättersee. Insbesondere wird aufgezeigt, wie mit Hilfe von geophysikalischen, sedimentologischen, in situ geotechnischen und numerischen Modellierungs-Methoden detaillierte Untersuchungen von subaquatischen Hangrutschungen und deren Ablagerungsprodukten zum Verständnis solcher Naturgefahren beitragen können.

Subaquatische Rutschungen treten sowohl in Ozeanen als auch in Seen auf und können eine Gefährdung für Bauten und Verankerungen am Boden der Gewässer sowie für Mensch und Infrastruktur am Ufer darstellen. Solche Hanginstabilitäten können durch verschiedene Mechanismen ausgelöst werden, wie zum Beispiel durch Erdbeben oder durch erhöhte Sedimentzufuhr. Die fjordähnlichen Schweizer Alpenrandseen, wie Zürich- und Vierwaldstättersee, sind besonders geeignet, den Einfluss von seismischen bzw. nichtseismischen Auslösemechanismen zu erforschen und die Hangstabilität als Funktion von statischer und dynamischer Belastung im Detail zu studieren. In den untersuchten Seen sind seitliche Unterwasserabhänge, welche nicht von Delta-Prozessen beeinflusst werden, unter statischer Belastung stabil. Erst zusätzliche dynamische Belastungen, welche durch Erdbebenerschütterungen hervorgerufen werden, lösen Hangrutschungen aus. Die Rutschungsflächen bilden sich bevorzugt entlang der lithologischen Grenze zwischen leicht unterkonsolidierten spätglazialen Tonen mit relativ geringen Scherfestigkeiten und den darunterliegenden überkonsolidierten, glazial deformierten Gletscherseeablagerungen mit erhöhten Porenwasserdrücken. Grossräumige Versackungen und Massenbewegungen während des endeiszeitlichen Gletscherrückzugs sowie nacheiszeitliche Hanginstabilitäten entlang von Deltaabhängen können unter dem Einfluss von erhöhtem Sedimenteintrag hingegen auch aseismisch ausgelöst werden.

Frühere Studien in der Region Luzern haben bereits aufgezeigt, dass historische und prähistorische Erdbeben die Region mehrfach erschüttert und im Vierwaldstättersee gleichzeitig mehrere subaquatische Rutschungen verursacht haben. Mit rechnerischen Analysen der Hangstabilität, welche dank Daten von in situ geotechnischen Messungen quantitativ durchgeführt werden können, wird neu die für das Auslösen der Rutschungen nötige kritische seismische Bodenbeschleunigung vergangener Beben rekonstruiert. Demnach entsprach die Erschütterung während des historischen $M_w \sim 6.2$ Erdbebens im Jahre 1601 einer Bodenbeschleunigung von ca. 0.08 g. Für ein prähistorisches Beben 2220 Jahre vor heute ergeben sich Werte von ~0.14 g Die Resultate der 1601-Erdbeben-Rekonstruktion liegen in der gleichen Grössenordnung wie die mit stochastischen Simulationsmethoden errechnete theoretische Bodenbeschleunigung. Sie sind ebenfalls vergleichbar mit lokalen Intensitätsangaben in historischen Quellen. Somit zeigt diese Studie auf, dass die quantitative Analyse von vergangenen subaquatischen Hanginstabilitäten eine vielversprechende Methode für die Rekonstruktion prähistorischer Erdbebenintensitäten darstellt.

Für die Region Zürich war es bis anhin nicht bekannt, ob in der Vergangenheit grössere Erdbebenerschütterungen stattgefunden haben. Die neuen Untersuchungen im Zürichsee, wo mit Hilfe von 300 km reflektionsseismischen Profilen, 6 Sedimentkernen und 15 Radiokarbondatierungen die zeitliche und räumliche Verbreitung von Unterwasserrutschungen im Detail rekonstruiert wurde, zeigen aber drei grosse Ereignisse mit simultan ausgelösten Rutschungen auf, was auf drei prähistorische Erdbeben schliessen lässt. Auffallenderweise stimmen die Alter der drei Beben (2220, 11600 und 13770 Jahre vor heute) mit den Altern von im Vierwaldstättersee rekonstruierten Beben überein, was einen genetischen Zusammenhang impliziert. Mit Hilfe von makroseismischen Rekonstruktionen, für welche die für die Auslösung von Rutschungen kritischen Intensitäten sowie empirische seismische Wellenausbreitungsmodelle verwendet wurden, wird die minimale Magnitude dieser drei Erdbeben auf $M_w > 6.5$ geschätzt. Die Epizentren dürften wohl irgendwo entlang des nördlichen Alpenrandes gelegen haben. Diese Resultate lassen vermuten, dass aktive alpin-tektonische Kräfte zur Aktivierung von seismogenen Zonen in den Alpen geführt haben und auch in Zukunft führen könnten.

Im Weiteren wurden im Zürichsee Sedimentstrukturen beobachtet, welche im Zusammenhang mit dem ältesten dieser drei Erdbeben entstanden sein müssen und auf grosse Wasserströmungen hinweisen. Zusätzliche geomorphologische Daten und Bohrkernaufnahmen im Raum Zürich zeigen auf, dass diese Strukturen durch einen Zürichsee-Ausbruch mit durchschnittlichen Ausflussraten von mindestens 2400 m^3s^{-1} und einer resultierenden Seespiegelabsenkung von ~12 m gebildet wurden, welcher sich als Folge eines Durchbruchs durch den stauenden Moränenriegel von Zürich ereignet hatte. Maximale Spitzenabflussraten dürften in der Grössenordnung von ~20600 m^3s^{-1} gelegen haben. Der Moränendurchbruch selbst wurde entweder primär durch die seismische Erschütterung oder sekundär von überschwappenden Wellen ausgelöst, welche durch die Wasserverdrängung von erdbebeninduzierten Rutschungen im See entstehen können.

Zusammengefasst dokumentiert diese Arbeit das Auftreten verschiedener geologischer Ereignisse, wie Massenbewegungen, Erdbeben und Seeausbrüche, welche sich im Verlaufe der letzten rund 17000 Jahren in der Zürich- und Vierwaldstättersee Region ereignet haben. Daten und Resultate dieser Studie erlauben es, Intensitäten und Wiederkehrraten solcher Prozesse quantitativ abzuschätzen. Der angewandte multidisziplinäre Ansatz, die Entstehung und Konsequenzen von subaquatischen Hangrutschungen im Detail zu erforschen, kann daher als relevante und vielversprechende Methode betrachtet werden, um das Gefährdungspotential von solch seltenen aber möglicherweise katastrophalen geologischen Ereignissen abzuschätzen.

1 INTRODUCTION

1.1 Research motivation and general objectives

Natural hazards, such as earthquakes, landslides, and lake outbursts can have severe impacts on civil infrastructures and human society. Hence, understanding geological processes that govern nature and evolution of such geohazards is a fundamental and societal relevant goal of modern Earth Science. Enormous scientific and economic efforts are undertaken to assess the hazard potential associated with such rare but potentially-destructive events and to develop future scenarios, especially in highly populated areas. In order to achieve these fundamental goals, studying in detail past events, assessing their recurrence intervals and quantitatively reconstructing magnitudes and intensities of both causal and subsequent processes and impacts are key requirements. Most extreme geological events, however, show recurrence rates typically exceeding the time span covered by instrumental data and often also by historical archives. Hence, studying prehistoric events preserved in the geological record is essential to assess the geohazard potential associated with such rare events.

This thesis investigates Late Quaternary natural hazards as recorded in the lacustrine record of Swiss Lakes. As an overall scientific objective, it aims to better determine and quantify causes and effects of natural hazards related to subaquatic landslides. Large subaqueous mass-movement events gained wide attention in the marine environment not only because of their catastrophic impacts on both offshore infra-structures (e.g. pipelines, cables and platforms) and coastal areas (e.g. landslide-induced tsunamis) (e.g. Locat and Lee, 2002; Camerlinghi et al, 2007; and references therein), but also because they can be directly related to primary trigger mechanisms including earthquakes, rapid sedimentation, gas release, glacial and tidal loading, wave action, or clathrate dissociation, many of which representing potential geohazards themselves (e.g. Hampton et al, 1996; Locat and Lee, 2002; Sultan et al., 2004; Solheim, 2006; Owen et al., 2007; and references therein).

Similarly, subaquatic mass movements have also been observed and described in lakes (e.g. Heim, 1908; Kelts and Hsü, 1980; Siegenthaler et al, 1987; Shilts and Claque, 1992; Daut, 1998; Chapron et al., 1999; Schnellmann et al. 2002; 2005; 2006; Monecke et al, 2004; 2006; Moernaut et al, 2007; Girardclos et al., 2007). Due to their well-constrained boundary conditions, their smaller size and the possibility to be investigated on a complete basinwide scale, mass movements in lacustrine environments offer a series of advantages that make lake studies vital to also improve our knowledge on marine processes. With their regular sedimentation, steep lateral slopes and great water depths, Swiss perialpine fiord-type lakes, therefore, provide ideal model basins to study in detail subaquatic slope failure and mass-movement processes.

Furthermore, lakes have been shown to provide valuable archives to reconstruct the regional earthquake history (Sims, 1973; Shilts and Claque, 1992; Schnellmann et al. 2002; 2006; Monecke et al, 2004; 2006; Nomade et al, 2005; Moernaut et al, 2007). It has been shown that seismic shaking leaves its characteristic fingerprint (in particular multiple coeval landslide deposits and soft sediment deformation) in the otherwise-continuous lacustrine sedimentary record that can be spatially correlated and precisely dated. Primary objectives addressed in this thesis thus are to test the utility of (i) assessing critical seismic threshold intensities for triggering sub-aquatic slope failures and of (ii) temporal and spatial correlation of subaquatic landslides deposits in different lake archives as paleoseismologic tool to quantitatively reconstruct past local ground shaking intensities and to constrain chronology, magnitudes and epicenters of prehistoric seismicity. These scientific objectives are addressed by investigating Lake Zurich and Lake Lucerne (Central Switzerland; Fig. 1.1) using combined sedimentological, geophysical, in situ geotechnical and numerical modeling techniques. The combination of these methods represents a novel approach for lacustrine slope stability assessment and for quantitative paleoseismologic reconstructions. Additionally, the benefit of systematic quasi 3-D seismic stratigraphic mapping, coring and dating is not limited to investigation of subaqueous mass-movement processes and paleoseismologic reconstructions. It also allows identifying and reconstructing other potentially-hazardous processes and impacts that affected the lake and its surroundings over geological timescales. An additional objective of this thesis, therefore, is to shed light on a Late Pleistocene outburst of Lake Zurich that was postulated by Schindler (1971) but that has so far lacked conclusive interpretations of trigger mechanism(s), accurate timing and consequences.

1.2 Regional setting

1.2.1 Study areas

Lake Lucerne and Lake Zurich occupy perialpine, glacigenic overdeepend troughs situated in central Switzerland in the Swiss Plateau and at the North-Alpine front, respectively (Fig. 1.1). Both lakes consist of several sub-basins separated by subaqueous sills. The sub-basins generally are characterized by elongated shapes, steep lateral slopes and sharp lower slope breaks towards intermediate flat basin plains. The sedimentary infill in both lakes generally consists of

a thick succession of mainly glacial and glacio-lacustrine deposits. The majority of theses sediments were accumulated in a subglacial environment and only the uppermost ~10-30 meter were deposited after the glacier retreated from the lake basins (Finckh et al., 1984; Hsü and Kelts, 1984 and references therein; Schnellmann, 2006).

Lake Lucerne

In the subsurface of Lake Lucerne, previous studies by Siegenthaler et al. (1987), Lemcke, (1992), and Schnellmann et al. (2002; 2005; 2006) identified numerous mass-movement deposits related to a historic M_W ~6.2 earthquake occurring in 1601 A.D. (Schwarz-Zanetti et al., 2003; Gisler et al., 2004). 13 synchronous mass movements related to this event triggered a tsunami wave up to 4 meter in height and a subsequent seiche wave that lasted for several days (Cysat, 1601; Schnellmann et al., 2002). In the deeper subsurface, several mass-movement deposits comprising five additional seismically-triggered synchronous mass-movements events were identified (Schnellmann et al. 2006). This complete chronological catalogue of Late Glacial and Holocene mass-movement deposits in Lake Lucerne provides an ideal basis to systematically and quantitatively investigate slope stability during both seismic and static loading conditions and to shed light on slide plane development and slope failure initiation mechanism(s).

Lake Zurich

In Lake Zurich, previous studies in the 1970's and 1980's described Lake Zurich's geology and its general sedimentary and environmental evolution since the Last Glacial Maximum (Hsü and Kelts, 1970; 1984; Schindler, 1971; 1974; 1976; Kelts, 1978; Giovanoli, 1979; Pika, 1983; Lister, 1985; 1988; Sidler, 1988). In early Late Glacial times lake level was significantly higher than today, because during an intermediate stagnation phase during overall deglaciation, the retreating Linth Glacier deposited a large frontal moraine that dammed (paleo) Lake Zurich at a higher level (Schindler, 1971). On the basis of geomorphological data and information from drill cores and open construction pits in downstream areas of Lake Zurich, Schindler (1971) proposed that the drop in lake level may have been instantaneous as a consequence of the collapses of the Zurich moraine dam and a subsequent lake outburst. Since the early 1970's, however, only very few studies tested this hypothesis (Furger, 1991; Schindler, 2004) but occurrence, timing and trigger mechanism(s) of such an event could not be conclusively revealed.

Subaquatic mass-movement deposits in Lake Zurich have been described both in core and seismic data acquired during previous studies (Schindler, 1976; Kelts, 1978; Giovanoli, 1979; Pika, 1983; Hsü and Kelts, 1984). In particular, a series of subaqueous slumps that were triggered by human landfill along the shore near Horgen in 1875 A.D. was extensively studied and described by Heim, (1976), Kelts (1978), Kelts and Hsü (1980) and Siegenthaler et al. (1984). In the deeper sedimentary section, however, none of the previous studies particularly examined spatial and temporal distribution of Late Glacial-to-Holocene mass-movement deposits and their causes remain speculative. It thus remains open, whether Late Glacial and Holocene mass movements in Lake Zurich systematically occurred during specific events and whether their deposits may record information on past seismic and/or environmental impacts.

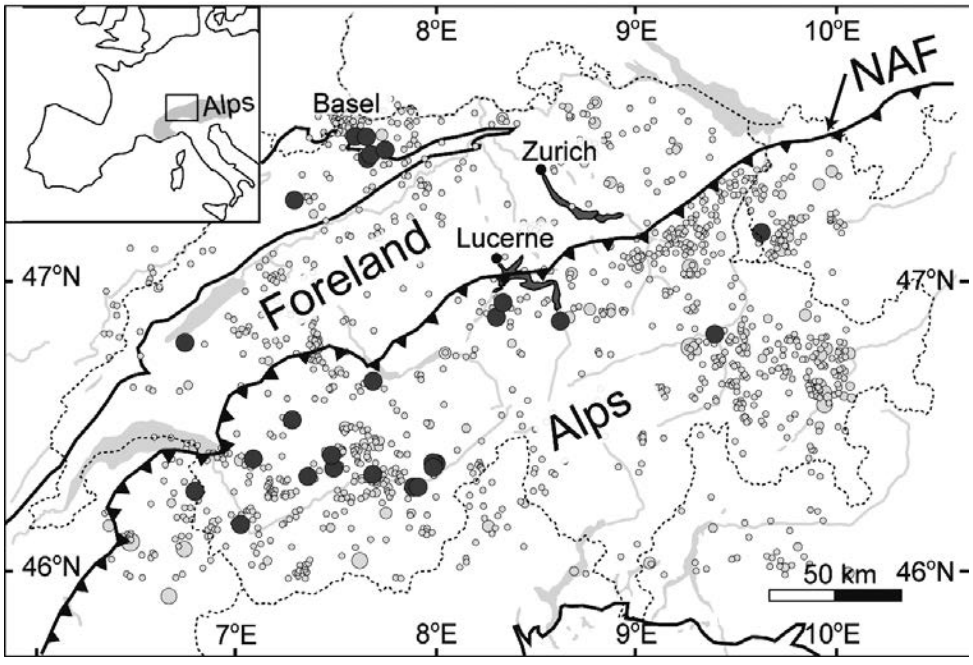

Figure 1.1: Map of Switzerland locating study areas Lake Zurich and Lake Lucerne (dark-grey areas) and showing general tectonic units and epicenters of instrumentally (gray dots) and historically ($M \geq 5.5$, dark-gray dots) recorded earthquakes (Fäh et al., 2003). NAF=North-Alpine nappe front.

1.2.2 Seismotectonic setting and previous paleoseismic studies

The cities of Lucerne and Zurich are situated in the north alpine foreland basin, 7 and 40 km north of the North-Alpine nappe front, respectively (Fig. 1.1). This frontal thrust strikes WSW-ENE and marks the northern topographic boundary of the Alpine nappes that overthrust the Molasse basin. The instrumentally registered recent seismicity in central Switzerland over the last 30 years has been very low. In the foreland, small earthquakes generally occur throughout the crust to Moho level (~30 km), nucleating in crystalline basement with predominantly strike-slip focal mechanisms and minor normal faulting components. Upper-crust shallow thrust and strike-slip faulting dominates the external Alpine nappes (KASTRUP et al., 2004). The observed changes in earthquake-depth distribution and style of faulting between the foreland and the inner-alpine zones reflect the superposition of the regional compressional stress, induced by large-scale continental convergence, with the uniaxial tensional stress related to lateral spreading within the Alpine orogenic belt (KASTRUP et al., 2004). However, the sparse data do not allow to identify or even to speculate on seismically active fault zones capable of generating large and potentially-destructive earthquakes.

In the foreland, the largest known historic earthquake (M_w ~5.4) occurred in 1674 A.D. near Thalwil, ~20 km southeast of Zurich (FÄH et al., 2003), whereas the inner-alpine central Switzerland region south of Lucerne was seismically more active throughout the historic period. Three events with $M_w \geq 5.7$ were chronicled during the past millennium (Fig. 1.1), including the 1601 A.D. Mw ~6.2 event, that may be associated with a ~20-km-long, left lateral shallow-seated strike-slip fault system within the Helvetic nappes located approximately along the valley of Obwalden (GISLER et al., 2004). The historical record of seismicity in central Switzerland, however, spans only ~1000 yr, and certainly does not reflect the overall seismic potential. Previous paleoseismological studies calibrated the effect of historic earthquakes on sediments in different lakes in the greater Lucerne area and identified 6 additional prehistoric paleoseismic events (with effects similar to those produced by the 1601 A.D. event) that occurred in the past 15 k.y. (SCHNELLMANN et al, 2002; 2006; MONECKE et al, 2006). MONECKE et al. (2004; 2006) further documented that the northwestern part of central Switzerland was also influenced by large earthquakes with epicenters in the Basel region that is characterized by enhanced seismicity both during historic (Basel earthquake 1356 A.D. M_w 6.9 (MEGHRAOUI et al., 2001)) and during prehistoric times (BECKER et al, 2002; FERRY et al, 2004; MONECKE et al, 2006).

The greater Lake Zurich area, however, so far lacks any paleoseismic information and it remains unknown, whether the reconstructed earthquakes in the greater Lucerne and/or Basel area or so far unknown prehistoric seismic events may have affected Lake Zurich and its surroundings. Due to the limited geographical distribution of the previously investigated archives in the greater Lucerne area, estimations of epicenters and magnitudes of prehistoric events remained dubious and, therefore, it is not known whether these events may be associated with the proposed fault zone along the Obwalden valley (GISLER et al, 2004) or with other, so far unknown, neotectonic faults zones capable of generating rare but large earthquakes.

1.3 Outline of the thesis

Chapters 2 to 5 represent four individual peer-reviewed scientific articles that either are published (Chapters 2 and 4) or in press (Chapter 5) in scientific journals or within this publication (Chapter 3). They cover different aspects within the overall thesis framework of «Late Quaternary Natural Hazards in Swiss Lakes» and aim to better determine and quantify causes and effects of natural hazards related to subaquatic mass movements. The general organization of the thesis is as follows:

Chapter 2, published in «Marine Geology», presents three detailed case studies of seismically-triggered slope failures in Lake Lucerne. Sedimentological and geotechnical data from coring and from on-site deployment of in situ geotechnical testing devices allow for reconstruction of the geological and sedimentological processes acting on submerged slopes and for discussion of their influence on physical and geotechnical properties that affect the subaqueous stability conditions and slope failure initiation. The obtained data eventually are implemented into limit equilibrium slope stability calculations that reveal quantitative information on threshold conditions for subaqueous landslide initiation.

In Chapter 3, a chronological catalogue of Late Glacial-to-Holocene mass-movement activity in Lake Zurich is established. The systematic characterization of types and distribution of different mass-movement deposits allow determining the associated depositional, transport and slope-failure trigger mechanism(s) and provide the basis for deciphering various seismic and environmental impacts that affected Lake Zurich and its surrounding during the last 17000 years.

Chapter 4, published in «Geology», identifies striking evidences for three large paleo-earthquakes ($M_w > 6.5$) in central Switzerland by spatial and temporal correlation of multiple coeval lacustrine deposits in Lake Zurich and Lake Lucerne. A novel quantitative paleoseismic approach applying macroseismic reconstructions on the basis of empirical seismic attenuation models and calibrated threshold values for landslide initiation then reveals estimates on earthquake magnitudes and potential epicenter locations. This allows for discussion of seismotectonic implications and provides, for the first time, quantitative information on the seismic hazard potential for the greater Zurich area.

In Chapter 5, in press in «Journal of Geophysical Research: Earth Surface», several independent evidences for the occurrence of a Late Pleistocene moraine collapse and subsequent Lake Zurich outburst are presented that also allow for discussion of causes and consequences of this unique event. Furthermore, the potential outburst magnitude is estimated using hydrodynamic calculations to reconstruct outflow discharge scenarios. The findings then are placed in a broader context to generally discuss natural hazards related to outbursts from moraine-dammed lakes.

2 QUANTIFYING SUBAQUEOUS SLOPE STABILITY DURING SEISMIC SHAKING: LAKE LUCERNE AS MODEL FOR OCEAN MARGINS

Published as: Strasser, M., Stegmann, S., Bussmann, F., Anselmetti, F.S., Rick, B., and Kopf, A. (2007): Quantifying subaqueous slope stability during seismic shaking: Lake Lucerne as model for ocean margins. Marine Geology, 240, 77–97.

Abstract

Lakes can be used as model basins to investigate subaqueous slope stability under static and dynamic loading conditions. This study combines geophysical, sedimentological and in situ geotechnical methods with limit equilibrium calculations in order to discuss (i) the geological and sedimentological processes acting on submerged non-deltaic lateral slopes in Lake Lucerne; (ii) their control on physical and geotechnical properties that eventually affect the subaqueous stability conditions and slope failure initiation, and (iii) the quantitative assessment of subaqueous slope stability. Three detailed case studies are presented to describe and quantitatively reconstruct stability conditions of slopes that failed during a well-documented historic earthquake in 1601 A.D. and during a prehistoric Late Holocene earthquake around 2220 cal yr. BP (both $M_w > 6$).

Glacio-lacustrine sedimentation dominated by suspension settling from meltwater plumes and slight overconsolidation from ice-grounding during small readvances of a generally retreating glacier lead to a peculiar glacial-to-postglacial lithologic slope succession that eventually was burried by the Holocene sediment drape. During past earthquake shaking, the slopes that were stable under static loading conditions (factor of safety of 1.5–2) failed along planar sliding surfaces that developed at the lithological boundary between fine grained, thinly-laminated, slightly underconsolidated cyclic plume deposits with low undrained shear strength values above and overconsolidated, glacially-deformed, glacio-lacustrine deposits with excessive formation pore pressure below. Measured in situ shear strength characteristics and sediment geometries were implemented into limit equilibrium models that allow for quantitative reconstruction of critical ground accelerations of past earthquakes in Central Switzerland. Results reveal seismic peak ground acceleration (PGA) of ~0.08 g and ~0.14 g for the historic 1601 A.D. M_w ~6.2 earthquake and the prehistoric, ~2220 cal yr. B.P. earthquake, respectively. Additionally, results reveal that stability conditions change over relative short geological time scales because the postglacial sedimentation rate, which mainly controls the static weight of the slope sediment acting on the critical lithological boundary, turns out to be a key parameter in «charging» slopes susceptible to sliding.

Zusammenfassung

Diese Studie befasst sich mit der Stabilität von Unterwasserabhängen unter statischer und dynamischer (i.e. seismischer) Belastung. Mit Hilfe von geophysikalischen, sedimentologischen, in situ geotechnischen und numerischen Modellierungs-Methoden wird untersucht (i) wie die geologischen, sedimentären- und postsedimentären Prozesse entlang Unterwasserabhänge wirken, (ii) was deren Einfluss auf die physikalischen Sedimenteigenschaften ist und (iii) wie diese die Hangstabilität kontrollieren. In drei detaillierten Fallstudien wird die Hangstabilität berechnet, um subaquatische Rutschungen, ausgelöst durch ein historischen Erdbeben im Jahre 1601 n. Chr., bzw. durch ein prähistorisches Erdbeben ~2220 Jahre vor heute, quantitativ zu rekonstruieren.

Die Untersuchungen zeigen auf, dass glazio-lakustrine Sedimentationsprozesse, welche durch Ablagerung aus Gletschermilch-Suspensionwolken dominiert wurden, sowie eine postsedimentäre leichte Überkonsolidierung verursacht durch Eiskontakt, zu einer besonderen glazial-bis-spätglazialen lithologischen Abfolge entlang der Unterwasserabhänge führten. Diese Abfolge wurde schliesslich von Holozänen Seeablagerungen überlagert. Während vergangener Erdbeben entwickelten sich entlang der lithologischen Grenze zwischen den feinkörnigen, feinlaminierten, leicht unterkonsolidierten spätglazialen Sedimenten, welche geringe Scherfestigkeiten aufweisen, und den darunter liegenden glazial-deformierten, leicht überkonsolidierten glazio-lakustrinen Ablagerungen, welche zusätzlich durch leichte Porenwasserüberdrücke charakterisiert sind, planare Rutschungsflächen, entlang welcher das unter statischer Auflast stabile post-glazialen Sedimentpacket (Sicherheitsbeiwerte von 1.5–2) abrutschte.

Limit Equilibrium Hangstabilitätsberechnungen, welche die in situ bestimmten Sedimentfestigkeiten sowie die aus reflexionsseismischen Untersuchungen bekannten Hanggeometrien berücksichtigen, erlauben es die kritischen seismischen Bodenbeschleunigungen für die vergangenen Erdbeben quantitativ zu rekonstruieren. Die Resultate liefern minimale Bodenbeschleunigungen in der Grössenordnung von 0.08 g für das historische Erdbeben im Jahre 1601 n. Chr. und 0.14 g für das prähistorische Beben vor ~2220 Jahren. Die Resultate zeigen im Weitern auf, dass sich die Hangstabilitätsverhältnisse geologisch betrachtet über relative kurze Zeiträume signifikant ändern können. Dies wird als Folge von unterschiedlichen post-glaziale Sedimentationraten, welche schlussendlich die statische Auflast des Sedimentpakets auf die kritische glazial-postglaziale lithologische Grenze kontrollieren, interpretiert.

2.1 Introduction

Local instability of submerged sediment-covered slopes are common features in both marine and lacustrine environments and may have considerable catastrophic impact on offshore and coastal infrastructure (e.g. Shilts and Clague, 1992; Chapron et al., 1999; Locat and Lee, 2002; Boe et al, 2004; Lee, 2005). They originate from various processes such as erosion, rapid sedimentation, gas release or migration, earthquake shaking, diapirism, glacial and tidal loading, wave action, or clathrate dissociation (Hampton et al., 1996, Locat and Lee 2002). Some of these geological processes act on the submerged slopes over longer time periods and are considered as causal factors whereas others are of instantaneous nature (e.g. earthquakes) and are thus referred to as short term trigger mechanisms (Locat and Lee, 2002; Sultan et al., 2004;). To understand past slope failure events and to eventually assess subaqueous landslide hazard, it is essential to reconstruct the prefailure and failure conditions associated with subaquatic landslides (Leroueil et al., 1996), and also to quantitatively distinguish between long-term and short-term trigger processes.

Much of what is known today about subaqueous slope stability and hazard-related issues of underwater mass movements has been established from case studies during international campaigns along continental margins (e.g Costa-Project (Mienert, 2004; and references therein) and Strataform-Project (Nittrouer, 1999; and references therein); see Locat and Lee (2002) for general summary) or from theoretical approaches using laboratory data or numerical modeling techniques (e.g. Biscontin et al., 2004; Azizian and Popescu, 2006). These studies present major advances in the quantitative assessment of submarine slope stability, but have also shown the challenges in determining in situ physical and geotechnical properties (e.g. shear strength and pore pressure) that are crucial for quantitative slope stability analysis. In the submarine environment, coring and in situ testing tools are expensive and critical subsurface structures along which failure occurred (or might occur in the future) are often located in depths inaccessible by those devices. Therefore, the acquired shallow subsurface data have to be extrapolated to critical depths (e.g. Urgeles et al., 2006) or the stability has to be assessed through normalized approaches (Lee and Edwards, 1986).

This study uses the lacustrine environment as a «model ocean» to quantitatively analyze subaqueous slope stability under static and dynamic loading. Due to their well-constrained boundary conditions, their smaller size and the possibility to be investigated on a complete basinwide scale, mass movements in lacustrine environments offer a series of advantages that make lake studies vital to improve our knowledge on marine processes. The three case studies of seismically-triggered slope failures in perialpine, fjord-type Lake Lucerne (Central Switzerland) presented here allow a quantitative discussion about the relationship between long-term causal factors and short-term trigger mechanisms. Methods developed for oceanographic and geotechnical investigations campaigns were utilized for site characterization. The limited sediment thickness covering the bedrock allows a complete in situ characterization of the slope-covering strata in failed as well as in stable areas. The combined geophysical, sedimentological, in situ geotechnical and limit equilibrium study presents a novel approach for slope stability assessment in the lacustrine environment, but resulting conceptual ideas give also new inputs in the context of larger slope instabilities occurring in particular in fjords or - more generally - on continental margins.

The primary objectives of the study are: (i) to understand the sediment dynamics and their control on the stability conditions along the lateral, non-deltaic slopes of Lake Lucerne; (ii) to quantify the sliding related key-characteristics (morphology, sedimentology, physical properties and in situ geotechnical parameters) of three earthquake-triggered slopes failures; and (iii) to quantitatively reconstruct seismic ground accelerations that affected the slopes at the time of failure.

2.2 Geological Setting/Lake Lucerne

Lake Lucerne is a fjord-type, perialpine lake of glacial origin situated in Central Switzerland (~47°N, 8.5°E; 437 m asl.; area = 116 km^2; Fig. 2.1). It consists of seven steep-sided sub-basins with relatively flat basin plains down to 220 m maximum water depth (Bührer and Ambühl, 1996). The substratum of Lake Lucerne is composed from S to N by the Helvetic Nappes, the Subalpine Molasse and the Plateau Molasse which are separated by the Northern Alpine thrust and Subalpine thrust, respectively (Fig. 2.1). The lake's complex shape and morphology result from efficient glacial erosion along weak zones associated with the regional geology. Past lake levels were slightly lower (~-9 m) and probably increased stepwise related to the growth of two opposing deltas in the outlet region near the city of Lucerne (Kopp, 1938).

This study concentrates on the lateral non-deltaic slopes of the external Chrüztrichter and Vitznau basins (Figs. 2.1 and 2.2) that are separated from the major deltas by sills formed by submerged moraines (Hantke, 2003). The three discussed study sites (i.e. the Weggis, St.Niklausen and Chrüztrichter sites) are located north of the Northern Alpine Front in areas with a molassic substratum consisting of sandstones and conglomerates.

In the central region of the investigated sub-basins the bedrock is covered with an up to 120 m-thick, mainly glacial and glacio-lacustrine infill (Finckh et al., 1984). The majority of these sediments were deposited in a subglacial environment within relatively short time during the end of the last Glacial period. The Late Glacial basin sediments comprise thinly-laminated light gray to yellowish mud with frequent intercalated graded turbidite beds. The Holocene sediments consist of 5 to 15 m-thick, faintly laminated grayish to brownish mud with dark layers rich in organic matter and some intercalated graded turbidite beds (Schnellmann et al., 2006). Previous stud-

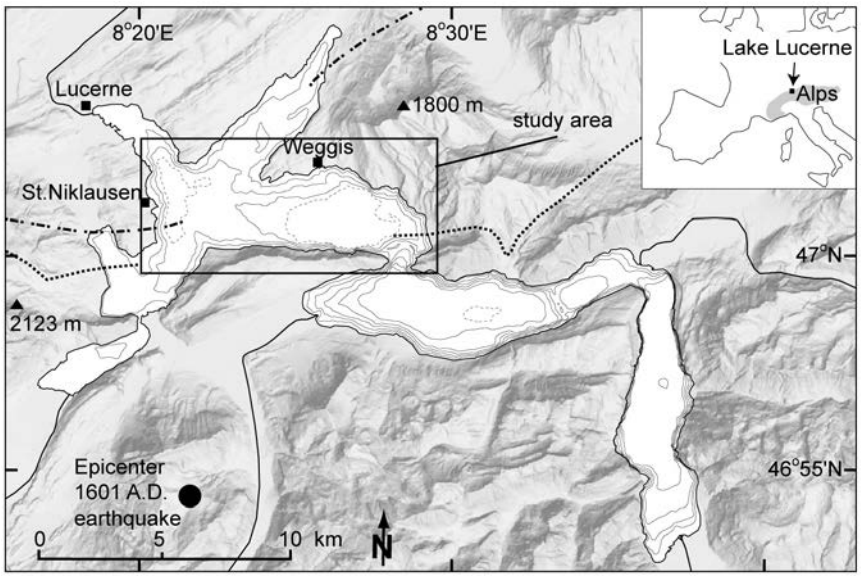

Figure 2.1: Overview map of Lake Lucerne and its surroundings (shaded relief from 25 m digital terrain model, Swisstopo) showing the seven steep-sided sub-basins with flat basin plains. Bathymetric contour interval is 40 m. Dotted contour lines represent 20 m intervals and aim to clarify bathymetry. The rectangle indicates the study area and outlines location of subsequent Figure 2.2. The dotted and dashed lines mark the Alpine and the Subalpine Front, respectively (see section 2.2). Black circle in the SW corner of the map indicates estimated epicentral location of 1601 A.D. Mw ~6.2 Unterwalden earthquake (Schwarz-Zanetti et al., 2003; Gisler et al., 2004).

ies identified numerous mass-movement deposits related to a historic Mw 6.2 earthquake occurring in 1601 A.D. (Unterwalden Earthquake; Schwarz-Zanetti et al., 2003; Gisler et al., 2004) in the subsurface of Lake Lucerne (Siegenthaler et al, 1987, Lemcke, 1992; Schnellmann et al., 2002, 2005, 2006). 13 synchronous mass movements related to this event triggered a tsunami wave up to 4 meter in height and a subsequent seiche wave that lasted for several days (Cysat, 1601; Schnellmann et al., 2002). In the deeper subsurface, five additional event horizons containing seismically triggered synchronous mass movements were identified that have occurred in the last 15000 years. Schnellmann et al. (2006) provide a chronological catalogue of Late Glacial and Holocene mass-movement deposits and related subaqueous landslide scars in the two studied sub-basins. Slope failures are mostly characterized by translational movement and occurred in water depths ranging from 30–100 m. This study focuses on the source areas and on the prefailure and failure conditions of three well-dated landslides, the deposits and depositional mechanisms of which are well constrained and for which strong seismic shaking was singled out as trigger mechanism (Schnellmann et al, 2005, 2006; Fig 2.2).

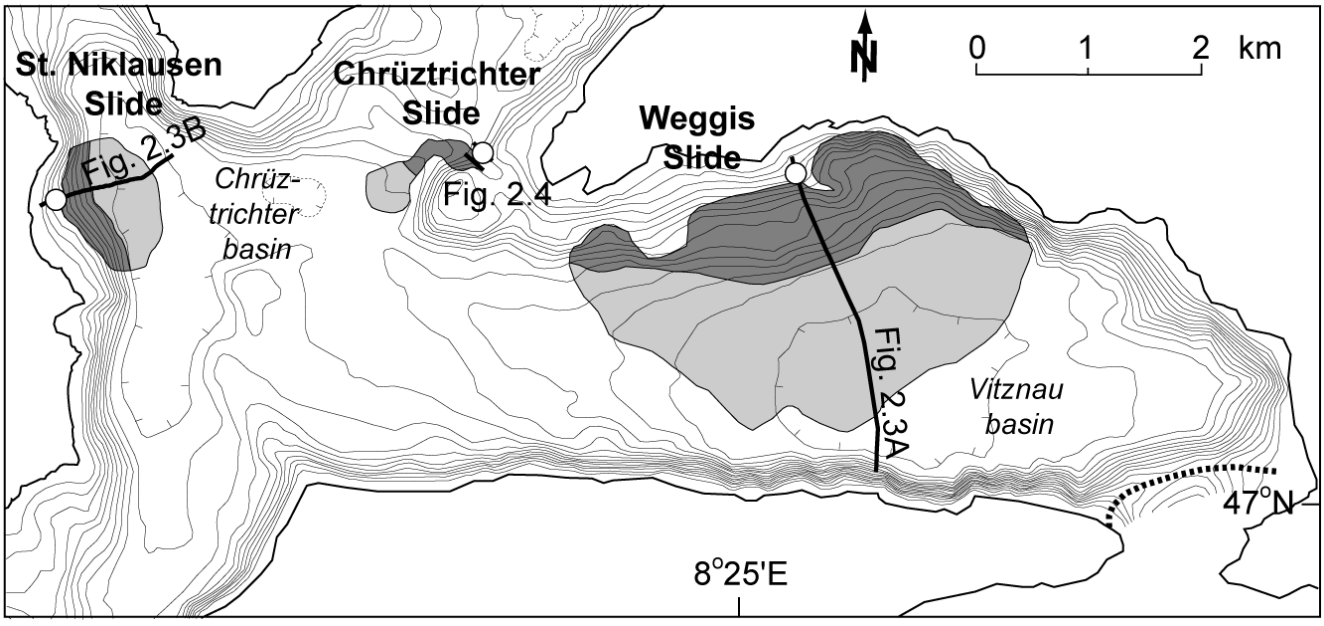

Figure 2.2: Modified after Schnellmann et al., 2005. Bathymetric map of Chrüztrichter and Vitznau basins showing the outline of the Weggis, St. Niklausen and Chrüztrichter Slides (see Figure 2.1 for location of the map segment). Slide complexes are marked with grey shadings, whereby dark and light grey indicate erosional and depositional zones, respectively. Contour interval is 10 m. The bold dotted line in the SE corner indicates a major subaqueous sill and corresponds to an intermediate glacier-front stage during deglaciation (Hantke, 2003). Bold lines indicate position of 3.5 kHz seismic profiles presented in subsequent figures. Open white circles give position of piston cores and in situ testing sites.

2.3 Methods

2.3.1 Subbottom profiling

Closely spaced (~30–50 m grid spacing), single channel high-resolution 3.5 kHz seismic profiles (pinger source) were acquired in 2005 in order to refine the existing basinwide seismic data set (SCHNELLMANN et al, 2006) in the areas of the three study sites. The source/receiver was mounted on a cataraft that was pushed in front of a small vessel. DGPS-positioning with a maximum error of ±2 m guaranteed accurate navigation. The digitally recorded data was processed using both a flat gain and band-pass filtering. Two-way travel time was converted to water depth and sediment thickness using a constant velocity of 1450 ms^{-1}. No migration was applied to the data because visual quality and readability is better in the non-migrated data and slope dip errors due to non-migration of the seismic sections are negligible (< 2 %).

2.3.2 Coring and laboratory analysis

At each study site, two Kullenberg-type gravity piston cores (KELTS et al., 1986), each 4.5–7 m in length, were recovered in the undisturbed slope-covering sediments adjacent to the failure scars. These cores provide material for both detailed characterization of sedimentological and physical properties, and for further geotechnical analysis on undisturbed samples. Additionally, at each study site 3 short gravity cores with a maximum length of 2 m were recovered along the failed slopes downslope of the failure scar.

The cores were logged in the Limnogeology Laboratory at ETH Zurich using a GEOTEK multisensor core logger (MSCL), which measures Gamma Ray Attenuation bulk density, compressional wave velocity and magnetic susceptibility. Afterwards, cores were split for sedimentological description (macroscopically and using smear slide techniques; ROTHWELL, 1989; KELTS 1998). Immediately after splitting, cores were photographed and natural water content measurements were performed by weighing 10 cm^3 of sediment before and after drying in an oven at 105°C. On the freshly split sediment surface, undrained shear strength was measured perpendicular to bedding at ~15 cm intervals using a pocket vane shear testing device (Eijkelkamp). Atterberg limits were determined according to British Standards 1377 (Institute B.S., 1977) using a Casagrande apparatus. Grain size analysis were performed using laser diffraction techniques (Malvern Mastersizer Hydro 2000S) at ~10 cm intervals along the split core. Gravel clasts > 2000 µm in the glacio-lacustrine sediments recovered at the bottom of the cores were removed by sieving prior to analysis, and clast diameters were estimated visually. Additionally, selected samples were analyzed for solid volume using a helium pycnometer device at the Rock Deformation Laboratory at ETH Zurich to derive grain density values. To characterize the consolidation history of the material, one dimensional consolidation tests (oedometer) were performed on two end-member lithologies from undisturbed samples taken from core 4WS05-K5 (Weggis Site) at the Research Centre Ocean Margins (RCOM), in Bremen. Specimens of 2 cm height and 5 cm in diameter were trimmed out of whole-round core samples and incrementally subjected to normal loads of up to 4 MPa.

2.3.3 In situ geotechnical testing

At the Weggis and St.Niklausen sites (see Fig. 2.2 for location) in situ geotechnical strength measurements were performed at ~50 cm intervals throughout the sediment profile. Both vane shear tests and Cone Penetration Testing (CPT; with pore pressure measurements) were performed to identify the in situ undrained strength profile. By using two independent methods the strength versus depth profile could be independently confirmed. Additionally, local induced excess pore pressure response could be measured and monitored to approximate the in situ pore pressure distribution.

The in situ vane shear tests were performed using a vane shear probe of 6.5 cm diameter (Geonor A/S) that was lowered in a casing mounted on an anchored platform. At each target depth the probe was extruded carefully from the casing into the undisturbed sediment and rotated mechanically from the platform at constant rate (6°/min) until failure occurred. In the water saturated, fine-grained sediment, the hereby induced excess pore pressure does not have time to dissipate, thus the measured peak strength is inferred to be the in situ undrained shear strength ($c_{u\ in\ situ}$). The residual strength was then deduced from a consecutive test at the same interval. Only in the lowermost part of the section the measurements might be biased by the presence of gravels that occasionally block the vane shear device during rotation. Calibrating the system in the casing in the water above the lake bottom revealed negligible additional friction of the rotating rod. However, some inaccuracy results from the slight sediment disturbance when the probe is lowered. This results in underestimating the real in situ strength condition. Although the measurements were performed during calm periods with no wind-driven waves on the lake, minor waves from boats could not always be avoided so that early failure due to wave induced vertical movement of the vane shear device during the tests cannot always be excluded, potentially providing a second source for underestimating the actual in situ strength values.

A marine free-fall penetrometer from RCOM Bremen was used to measure strength and pore pressure in situ (STEGMANN et al. 2006). The autonomous working tool consists of a standard industrial 15 cm^2 CPT cone and a pressure housing containing the power supply, data acquisition and an acceleration sensor. The tests were performed at the same location and at comparable depth intervals as the vane shear test. The CPT-instrument was lowered carefully from the anchored platform using a 4x4 car winch at the lowest possible rate (average rate ~2 cm/sec) into the sediment, rested at each level for 10 minutes for pore pressure dissipation, and was then lowered to the next level, and so on. Insertion of the probe results in a compaction of the

sediment, which generates an artificial excess pore pressure spike followed by pressure decay that approaches ambient values. By monitoring and evaluating the pore pressure dissipation after insertion, qualitative permeability conditions can be estimated (for details see TERZAGHI, 1925). Additionally, these measurements provide confirmation that the strains induced during testing result in excess pore pressures and thus undrained loading at the test locations. Undrained shear strength ($c_{u\ in\ situ}$) was derived based on an empirical equation with the measured cone resistance during CPT-lowering using a standard cone factor (N_k) of 15 and 17 for normally consolidated clays and overconsolidated clays, respectively (for details see LUNNE et al, 1997). Vane and cone penetration derived undrained shear strength cannot be directly compared because absolute values may differ significantly due to fundamental differences in the mechanical behavior between vane shearing and cone penetration (LU and BRYANT, 1997). Thus, the two independently measured cu in situ values are only considered for first-order comparison of magnitude, but they can be used to identify characteristic strength versus depth trends.

2.3.4 Slope Stability evaluation

2-D limit equilibrium slope stability analysis (for details see e.g. DUNCAN, 1996) were carried out using the commercially available software package Slide (Rocscience Inc.) that is widely used in geotechnical engineering for slope stability assessments under subaerial conditions, but allows for adaptation to the subaqueous environment. The program uses equal-width slices and allows for input of a slope profile, sub-bottom geometry of layers, their geotechnical properties and a predefined failure surface geometry. Additionally, a pseudostatic acceleration can be used to model the peak ground acceleration generated by earthquakes and to evaluate the seismic slope stability. This parameter assumes that the earthquake acceleration is applied over a significantly long period of time so that the induced stresses can be considered constant (HAMPTON et al., 1996). Thus, the dynamic response of the sediment cannot be taken into account. The output factor of safety (FS; i.e. the ratio between the resisting shear strength and the sum of all loading forces (mobilized shear stress)) is calculated using a combined General Limit Equilibrium (GLE)/Morgenstern-Price method (FREDLUND and KRAHN, 1977; MORGENSTERN and PRICE, 1965).
Two types of analysis were performed: (i) Deterministic back-analysis of seismically-triggered slope failures, and (ii) probabilistic limit equilibrium slope stability calculations. The back-analysis approach assumes FS=1 at failure and tries to constrain the parameter combinations that could produce instabilities. Contrary to this deterministic method that uses one single constant value for each input parameter, the probabilistic approach considers variability and hence uses a mean and standard deviation value. Here, the input data samples are randomly generated using the Monte Carlo sampling method simulating the uncertainty and variability of each input parameters. FS is calculated for > 1000 runs and model outputs reveal mean FS value of the modeled slope and the corresponding probability of failure (i.e. % of all analyses with FS < 1).

2.4 Data and Results

Seismic interpretation and bathymetric evaluation allowed three target locations to be identified that are well suited for the purpose of this study (i.e. the Weggis, St.Niklausen and Chrüztrichter sites). They are characterized by (i) clear landslide scars related to known mass-movement events, (ii) undisturbed postglacial drape thickness adjacent to the failure scar < 8 m (i.e., can be penetrated with coring and in situ testing probes), and (iii) water depth < 40 m for in situ vane shear testing. In this section the analyzed morphological, sedimentological and geotechnical characteristics of this three studied lateral slopes that failed during past earthquakes are presented.

2.4.1 Case study sites

2.4.1.1 Weggis Slide

The largest slide in the study area, the Weggis Slide, mobilized ~8.5 x 10^6 m^3 of sediment and is located on the northern slope of the Vitznau sub-basin (Figs. 2.2 and 2.3A). Previous studies by SIEGENTHALER et al. (1987), LEMCKE (1992) and SCHNELLMANN et al., (2002, 2005, 2006) have shown that this landslide is related to the 1601 A.D., M_w ~6.2 earthquake. The slide scar reaches a maximum height of 6 m and extends laterally over more than 6 km in water depths ranging from 30 to 100 m along the relatively gently dipping, 5° to 15° steep lateral slope. In Figure 2.3A, the slide scar appears in approximately 35 m water depth in a zone, where the slope inclination increases downwards from < 10° to ~15°. In the uppermost part of the eroded slope acoustically chaotic to transparent proximal mass-movement deposits can be identified. The observed bathymetric step in the lower part of the slope is caused by conglomerate banks of subalpine molasse rocks in the substratum. The slide scar cuts through a 4 m-thick, acoustically laminated sedimentary drape (referred to Holocene and Late Glacial deposits in Fig. 2.3) that overlies a thin seismostratigraphic unit characterized by a high-amplitude chaotic reflection pattern that is hardly distinguishable from the acoustic basement. This observation suggests that bedrock is covered by a few meters of glacial deposits. However, seismic penetration and resolution do not allow for exact mapping of this boundary. The absence of the entire drape clearly points towards a translational sliding mechanism with the glacial deposits acting as a base for the failure surface.

2.4.1.2 St. Niklausen Slide

Offshore the village of St. Niklausen in the western Chrüztrichter sub-basin (Fig. 2.2), stacked debris-flow deposits in the basin plain (Fig. 2.3B) indicate that parts of the slope

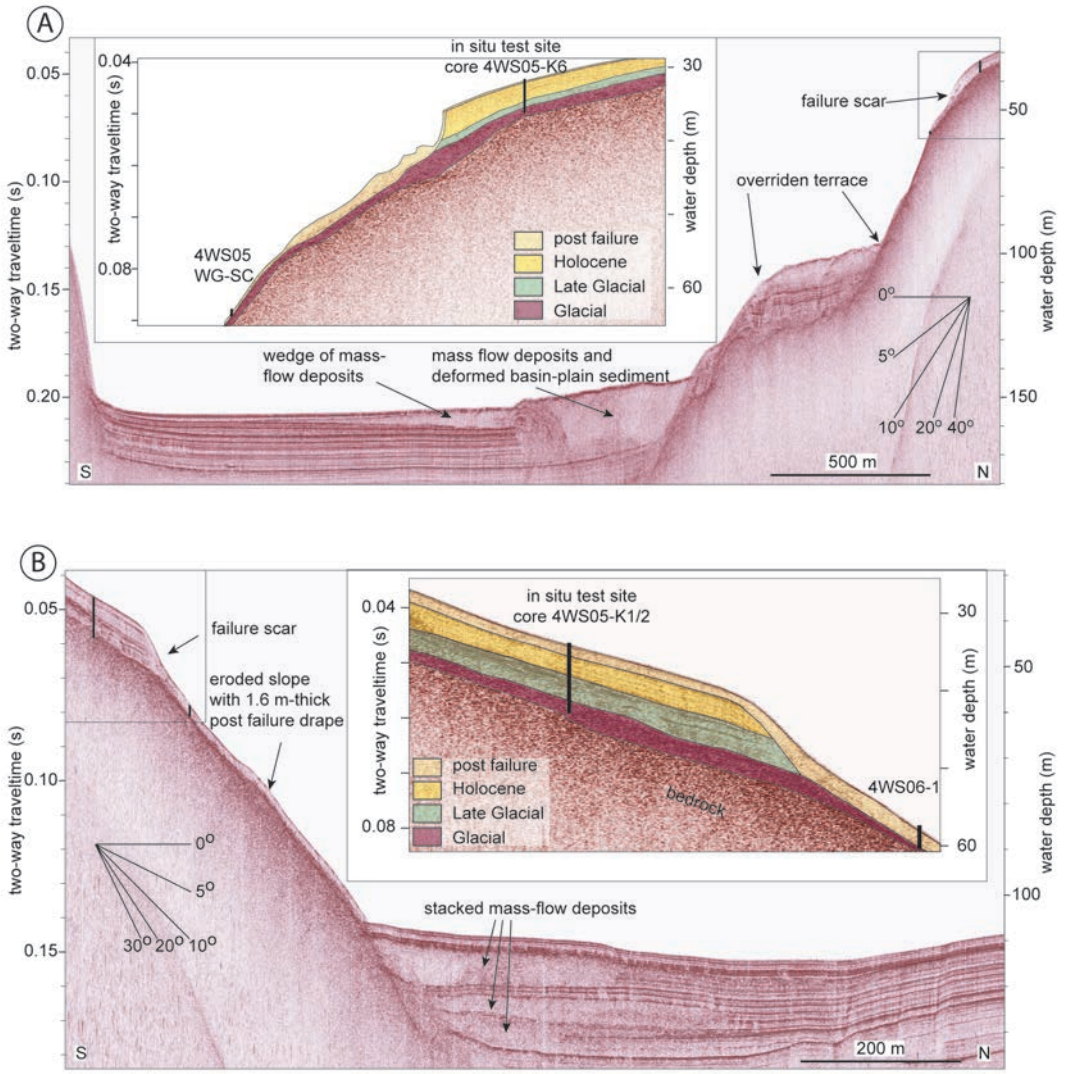

Figure 2.3: 3.5 kHz seismic lines illustrating the structure of the Weggis Slide (A) and St.Niklausen Slide (B). See Figure 2.2 for location of seismic lines. Inlets show enlarged details of the scars with slope model interpretations of lithological units as cored in reference cores. In the uppermost part of the eroded Weggis slope (A) the acoustically chaotic to transparent unit with an irregular upper surface is interpreted as proximal mass-movement deposit.

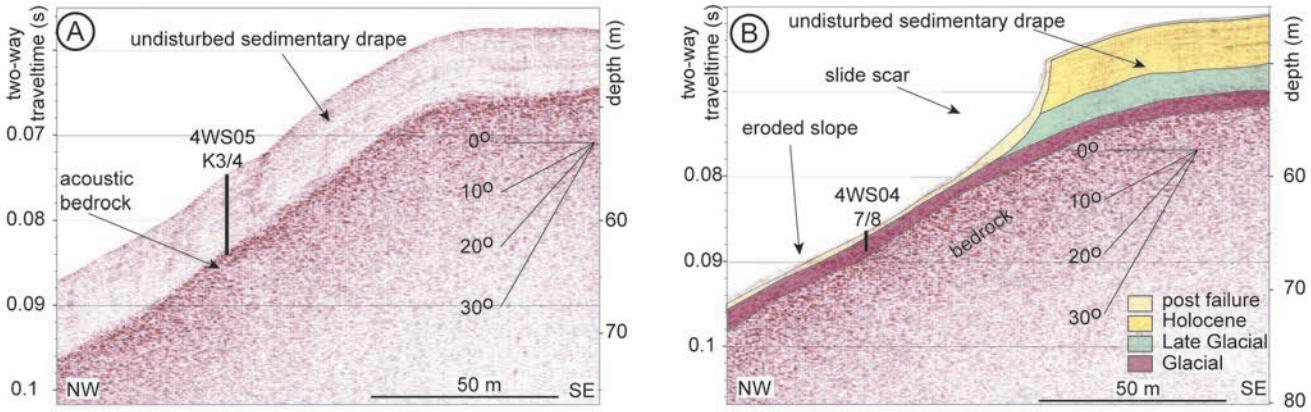

Figure 2.4: Two parallel-oriented 3.5 kHz seismic lines across the sub-lacustrine slope in the northeastern edge of Chrüztrichter basin. Distance between the lines is about 80 m. For location see Figure 2.2. (A) Profile shows an undisturbed slope characterized by an approximately 6 m-thick continuous sedimentary drape directly overlaying acoustic bedrock and location of cores 4WS05-K3 and K4. (B) Profile displays failure scar of Chrüztrichter slide with slope model interpretation of lithological units as cored in reference core 4WS05-K4 and short cores 4WS04-7 and 8, which recovered the failure plane of the 1601 A.D. slope failure in core depths of 0.4 m below lake floor. Figure modified after Schnellmann et al., (2005).

have repeatedly been active in Late Glacial and Holocene times, with the youngest being the largest event that affects a total mobilized volume of ~1.5 x 10^6 m^3. St. Niklausen Slide is smaller than the Weggis Slide described above and is of medium size compared to other Lake Lucerne subaqueous mass movements (SCHNELLMANN et al., 2005, 2006). It was dated at 2180–2410 cal. yr B.P. (SCHNELLMANN et al., 2006) and is part of a multiple-slide event that was triggered by a major northern alpine earthquake (M_W > 6.5; 2220 ±40 cal yr B.P.; STRASSER et al., 2006). A 1.5 km long and up to 6 m high slide scar assigned to this 2220 cal. yr B.P. slope failure event is located on a steepening-downward slope in 40–50 m water depth (Fig. 2.3B). Below the failure scar, a 1.6 m-thick post-landslide sedimentary drape covers the ~13° steep slope. Seismic data reveal the same acoustic characteristics as observed on the Weggis slope described above, with slightly more pronounced continuous, parallel high-amplitude reflections in the undisturbed, acoustically-laminated drape up-slope the failure scar (Fig 2.3).

2.4.1.3 Chrüztrichter Slide

A third subaqueous landslide, triggered by the 1601 A.D. earthquake (SCHNELLMANN et al, 2005), was surveyed in great detail. The relatively small Chrüztrichter Slide (~0.18 x 10^6 m^3 eroded volume) is located on the northeastern edge of the Chrüztrichter basin and affects an area of 0.3 km^2 from the failure scar to the toe of the deposits. The failure scar lies on a ~13° steep, northward-dipping slope of a small subaqueous mound at 30–40 m water depth. It cuts a ~6 m thick, acoustically laminated sedimentary drape that overlies acoustic basement in the undisturbed slope environment, both upslope and lateral to the failure scar (Fig. 2.4).

2.4.2 Lithostratigraphy

The continuous glacial-to-postglacial sedimentary succession covering the undisturbed lacustrine slope at the three study sites was recovered in 6 piston cores (two at each site) immediately upslope (Weggis/St.Niklausen) or adjacent (Chrüztrichter) to the failure scar (see Figs. 2.2–2.4 for location). Figures 2.5, 2.6 and 2.7 show the composite plots of all data obtained at the three study sites. The sedimentary succession is very similar at all three sites and shows three distinct lithologic units composed of (from top to bottom): Unit 1 (2.5–4.9 m thick): homogenous to mottled, olive gray, silty clays with abundant organic material. The sediment is mainly of detrital origin with variable amounts of authigenically-produced carbonates and diatoms; Unit 2 (1.2–1.6 m thick): yellowish light gray, thinly-laminated (mm to sub-mm-scale), clays and clayey silts of detrital origin (Fig. 2.8A); Unit 3 (1–2 m thick) tilted and deformed thinly-laminated yellowish to light gray clayey silts to silty clays with sparse (< 20%) sand and medium-sized gravels up to 4 cm in diameter (Fig. 2.8B) floating in the fine-grained matrix. These angular, poorly sorted gravels show clear glacial striation and cover a wide range of lithologies also including crystalline basement rocks that only outcrop far south of Lake Lucerne. At the base of core 4WS05-K1 (St. Niklausen), a 15 cm-thick diamict deposit with clasts of glacial origin in a poorly sorted, clay-silt-sand matrix was recovered. Although the lowermost part of this core shows coring disturbances, this basal layer can be interpreted as a till deposit.

Unit 3 can be assigned to the thin seismostratigraphic unit showing high amplitude, chaotic reflection patterns as observed at the Weggis site (see subsection 2.4.1.1) and is interpreted to represent glacially deformed glacio-lacustrine deposits (see discussion in subsection 2.5.1.1). Units 1 and 2 can be correlated by seismic stratigraphy, lithological facies and physical properties (mainly magnetic susceptibility and bulk density) to lithologies recovered and dated in sediment cores from the deep basin (SCHNELLMANN et al., 2006; Thevenon and Anselmetti, 2007) revealing Holocene (< 11500 cal yr. B.P.) and Late Glacial (> 11500 cal yr B.P.) ages, respectively. They represent the draping «slope-cover» sediment facies deposited in Lake Lucerne since the glacial retreat from the Swiss Plateau around 17500 cal yr B.P (LISTER 1988; WESSELS 1998; see discussion in subsection 2.5.1.2). Sedimentation rates in the Late Glacial Unit 2 are similar at the Weggis and Chrüztrichter sites (20–21 cm/ka) and slightly higher at the St. Niklausen site (~26 cm/ka). There, the sediments have slightly higher silt contents and few 0.5–2 cm-thick sand layers in the lower part of the postglacial section indicate higher detrital input possibly from a small local creek entering the lake nearby. In contrast, sedimentation rates for the Holocene Unit 1 differ significantly from site to site. At the Weggis site, they are in the same order as during Late Glacial times (~22 cm/ka), while they are clearly higher along the submerged slope offshore St. Niklausen (~36 cm/ka) and reach maximal values at the Chrüztrichter site (42 cm/ka). The difference in sedimentation rate may be caused by small local creeks, currents (AESCHBACH-HERTIG, 1994) and different amounts of biogenic sedimentation that favors deposition along the St. Niklausen and Chrüztrichter slope.

2.4.3 Physical properties

Physical property data from all three sites reveal significant contrasts in most measured parameters between the postglacial (Units 1 and 2) and the glacio-lacustrine deposits (Unit 3; Figs 2.5, 2.6 and 2.7). Generally, the Holocene section is characterized by downward increasing values of bulk density (ρ_{bulk}) with depth, whereas natural water content and Atterberg limits decrease gradually down-section. Only solid grain densities are more or less constant throughout the section with values of ~2.75 g/cm^3 and ~2.8 g/cm^3 in the Holocene deposits and in the Glacial to Late Glacial material, respectively. At the Weggis Site, absolute ρ_{bulk} values increase stepwise at lithological boundaries from 1.3–1.4 g/cm^3 in Unit 1 to 1.45–1.55 g/cm^3 in Unit 2, whereas at the two other sites, ρ_{bulk} values more gradually increase from ~1.3 g/cm^3 in the middle part of the Holocene section to ~1.55 g/cm^3 in the Late Glacial deposits.

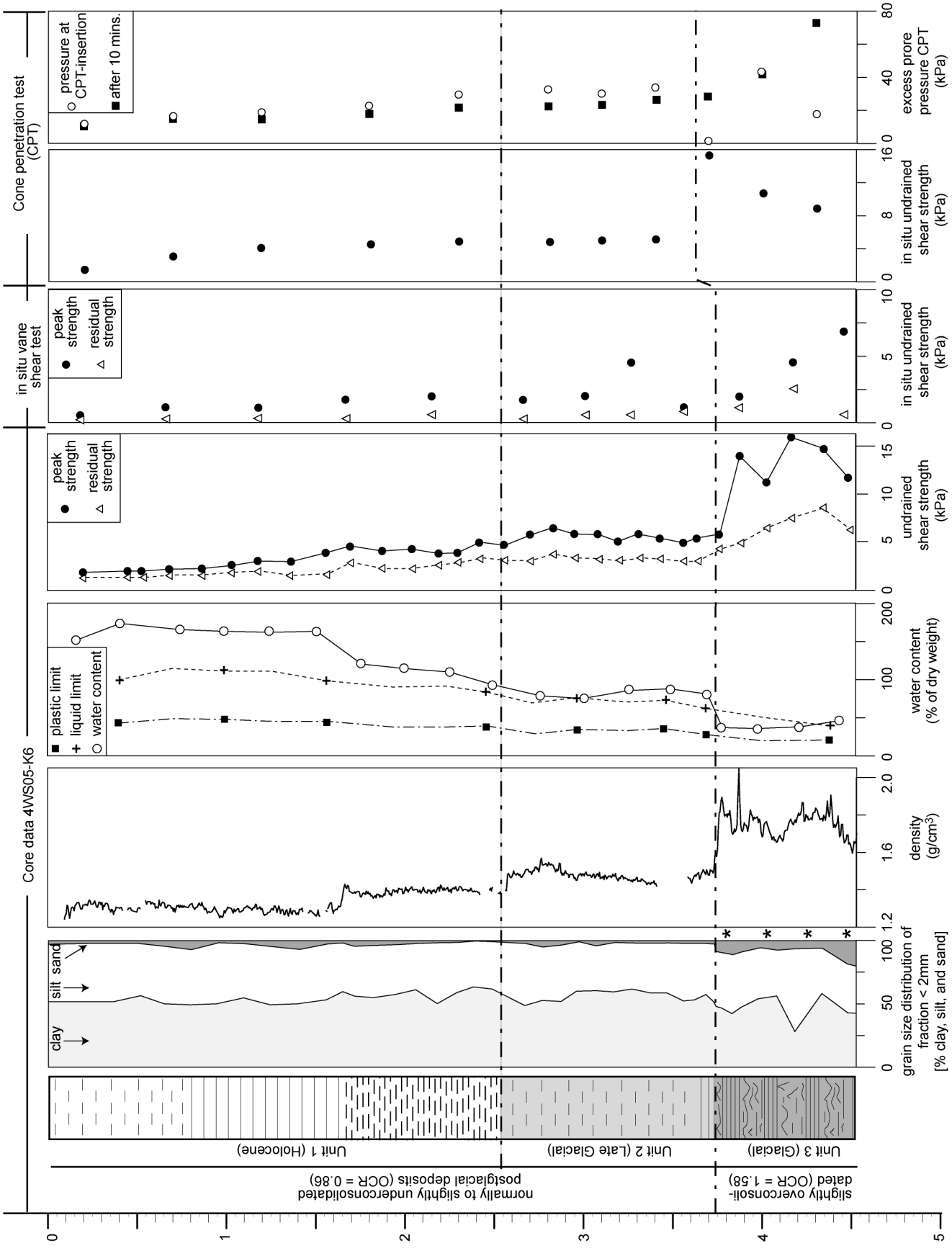

Figure 2.5: Data obtained from core 4WS05-K6 and from in situ tests summarizing sedimentological and geotechnical characteristics of the undisturbed continuous glacial-to-postglacial sedimentary succession covering the sublacustrine slope offshore Weggis. The site is located immediately upslope the failure scar (see Figs. 2.2 and 2.3A for location). Asterisks indicate the presence of material with grain size > 2 mm (that are not considered in this plot).

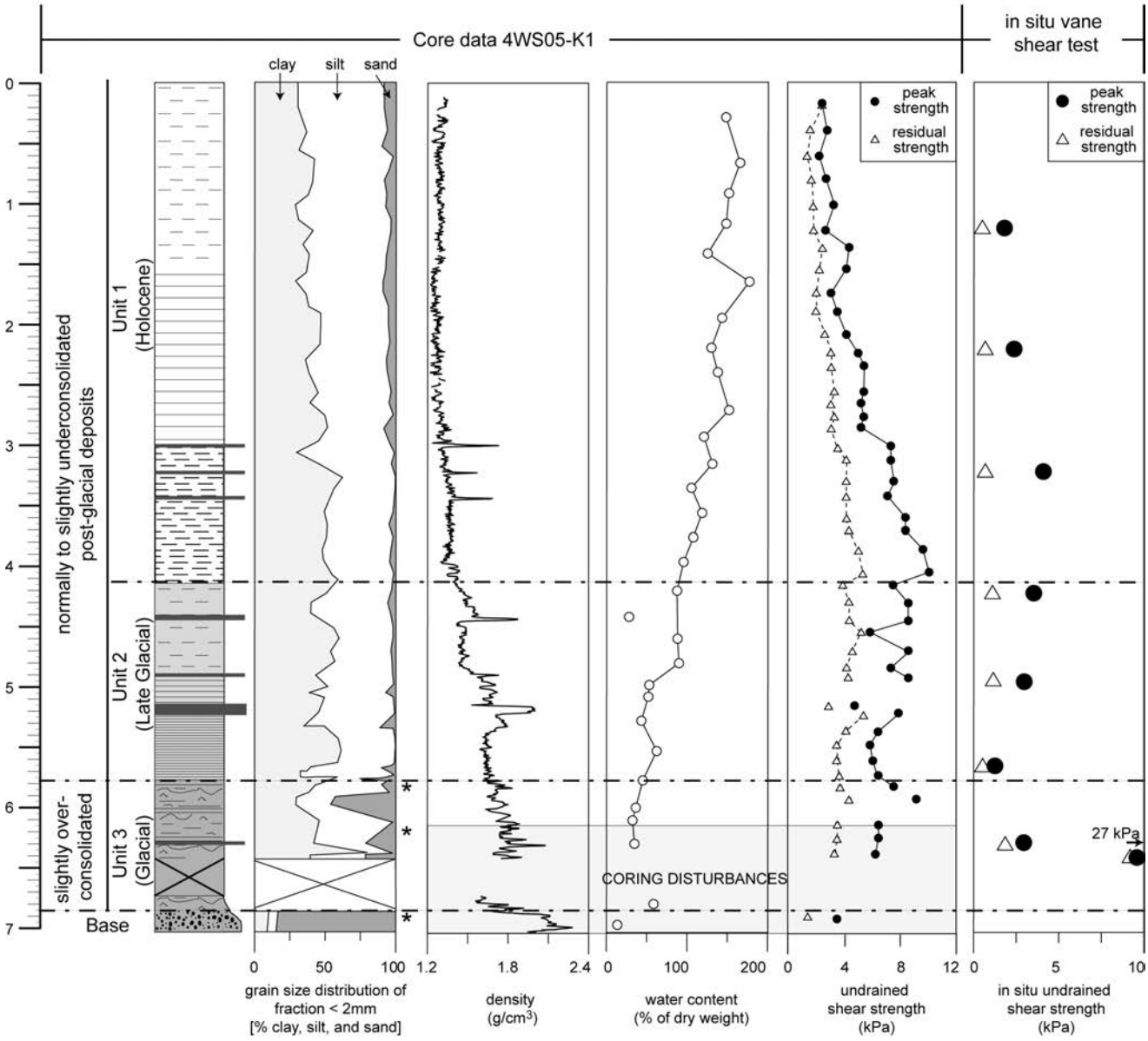

Figure 2.6: Data obtained from core 4WS05-K1 and from in situ tests summarizing sedimentological and geotechnical characteristics of the undisturbed continuous glacial-to-postglacial sedimentary succession covering the sublacustrine slope offshore St.Niklausen. The site is located immediately upslope the failure scar (see Figs. 2.2 and 2.3B for location). Asterisks indicate the presence of material with grain size > 2 mm (that are not considered in this plot).

The boundary between the postglacial and the glacial deposits is characterized by a dramatic increase in ρ_{bulk} of ~0.3 g/cm^3 at Weggis and Chrüztrichter sites. This boundary is further characterized by a significant change in the liquidity index, because natural water contents (w) in the postglacial sediments (decreasing from ~150–175% of dry weight in the uppermost part to ~60–75% in the laminated Late Glacial clays) are higher than the liquid limits (w_L) of theses sediments, whereas w values (~40–50%) plot below the respective w_L-values in the glacio-lacustrine deposits of Unit 3. However, at the St. Niklausen site the contrast in physical properties between the postglacial sediments and glacial deposits is less pronounced than at the other sites (Fig. 2.6). This is most likely caused by coring disturbances in the lowermost part of core 4WS05-K1.

At the Weggis site, two samples from immediately above and below the characteristic boundary between Units 2 and 3 were examined with one dimensional consolidation tests (oedometer) to determine the consolidation history and relative permeability of the material. Results reveal that the laminated Late Glacial clays are slightly underconsolidated (OCR = 0.86) whereas the glacio-lacustrine deposits of Unit 3 are overconsolidated (OCR = 1.58). Both sediment types show low permeability, with the plastic glacial material from Unit 3 being less permeable (hydraulic conductivity (K) = 5.35 x 10^{-10} m/s) than the postglacial sample (K = 5.32 x 10^{-9} m/s) (for details see Stegmann et al., 2007).

2.4.4 *Shear strength*

Undrained peak (c_u) and residual shear strengths slightly vary with respect to the three different test methods utilized, but all three approaches reveal the same relative trend (Figs. 2.5, 2.6 and 2.7): The Holocene Unit 1 is characterized by linearly increasing cu values with depth, whereas values in the upper part of the Late Glacial Unit 2 are constant and even show a clear downward decrease immediately above the contact with the glacial deposits that again show significantly higher strength values (well pronounced at St. Niklausen and Chrüztrichter sites; Figs. 2.6 and 2.7).
Measured $c_{u\ in\ situ}$ values from in situ vane shear tests generally show slightly lower values than those from in situ CPT and laboratory test. This result is interpreted to be caused by disturbances to the material during probe insertion and small waves during the vane shear testing, resulting in slight underestimates of $c_{u\ in\ situ}$ (see subsection 2.3.3). At the Weggis site, $c_{u\ in\ situ}$ values derived from CPT testing and c_u values obtained from laboratory tests correlate well and reveal similar values that increase within the upper 2.5 m (Unit 1) to ~5 kPa. At the St. Niklausen and Chrüztrichter site, highest laboratory-derived cu values at the base of the Holocene Unit 1 reach 9 and 7.5 kPa, respectively. In the laminated Late Glacial clays of Unit 2, c_u values vary between 5–8 kPa (laboratory and in situ CPT-test) and 2–5 kPa (in situ vane shear test) but indicate more or less constant strength characteristics in the upper part and a clearly downwards decreasing trend in the lowermost part of the cores. The glacio-lacustrine sediments of Unit 3 show significantly higher strength values, but absolute values derived from the different methods scatter between 3 and 27 kPa. Given the fact that Unit 3 shows some heterogeneity with slightly higher sand content (up to 20 %) and presence of gravels (see subsection 2.4.2), vane shear tests might not be perfectly applicable and partly account for the scatter. However, as the bulk sediment in this lower section consists mainly of silty clay with a relative low permeability, undrained loading conditions predominate (Lambe and Whitman, 1979). Thus, the measured undrained strength values are interpreted to adequately represent the strength characteristics in this unit.

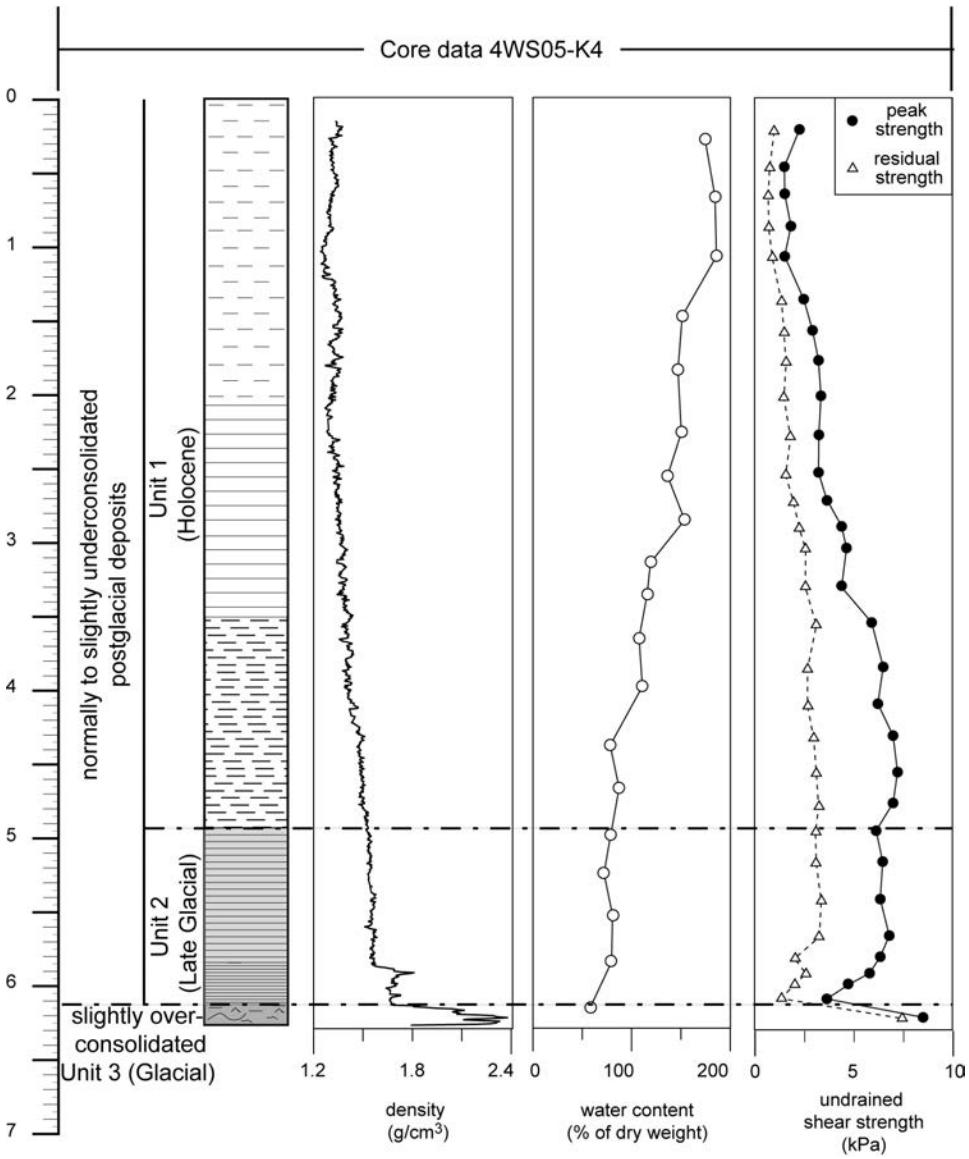

Figure 2.7: Data obtained form core 4WS05-K4 summarizing sedimentological and geotechnical characteristics of the undisturbed continuous glacial-to-postglacial sedimentary succession covering the sublacustrine slope at the study site in the source area of the Chrüztrichter Slide. The site is located adjacent to the failure scar (see Figs. 2.2 and 2.4 for location).

2.4.5 *In situ pore pressure (Weggis site)*

At the Weggis site, in situ formation pore pressure ($u_{in\ situ}$) was estimated after 10 minutes of monitoring the pressure evolution after CPT insertion at different target depths. Figure 2.5 shows measured excess pore pressure values (i.e. absolute measured pressure minus hydrostatic pressure) at CPT-insertion and after 10 min. All tests conducted in the postglacial section reveal dissipation curves with a pore pressure spike upon impact of the probe, followed by a non-linear asymptotical decay. Although ambient excess formation pore pressure cannot be extrapolated from only 10 minutes of monitoring, the characteristic exponential decay of the dissipation curves points toward equilibrium values slightly above hydrostatic. In the glacio-lacustrine sediments of Unit 3, however, the monitored pore pressure after insertion shows the opposite trend. Insertion pressures are relatively low compared to the postglacial sediments, possibly due to suction and fluid displacement at the tip during insertion or due to a dilatant material response. With time, however, pressure increases significantly. This observation is interpreted to result from considerably elevated formation pore pressure in Unit 3. One test carried out for about 45 minutes attested that a plateau in pore pressure rise is reached after approximately 25 minutes.

2.4.6 *Failure plane characteristics*

Short gravity cores from the slide-eroded slopes at all three sites recovered tilted and deformed glacio-lacustrine deposits (Unit 3) in 0.36, 0.4 and 1.6 m core depth at the Weggis, Chrüztrichter and St.Niklausen sites, respectively. The upper boundary of the glacial deposits in all cores is sharp and erosive. These boundaries are interpreted as the failure surfaces of the 1601 A.D. and 2220 cal yr. B.P earthquake-triggered landslides (Weggis-/Chrüztricher and St. Niklausen slide, respectively). At the two 1601 A.D. landslide sites, the thickness of overlying post-landslide deposits (Unit 1) reveals sedimentation rates for the last

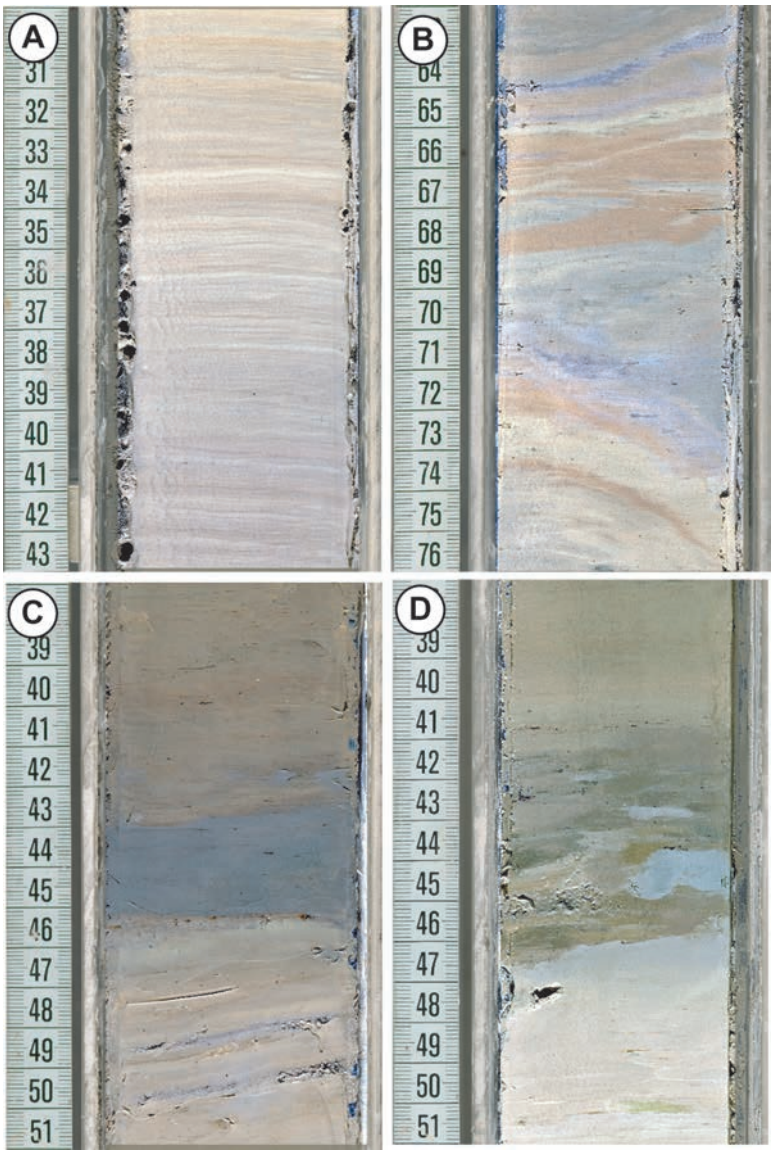

Figure 2.8: Core photographs showing:
A) thinly laminated Late Glacial clays (core 4WS05-K6);
B) glacially deformed overconsolidated glacial-lacustrine deposits (core 4WS05-K6);
C) 2 cm-thick, grey homo-genous silty clay layer between 44 and 46 cm of core 4WS05-WG/SC assigned to the Weggis Slide overlying tilted glacio-lacustrine deposits;
D) sharp and erosive boundary at 46 cm of core 4WS04-7 (i.e. failure plane of Chrüz-trichter Slide) between glacially deformed glacio-lacustrine de-posits and post-landslide deposits. Note reworked glacial mud clasts (at 45 cm) at the base of the overlying post-landslide deposits.

400 years of ~1 mm/a, which is consistent with estimated recent sedimentation rates by Lemcke (1992). At St. Niklausen, the 1.6 m thick deposition of post-landslide sedimentary drape on the eroded slope reveals mean sedimentation rates over the last 2220 yr in the order of ~0.75 mm/a. At the Weggis site, a gray, 2 cm-thick, homogenous silty clay layer overlying the failure surface can be related to the Weggis Slide (Fig. 2.8C). Additionally, reworked glacial mud clasts recovered at the base of post-landslide deposits at the Chrüztrichter and St. Niklausen sites (Fig. 2.8D) clearly pinpoint the failure surfaces to be related to the glacio-lacustrine Unit 3. However, as observed in the seismic data, there are no evidences for significant erosion of Unit 3 during translational sliding (Figs. 2.3 and 2.4). Therefore, combined geophysical subsurface and core data suggests the failure to be located immediately at the top of the glacial Unit 3.

2.5 Discussion

Results from our study consistently imply that, regardless of regional variations between the sub-basins, initiation and evolution of earthquake-triggered lateral subaqueous slope failures occurred along glide planes that developed at the lithological boundary between overconsolidated, overpressured glacio-lacustrine deposits (Unit 3) and weak, slightly underconsolidated laminated Late Glacial clays (Unit 2). Similarly, it has been reported from other studies in peri-alpine, fjord-type lakes and fjords that slides also mobilized the slope-covering drape down to glacial deposits comparable to those described here (e.g. Horgen Slide and Oberrieden Slide in Lake Zurich, Switzerland (Kelts 1978; Strasser and Anselmetti, 2008); Pointe-Du-Fort Slide in Saguenay Fjord, Canada (Locat et al., 2003); submarine slides in Karmsundet and Skudenesfjorden, Norway (Boe et al., 2000)). It is thus interpreted that the glacial-to-postglacial evolution in sedimentation processes along the lateral slopes in similar settings as Lake Lucerne results in characteristic physical and geotechnical properties that eventually control the stability conditions and that in turn favor subaqueous slope failure initiation at systematic stratigraphic levels.
In the following section, a conceptual slope-sedimentation model since the last glaciation is presented (Fig. 2.9), and its control on the evolution of the physical properties is discussed. In the subsequent section, the measured geotechnical parameters are implemented into limit equilibrium models in order to quantitatively assess the slope stability condition of the submerged slopes at the time of failure.

2.5.1 Sedimentation model and its influence on the geotechnical properties

2.5.1.1 Glacial

The sedimentary facies of the tilted and deformed laminated clayey silts with sparse sand and glacially striated, allochtonous gravels (Unit 3) clearly point towards deposition in a glacio-lacustrine environment and subsequent glacial deformation by ice-grounding and/or ploughing. The fact that the material experienced higher pre-consolidation pressure than the effective overburden stress today (OCR > 1) can in this context be interpreted to result from glacial compaction under the additional weight of ice mass acting on the material. Additionally, long-term postglacial secondary compression within the compressible glacio-lacustrine clays and silts (Terzaghi, 1996) may also partly explain the observed formation-wide overconsolidation. Other processes that would lead to overconsolidation, such as erosion of previously overlying material or diagenetic cementation, are ruled out, because evidence favoring these processes was neither observed in the seismic data nor in cored material. Glacial compaction and secondary compression also results in reduction of permeability. Therefore, the observed pore fluid overpressures in Unit 3 are interpreted to be a result of the limited drainage capacity in these relative low permeable deposits. The process of overpressuring, however, remains unknown. One possibility is that elevated pore pressures were initially induced during partially undrained glacial-compaction and sustained thereafter, although one would rather expect the formation pore pressure to stabilize over such a long time period. Alternatively, and more likely, there could be an influence from a recent local groundwater flow sustaining a positive lateral flux that results in higher pore pressures than expected under hydrostatic conditions.
Because the observed glacial overconsolidation of the deposits is relatively low (OCR = 1.58), we exclude that glacial compaction took place during times when the glacier fully occupied the deep basins and the study sites were covered by ~800 meters of ice (Florineth and Schlüchter, 1998). Therefore, the glacio-lacustrine deposits have to be younger then the Last Glacial Maximum (~24–19 ka B.P; Ivy-Ochs et al., 2004). Generally, deglaciation of glacially over-deepened basins such as Lake Lucerne occurred by stagnation-zone retreat rather than by the retreat of an active glacier front (Lister et al, 1984). Deposition of glacio-lacustrine sediments first takes place in the deep basin of a sub-glacial lake that formed once the buoyancy of the ice body exceeds its weight and the glacier floats up. Further ablation, water-contact melting, and calving lead to rapid disintegration of remaining glacial ice back to shallower up-valley parts (e.g. Haeberli and Schlüchter, 1987). Most of the sediment is deposited in the topographic depressions but a thin veneer of fine grained glacio-lacustrine sediments is also deposited along the lateral slopes settling out of meltwater plumes containing suspended glacial mud (e.g. Mackiewicz et al., 1984; Blass et al., 2003; Anselmetti et al., 2007; Fig. 2.9C). Sand and gravel

clasts occasionally are deposited as ice-rafted debris. In this highly dynamic periglacial setting, relatively short-lived periods of colder climate conditions result in minor glacial readvances with higher intensities of ice-calving, during which ploughing and grounding of icebergs along the lateral slopes result in deformation and compaction of the glacio-lacustrine sediment (Fig. 2.9D).

2.5.1.2 Post Glacial

After the final glacier retreat (~17500 cal yr. B.P.; Lister 1988; Wessels 1998), most of postglacial sedimentation occurs on deltas and is focused in the topographic depressions of the deep basins through underflow processes. However, suspension settling from meltwater plumes that uniformly distribute the fine fraction of the suspended glacial mud over the lake basin also drapes the submerged lateral slopes. Cyclic (e.g. seasonal) fluctuations in meltwater discharge result in thinly-laminated and fine-grained draping slope deposits as recovered in the lower part of Unit 2 (Fig. 2.8A), which potentially could represent proglacial clastic varves (Mackiewicz et al., 1984; Blass et al., 2003, Anselmetti et al., 2007). With further glacial retreat into the alpine valley during Late Glacial times, the influence of glacial meltwater plumes on the lacustrine sedimentation is continuously diminished and suspended material entering the lake as under-, inter- and overflows after high precipitation and flood events continuously dilutes the rhythmically laminated Late Glacial clays. With climate amelioration at the Late Glacial to Holocene transition around 11500 cal yr B.P., sedimentation along the slope is increasingly influenced by both authigenic carbonate and biogenic production as well as

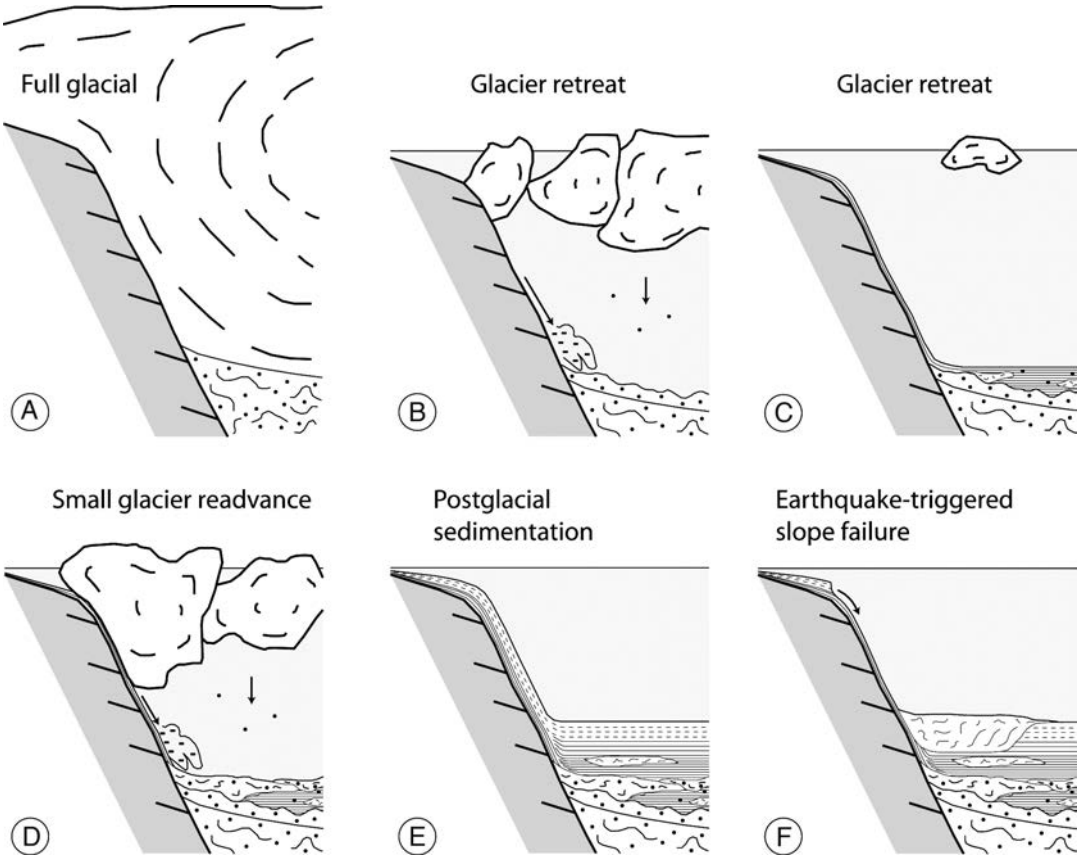

Figure 2.9: Conceptual glacial-to-postglacial sedimentation model along lateral non-deltaic slopes in perialpine fjord-type lakes. Schemes (not to scale) are perpendicular to the basin axis and show schematically the depositional and post-depositional processes acting on the submerged slope: (A) Last Glacial Maximum: the basin is fully occupied by the glacier. Glacial bedrock erosion rather then sedimentation occurs along the slopes; (B) Glacial decay results in the formation of a subglacial lake (see subsection 2.5.1.1). Glacio-lacustrine deposition occurs focused in the deep basin; along the lateral slope, little sedimentation, erosion, creeping and slumping occurs. (C) Further rapid desintegration of remaining glacial ice back to shallower up-valley parts results in a periglacial setting where a fine veneer of fine-grained sediments also is deposited along the lateral slopes settling out from meltwater plumes. (D) Relatively short-lived periods of colder climate conditions result in minor glacial readvances, during which ploughing and grounding of icebergs along the slope leads to deformation and compaction of the glacio-lacustrine sediment. (E) After the final glacier retreat suspension settling from meltwater plumes and settling from flood-induced over- and interflows mixed with authigenic carbonate production occurs during the Late Glacial and Holocene, respectively. Continuous sedimentation «charges» the slopes until external trigger mechanism triggers slope failures. (F) Post-failure situation.

detrital input from small local rivers during high discharge events (Sturm and Matter, 1978). This observed change in the sedimentation processes along the lateral slopes reflects the general Late Glacial to Holocene shift in the sedimentary system also recorded in many other perialpine lakes (e.g. Van Rensbergen et al, 1999; Eyles et al., 2000; Beck et al., 2001) and fjords (e.g. Evans et al., 2002; Lysa et al., 2004). It further explains the increased sedimentation rates along the lateral slopes during the Holocene compared to Late Glacial times, as estimated from the core data (see subsection 2.4.2).

The distinct differences in Late Glacial and Holocene sedimentation mechanisms also influence the strength characteristics of the slope covering material. In the Holocene Unit 1 gradients of undrained shear strength with depth (∇c_u) are constant in the order of ~1.8 kPa/m (Weggis ~1.75 kPa/m, St. Niklausen ~2.0 kPa/m, Chrüztrichter 1.75 kPa/m). Similar Holocene - ∇c_u values also have been reported from in situ testing results in other Swiss lakes (Gyger et al., 1976). Sediment strength thus correlates with effective stress (ratio c_u/σ'_v ~0.2–0.4) and the characteristic profiles suggest a continuous self weight consolidation associated with a relatively continuous sedimentation rate. In contrast, cu values in the Late Glacial clays (Unit 2) are constant in the upper part and even reveal negative cu-gradients at their base, where the lamination of proglacial cyclic plume deposits is well pronounced. This observation suggests a connection between the laminated clays and their unfavorable stability conditions. Indeed, geotechnical investigations of similar Late Glacial varve-deposits in Switzerland and Canada show significant influences of the clay lamination and microstructure on strength characteristics and mechanical behavior (e.g. Quigley and Ogunbadejo, 1972; Plötze et al 2003). Additionally, the postglacial deposits are characterized by slight formation overpressures, which is interpreted to be related to the relatively high sedimentation rates (20–40 cm/ka) and incomplete drainage of the low-permeable sediments. As a consequence, the normal consolidation phenomenon is retarded and the sediment is in an underconsolidated state (Sultan et al, 2004), as measured by consolidation tests (OCR = 0.86).

In summary, the depositional and consolidation mechanism of sediments covering the submerged lateral slope of Lake Lucerne created particular sedimentological and geotechnical slope characteristics that control the stability condition and that predefine the eventual failure location. With an external trigger mechanism (i.e. strong seismic shaking) these lithologically inherited conditions result in subaqueous slope failure initiation along the boundary between overconsolidated glacio-lacustrine deposits with overpressured formation pore pressures (Unit 3) and slightly underconsolidated laminated Late Glacial clays (Unit 2) characterized by low shear strength values at their base. Based on the principle of effective stress, Stegmann et al. (2007) show in detail that, as a result of co-seismic stress fluctuations and stress-transfer upward to the base of the weaker unit, pore pressure exceeds lithostatic load and initiates sliding along a failure plane developing at the boundary between Unit 2 and 3.

2.5.2 Limit Equilibrium slope stability analysis

In order to reconstruct slope failure conditions at the study sites and to quantify seismic ground accelerations affecting the slopes at the time of failure, the obtained data were implemented into a limit equilibrium slope stability model that serves to back-analyze the slope failures triggered by the historic 1601 A.D. and the prehistoric 2220 cal yr. B.P earthquakes. At both Weggis and St.Niklausen sites, the pre-failure slope geometry was reconstructed as a 3-layer model (Units 1–3) assuming constant sediment thicknesses as recovered in the reference cores immediately upslope of the failure scars and subtracting the uppermost post-landslide deposits as recovered in short cores along the eroded slopes. This assumption is justified by seismic data that show constant sediment thicknesses in undisturbed sections draping the slope adjacent to the slide. The lower model boundary was chosen to be 1 m below the boundary between Units 2 and 3, modeling the thickness of the overconsolidated glacial Unit 3 as indicated in the seismic data (see subsection 2.4.1). Mean ρ_{bulk}, c_u at the layer top and ∇c_u were assigned to each layer according to results from core analysis and in situ testing (Table 2.1). Based on the observation in the geophysical subsurface data and on the results from in situ and cores analysis, the glide plane along which translational sliding occurred, is interpreted to correspond to the lithological boundary between Unit 2 and Unit 3 (see subsection 2.4.6 and 2.5.1). Therefore, a failure plane at the boundary between these to units was predefined in the slope stability analysis.

For all analysis it was assumed that the sediment is subjected to undrained loading conditions because cyclic loading during earthquake shaking is rapid enough that excess pore pressure does not have time to dissipate through the fine grained medium. The slightly higher sand content in Unit 3 potentially could indicate that loading conditions in the lowermost unit might not fully be undrained. Also, liquefaction induced by pore pressure increase during seismic shaking cannot completely be excluded as potential failure initiation mechanism. However, given the relatively low permeability and predominant fine-grained character of the glacial deposits, undrained loading is interpreted to be the predominant mechanism at the critical depth where failure occurs. Liquefaction as potential failure initiation processes is interpreted to by unlikely because estimations of the susceptibility for liquefaction based on a rough criterion proposed by Andrews and Martin (2000) reveal no critical conditions (i.e. measured clay contents and liquid limits at critical depth in all cores are much higher than critical values of 10% and 32%, respectively). Additional uncertainties in our slope stability analysis arise from the fact that the used pseudostatic modeling approach does not consider the dynamic behavior of the sediment and therefore does not account for potential failure mechanism in addition to the load generated by horizontal seismic acceleration (e.g. degradation of soft clays, accumulation of plastic strains and shear-induced excess pore water pressure with increasing number of cycles (Sultan et al, 2004; Biscontin et al., 2004)). Future investigations on the

Table 2.1: Geotechnical parameters used for deterministic limit equilibrium back-anaylsis.

	layer thickness d [m]	*Unit weight γ* [kN m^{-3}]	*undrained shear strength at the top of layer* c_u [kPa]	*undrained shear strength gradient with depth* ∇c_u [kPa m^{-1}]
Weggis Site at 1601 A.D.				
layer 1 (Holocene)	*2.5*	*13.25*	*1*	*1.75*
layer 2 (Late Glacial)	*1.25*	*14.72*	*5.4*	*0*
layer 3 (Glacial)	*1*	*17.7*	*varying values*	*5*
St.Niklausen Site at 2220 cal. yr B.P.				
layer 1 (Holocene)	*2.7*	*12.8*	*1*	*2*
layer 2 (Late Glacial)	*1.6*	*14.72*	*7.1*	*0*
layer 3 (Glacial)	*1*	*17.7*	*varying values*	*5*

dynamic behavior of the material under cyclic loading as well as detailed clay mineralogy analysis are required in order to better constrain these uncertainties. Therefore, our pseudostatic limit equilibrium model used here only represents a first order estimation of quantifying seismic ground accelerations that affected the Lake Lucerne slopes during past earthquakes.

Sensitivity analysis of the model used in this study revealed that the impact of c_u at the depth of failure and the horizontal acceleration a_H is several-fold higher in comparison with the other parameters for the chosen slope geometry and failure plane location. Absolute cu values slightly vary with respect to the three different measurement methods and therefore add uncertainties in the back-calculated critical pseudostatic seismic ground acceleration. The back-analysis was therefore carried out with varying values of c_u at the top of Unit 3 and results are presented as contour plots showing the factor of safety (FS) as a function of both c_u at the depth of failure and a_H (Fig. 2.10).

For the Weggis site, measured c_u values at the top of Unit 3 vary between 3 and 6 kPa as measured with the different independent methods, whereas they are slightly higher at the St. Niklausen site. Results of deterministic stability analysis using these c_u ranges reveal that both slopes are stable under static loading condition (i.e. $a_H = 0$) with FS ranging between 1.1 to 1.7 and 1.3 to > 2, respectively. As discussed above, the lower values estimated from in situ vane shear tests most probably underestimate the actual strength conditions, so that realistic $c_{u\ in\ situ}$ should be ~5 kPa at the Weggis and ~6 kPa at St. Niklausen site, as inferred from in situ CPT tests. Using these values for the model input reveal static FS between ~ 1.5 and 2 at Weggis and St. Niklausen, respectively. To trigger slope failure at the Weggis site, an additional pseudostatic seismic acceleration between 0.01 and 0.06 g (~0.04 g, if applying the estimated probable $c_{u\ in\ situ}$ value of ~5 kPa) is required, whereas the slope at St. Niklausen remains stable up to critical a_H values between 0.03 and 0.08 g (~0.07 g, if applying the estimated probable $c_{u\ in\ situ}$ value of ~6 kPa) (Fig 2.10).

Leynaud et al. (2004) suggested that the pseudostatic horizontal seismic acceleration only represents about 50% of the effective earthquake peak ground acceleration (PGA). Results from slope stability back-calculations thus imply minimal PGA's of about 0.08 g (range of uncertainty ~0.02–0.12 g) and ~0.14 g (range of uncertainty ~0.06–0.16 g) during the 1601 A.D. and the 2220 cal yr B.P. earthquake, respectively. The result for the 1601 A.D. event from the Weggis site lies in the range of calculated values for PGA's deduced from predictive ground motion models for Central Switzerland (Bay et al., 2005), assuming a M_W 6.2 earthquake and an epicentral distance of 12 km (Fig. 2.1). The estimated PGA value for the prehistoric 2220 cal yr B.P earthquake in the order of 0.14 g, however, is slightly higher than the expected ground motion induced by low frequency (1Hz) seismic waves with a return period of 2500 year as estimated by probabilistic earthquake hazard assessment for the Lake Lucerne area (Giardini et al., 2004).

Although one would need to consider site effects that might amplify or attenuate seismic shaking and the fact that the accuracy of the used pseudostatic approach is governed by the simplification, with which the pseudostatic inertial forces represent the complex dynamic inertial forces during earthquake shaking (Kramer, 1996), the results from slope stability back-analysis suggest that during the prehistoric 2220 cal yr B.P earthquake that triggered the St.Niklausen Slide the Lake Lucerne area experienced significantly higher ground motions than during the historic 1601 A.D. M_W ~6.2 earthquake. This interpretation is supported by the fact that the 2220 cal yr BP earthquake also triggered subaqueous landslides in Lake Zurich at a distance of 40 km from Lake Lucerne, requiring a significantly larger magnitude (M_W > 6.5) than the historic 1601 A.D. earthquake (Strasser et al., 2006). However, the interpretation of higher ground motions during the 2220 cal yr B.P. event seems to contradict the observation that the Weggis and Chrüztrichter slopes remained stable during this stronger prehistoric event.

In order to investigate this apparent contradiction, the Weggis and Chrütztrichter slope stability conditions at

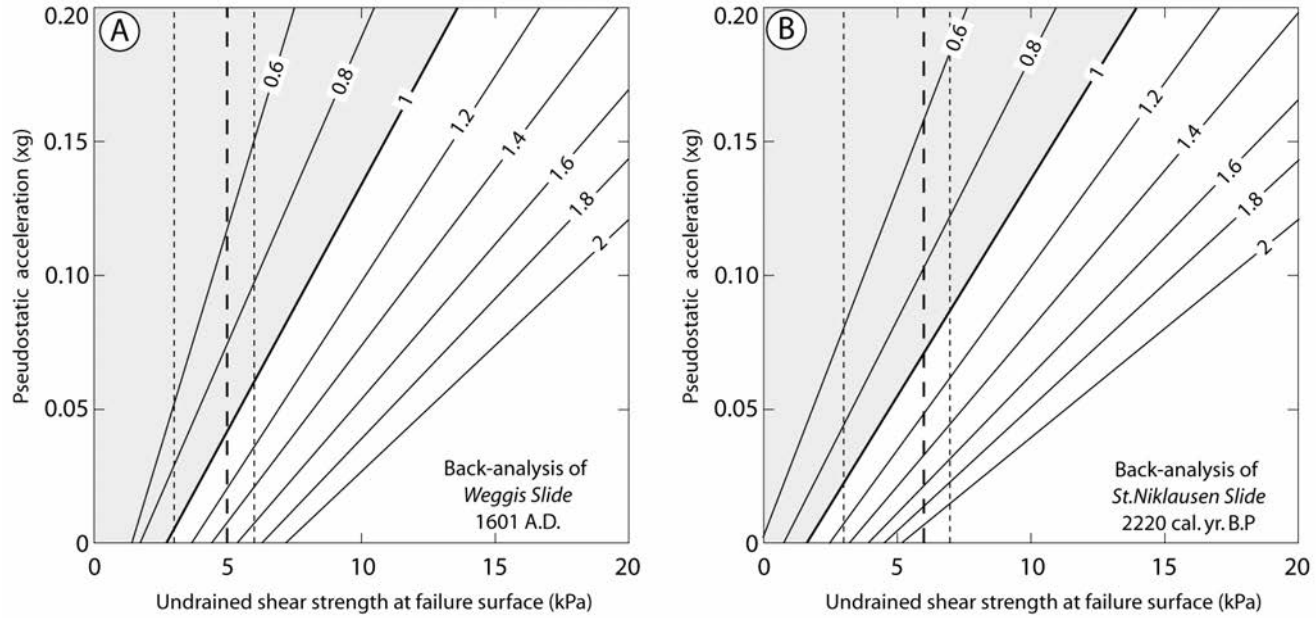

Figure 2.10: Results of deterministic limit equilibrium slope stability back-analysis of Weggis (A) and St. Niklausen (B) Slides during the 1601 A.D. M_w ~6.2 earthquake and the 2220 cal. yr B.P. earthquake (M_w > 6.5), respectively. Contour plots show factor of safety (FS) as a function of the undrained shear strength at the failure surface and the pseudostatic acceleration (fraction of gravitational acceleration g). The gray shaded areas indicate solutions leading to instable conditions (FS < 1). The range and reliable in situ values of measured undrained shear strength at the two study sites is shown as a fine dotted and bold dashed line, respectively. See Table 2.1 for model input data.

2220 cal yr B.P. were analyzed with a probabilistic limit equilibrium approach using the calculated critical horizontal seismic accelerations by the back-analysis described above (Table 2.2 summarizes the input parameters used). Both scenarios reveal mean FS values > 1 (1.03 and 1.14) and failure probability of < 50% (45.6 % and 43.7 %) for both the Weggis and Chrüztrichter slopes, respectively. Both slopes were relatively close to failure, but obviously remained stable during the 2220 cal yr. B.P. event. These results indicate that the «charging» state of a submerged slope is a function of the sedimentation rate during the Holocene (i.e. the only parameter changing significantly from site to site), that controls the static weight of the slope-covering drape. Similar conclusions were drawn based on a significant increase in the frequency of lateral mass-movement deposits identified during Holocene times in other lakes (e.g. Waldmann et al., 2008).

Table 2.2: Geotechnical material statistics used for probabilistic limit equilibrium slope stability analyses.

	d [m]	*γ [kN m^{-3}]*				*c_u[kPa]*				*∇c_u[kPa m^{-1}]*			
		mean	*std.dev*	*rel.min*	*rel. max*	*mean*	*std.dev*	*rel.min*	*rel. max*	*mean*	*std.dev*	*rel.min*	*rel. max*
Weggis Site at 2220 cal. yr B.P.													
Layer 1	*1.5*	*13.25*	*0.3*	*0.5*	*0.5*	*1*	*0.5*	*0.5*	*0.5*	*1.75*	*0.5*	*0.75*	*0.5*
Layer 2	*1.25*	*14.72*	*0.5*	*0.5*	*0.5*	*5.4*	*3*	*3*	*3*	*0*	*-*	*-*	*-*
Layer 3	*1*	*17.7*	*1*	*1*	*3*	*5.4*	*2.5*	*2.4*	*2*	*5*	*2*	*3*	*5*
Chrüztrichter Site at 2220 cal. yr B.P.													
Layer 1	*3.4*	*13.25*	*0.3*	*0.5*	*0.2*	*1*	*0.5*	*0.5*	*0.5*	*1.75*	*0.5*	*0.75*	*0.5*
Layer 2	*1.2*	*14.72*	*0.5*	*0.5*	*0.5*	*7.5*	*3*	*5*	*0.5*	*-2*	*0*	*1*	*2*
Layer 3	*1*	*20.6*	*1*	*3*	*1.5*	*8.5*	*2.5*	*4.5*	*2*	*5*	*2*	*3*	*3*

Pseudostatic acceleration k_h during 2220 cal yr B.P earthquake [x g]	*mean*	*std.dev*	*rel.min*	*rel. max*
	0.07	*0.03*	*0.012*	*0.023*

These observations further imply that ongoing sedimentation along the submerged slopes will continuously load the slopes so that the susceptibility for slope failure will increase in the future. As an end member scenario we investigated how long it would take to charge the Weggis slope (assuming constant sedimentation rates), so that the sediments acting on the critical surface would become unstable under static loading conditions. Solving the infinite slope equation (MORGENSTERN, 1967) for critical sediment thickness to initiate failure reveals as a first order assumption that the slopes only will become statically unstable in ~24500 years (input parameters: mean values for c_u, γ' and α as observed in the data described above). This is one order of magnitude longer than the time that separated the last two major earthquakes around Lake Lucerne implying that the occurrence of seismic events acts as main control on landslide triggering. Local differences in site-specific stability conditions, however, are governed by regional variations in sediment supply so that slope stability conditions may change locally over relative short geological time scales.

2.6 Summary and conclusions

This study presents the results from three comprehensive case studies of seismically-triggered, lateral non-deltaic subaqueous slope failures in perialpine, fjord-type Lake Lucerne (Central Switzerland). The combined sedimentological, geophysical and in situ geotechnical approach provides a better understanding of the influence of the glacial-to-postglacial evolution in sedimentation processes along the investigated lateral slopes and their impact on the characteristic physical and geotechnical properties of the slope-covering sediments that control the stability condition and subaqueous slope failure initiation. On a larger scale, comparable slope stability conditions may evolve in fjords and high-latitude ocean margins, where glacially overconsolidated deposits are overlain by postglacial (glacio-) marine sediments accumulated during deglaciation periods and by pelagic and hemi-pelagic sediments deposited during interglacials (e.g. BOE et al, 2000; 2004, LOCAT et al., 2003). Our comprehensive lake study and resulting conceptual ideas thus also improve our understanding of larger slope instabilities occurring along formerly glaciated ocean margins.
A summary list of the main conclusions includes the following:

(1) Sedimentation dominated by suspension settling from meltwater plumes, slight overconsolidation by ice-grounding and postglacial draping lead to particular slope conditions characterized by: (i) fine-grained, thinly-laminated, slightly underconsolidated Late Glacial cyclic plume deposits with low undrained shear strength values overlying (ii) overconsolidated, glacially deformed glacial deposits with overpressured formation pore pressure. This particular succession is overlain by a Holocene drape with variable thickness that acts as a surcharge on the lower sediment layers.

(2) During past earthquake shaking, slopes that were stable under static loading conditions (FS of 1.5–2) failed along glide planes that developed at this lithological boundary.

(3) This glide plane location is a consequence of the comparably low strength conditions within the overlying thinly-laminated Late Glacial clays and the additional excess in situ pore pressure in the underlying overconsolidated, low permeable material reducing effective strength at and below the zone of failure.

(4) Limit equilibrium back-analysis reveal seismic peak ground accelerations (PGA) at the study sites of ~0.08 g (range of uncertainty ~0.02–0.12 g) and ~0.14 g (range of uncertainty ~0.06–0.16 g) for the historical 1601 A.D. M_w ~6.2 earthquake and a prehistoric, 2220 cal yr. B.P., $M_w > 6.5$ northern alpine earthquake, respectively.

(5) The results thus pinpoint the potential of detailed subaqueous slope stability analysis as paleoseismological tool that allow for quantitative reconstruction of past earthquake shaking.

(6) Holocene sedimentation rates are a key parameter in «charging» subaqueous slopes susceptible for sliding. Stability conditions thus may change over relative short geological time scales.

(7) Lessons learned from the high-resolution case studies presented here should be implemented in future studies on a basinwide scale. In combination with more detailed analysis on the dynamic behavior of the material under cyclic loading these results eventually will yield strong arguments in identifying sites of potential slope instability in the future.

3 MASS-MOVEMENT EVENT STRATIGRAPHY IN LAKE ZURICH: A RECORD OF VARYING SEISMIC AND ENVIRONMENTAL IMPACTS

Peer-reviewed article co-authored by F.S. ANSELMETTI.

Abstract

Combining basin-wide high-resolution seismic imaging with coring in perialpine Lake Zurich (Switzerland) reveals a chronological catalogue of Late Glacial-to-Holocene mass-movement units, documenting a complex history of varying tectonic and environmental impacts affecting the lake and its surrounding. A total of 149 mass-movement deposits have been identified and mapped with a dense grid of seismic profiles ~300 km in length. They are allocated to 21 seismic stratigraphic event horizons, each of which comprising 1–23 individual mass-movement deposits. An age model based on information from previous studies, 6 new long piston cores and 15 new AMS-^{14}C ages allowed establishing a well-constrained chronological mass-movement event catalogue covering the last ~17000 years. Results include the documentation of 3 major (2210, 11600, 13760 cal yr. B.P.) and 2 minor (640 and 7270 cal yr. B.P), simultaneously-triggered basin-wide lateral slope failure events interpreted as the fingerprint of paleo-seismic activity in the Zurich area. Furthermore, two major slide events were discovered, which occurred during the transition from the Pleniglacial to the Late Glacial time period and thus are likely related to the activity of the nearby Linth glacier. Additionally, our record reveals higher frequency of Holocene mass movements in deltaic settings during specific periods that may be related to climate-controlled increase of sediment supply, supposing climatic causing factors for subaqueous delta slope failures. These findings thus point at a variety of potentially hazardous processes, such as earthquakes, lake outbursts and floods, that affected the Zurich area over the last ~17000 years.

Zusammenfassung

Hochauflösende reflexionsseismische Profile, welche den Untergrund des schweizerischen Zürichsees beckenweit abbilden, und Sedimentproben an gezielt ausgewählten Kernlokalitäten erlauben es, Spätglaziale und Holozäne Ablagerungen subaquatischer Massenbewegungen im See räumlich und zeitlich auszukartieren. Der somit erfasste Ereigniskatalog lässt auf eine Vielzahl unterschiedlicher geologischen, tektonischen und klimatologischen Einflüsse schliessen, welche in der Vergangenheit auf den See und auf dessen Umgebung eingewirkt haben müssen.

In den ~300 km umfassenden seismischen Profilen, welche in einem engmaschigen Gitter über den See verteilt aufgenommen wurden, lassen sich total 149 einzelne Massenbewegungsablagerungen kartieren. Diese finden wir in 21 stratigraphischen Niveaus (i.e. seismostratigraphische Ereignishorizonte), welche jeweils 1–23 individuelle Ablagerungen umfassen. Mit Hilfe von Informationen aus früheren Studien und 6 neu abgeteuften Kolbenlotkernen, an welchen insgesamt 15 neue Radiokarbondatierungen (^{14}C) durchgeführt wurden, lässt sich ein hochauflösendes Altersmodel der Sedimentationsgeschichte im See erstellen. Daraus ergibt sich die Chronologie der Massbewegungsereignisse im Zürichsee über die letzten ~17000 Jahre. Die Studie dokumentiert 3 grosse (2210, 11600, 13760 Jahre vor heute) und 2 kleinere (640 und 7270 Jahre vor heute) Ereignisse, welche durch gleichzeitig ausgelöste, beckenweite Rutschungen entlang der seitlichen Unterwasserabhängen charakterisiert sind, und welche als Zeugen vergangner Erdbebenaktivität im Raum Zürichsee interpretiert werden. Im Weiteren wurden zwei grossräumige Versackungens- und Massenbewegungsereignisse während des endeiszeitlichen Gletscherrückzugs entdeckt, welche wohl im Zusammenhang mit der Aktivität des damals nahegelegenen Linth Gletschers stehen dürften. Entlang von Deltaabhängen konnten nacheiszeitliche Hanginstabilitäten während bestimmten Zeitintervallen nachgewiesen werden, welche möglicherweise mit Klimaphasen zusammen fallen, die zu einem erhöhtem Sedimenteintrag in den See führten. Dies lässt einen klimatischen Kontrollfaktor für die Stabilität von subaquatischen Deltaabhängen vermuten.

Die Resultate der Studie dokumentieren somit das Auftreten verschiedener geologischer Ereignisse, wie Erdbeben, Seeausbrüche oder Hochwasser, welche sich im Verlaufe der letzten rund 17000 Jahren in der Zürichsee Region ereignet haben und welche, aus heutiger Sicht betrachtet, mögliche Naturgefahren darstellen könnten.

3.1 Introduction

Subaqueous mass movements such as slides, slumps, mass flows and turbidity currents are important players for sediment transport and redeposition mechanism in both marine and lacustrine environments. They also pose societal and environmental risks to offshore infrastructures (e.g. pipelines, cables and platforms) as well as to coastal areas (e.g. due to shore collapses and landslide-induced tsunamis) (Camerlinghi et al, 2007). Mass flows and turbidity currents often evolve from mass-failure processes along the submerged sediment-covered slopes (e.g. translational or rotational slides) that may originate from various processes including rapid sedimentation, gas release or migration, earthquake shaking, glacial and tidal loading and wave action (Hampton et al, 1996; Mulder & Cochonat, 1996; Locat & Lee, 2002). Some of these geological processes act on the submerged slopes over longer periods whereas others are of instantaneous nature (e.g. earthquakes). Studying the geological record of subaquatic mass-movement deposits, determining and characterizing their type, distribution and frequency as well as deciphering their causes and effects, thus may reveal important information to evaluate the geo-hazard potential arising from such processes.

Lakes provide ideal sedimentary archives to track such processes, as lacustrine deposits usually are spatially and temporally continuous (e.g. Sturm & Lotter, 1995). This allows investigation on a basin-wide scale and offers a well-constrained age control. Characteristic mass-movement event beds in lake sediments have been allocated to historically described catastrophic events, including earthquakes (e.g. Shilts & Claque, 1992; Chapron et al., 1999; Schnellmann et al, 2002; 2006), human-induced shore collapses (e.g. Kelts & Hsü, 1980; Hsü & Kelts, 1985; Longva et al., 2003) and delta failures (e.g. Siegenthaler & Sturm, 1991). Based on the fingerprints of such historic events in «recent» sediments, similar prehistoric events can be recognized in the sedimentary archive (e.g. Schnellmann et al., 2002; 2006; Sletten et al., 2003; Strasser et al., 2006) and allow for evaluating recurrence times of related geological impacts that often exceed the time span covered by historical archives.

However, the here studied perialpine Lake Zurich (Switzerland) was so far not specifically investigated for studying prehistoric subaqueous mass movements and for exploring their related geological processes. In this study, the presented combined basin-wide high-resolution reflection seismic and coring approach aims (i) to identify and date Late Glacial-to-Holocene mass-movements deposits, (ii) to characterize their types and distribution, (iii) to determine the associated depositional, transport and slope-failure trigger mechanism(s), and (iv) to establish a chronological catalogue of past mass-movement events, which eventually provides the basis to (v) discuss impact and frequency of various potentially-hazardous natural processes that affected the Lake Zurich area over the last ~17000 years.

3.2 Geological setting and previous studies

Lake Zurich occupies a perialpine, glacigenic overdeepened, NW-SE trending trough situated in the northern part of the Swiss Plateau (Fig. 3.1). It can be divided into two basins that are carved into mainly flat-lying sandstones, siltstones and marls of the Tertiary «Obere Süsswasser Molasse» (OSM) formation. The general morphology consists of (i) a northwestern, elongated deep basin (max water depth 135 m) with steep lateral slopes and a flat basin plain, and (ii) a flat and shallow (~20 m water depth), sediment-filled upper basin, which is divided from the lower basin by a sediment-covered subaqueous rock barrier showing a complex, step-like morphology descending towards NW (Hsü and Kelts, 1970; Schindler, 1976) (hereafter termed «escarpment structure»). A mostly sub-aerial sill formed by the Hurden Moraine between Rapperswil and Pfäffikon with only 2 m deep lake passages separates Lake Zurich in the northwest from Obersee in the east. Note that Obersee often also is referred to be a part of Lake Zurich. In this study, however, «Lake Zurich» only comprises the lower deep and the upper flat and shallow basins, whereas Obersee is treated as separate lake.

The main rivers (Linth, Jona, and Wägitaler Aa), contributing about 90 % of Lake Zurich's water supply, discharge into Obersee, which acts as the dominant sink for the clastic sediment supply from the mainly alpine catchment. During the Late Glacial period, the Sihl river temporarily discharged into the lower Lake Zurich basin depositing a large, nowadays inactive delta (Huber, 1938; Schindler, 1968), which, together with the moraine from the Zurich Stadium, boarders the lake on its northwestern margin (Fig. 3.1). Since Early Holocene times, the here studied Lake Zurich lacks major active deltas and, as a consequence, shows relatively low sedimentation rates. However, local creeks laterally entering the lake contribute to Lake Zurich's clastic sediment supply and form small local deltas along the shorelines (e.g. deltas of Küsnacht, Erlenbach, Meilen and Horgen/Käpfnach; Fig 3.1). Lake level during that time generally was stable and only oscillated by max. 2–3 m corresponding to climatic variations, precipitation pattern and Sihl river sediment discharge that may have influenced the Limmat river outflow situation (Schindler, 1971; Magny, 2004; Riesen and Neaf, 2007).

Several previous studies in the 1970's and 1980's described Lake Zurich's geology and its sedimentary and environmental evolution since the Last Glacial Maximum (Hsü and Kelts, 1970; 1984; Schindler, 1974; 1976; Kelts, 1978; Giovanoli, 1979; Pika, 1983; Lister, 1985; 1988; Sidler, 1988). These studies are mainly based on data from the deep northwestern basin comprising some seismic lines and piston cores, and one deep drill hole termed «Zübo» (see Hsü and Kelts, (1984) and references therein). These data reveal that in the lower Lake Zurich basin, the molassic bedrock is covered with an up to 140 m-thick, mainly glacial and glacio-lacustrine infill. The majority of theses sediments were accumulated in a subglacial environment. Only the uppermost ~30 m were deposited after the glacier retreated from the lower Lake Zurich basin (see lithostratigraphic description in subsection 3.4.2.1).

In this upper sedimentary succession, none of the previous studies specifically addressed interpretation and correlation of Late Glacial-to-Holocene mass-movement deposits throughout the lake. Only a series of subaqueous slumps on the shore near Horgen that occurred in 1875 A.D. was extensively studied and described by Heim (1976), Kelts (1978), Kelts & Hsü (1980) and Siegenthaler et al. (1984). Additionally, shore collapses near Rüschlikon in 1898, 1900 and 1907, near Oberrieden in 1918 and near Küsnacht in 1943 and 1955 were mentioned in the literature (e.g. Nipkow, 1920; Kuen, 1999). All these slopes instabilities resulted directly from human-induced loading of sand and gravel landfill on a weak foundation of lacustrine chalk. These shore collapses and slumps resulted in mud-flow and mud-flow-evolved turbidite deposits that can be traced in the sedimentary record throughout the lower Lake Zurich basin (Kelts, 1978; Pika, 1984).

3.3 Methods

With the objective to identify, characterize, map and date Late Glacial-to-Holocene mass-movement deposits, the existing sedimentary model of the postglacial infill of Lake Zurich was refined by acquiring new high-resolution seismic reflection data and 6 new long sediment piston cores (Fig 3.2). Additionally, a sidescan-sonar survey covering a limited area offshore Oberrieden aimed to characterize the lake floor surface expression and spatial geometry of a prominent sub-recent mass-movement deposit.

3.3.1 Reflection seismic subsurface imaging and seismic stratigraphic mapping

A dense grid of ~300 km of single channel 3.5 kHz seismic profiles (acoustic pinger source) was acquired to image the subsurface in quasi 3-D. The source/receiver was mounted on a cataraft that was pushed in front of a small vessel. DGPS-positioning with a maximum error of ±2 m guaranteed accurate navigation. The digitally-recorded data were processed using a flat gain and a band-pass filter. Two-way travel time was converted to water depth and sediment thickness using a constant velocity of 1450 ms^{-1}.
Landslide deposits in the seismic data were identified based on characteristic chaotic to transparent seismic facies that contrasts with continuous reflections produced by regular, undisturbed sediments (see subsection 3.4.1.2). The top of each mass-movement deposit was defined at its pinch-out point and assigned to a distinct «event horizon» (i.e. seismic stratigraphic horizon related to at least one mass-movement deposit (Schnellmann et al, 2006)). Such horizons represent isochrons that can be traced throughout the entire lake basin, establishing a basin-wide catalogue of mass-movement deposits and allowing recognition of synchronous landslide events.

3.3.2 Sidescan-sonar imaging

Offshore Oberrieden, a limited lake floor area was imaged using a digital dual frequency (100/325 kHz) sidescan-sonar system (C-Max sidescan with a 760 CodaOctopus acquisition system). The fish was deep-towed maintaining a constant fish-to-lake floor offset of ~15 m and a constant boat speed along parallel track lines to obtain a uniform spatial footprint without distortion. The digitally-recorded data of each single track was processed using slant-range and signal-attenuation corrections implemented in the processing software (Octopus 461 Processing Toolkit). For positioning of the lake floor images, the layback of the fish has been calculated by matching the positions of acoustically prominent lake floor features imaged in two parallel lines that advance in opposite directions. Resulting images of single track lines were exported and manually mosaiced using Adobe Photoshop.

3.3.3 Coring and dating

Six Kullenberg-type gravity piston cores (Kelts et al., 1986), each 8–10 m in length, were recovered at key positions to groundtruth the seismic data, for detailed sedimentological analyses and dating. The cores were scanned with a GEOTEK multisensor core logger, which measures gamma ray attenuation bulk density, compressional wave velocity and magnetic susceptibility. Afterwards, cores were split, photographed and sedimentologically described (macroscopically and using smear slide techniques). Accelerator mass spectrometry ^{14}C analysis on terrestrial organic matter (ideally leaf fragments to minimize the risk of dating reworked material) sampled at different stratigraphic levels in four cores were performed at the Particle Physics Laboratory of ETH Zurich to date the sedimentary succession. Radiocarbon ^{14}C-ages were calibrated using the IntCal04 calibration curve (Reimer et al., 2004). In addition, core and age information from previous studies (Kelts, 1978; Giovanoli, 1979; Pika, 1983; Lister 1988; Sidler, 1988) were incorporated using core-to-core and seismic-to-core correlation. Non-calibrated radiocarbon ages given in these previous studies were also calibrated (Reimer et al., 2004), so that all ages in this study refer to the same time scale.
For dating an individual event horizon the lithostratigraphically closest 1–4 ^{14}C-ages were selected (in different cores, if possible). The error introduced by the offset between the lithostratigraphic position of ^{14}C-ages and the event horizon was corrected using the estimated sedimentation rates applied to the sample-horizon offset. Sedimentation rates were estimated for each individual core by linearly interpolating between two ^{14}C samples after correcting for the thickness of instantaneously deposited turbidite layers. For each of the 1–4 selected samples an age range for the event horizon then was calculated. Subsequently, the overlap of the obtained age-ranges and its center was determined. The same procedure was repeated for each of the event horizons. Additionally, counting of sediment laminations in lithostratigraphic Unit 1a and 1b (see subsection 3.4.2.1) that have been interpreted as varve couplets by Giovanoli (1979), Zao (1984), and Niessen et al. (1992), as well as age information based on geomagnetic correlations (Baster, 2002) were used to refine the estimated sedimentation rates and resulting age model for the sedimentary succession prior to ~14000 cal yr B.P..

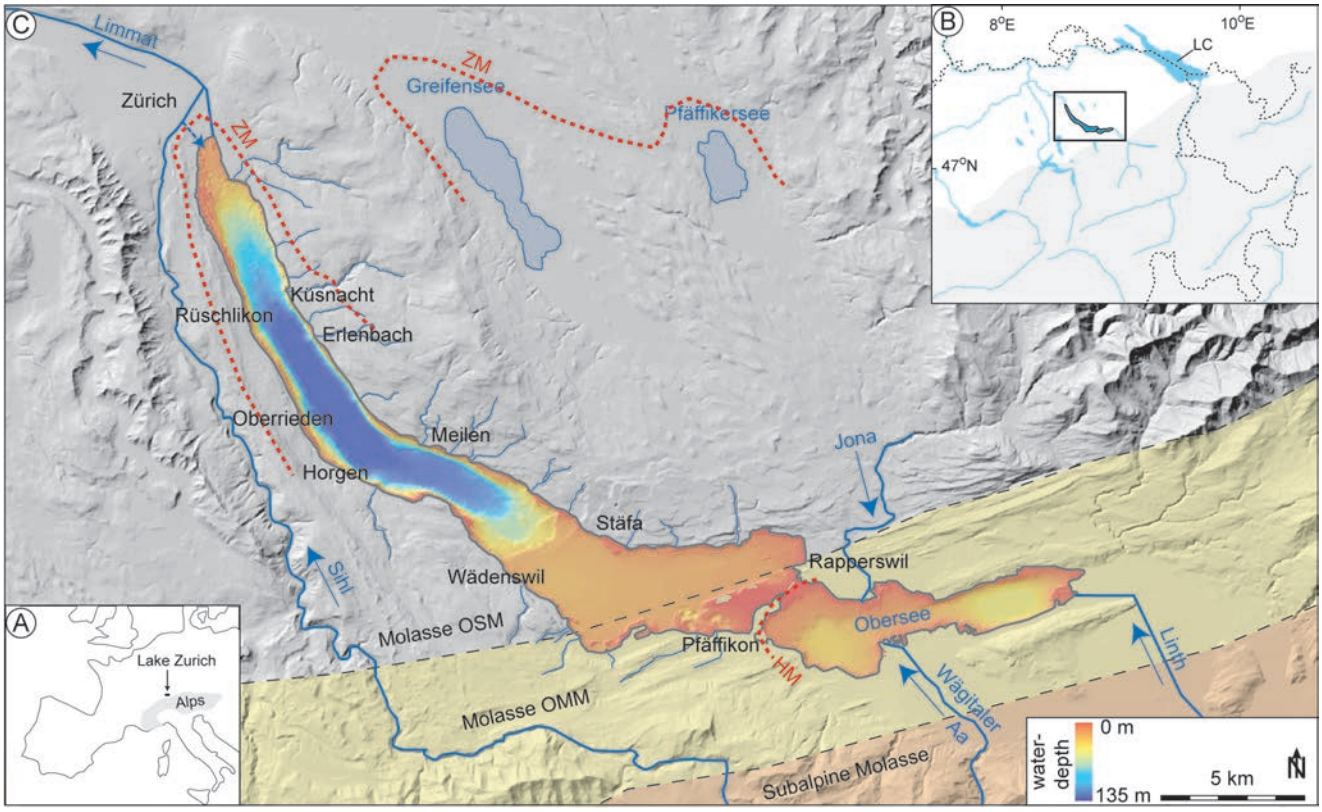

Figure 3.1: Geographic location of Lake Zurich: A) location with respect to Europe and the Alpine chain (gray shaded area). B) Close up view showing the Alps (gray shaded area) and the northern Swiss Plateau (white area). Dotted lines mark country borders of Switzerland, Germany, Austria, Liechtenstein and Italy. Rectangle indicates position of Fig. 3.1C. LC = Lake Constance. C) Lake Zurich's and Obersee's colored bathymetric map embedded in its geographic and geological context. Dashed red lines show prominent geomorphic features resulting from retreatal moraines that were formed during overall glacier retreat (ZM = Zurich Moraine, HM = Hurden Moraine). Blue arrows and annotations indicate flow direction and major rivers, respectively. Background: Shaded relief of digital elevation model (dhm25, Swisstopo) overlain by the general geological setting (OSM = Obere Süsswasser Molasse; OMM = Obere Meeres Molasse).

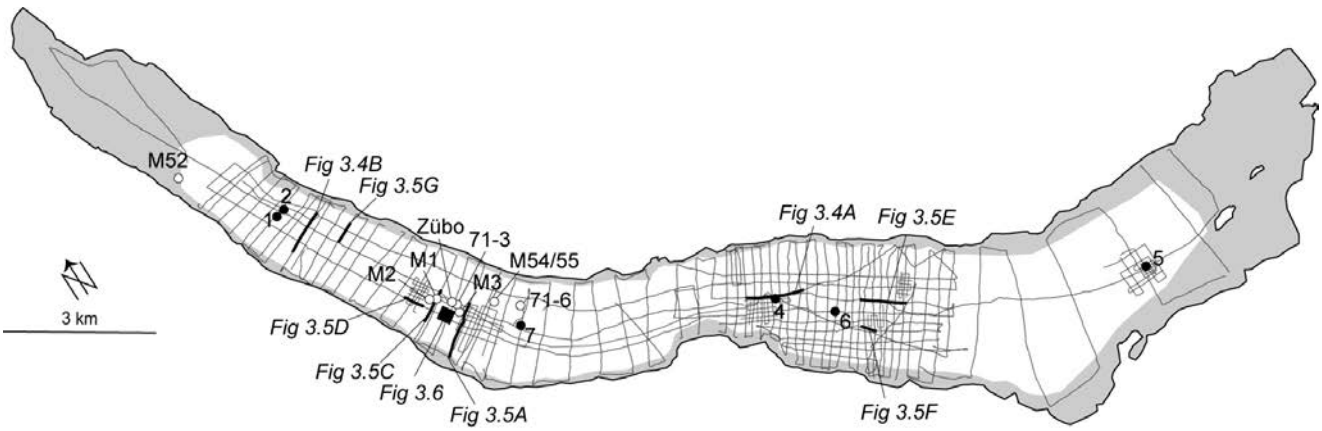

Figure 3.2: 3.5 kHz seismic survey grid in Lake Zurich and location of cores. Black dots and open circles indicate positions of new cores ZHK04-1 to 7 (this study) and from previous studies (Kelts, 1978; Giovanoli, 1979; Pika 1983; Lister, 1988; Sidler 1988), respectively. Solid black lines mark locations of seismic lines shown in subsequent figures. Gray shaded areas indicate marginal areas where the acoustic signal did not penetrate into the subsurface. Black square marks location of sidescan-sonar survey area and map shown in Figure 3.6.

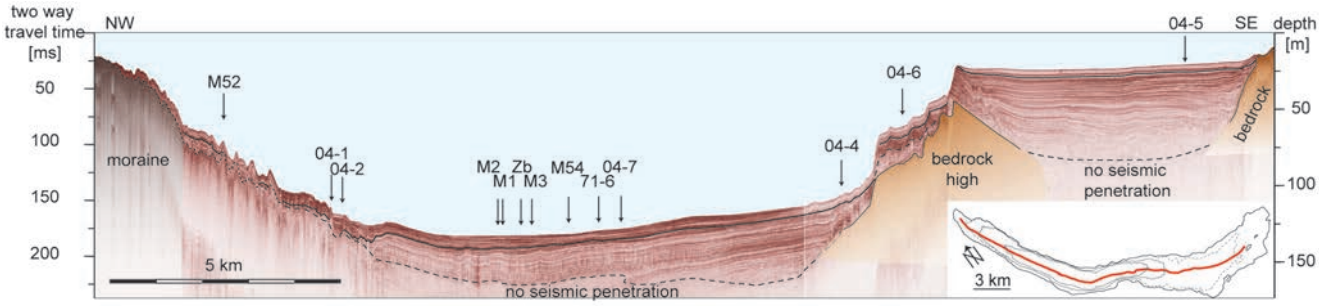

Figure 3.3: 3.5 kHz reflection seismic profile (pinger source) imaging the subsurface of Lake Zurich along the whole longitudinal lake axis with projected locations of cores shown in Figures 3.7 and 3.8. Black line in the seismic data corresponds to the boundary between seismic stratigraphic Unit A below and Unit B above. Inlet in the lower right corner shows location of the seismic line (solid red line). Contour interval is 50 m. Dotted contour line marks 20 m-depth contour line and aims to clarify basin morphology in the upper flat basin.

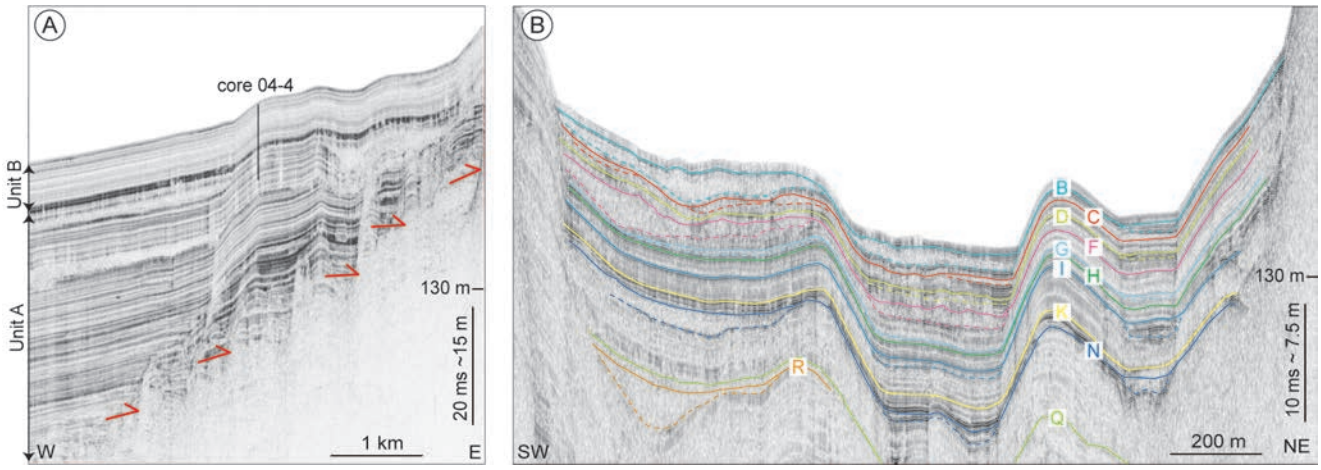

Figure 3.4: 3.5 kHz reflection seismic profiles illustrating general features of the seismic stratigraphy of Lake Zurich. See Figure 3.2 for location of seismic lines. A) Seismic section illustrating the two distinct differences in the geometry-style (ponding vs. draping) of Unit A and B, respectively. Red arrows indicate onlap patterns. A coring site is indicated with a vertical solid black line. B) Seismic line perpendicular to the lake axis in the northwestern part of Lake Zurich illustrating stacked mass-movement deposits of a few 10's to 100's of meters horizontal extension with internal chaotic-to-transparent seismic facies and clear lateral pinch-out geometries. Different-colored solid lines mark seismic stratigraphic horizons relating to the top of individual mass-movement deposits (i.e. event horizons B to R). Dashed colored lines mark the base of individual mass-movement bodies. The thin package of coherent, high-amplitude reflections between event horizons N and K corresponds to the transition zone between seismic stratigraphic units A and B.

3.4 Data and Results

3.4.1 Reflection seismic data

3.4.1.1 Seismic stratigraphy

Two seismic stratigraphic units can be identified in the seismic data that image ~50 and ~75 ms or the upper ~35 and ~60 m of the sedimentary infill of the lower and the upper basin, respectively (Fig. 3.3). In the deep basin the two seismic units are separated by a thin package (0.5 to 1 m thick) of coherent, high-amplitude reflections (Fig.3.4A). The two seismic units are characterized as follows:

(i) The seismic Unit A comprises a thick (~15 to 25 m and up to 55 m in the lower and upper basin, respectively) succession of acoustically stratified sediments characterized by parallel reflections of varying amplitudes. Towards the basin margins, the vertical amplitude variations are more closely spaced and the reflections often onlap onto the acoustic basement, indicating a dominant ponding-style of sedimentation (Fig. 3.4A).

(ii) The overlying seismic Unit B (~5 to 7 m thick) is characterized by closely-spaced, parallel reflections of medium-to-high and low-to-medium amplitudes

in the lower and the upper basin, respectively. Unit B forms a drape across the entire basin generally also covering the slopes. However, the drape is absent on the uppermost ~ 20 m-high scarp where glacio-lacustrine deposits outcrop along the escarpment structure (Boner et al., 1999) and moat features suggest current-induced erosion and/or non-sedimentation (Fig. 3.5E).

3.4.1.2 Types of mass-movement deposits

Sedimentary bodies of a few 10's to 100's of meters horizontal extension with internal transparent to chaotic-to-transparent seismic facies and clear lateral pinch-out geometries can be identified throughout the sedimentary succession in the lower basin and along the escarpment structure (Figs. 3.4B and 3.5). On the basis of different geometries, seismic facies and geographical occurrence, four different types of mass-movement deposits can be distinguished. They are described in the following section, which also delineates the interpreted transport and depositional mechanism associated to these types of mass-movement deposits.

Mass-flow deposits resulting from translational sliding along lateral steep slopes

The most prominent mass-movement deposits identified in the study area occur in the lower basin close to the slope breaks and are characterized by basinward-thinning bodies with distinct distal terminations, a transparent to sometimes partly chaotic-to-transparent seismic facies and generally smooth top surfaces (Figs, 3.4B, 3.5A, C and D). These observed geometries and seismic facies are typical characteristics of subaquatic mass-flow deposits (e.g. Prior et al, 1984; Mulder & Cochonat, 1996; Schnellmann et al. 2006) and indicate mass transport from the 15–20° steep lateral slopes towards the basin. Along the lateral slopes, failure scars related to the mass-flow deposits can be identified in seismic profiles (Figs. 3.5A and B). They reach > 5 m in height and generally occur on steepening-downwards slopes in water depth > 40 m. Observed geometries indicate translational sliding of the whole sedimentary drape covering the slopes along a basal gliding plane. A short gravity core recovered along the eroded slope offshore Oberrieden (i.e. slope failure event associated to the mass-flow deposit shown in Figures 3.5C and D) revealed that the sliding plane consists of glacial deposits and indicate comparable characteristics as described for lateral slope failures in Lake Lucerne (Strasser et al., 2007).
In Lake Zurich mass-flow deposits that evolved from translational sliding along the steep lateral slopes reach thicknesses of 1 to 7 meters and cover areas of a few 10's to 100's of meters horizontal extension. Seismic profiles crossing thick mass-flow deposits often indicate that the chaotic-to-transparent seismic facies reaches deeper than the mass-flow deposit itself indicating deformation of the overridden basal basin-plain sediments. This deformation sometimes is visualized by steeply dipping, high-amplitude reflections/diffractions in the frontal part of the acoustically chaotic-to-transparent bodies (Fig. 3.5C) suggesting frontal thrusting as the result of an adjustment of the underlying sediments to the increased static and dynamic loading during mass-flow deposition (Schnellmann, 2005). Sidescan-sonar data of a sub-recent lateral mass-flow deposit offshore Oberrieden show arcuate frontal compressional ridges associated with the mass-movement deposit (Fig. 3.6), supporting the interpretation of gravity spreading induced by loading of the slope-adjacent lake floor during lateral mass-flow deposition.

Mass-flow deposits resulting from rotational sliding along the escarpment structure

A second type of acoustically transparent mass-flow deposits was identified in the seismic data at the toe and in the intermediate sub-basins of the step-like escarpment structure (Fig. 3.5E). They only occur within seismic Unit A. On the basis of their geometries they clearly indicate mass-transport direction parallel to the lake axis. The source area of theses mass movements thus is interpreted to be situated along the upper scarps of the escarpment structure. However, complex geometries and potentially current-induced erosion and/or non-sedimentation as indicated by moat structures and outcropping of glacio-lacustrine deposits along the uppermost ~ 20 m-high scarp (Boner et al, 1999) (Fig. 3.5E) mask clear indicators of slope failure processes associated with this type of mass-flow deposition. Nevertheless, few seismic lines indicate rotational slide blocks associated with these mass-flow deposits (Fig. 3.5F), which thus are interpreted to have evolved from rotational sliding along the escarpment structure.

Wedge-shaped mass accumulation bodies in distal deltaic areas

Apart from the well-defined mass-flow deposits described above, seismic data in distal areas of small lateral deltas often show small wedges that taper off towards the basin. They generally comprise one to 3 low-amplitude reflections that downlap on a single seismic stratigraphic horizon in a basinward direction (Fig. 3.5G). No single mass-movement can be assigned to such wedge-shaped bodies because seismic penetration often is limited in delta-proximal areas and individual remobilization events along the delta supposedly are too small to be resolved on seismic sections. Therefore, these depositional units mapped as the correlated seismic stratigraphic horizons rather represent a series of individual small events and are interpreted to indicate periods of increased mass accumulation in the distal part of small lateral deltas resulting from small-scale remobilization on the steep delta slopes (e.g. mass flows induced by delta front collapses) and partially from higher clastic input from small creeks laterally entering Lake Zurich (see subsection 3.5.3).

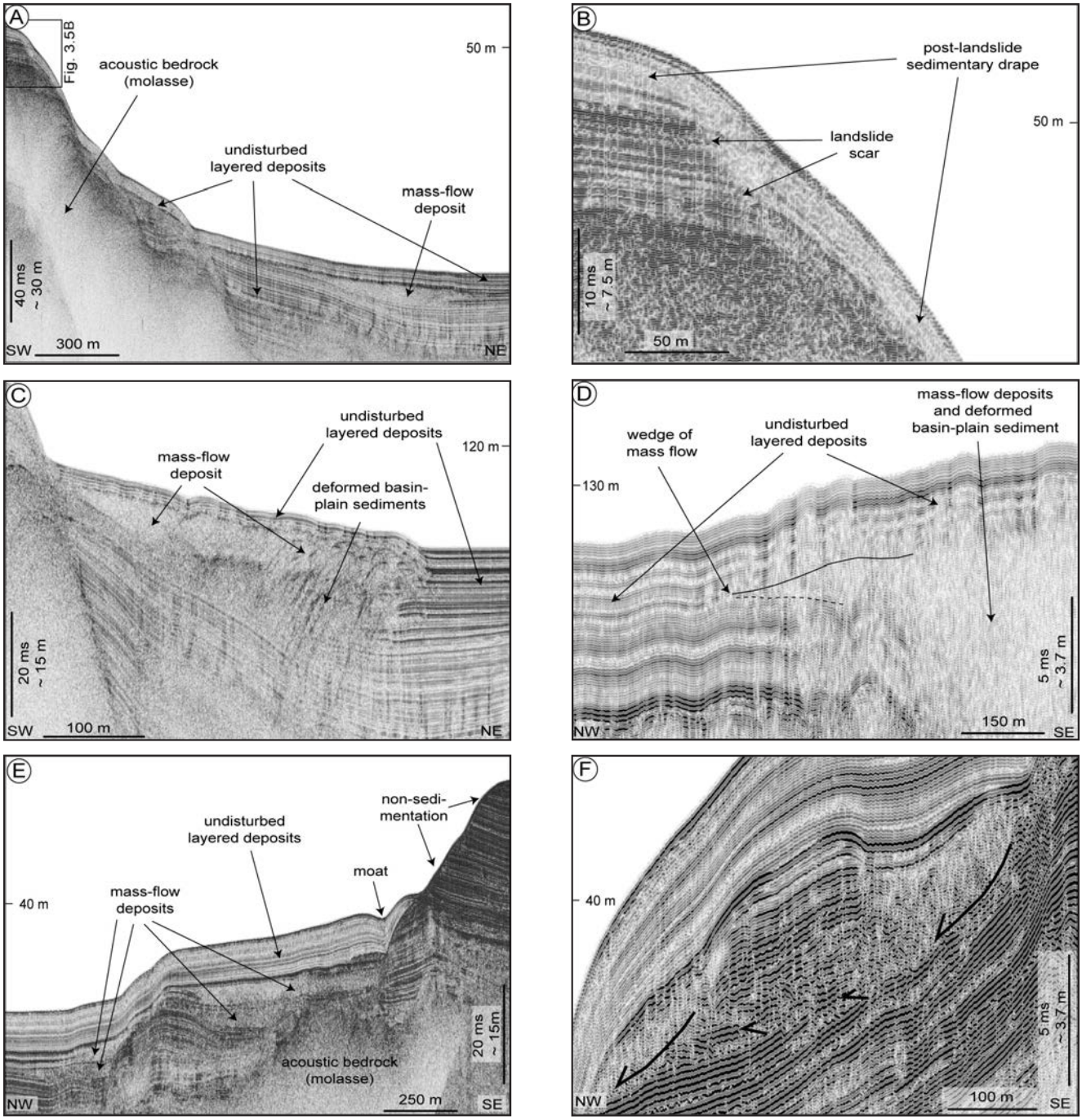

Figure 3.5: Selected 3.5 kHz seismic profiles illustrating mass-movement deposits in Lake Zurich. See Figure 3.2 for location of seismic lines. A) Lateral slope with failure scar and acoustically transparent mass-flow deposit of event N. B) Close-up of subaquatic landslide scar in ~50 m water depth. C) Prominent acoustically transparent to chaotic mass-flow deposit from lateral slope failure event F. D) Seismic line along the longitudinal lake axis crossing event F mass-flow deposits shown in panel C. Note well-defined lateral pinch-out geometry indicated by solid and dashed line. E) Longitudinal profile along the upper part of the escarpment structure showing two prominent Late Glacial mass-flow deposits (events Q and U). Note moat structures and lack of Holocene sedimentation indicating currents along the upper scarp. F) Close-up of rotational slide block (event Q) along the escarpment structure. G) Seismic line showing the distal part of Erlenbach Delta and mapped wedge-shaped mass accumulation bodies.

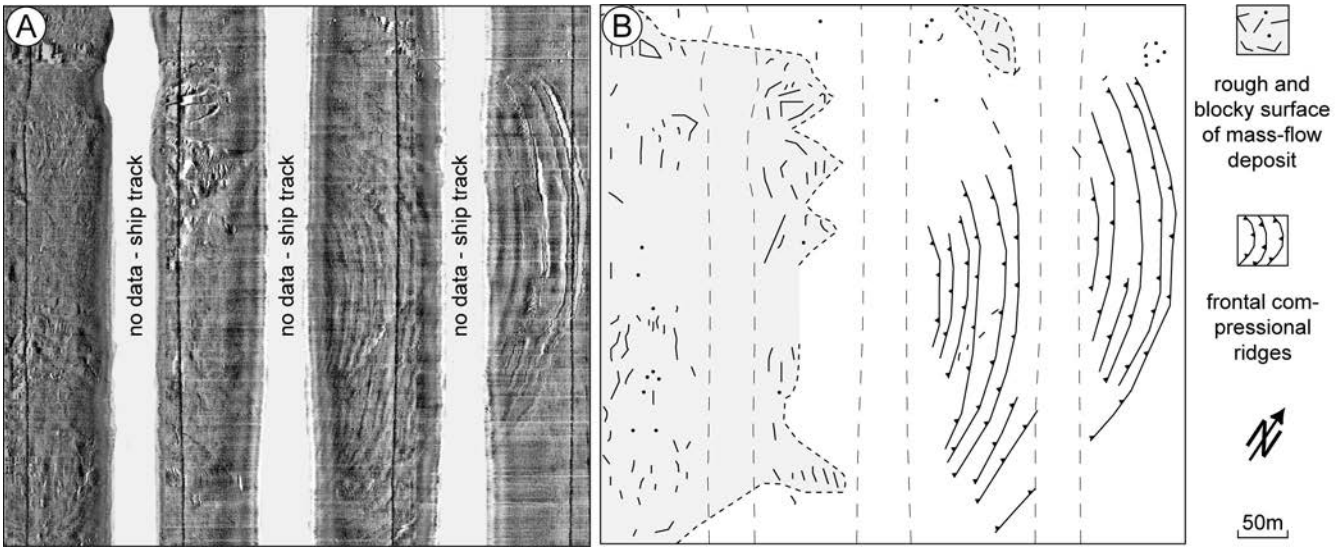

Figure 3.6: A) Sidescan-sonar image illustrating the lake floor surface expression and spatial geometry along the distal part of the 1918 A.D. Oberrieden mass-flow deposit (see Figure 3.2 for location of map segment). B) Interpretation of sidescan-sonar image showing the rough and blocky surface of the mass-flow deposit (mass-movement transport downslope from left to right) and associated arcuate frontal compressional ridges propagating into the basin plain.

Turbidite deposits

In the deepest depressions of the lower basin, event horizons assigned to mass-movement deposits often correlate to few dm to m-thick, acoustically almost transparent bodies that are characterized by smooth top surfaces and by well-defined ponding geometries. This geometry and acoustic signatures is typical for thick, extensive turbidite and homogenite deposits, which generally result from large mass flows (e.g. Sturm & Matter, 1978; Hsü & Kelts 1985; Bouma, 1987; Schnellmann et al, 2006). In Lake Zurich, only event horizons related to larger mass-flow deposits are associated with seismically resolvable turbidite deposits. However, smaller events often are associated with seismic reflections showing higher amplitudes indicating the presence of smaller turbidite layers (see subsection 3.4.2.3).

3.4.2 Core data

3.4.2.1 Lithostratigraphy

All six newly acquired sediment cores (see Figure 3.2 for core locations) recovered the characteristic postglacial stratigraphic succession that reflects the general sedimentary and environmental evolution of Lake Zurich as already described in previous studies (Kelts, 1978; Giovanoli, 1979; Pika, 1983; Hsü and Kelts, 1984; Lister, 1988; Sidler, 1988). Figure 3.7 shows a compilation of all available core information from Lake Zurich. The general sedimentary succession comprises three lithologic units (from bottom to top):

Lithologic Unit 1 «glaziale Seebodenlehme» - plastic mud

Sticky, medium-gray, plastic clays to silty clays with high bulk densities showing distinct up to 5 cm-thick laminations in the lower part (U1a - laminated plastic mud), thin mm-scale laminations intercalated with yellowish, mm-scale silt to fine sand layers in the middle part (U1b - faintly laminated plastic mud) and homogenous to mottled textures in the upper part (U1c - mottled plastic mud). This lithologic unit corresponds to the upper part of seismic Unit A. Thicker laminae in deep-water cores contrast thinner laminae in shallow-water cores and thus confirm the ponding-style depositional character of this sedimentary unit. The lithology and infill pattern indicate glacio-lacustrine sedimentation by underflows in a proglacial environment. The lamination in the lower and middle part of this unit has been interpreted as varve deposits, reflecting annual pulses of suspension input from meltwater plumes of a nearby glacier (U1a) (Zao et al, 1984) and seasonal aeolian dust sedimentation (loess) during the Oldest Dryas (U1b) (Giovanoli, 1979; Niessen 1992)

Lithologic Unit 2 «Basaler Faulschlamm» - iron sulfide mud

Dark greenish-gray clays to silty clays with low carbonate content and low bulk densities showing a distinct appearance of several highly FeS-pigmented black laminations and intercalated cm-thick sandy to silty turbidites. From its stratigraphic position, this unit corresponds to the seismic high-amplitude reflections in the transition zone between seismic Units A and B. It is interpreted that, with postglacial climatic amelioration and the final retreat of the glaciers back into the Alps, catchment erosion and runoff

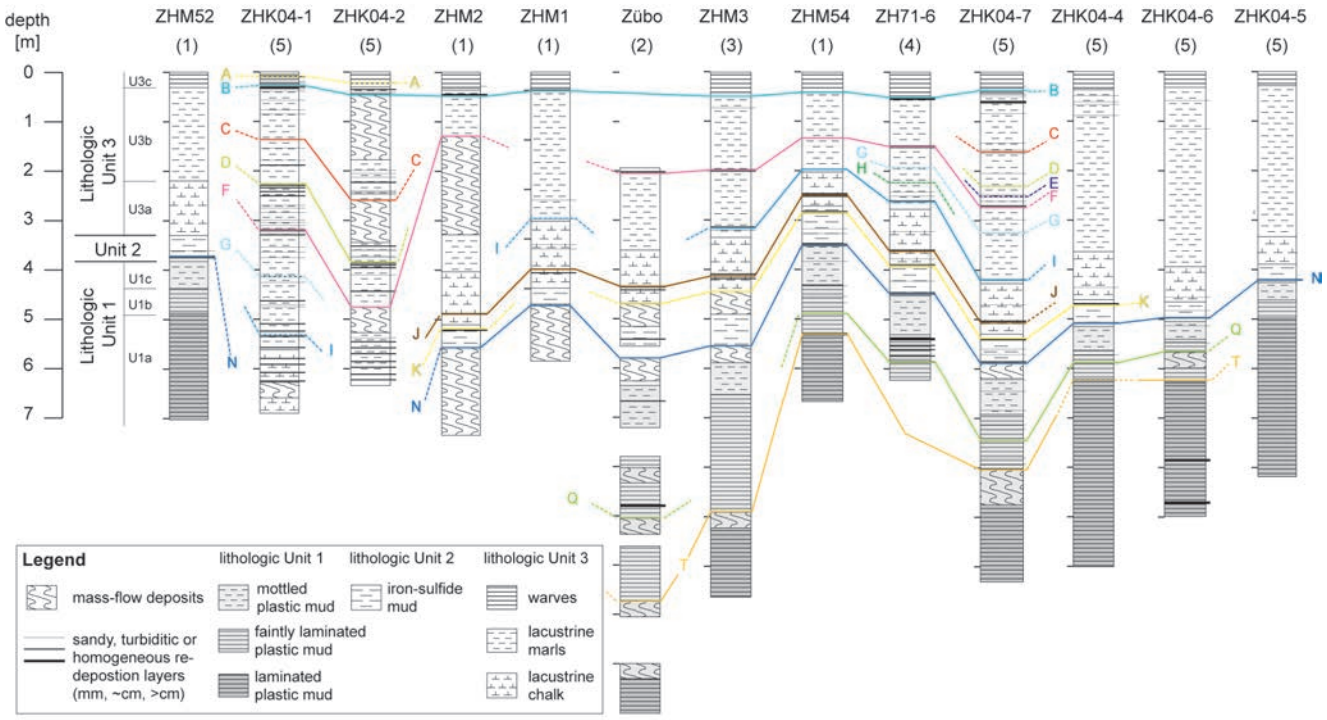

Figure 3.7: Core transect approximately along the longitudinal lake axis from NW to SE compiling all available core information from Lake Zurich ((1) Giovanoli, 1979, (2) Lister, 1988, (3) Pika, 1983, (4) Kelts, 1978, (5) this study). See Figure 3.2 for core locations. Note that core ZHK04-1 and ZHK04-2 represent sites close to Küsnacht and Erlenbach Deltas and thus show higher sedimentation rates. Core ZHM54 and ZH71-6 are from slightly elevated positions and are projected here onto the basin axis. Different-colored solid lines delineate core-to-core correlation of mass-movement horizons (i.e. event horizons A to T). Uncertain correlations are indicated with dashed lines and are mainly based on seismic-to-core correlation.

into the lake was reduced and the lake became stratified. Lacustrine biota is established and oxygen content in the bottom-water dropped occasionally to anoxic levels, resulting in characteristic FeS-pigmented black laminations of the lithologic unit (e.g. Kelts, 1978; Pika, 1983).

Lithologic Unit 3 «Seekreide» and «Seekreide-Mergel»-lacustrine chalk and marls

Light gray (U3a) to greenish gray (U3b), faintly layered lacustrine chalk (U3a) and marls (U3b) composed of terrigenous mud rich in authigenic carbonate, intercalated with cm-thick sandy and muddy turbidites. These deposits correspond to seismic Unit B and were deposited when bio-induced calcite precipitation and minor clastic input from small local creeks were the dominant sediment sources in the mesotrophic holomictic lake. Clastic input is especially evident at two coring sites close to the Küsnacht and Erlenbach deltas, where sedimentation rates are significantly higher than in the deep basin (Fig. 3.7). Cores ZHK04-1 and 2 recovered in the distal part of these deltas show frequent 0.5 to 2 cm-thick clastic layers with high organic content. The uppermost 50 to 70 cm of lithologic Unit 3 (U3c) show distinct rhythmically layered calcite/organic couplets (varves) throughout the deep basin representing human-induced lake eutrophication after 1897 A.D. (e.g. Kelts, 1978; Pika, 1983).

3.4.2.2 Age model

The general age model of the postglacial sedimentary infill of Lake Zurich has already been established based on few ^{14}C samples from the Zübo core (Lister, 1988) and based on palynological data from core M54 (Sidler, 1988). The new ^{14}C ages covering the last ~14000 years (Table 3.1) are in good agreement with these data and refine the age control since the beginning of the Bølling stage (Units 2 and 3). The new high-resolution age model established in core ZHK04-7 (Fig. 3.8) reveals Holocene ages for the lithologic Unit 3 (seismic Unit A) and Younger Dryas to Bølling ages for lithologic Unit 2.

The age model of the sedimentary succession in Unit 1 is only based on two ^{14}C ages of wood samples from the Zübo core. Lister (1988) dated the transition U1a/U1b and U1b/U1c to 17100–18050 and 16500–17300 cal yr B.P., respectively (Tab. 3.1). Counting of rhythmites (presumably varves) in cores ZHK04-4 and 7 reveal duration of ~575 yrs (565 and 587 in cores 4 and 7, respectively) for the deposition of U1b, which is in good agreement with the relative time span estimated from the two Zübo ^{14}C samples. However, geomagnetic correlation of this interval between Lakes Zurich, Constance, Lugano and Geneva (Baster, 2002, and references therein) consistently suggests younger absolute ages. Additional support for younger ages arises from sedimentological correlation

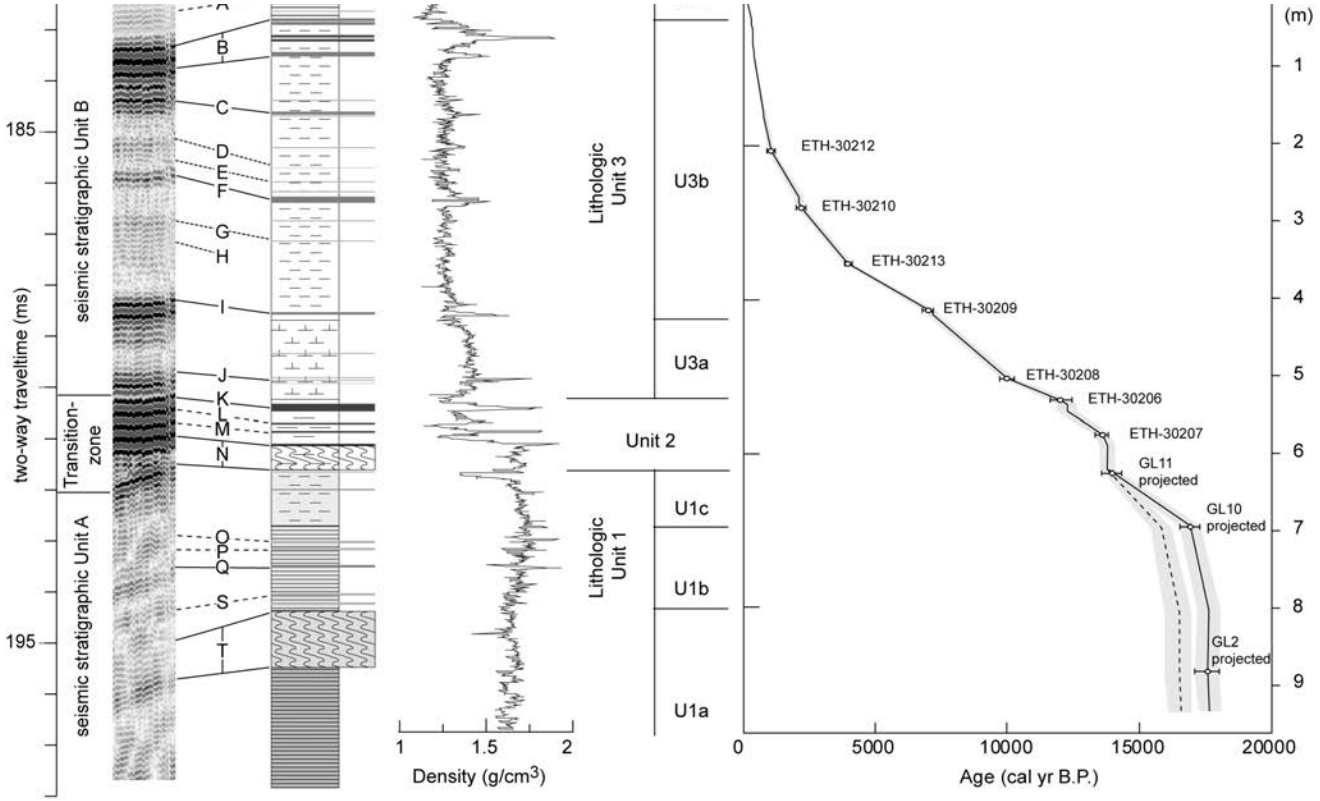

Figure 3.8: Compiled data from core ZHK04-7 (from left to right): Seismic stratigraphy at the coring site, seismic-to-core correlation, core log, bulk density log, lithostratigraphy and age model. See Figure 3.2 for core location and legend in Figure 3.7 for lithological symbols. Dashed line in the lower part of age model indicates correction for overestimated ^{14}C ages from the Zübo core (Lister, 1988) that are projected here (see subsection 3.4.2.2 and Table 3.2). Gray area marks 2σ-range of calibrated ages.

of loess deposits recovered in several Swiss Lakes (e.g. Lakes Constance (Niessen et al., 1992; Wessels, 1998) and Geneva (Baster, 2002; Girardclos et al., 2005). Geomagnetic correlation between Lakes Zurich and Constance reveal that Lake Zurich's Units U1b and U1c (faintly laminated and mottled plastic mud, respectively) correlate to laminated loess deposits (beige-brown rhythmites) in Lake Constance (Wessels, 1998). In his record, Wessels (1998) counted 1370 lamination couplets between the correlated lithologic boundaries U1b/U1c and U1/U2, which suggests that U1c covers ~1400 years. Following this interpretation and assuming a synchronous transition, as indicated by the geomagnetic correlation, between Units U1 and U2 in both lakes (dated to ~14500 cal yr B.P (Fig. 3.8 and Table 3.1)), the age model for lithologic Units U1a and U1b might be shifted by ~1000 (range: 650–1350) years towards younger ages (i.e. age (and range) discrepancy between Zübo date of U1b/U1c transition and correlated age in Lake Constance). Although only a first order assumption, this accounts for the (too) low sedimentation rates for U1c as estimated from the ^{14}C ages. While the Zübo ages propose that U1c sedimentation rates are in the same order of magnitude as in Unit 2 (Fig. 3.8), sediments of U1c still indicate a glacio-lacustrine sedimentation mode that clearly suggests higher sedimentation rates.

3.4.2.3 Sedimentary facies of mass-movement deposits

Mass-flow deposits

Coring the distal part of a mass-flow deposit that evolved from subaquatic translational sliding along the steep lateral slope in core ZHK04-7 recovered a characteristic succession showing a 2 cm-thick basal shear zone that is overlain by a fining upward matrix-supported mud-clast conglomerate (Fig. 3.9A). This typical mud-flow deposit is overlain by a 4 cm-thick graded turbidite layer characterized by a multiple, graded sandy to silty sequence at the base and by a homogenous clayey top layer. Similar sedimentary facies have been observed in core ZHK04-6 that recovered the distal part of a mass-flow deposit evolved from mass transport in an axis-parallel SE-NW direction along the escarpment structure. The lower part of this deposit shows a 15 cm-thick interval of heavily deformed and folded glacio-lacustrine sediments indicating slumping rather than full disintegration of the source material (Fig. 3.9B). This observation supports the interpretation that this type of mass-flow deposits evolved from rotational sliding of glacio-lacustrine sediments covering the bedrock sill in the uppermost part of the escarpment structure (see subsection 3.4.1.2).

Wedge-shaped mass accumulation bodies in distal deltaic areas

Core data from distal deltaic areas show frequent 0.5–2 cm-thick clastic layers with high organic content and sedimentation rates are significantly higher than in the central deep basin (Fig. 3.7). Seismic-to-core correlation reveals that intervals assigned to seismically imaged wedge-shaped mass accumulation bodies correspond to more frequent, thicker and coarser clastic layers (Fig. 3.9C). This observation confirms the interpretation that these wedge-shaped bodies do not represent single mass-movement events but rather periods of increased small-scale remobilization on the steep delta slopes (e.g. delta front collapses) and higher clastic input from small creeks laterally entering Lake Zurich (see subsection 3.5.3).

Turbidite deposits

A number of 1–5 cm-thick turbidite deposits have been recovered in cores retrieved in the central part of the deep basin (Fig. 3.7). In general, they show a coarser sandy to silty lower base, which sometimes comprises multiple graded sandy layers, and a fining upward sequence towards a homogenous clayey top layer (Fig. 3.9D). Smaller turbidite layers, however, do not always have a graded character and sometimes comprise only a 0.5–1 cm-thick homogenous silt or clay layer and/or a thin top layer with higher organic content (Fig. 3.9E). Occasionally, amalgamation of small individual turbidite layers lacking intercalated undisturbed sediment can be observed (Fig. 3.9F). Most of the turbidite layers recovered in cores from the deep basin can be correlated to event horizons assigned to mass-movement deposits mapped elsewhere in the deep basin (Fig. 3.8). In distal deltaic areas, however, they occur more frequent and probably also represent flood-related hyperpycnal-flows deposits.

3.4.3 Catalogue of past mass-movement deposits

A total of 149 mass-movement bodies have been identified in the seismic data (64 mass-flow deposits associated to lateral sliding, 19 mass-flow and rotational-slide deposits along the escarpment structure, 51 small wedge-shaped mass accumulation bodies and 15 turbidite deposits). They were mapped and correlated to a total of 21 individual event horizons, each of which was independently dated 1–4 times in different cores (see subsections 3.3.1 and 3.3.3,

Table 3.1: ^{14}C ages and calibration of samples from Lake Zurich.

Core Nr.	*Location* [1]	*Depth in core* [m]	*Sample Nr.*	*Sample age* [2] [^{14}C yr B.P.]	*Sample age* [3] [cal. yr B.P.]	*material*
ZHK04-1	*685585 / 240583*	*1.98*	*ETH-30711*	*1585 ± 50*	*1350 - 1570*	*leaf remains*
ZHK04-1	*685585 / 240583*	*3.19*	*ETH-30712*	*3230 ± 50*	*3360 - 3570*	*leaf remains*
ZHK04-1	*685585 / 240583*	*4.6*	*ETH-30713*	*4420 ± 60*	*4860 - 5290*	*leaf remains*
ZHK04-1	*685585 / 240583*	*6.26*	*ETH-30762*	*6505 ± 65*	*7270 - 7520*	*leaf remains*
ZHK04-2	*685744 / 240619*	*2.45*	*ETH-30707*	*470 ± 50*	*430 - 560*	*leaf remains*
ZHK04-5	*699687 / 230486*	*3.38*	*ETH-30216*	*5740 ± 70*	*6390 - 6730*	*leaf remains*
ZHK04-5	*699687 / 230486*	*3.78*	*ETH-30215*	*8995 ± 80*	*9750 - 10300*	*leaf remains*
ZHK04-5	*699687 / 230486*	*4.12*	*ETH-30715*	*11560 ± 90*	*13240 - 13640*	*wood*
ZHK04-7	*688526 / 236159*	*2.07*	*ETH-30212*	*1095 ± 50*	*920 - 1150*	*leaf remains*
ZHK04-7	*688526 / 236159*	*2.81*	*ETH-30210*	*2135 ± 55*	*1990 - 2320*	*leaf remains*
ZHK04-7	*688526 / 236159*	*3.52*	*ETH-30213*	*3615 ± 55*	*3820 - 4090*	*leaf remains*
ZHK04-7	*688526 / 236159*	*4.13*	*ETH-30209*	*6105 ± 70*	*6790 - 7170*	*leaf remains*
ZHK04-7	*688526 / 236159*	*5.03*	*ETH-30208*	*8895 ± 80*	*9700 - 10250*	*leaf remains*
ZHK04-7	*688526 / 236159*	*5.32*	*ETH-30206*	*10230 ± 85*	*11600 - 12400*	*leaf remains*
ZHK04-7	*688526 / 236159*	*5.76*	*ETH-30207*	*11710 ± 100*	*13340 - 13770*	*wood*
Zübo 1980 [4]	*687615 / 237266*	*5.75*	*GL8*	*9990 ± 150*	*11150 - 12100*	*wood*
Zübo 1980 [4]	*687615 / 237266*	*7.4*	*GL11*	*12400 ± 250*	*13750 - 15250*	*wood*
Zübo 1980 [4]	*687615 / 237266*	*7.5*	*GL15*	*12800 ± 250*	*14150 - 15850*	*wood*
Zübo 1980 [4]	*687615 / 237266*	*9.5*	*GL10*	*14150 ± 250*	*16500 - 17300*	*wood*
Zübo 1980 [4]	*687615 / 237266*	*13.8*	*GL 2*	*14600 ± 250*	*17100 - 18050*	*wood*

[1] Location is given in Swiss Grid (CH1903) Coordinates.

[2] Dating by AMS (accelerator mass spectrometry) with the tandem accelerator at the Institute of Particle Physics at the Swiss Federal Institute of Technology Zurich (ETH).

[3] Calibration (2σ range) was carried out applying the IntCal04-calibration curve (Reimer et al., 2004).

[4] Dates by Lister (1988).

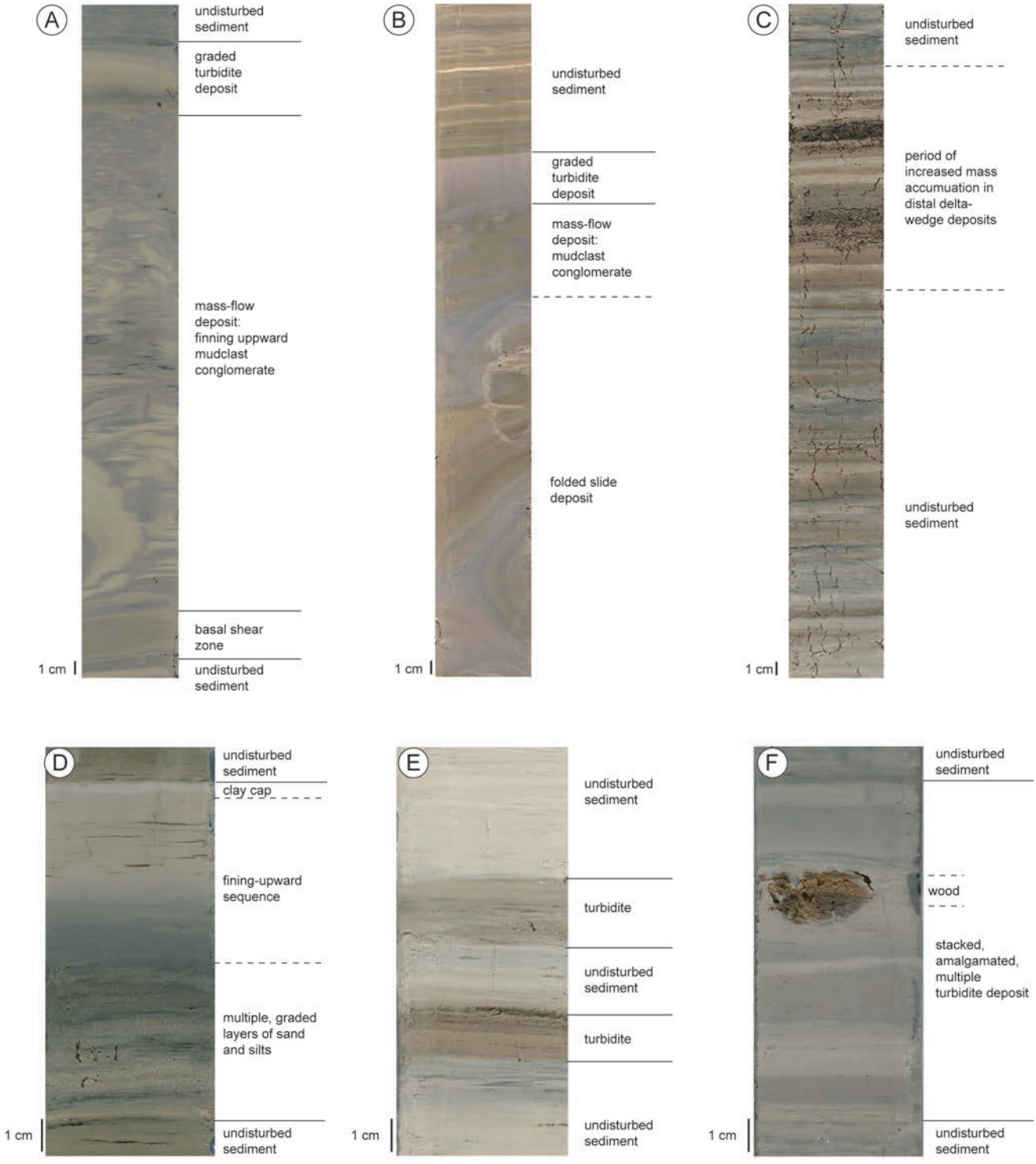

Figure 3.9: Core photos illustrating characteristics of mass-movement deposits in Lake Zurich. A) Core ZHK04-7 (event N): mass-flow and turbidite deposit evolved from translational sliding along the lateral slope. B) Core ZHK04-6 (event Q): slide, mass-flow and turbidite deposit evolved from rotational sliding and longitudinal flow along the escarpment structure. C) Sedimentary succession in core ZHK04-1 showing frequent clastic redeposition layers in a distal deltaic setting. Interval with higher frequency of coarser and thicker layers correlates to a wedge-shaped mass-accumulation body mapped in the seismic data (horizon D). D) Core ZHK04-7 (event K): Turbidite deposit showing multiple layers of sands and silts at the base, a fining-upward sequence and a fine homogeneous clayey cap. E) ZHK04-7 (event J): two small brownish redeposition layers in the lower part of Unit 3a (lacustrine chalk). F) ZHK04-7 (event F): Amalgamation of individual turbidite deposits evolved from multiple, coeval lateral landsliding lacking intercalated undisturbed sediment.

Tab. 3.2). The distribution of mass-movement deposits related to each event horizon (labeled as event A (young) to U (old) according to stratigraphy) are shown in Figure 10. Each of the individual event horizon comprises 1 to 23 mass-movement deposits.
The catalogue of past mass-movement activity in Lake Zurich shown in Figure 3.10 may not be complete because: (1) Limited seismic penetration in the northwestern-most part of the lower Lake Zurich basin, in proximal areas of lateral deltas and in shallow waters did not allow for mapping mass-movement deposits in these area (gray shaded area in Fig. 3.2), (2) relatively small and/or old deposits may not have been recognized due to reworking and deformation by younger and larger events, and (3) only the Holocene deposits were mapped out in the northwestern part of the lower basin due to the fact that the seismic signal did not penetrate into the Late Glacial succession in this area.

3.5 Discussions

The chronological catalogue of Late Glacial-to-Holocene mass-movement deposits together with the identification and characterization of different deposit types in terms of geometry, seismic and sedimentary facies, allows reconstructing an event-based history of slope failure, remobilization and sediment transport processes in peri-alpine Lake Zurich. It furthermore provides the basis for evaluating long-term causes and short-term trigger mechanism of subaquatic landslides in this setting. The following section aims to discuss Lake's Zurich mass-movement event history with respect to different geological processes and impacts that have affected the lake basin over the last ~17000 years.

3.5.1 Human-induced landslides within the last 150 years

During the last 150 years several shore collapses and slumps occurred along the shore of Lake Zurich (e.g. Horgen 1875, Rüschlikon 1898, 1900 and 1907, Oberrieden 1918 and Küsnacht 1943 and 1955 A.D. (Nipkow 1920; Kelts & Hsü, 1980; Kuen, 1999)). They directly resulted from human-induced loading of sand and gravel landfill on a weak foundation of lacustrine chalk and have been reported to leave characteristic traces in the sedimentary record of Lake Zurich (Nipkow, 1920; Kelts, 1978, Kelts & Hsü, 1980; Pika, 1984). In the seismic data, mass-movement deposits related to these documented shore collapses can clearly be identified and assigned to corresponding event horizons (events A and B; Note that for the mass-movement deposits near Rüschlikon and Küsnacht it remains unclear, which of the seismically imaged deposits corresponds to which reported event; Fig. 3.10). However, the seismic stratigraphic approach did not allow for assigning individual seismically resolvable event horizons to each of the historically documented events. Therefore they all occur within only two seismic stratigraphic horizons (events A and B) and the mapped turbidite deposit corresponding to horizon B thus comprise the stacked succession of all events that occurred between 1875 and 1918 A.D..

3.5.2 Events affecting the entire basin («glacial events» and paleo-earthquakes)

One of the most remarkable characteristics of the mass-flow deposits in the subsurface of Lake Zurich is the occurrence of event horizons with multiple coeval mass-flow deposits. 50 of the total 64 mapped mass-flow deposits associated to lateral sliding relate to only 3 event horizons (events F, K and N) and all 19 mass-flow and rotational-slide deposits along the western escarpment of the bedrock high occur only within two event horizons (events Q and U). These outstanding event horizons often also comprise seismically resolvable turbidite deposits, which are characterized in core data by multiple graded sandy layers and amalgamated redeposition layers lacking intercalated undisturbed sediment (Fig. 3.9F). These observations confirm the concurrence of individual landslides and show that regional triggers destabilizing simultaneously the subaquatic slopes repeatedly affected the Lake Zurich area in the past ~17000 years.
The two oldest events (events Q and U) occurred during the transition from the Pleniglacial to the Late Glacial period, when the retreating Linth glacier still was in proximity of Lake Zurich, as indicated by the sedimentary facies of lithologic Unit 1a and b. Lister (1988) interpreted the transition from Unit 1a to 1b to correspond to the time, when the Linth Glacier retreated back behind the Hurden moraine. During that time, deglaciation of the Linth Glacier has influenced to a large extent sediment input and depositional processes in the upper Lake Zurich basin and along the escarpment structure. High sedimentation rates, potentially punctuated by rapid glacier destabilization phases and/or episodic glacier outburst events, are likely to have influenced slope stability conditions of the glacio-lacustrine deposits. However, whether or not the two rotational sliding events Q and U along the escarpment structure can be related to such episodic «glacial events» remains open.
Alternatively, strong earthquake shaking might be a reliable regional trigger mechanism, as it has been reported in many other studies documenting the relation between synchronicity for a series of subaquatic landslides with strong seismic events that triggered slope failures on a regional scale (e.g., Shilts and Clague, 1992; Schnellmann, et al., 2002; 2006). Such an earthquake trigger also is the most likely process to explain the occurrence of the three younger event horizons F, K and N, each characterized by at least 10 individual slides along the lateral slopes throughout the lower Lake Zurich basin. In fact, Strasser et al., (2006) show that all three events correlate to multiple subaquatic landslide deposits in Lake Lucerne. This correlation indicates that three very large earthquakes ($M_w > 6.5$) shook central Switzerland in the past ~15000 years that were strong enough to trigger multiple mass movements in these two lakes located ~40 km apart.

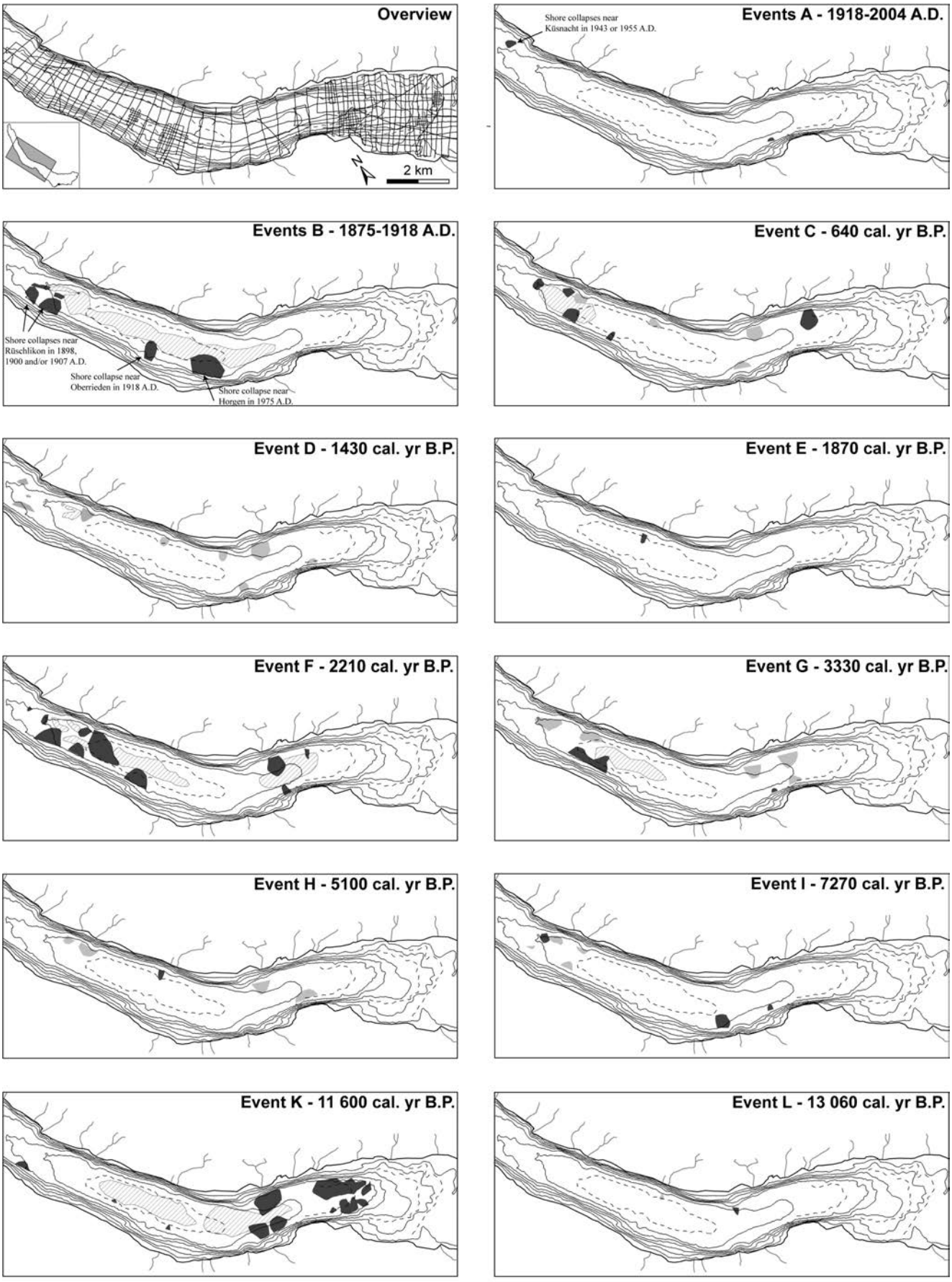
Overview
N
2 km
Events A - 1918-2004 A.D.
Shore collapses near
Küsnacht in 1943 or 1955 A.D.
Events B - 1875-1918 A.D.
Shore collapses near
Rüschlikon in 1898,
1900 and/or 1907 A.D.
Shore collapse near
Oberrieden in 1918 A.D.
Shore collapse near
Horgen in 1975 A.D.
Event C - 640 cal. yr B.P.
Event D - 1430 cal. yr B.P.
Event E - 1870 cal. yr B.P.
Event F - 2210 cal. yr B.P.
Event G - 3330 cal. yr B.P.
Event H - 5100 cal. yr B.P.
Event I - 7270 cal. yr B.P.
Event K - 11 600 cal. yr B.P.
Event L - 13 060 cal. yr B.P.

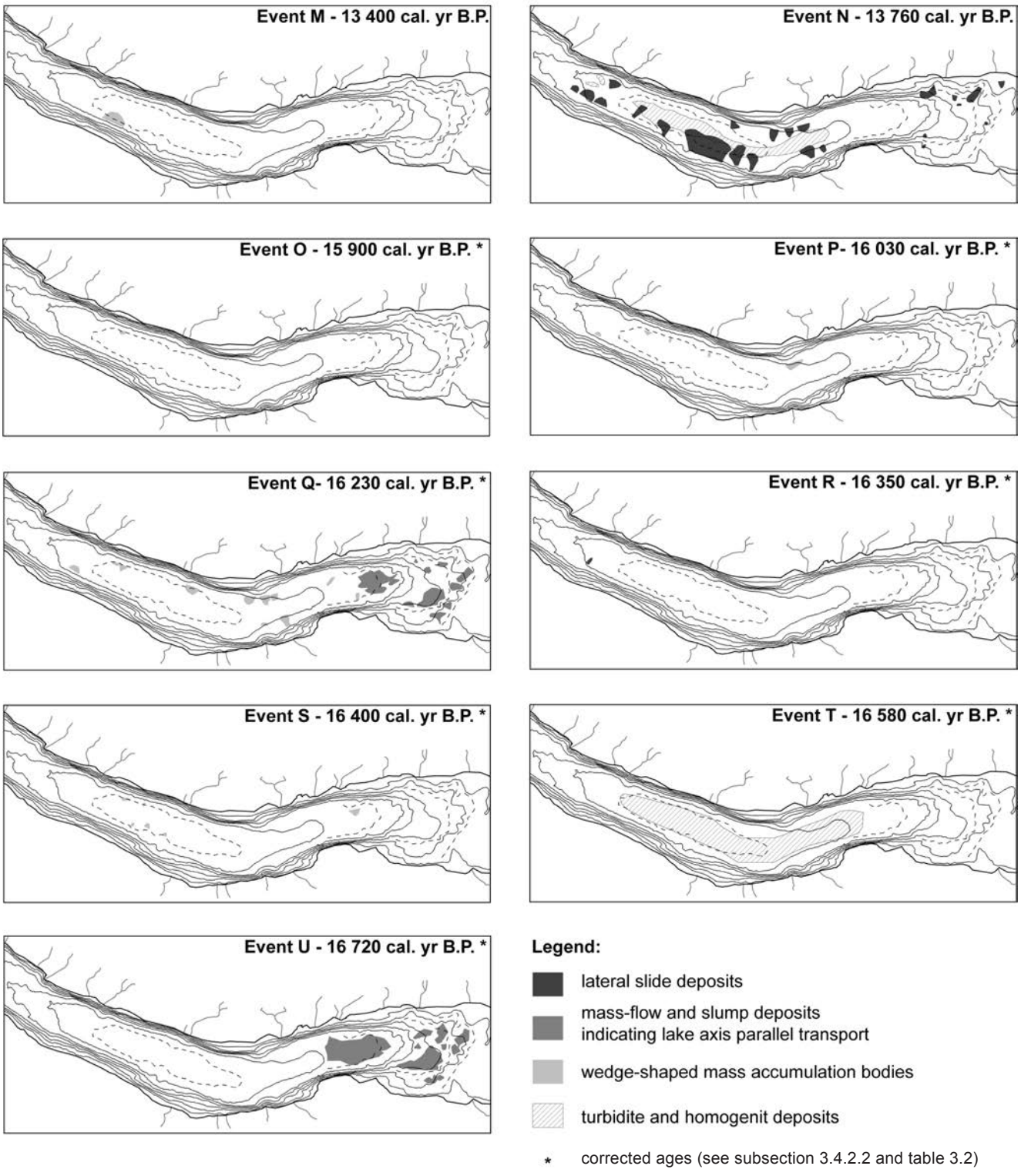

Figure 3.10: Catalogue of mass-movement deposits in the subsurface of Lake Zurich. The upper left panel shows the seismic survey grid, which was used for mapping and correlating the mass-movement deposits. The other panels show the aerial distribution of events A to U as imaged by the seismic data. For dating procedure and age ranges, see Tables 3.1 and 3.2. Asterisks in panel O to U indicate that the age was corrected by 1000 years towards younger ages (see subsection 3.4.2.2 and Table 3.2). Event J cannot be tracked on seismic data and was only observed in core data. It therefore is not included here.

Table 3.2. Dating of prehistoric event horizons.

Horizon Name	Sample Nr.	Sample age[1] [^{14}C yr B.P.]	Sample age[2] [cal. yr B.P.]	Offset[3] [cm]	Sed.rate[4] [cm/yr]	Horizon age [cal. yr B.P.]	Horizon age (overlap range) [cal. yr B.P.]	Center of overlap[5] [cal. yr B.P.]
C	ETH-30707	470 ± 50	430 - 560	-18	0.13	569 - 699		
	ETH-30212	1095 ± 50	920 - 1150	46	0.14	590 - 820	590 - 699	640
D	ETH-30212	1095 ± 50	920 - 1150	-21	0.06	1291 - 1521		
	ETH-30711	1585 ± 50	1350 - 1570	2	0.11	1331 - 1551	1331 - 1521	1430
E	ETH-30210	2135 ± 55	1990 - 2320	16	0.06	1707 - 2037	1707 - 2037	1870
F	ETH-30711	1585 ± 50	1350 - 1570	-37	0.05	2092 - 2312		
	ETH-30712	3230 ± 50	3360 - 3570	60	0.05	2157 - 2367		
	ETH-30210	2135 ± 55	1990 - 2320	3	0.06	1937 - 2267	2157 - 2267	2210
G	ETH-30213	3615 ± 55	3820 - 4090	24	0.04	3190 - 3460	3190 - 3460	3330
H	ETH-30713	4420 ± 60	4860 - 5290	-2	0.07	4889 - 5319	4889 - 5319	5100
I	ETH-30209	6105 ± 70	6790 - 7170	-3	0.03	6897 - 7277		
	ETH-30762	6505 ± 65	7270 - 7520	1	0.07	7255 - 7505	7255 - 7277	7270
J	ETH-30208	8895 ± 80	9700 - 10250	-	-	9700 - 10250	9700 - 10255	9980
K	ETH-30206	10230 ± 85	11600 - 12400	1	0.02	11534 - 12334		
	ETH-30215	8995 ± 80	9750 - 10300	-14	0.01	11109 - 11659		
	GL8[6]	9990 ± 150	11150 - 12100	-	-	11150 - 12100	11534 - 11656	11600
L	ETH-30206	10230 ± 85	11600 - 12400	-15	0.01	12656 - 13456	12656 - 13456	13060
M	ETH-30207	11710 ± 100	13340 - 13770	6	0.04	13189 - 13619	13189 - 13619	13400
N	ETH-30207	11710 ± 100	13340 - 13770	-3	0.04	13425 - 13855		
	ETH-30715	11560 ± 90	13240 - 13640	-5	0.03	13407 - 13807		
	GL11[6]	12400 ± 250	13750 - 15250	5	0.04	13607 - 15107		
	GL15[6]	12800 ± 250	14150 - 15850	15	0.04	13721 - 15421	13721 - 13807	13760
O	GL10[6]	14150 ± 250	16500 - 17300	-	-	16500 - 17300	16500 - 17300	16900
						corrected age[7]:	15500 - 16300	15900
P	GL10[6]	14150 ± 250	16500 - 17300	-25	0.20	16625 - 17425	16625 - 17425	17030
						corrected age[7]:	15625 - 16425	16030
Q	GL10[6]	14150 ± 250	16500 - 17300	-80	0.20	16900 - 17700		
	GL2[6]	14600 ± 250	17100 - 18050	100	0.20	16600 - 17550	16900 - 17550	17230
						corrected age[7]:	15900 - 16550	16230
R	GL2[6]	14600 ± 250	17100 - 18050	45	0.20	16875 - 17825	16875 - 17825	17350
						corrected age[7]:	15875 - 16825	16350
S	GL2[6]	14600 ± 250	17100 - 18050	35	0.20	16925 - 17875	16925 - 17875	17400
						corrected age[7]:	15925 - 16875	16400
T	GL2[6]	14600 ± 250	17100 - 18050	-	-	17100 - 18050	17100 - 18050	17580
						corrected age[7]:	16100 - 17050	16580
U	GL2[6]	14600 ± 250	17100 - 18050	-600	4.29[8]	17240 - 18190	17240 - 18190	17720
						corrected age[7]:	16240 - 17190	16720

[1] Dating by AMS (accelerator mass spectrometry) with the tandem accelerator at the Institute of Particle Physics at the Swiss Federal Institute of Technology Zurich (ETH).

[2] Calibration (2σ range) was carried out applying the IntCal04-calibration curve (Reimer et al., 2004).

[3] Position of the dated sample relative to the event horizon.

[4] Estimated by lineraly interpolating between two ^{14}C samples after correcting for the thickness of instantaneously deposited turbidite layers.

[5] Ages are rounded to the decade.

[6] Dates by Lister (1988).

[7] Correction of -1300 yrs to account for the likelyhood of overestimated ^{14}C ages (see text section 3.4.2.2).

[8] Sedimentation rates from Zao et al., (1984).

Beside the 5 above mentioned event horizon F, K, N, Q and U that all comprise at least 10 prominent large mass-flow and thick turbidite deposits in the central basin, two identified event horizons are also characterized by more than one evidences for lateral landsliding (event horizon C and I). Event horizon I is associated with 3 small mass-flow deposits in the vicinity of small lateral deltas and event horizon C shows 5 small to medium-sized mass-flow deposits, among which three occur close the deltas. Both horizons are also associated with deltaic wedge-shaped mass accumulation bodies indicating phases of higher remobilization along lateral deltas (see subsection 3.5.3). However, the multiple-deposit pattern might also suggest an earthquake trigger, although strong seismic shaking can be excluded as they would presumable destabilize more slopes at the same time.

Event horizon C is dated to 590–700 cal yr B.P. (1250–1360 A.D.) and might coincide with the M_W 6.9 Basel earthquake in 1356 A.D. (Meghraoui et al, 2001). Macroseismic reconstructions based on historical documents suggest that the northwestern part of Lake Zurich may have experienced macroseismic intensities close to VII (Mayer-Rosa & Cadiot, 1979), which is interpreted to be the threshold intensity for multiple subaquatic landslide initiation (Monecke et al, 2004; Strasser et al., 2006). However, an interdisciplinary revision of the 1356 A.D. Basel earthquake rather suggests slightly lower intensities for the study area (Fäh et al., subm.). In any case, the Basel earthquake remains a candidate to have triggered the Lake Zurich event C, because the mass-flow deposits are partly related to slope failures along lateral deltas where threshold stabilities might be lower (see subsection 3.5.3) and delta slopes may have been additionally «charged» by a historically documented super-regional flooding event in 1342 A.D. (Schwarz-Zanetti, 1998).

3.5.3 Deltaic remobilization events during climatic periods of higher clastic sediment supply

Event horizons D, E, G, H, L, M, O, R and S are characterized by either single lateral mass-flow deposits lacking more than one counterpart and/or by wedge-shaped mass accumulation bodies in distal deltaic areas. Given the fact that also the single lateral mass-flow deposits often occur close to lateral deltas these 9 event horizons are interpreted to reflect sediment remobilization events/periods along the lateral deltas. Additionally, periods of higher frequency of exceptional high discharge events in the small catchment and resulting hyperpycnal flows may partly explain the occurrence of the distal deltaic wedge-shaped mass accumulation bodies. For instance, such deposits are also associated with above-mentioned event horizon C (Fig. 3.10) and, hence, might partly be related to the historically documented super-regional flooding event in 1342 A.D. (Schwarz-Zanetti, 1998).

Slope stability conditions of deltas, especially in the proximal area, where the slope is steep, may be relatively close to a critical state where sediment failure may be triggered by only small external disturbances (e.g. weak seismic shaking) or even can occur spontaneously (Girardclos et al, 2007). Reduced stability conditions and thus the likelihood of delta collapse initiation can be caused by a variety of geological processes, among which the two most dominant are: (i) high sedimentation rates increasing the gravitational load and leading to the formation of excess pore pressure (Sultan et al, 2004) and (ii) biogenic gas production from decomposition of organic material reducing the inter-particle cohesion and friction (Coleman & Prior, 1988). Both the input of organic material and sedimentation rates are likely to be higher during periods of enhanced precipitation and run-off in the catchment of the small creeks laterally entering Lake Zurich.

The proposed influence of climate-controlled increase of sediment supply as the causing factor for subaquouse delta slope failures in Lake Zurich can be tested by plotting the occurrences of Holocene event horizons C, D, E, G, H, against reconstructed phases of mid-European lake level high-stands interpreted as proxy for higher precipitation and increased river run-off (Magny, 2004) (Fig. 3.11). However, the resulting correlation is ambiguous and, therefore, the Lake Zurich dataset does not allow for conclusive interpretation.

3.5.4 Exceptional event layers in Lake Zurich

Two event horizons (J and T) have been identified that are not associated with any mass-flow deposits or wedge-shaped mass accumulation bodies. Event T comprises an up to 1 m-thick deposit characterized by a ponding geometry with internal laterally-continuous very-low-amplitude reflections and thick homogeneous clay deposits in the seismic and core data, respectively (Fig. 3.7). It occurs at the lithological boundary between Unit 1a and 1b which has been interpreted to correspond to the time when the Linth glacier retreated behind the Hurden moraine (Lister, 1988). Therefore, it is likely that event T is somehow related to the termination of the Hurden Stage, but the physical process of sediment mobilization and deposition remains unknown.

Event J only is defined in cores from the central part of the deep basin (Fig. 3.7) and can not be resolved in the seismic data. It consist of two characteristic 1–2 cm-thick brownish turbidite layers only 2 cm apart (Fig. 3.9E) that occur in the lower part of lithostratigraphic Unit 3a (lacustrine chalk) and that can be correlated as marker beds throughout the deep basin in all cores. Palynological data from core ZHM54 (Sidler, 1988) show that these two layers comprise high amounts of pre-Quaternary pollen grains indicting a major clastic input from an alpine catchment (Hochuli, 2004, personal communication). The occurrence of the two characteristic clastic layers thus suggests two exceptional events likely related to exceptional flood events. They may have resulted for instance from outbreaks of a naturally-dammed lake somewhere in the alpine catchment of Lake Zurich, because floods resulting from local high precipitation events may not explain the deposits throughout the lower basin. It remains unclear whether the source of such events may be within the Sihl

catchment (if the Sihl at that time still was discharging into Lake Zurich) or within the catchment of the Linth or Wägital Aa. The latter appears to be less likely as the flood deposits would rather be expected to be deposited in upstream depocentres (e.g Obersee). However, the two layers of event J are somewhat similar and in comparable stratigraphic position as two exceptional clastic layers described in Lake Constance (Schneider et al, 2004). These two layers have been interpreted to be related to the failure of two rockslide dams in the catchment area of the Rhein river (deposited by the Flims and Tamins rockslides) and the catastrophically drainage of the landslide-dammed lakes resulting in major floods. However, although it would theoretically be possible that these exceptional flood events could somehow be connected to the catchment area of Lake Zurich (i.e. through the Walensee/Seez valley and the Linth river), the slightly older ages of event J (9700–10250 cal yr B.P) compared to the age of the Flims rockslide (9460–9490 cal yr. B.P. (Deplazes et al., 2007)) and the unlikelihood of clastic material reaching all the way down to the lower Lake Zurich basin, do not suggest a causal relation between event J and the Flims rockslide.

Among all reconstructed mass-movement events, event N is the most prominent showing 23 individual landslides deposits all over Lake Zurich and it is the only horizon, along which mass-movements deposits have been recovered in all cores (including shallow water cores ZHM52 and ZHK04-5; Fig 3.7). Strasser et al, 2008 show that this exceptional event horizon furthermore is associated with sediment waves indicating strong currents in the upper flat basin. On the basis of geomorphological and core data in downstream areas of Lake Zurich and of data presented here, Strasser et al., 2008 interpret that a reconstructed earthquake ~13760 cal yr B.P. may not only have triggered subaquatic landslides all over Lake Zurich but that primary earthquake shaking or secondary effects, such as landslide-generated waves, may have resulted in a sudden collapse of the Zurich moraine leading to a subsequent lake outburst flood lowering the lake level by ~12 m.

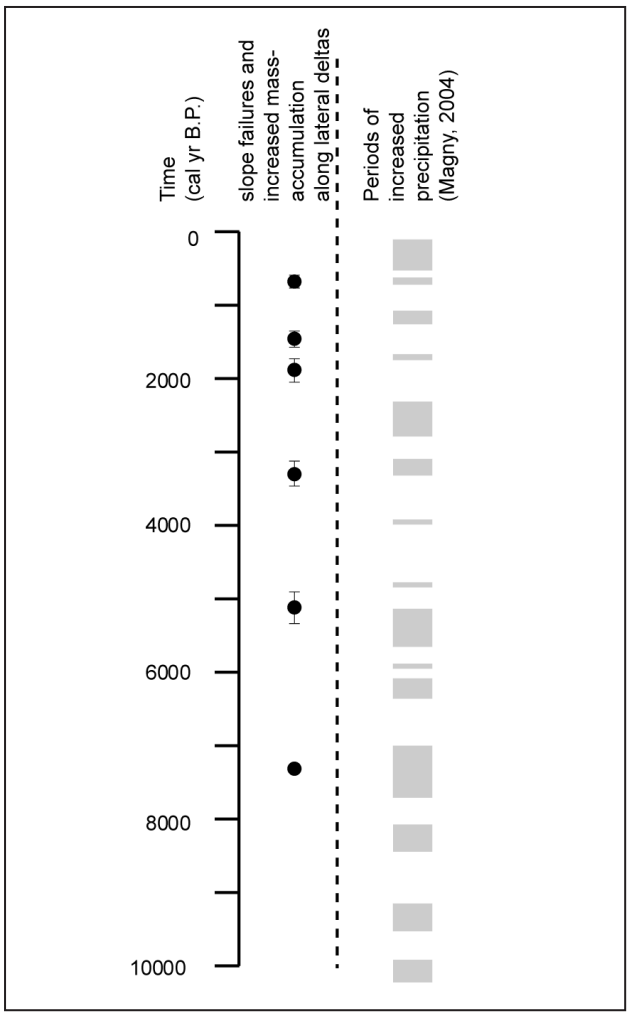

Figure 3.11: Left panel: Stratigraphic distribution of identified mass-movement horizons C, D, E, G, H, and I comprising single lateral mass-flow deposits closed to small lateral deltas and/or distal deltaic wedge-shaped mass-accumulation bodies interpreted to result from increased remobilization and slope failure processes along the delta. Right panel: Gray bars mark reconstructed periods of mid-European lake level high-stands interpreted as proxy for higher precipitation and increased river run-off (Magny, 2004).

3.6 Summary and conclusions

The combined basin-wide high-resolution seismic and core study of the subsurface of Lake Zurich enable identification and dating of Late Glacial-to-Holocene mass-movements deposits and allow for determination and characterization of their type, distribution and frequency. The resulting chronological event catalogue presents a record of varying environmental impacts and provides the basis for deciphering seismic vs. climatic trigger mechanism of subaquatic slope failures. Results reveal that a variety of potentially hazardous processes, such as earthquakes, outbursts and floods, affected the study area over the last ~17000 year. The presented mass-movement event stratigraphy provides first information on their frequency and impact, and eventually may yield the means for assessing the geo-hazard potential arising from such natural processes in the densely populated region around Lake Zurich.

A summary list of the main conclusions includes the following:

(1) 3 major simultaneously-triggered basin-wide lateral slope failure events (translational sliding) occurred at ~2210, 11600 and ~13760 cal yr. B.P. and are interpreted as the fingerprint of strong paleo-seismic activity in the Zurich area.
(2) Additionally, 2 smaller simultaneously-triggered slope failure events were identified (640 and 7270 cal yr. B.P), which also might be related to seismic events of lower local intensity. The younger event potentially corresponds to the historic 1356 A.D. Basel earthquake and suggests far-field seismic intensities in the Zurich area, strong enough to trigger subaqueous landslides.
(3) Two major mass-movement events (rotational sliding) occurred during the transition from the Pleniglacial to the Late Glacial time period and are likely related to the activity of the nearby Linth glacier.
(4) The record reveals higher frequency of Holocene mass movements in deltaic settings during specific periods that may be related to climate-controlled increase of sediment supply, supposing climatic causing factors for subaqueous delta slope failures.
(5) Two outstanding event layers, which are not related to lacustrine mass movements, suggest the occurrence of exceptionally high discharge events in the Alpine catchment around 9980 cal yr. B.P.
(6) The most prominent event layer (dated to 13760 cal yr. B.P.) shows 23 individual landslides deposits all over Lake Zurich and furthermore is associated with sediment waves indicating strong currents in the upper flat basin. These features are interpreted as the fingerprint of an earthquake-triggered collapse of the Zurich moraine dam that resulted in a large outburst of Lake Zurich.

4 MAGNITUDES AND SOURCE AREAS OF LARGE PREHISTORIC NORTHERN ALPINE EARTHQUAKES REVEALED BY SLOPE FAILURES IN LAKES

Published as: Strasser, M., Anselmetti, F.S., Fäh, D., Giardini, D., and Schnellman, M. (2006): Magnitudes and source areas of large prehistoric northern alpine earthquakes revealed by slope failures in lakes. Geology, 34, 1005–1008.

Abstract

This study presents evidences for three large paleo-earthquakes in central Switzerland with moment magnitudes (M > 6.5–7.0) significantly exceeding historically known values. These earthquakes occurred during the past 15000 years and were strong enough to simultaneously affect a large region that includes the present-day major cities of Lucerne and Zurich. Chronology, magnitudes and epicenters of these prehistoric earthquakes were reconstructed using temporal and spatial correlation of multiple subaqueous landslide deposits in Lake Zurich and Lake Lucerne through high-resolution seismic surveys, radiocarbon-dated sediment cores and spatial calculations using an empirical seismic attenuation model. Results indicate ongoing Alpine deformation that generated and could potentially generate destructive events in heavily-populated regions that are unaccustomed to seismic activity during historic times.

Zusammenfassung

In dieser Studie werden drei grosse Schweizer Paleo-Erdbeben rekonstruiert, welche Moment-Magnituden von > 6.5–7 erreicht haben und somit die bisherigen historisch bekannten Höchstwerte signifikant überschreiten. Diese Erdbeben, welche sich in den letzten 15000 Jahren ereigneten, waren so stark, dass sie gleichzeitig Gebiete, welche heute die Städte Zürich und Luzern umfassen, zum Erschüttern brachten und im Zürich- und Vierwaldstättersee subquatische Rutschungen auslösten. Die zeitliche Abfolge, Magnituden und Epizentren dieser Beben werden mittels Ablagerungen von subaquatischen Rutschungen rekonstruiert. Dazu werden hochauflösende reflexionsseismische Untersuchungsmethoden, radiometrische Datierungen an Sedimentkernen sowie empirische Gleichungen für die Ausbreitung und Abschwächung seismischer Wellen mit zunehmender Distanz vom Epizentrum und Erdbebenszenarien verwendet. Unsere Daten lassen vermuten, dass andauernde Alpine Deformation zu grösseren Erdbeben in der jüngeren geologischen Vergangenheit führte und auch in Zukunft zu Beben führen könnte, welche heute starkbesiedelte Gebiete ohne nennenswerte historische Erdbebenvergangenheit stark treffen würde.

4.1 Introduction

Long-term earthquake models and probabilistic seismic hazard assessments require knowledge of a well-dated and quantitative earthquake history. In intraplate continental regions with low crustal deformation rates, the recurrence interval of strong earthquakes often exceeds the time span covered by instrumental and historical records, making seismically active fault-zones difficult to identify. Hence, knowledge about the temporal and spatial distribution of prehistoric seismic events with long recurrence intervals is essential for understanding regional seismicity and for assessing earthquake hazard-potential of such regions. During the past 30 yr, paleoseismology has provided a wealth of information about paleoseismicity in a variety of geologic settings (Michetti et al., 2005; Vittori et al., 1991). This information usually relates to identification of specific events on recognized active faults (Sieh, 1978) or to more general descriptions of secondary effects (i.e., soil liquefactions, elevation changes, landslides) suggesting the occurrence of a prehistoric event (Keefer, 2002; Sims, 1975). However, earthquake parameter determination from only secondary effects still poses a challenge in paleoseismic research (Michetti et al., 2005). Here we constrain the chronology, magnitudes and epicenters for the intraplate area of central Switzerland by correlating in time and space sedimentary deposits of seismically-triggered subaquatic lacustrine landslides, and by spatial macroseismic reconstructions using a grid-search approach with a calibrated intensity-attenuation model.

Large earthquakes often spur mass movements, such as subaqueous landslides, that are recorded in sedimentary archives (Hampton et al., 1996). On 18 September 1601, the greater Lucerne area in central Switzerland was hit by one of the largest known earthquakes in central Europe (moment magnitude M = 6.2) that damaged parts of the city of Lucerne and its surroundings (Schwarz-Zanetti et al., 2003). The villages along the shoreline of Lake Lucerne experienced waves up to 4-m high and a subsequent seiche that lasted several hours. These effects were produced by 13 synchronous earthquake-triggered subaquatic landslides in Lake Lucerne (Schnellmann et al., 2002). In the temporally and spatially continuous sediments of perialpine lakes in central Switzerland coeval mass-movement deposits can thus be tracked throughout

the entire basin as the «fingerprint» of prehistoric seismic events. In the here-studied lake basins of Lake Zurich and Lake Lucerne (Fig. 4.1), paleoseismic shaking can be singled out as the trigger mechanism because these basins lack major stream deltas and lake-level fluctuations are minor, so that additional potential trigger mechanisms for multiple slope failures can be excluded (Hampton et al., 1996). Furthermore, lacustrine landslide-deposits in such settings record this intensity-threshold of seismic shaking independent of the earthquake focal-mechanism as revealed by calibration of multiple landslide deposits associated with historic earthquakes in central Switzerland. This demonstrates that sublacustrine slope-failures occurred only within areas that experienced shaking of macroseismic intensities (EMS98) VII or more (Monecke et al., 2004). These sedimentary archives are thus critical components for quantitatively assessing the seismic hazard potential in a region including the major urban centers of Zurich and Lucerne with their high population density, key communications nodes, and critical lifelines.

4.2 Seismotectonic setting

Lucerne and Zurich are situated in the North Alpine foreland basin, 7 and 40 km north of the North-Alpine nappe front, respectively (Fig. 4.1). This frontal thrust strikes WSW-ENE and marks the northern topographic boundary of the Alpine nappes formed during the Tertiary collision between Europe and Africa. In the foreland, earthquakes generally occur throughout the crust to Moho level (~30 km), nucleating in crystalline basement with predominantly strike-slip focal mechanisms and minor normal faulting components. Upper-crust shallow thrust and strike-slip faulting dominate the external Alpine nappes (Kastrup et al., 2004). The observed change in earthquake-depth distribution and style of faulting between the foreland and the inner-alpine zones reflect the superposition of the regional compressional stress, induced by large-scale continental convergence, with the uniaxial tensional stress related to lateral spreading within the Alpine orogenic belt (Kastrup et al., 2004). This is in agreement with the overall central-alpine geodynamic situation characterized by the indentation of the Adriatic block into the European Plate (Fig. 4.1) and isostatic plate forces acting on the steeply SSW dipping lithosperic slab (Kissling, 2004). It further suggests that the Aar massif basement uplift (Fig. 4.1) is still growing in response to ongoing Alpine collision (Persaud and Pfiffner, 2004).

In the foreland, the largest known historic earthquake (M = 5.4) occurred in 1674 A.D. near Thalwil, ~20 km southeast of Zurich (Fäh et al., 2003), whereas the inner-alpine central Switzerland region south of Lucerne was seismically more active throughout history. Three events with M ≥ 5.7 were chronicled during the past millennium, including the 1601 A.D. M = 6.2 event that may be associated with a ~20-km-long, left lateral strike-slip fault system (Sarnen fault system; Fig. 4.5B) (Gisler et al., 2004). However, the historical record of seismicity in central Switzerland spans only ~1000 yr, and certainly does not reflect the overall seismic potential. Previous paleoseismological studies in Lake Lucerne calibrated the effect of seismic shaking in lake basins using the 1601 A.D.

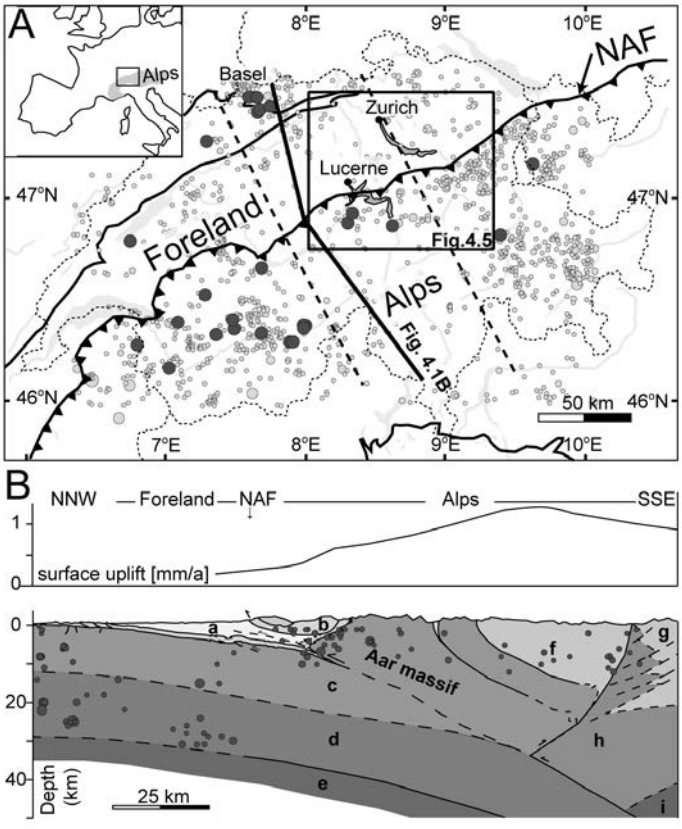

Figure 4.1: A) Location map showing tectonic units and epicenters of instrumentally (gray dots) and historically (M ≥ 5.5, dark grey dots) recorded earthquakes (Fäh et al., 2003). Box in the center locates the study area with Lake Zurich and Lake Lucerne. Profile line and swath (dashed lines) indicate Alpine profile and maximum earthquake-projection distance in Figure 4.1B. NAF = North-Alpine nappe front. B) Present-day uplift rates (after Schlatter and Marti, 2002) along Alpine tectonic profile (after Pfiffner and Heitzmann, 1997; Pfiffner and Kühni, 2001) with depth distribution of known earthquake (M > 2) hypocenters since 1975 (Deichmann et al., 2000). a = Molasse basin, b = European margin (EM) Mesozoic cover, c = EM upper crustal basement, d = EM lower crust, e = EM mantle, f = Penninic uppercrustal basement and cover, g = Apulian Plate (AP) upper crust and cover, h = AP lower crust, i = AP mantle.

earthquake and identified 5 additional paleoseismic events (with effects similar to those produced by the 1601 A.D. event) that occurred in the past 15000 years. (Schnellmann, 2004). Due to the limited geographical distribution of the investigated archives, however, estimations of epicenters and magnitudes remained dubious.

4.3 Paleoseismologic observation in Lake Zurich

To identify the occurrence of strong prehistoric seismic shaking in the foreland area of Zurich, we examined sediments in Lake Zurich for characteristic multiple landslide patterns by surveying a dense grid of high-resolution seismic profiles (3.5 kHz pinger source). We identified numerous landslide deposits in the seismic data based on chaotic-to-transparent seismic facies that contrast with continuous reflections produced by regular, undisturbed sediments (Fig. 4.3). We then connected the top of each mass-movement deposit at its pinch-out point with a distinct seismic-stratigraphic horizon. Such horizons represent isochrons that can be traced throughout the lake basin, allowing recognition of synchronous landslide events. Three event horizons were identified, each comprising at least 10 individual mass-movement deposits across the entire lake basin. In the deepest part of the lake, these event horizons are associated with multiple stacked turbidite deposits lacking intercalated background sediment (Fig. 4.4), confirming the simultaneity of individual sublacustrine landslides derived from source areas of varying distance. In analogy to observations in Lake Lucerne, we interpret these three event horizons as subsurface «fingerprints» of three prehistoric earthquakes.

To date these earthquakes we retrieved 6 piston cores of up to 11 m in length from key locations identified in the seismic data. Each of the three seismic-stratigraphic multiple landslide horizons were dated independently three to five times by combining AMS ^{14}C analysis of terrestrial organic matter, tephrachronology, sedimentation rate and seismic data-to-core correlations (Tables 4.1, 4.2). The resulting ages of the three events are 2200 ±55, 11530 ±185 and 13840 ±145 cal. yr B.P.

These results indicate that every few thousand years, the foreland region of Zurich experienced seismic events strong enough to trigger basin-wide slope instabilities. The ages of these three events match the ages of three of five reconstructed prehistoric earthquakes recorded in Lake Lucerne (Schnellmann, 2004) (Fig. 4.2). This correlation

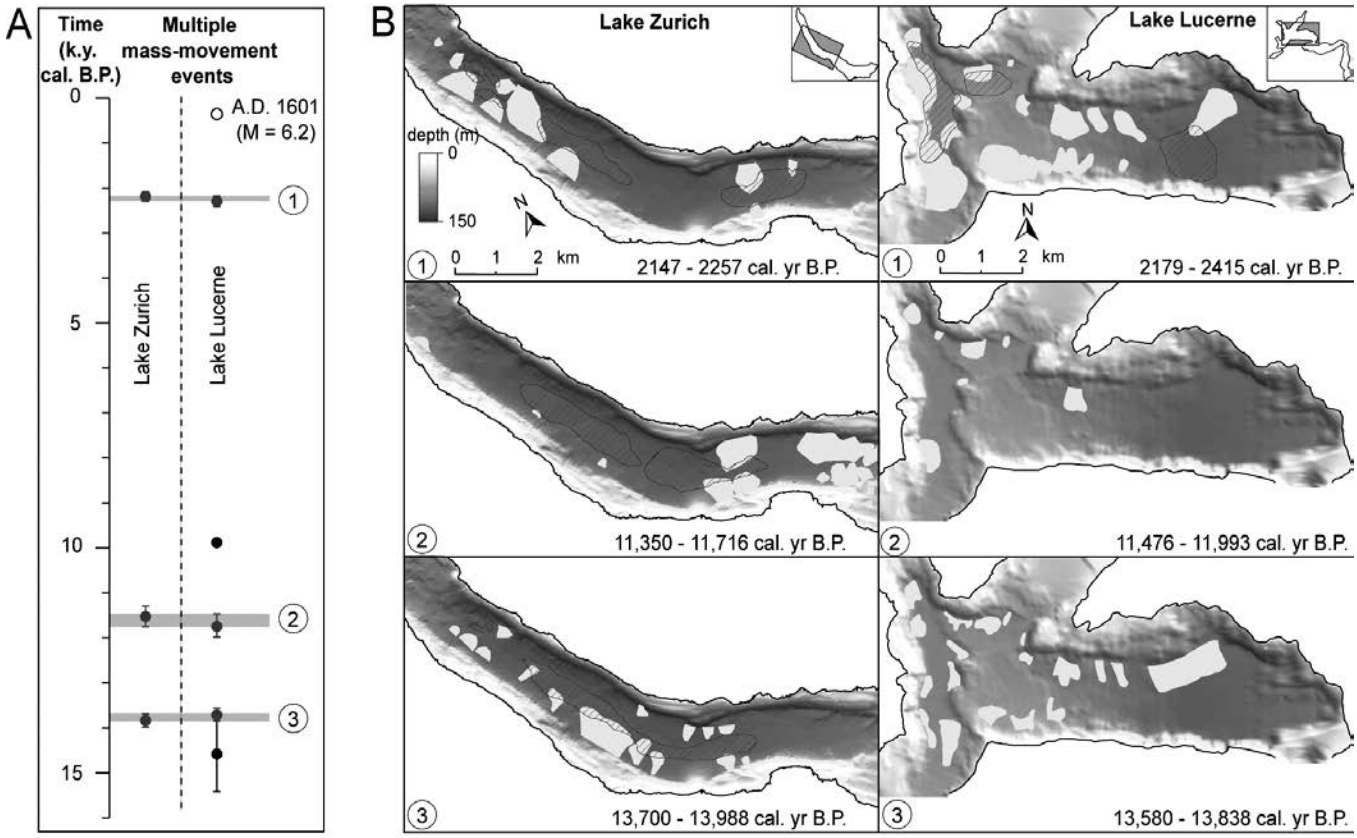

Figure 4.2: A) correlation between dated multiple mass-movement events assigned to paleo-earthquakes in Lakes Zurich (this study) and Lucerne (Schnellmann, 2004). The black open circle indicates the historic 1601 A.D. M=6.2 earthquake, black dots correspond to prehistoric regional events similar to 1601 A.D. event that are not recorded in Lake Zurich and grey dots correspond to 3 large prehistoric earthquakes recorded in both lakes (numbered from 1 to 3). Gray bars indicate age-range overlap of the two dated layers in both lakes. B) Maps showing simultaneous multiple mass-movement deposits (light grey areas) in both lakes for the three large paleo-earthquakes. Hatched areas mark extent of turbidite deposits associated with the landslides.

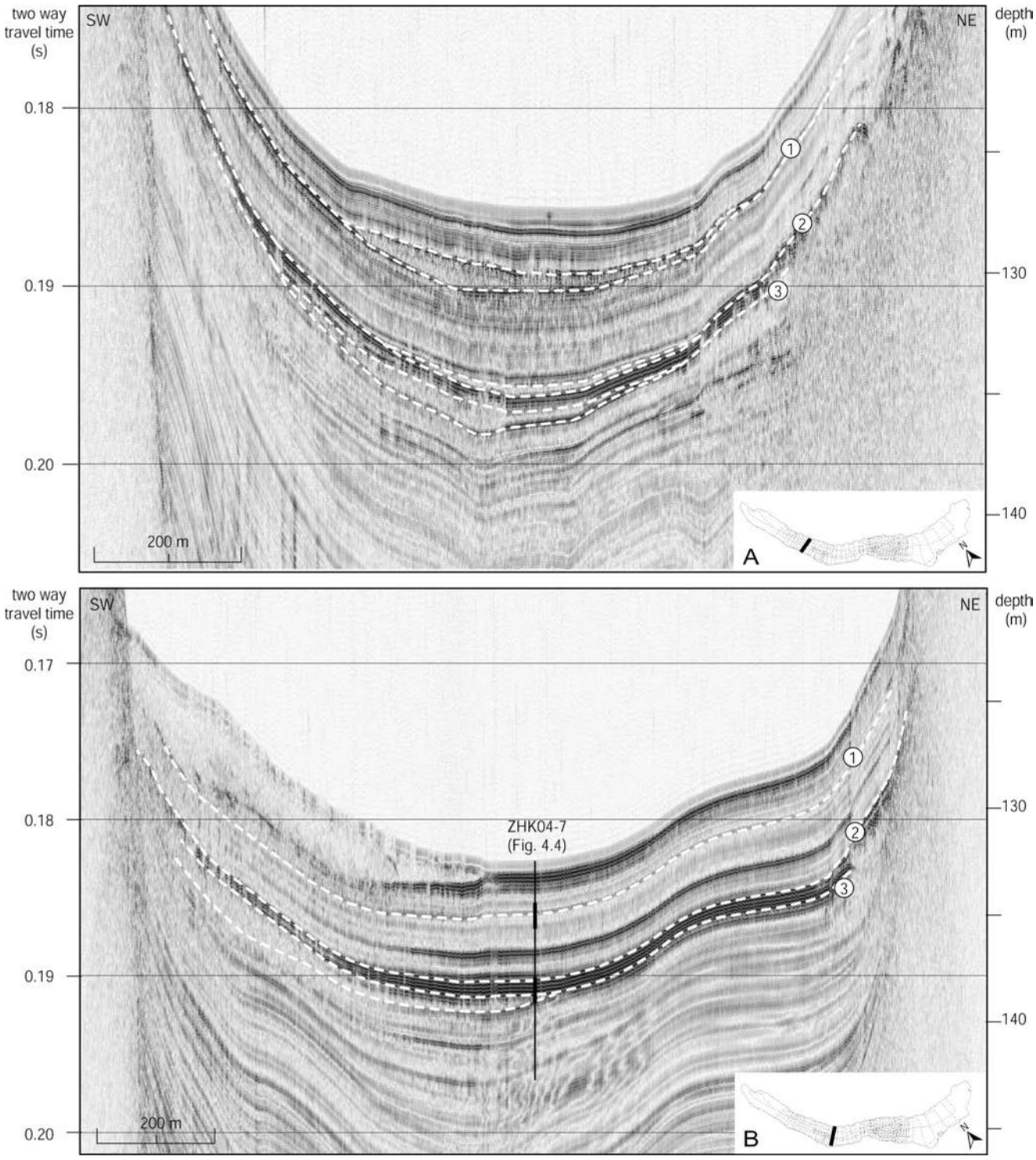

Figure 4.3: Two of the total 127 (see insets in the lower right corner) 3.5 kHz seismic profiles showing the subsurface of Lake Zurich where we identify the mass movement deposits due to their chaotic-to-transparent seismic facies and their characteristic onlap geometries. Dashed lines show the three seismostratigraphic horizons and their corresponding landslide deposits. 1, 2 and 3 correspond to the 2200±55, 11530±185 and 13840±145 cal yr B.P. event, respectively, where multiple simultanous slope failures occurred throughout the lake basin. b) Seismic profile with location of core ZHK04-7. Intervals marked with bold lines are shown as photographs in Figure 4.4. Note prominent mass-movement deposit in the uppermost part on the left side. It corresponds to the 1875 A.D. landslide triggered by human construction along the shore (Kelts, 1980).

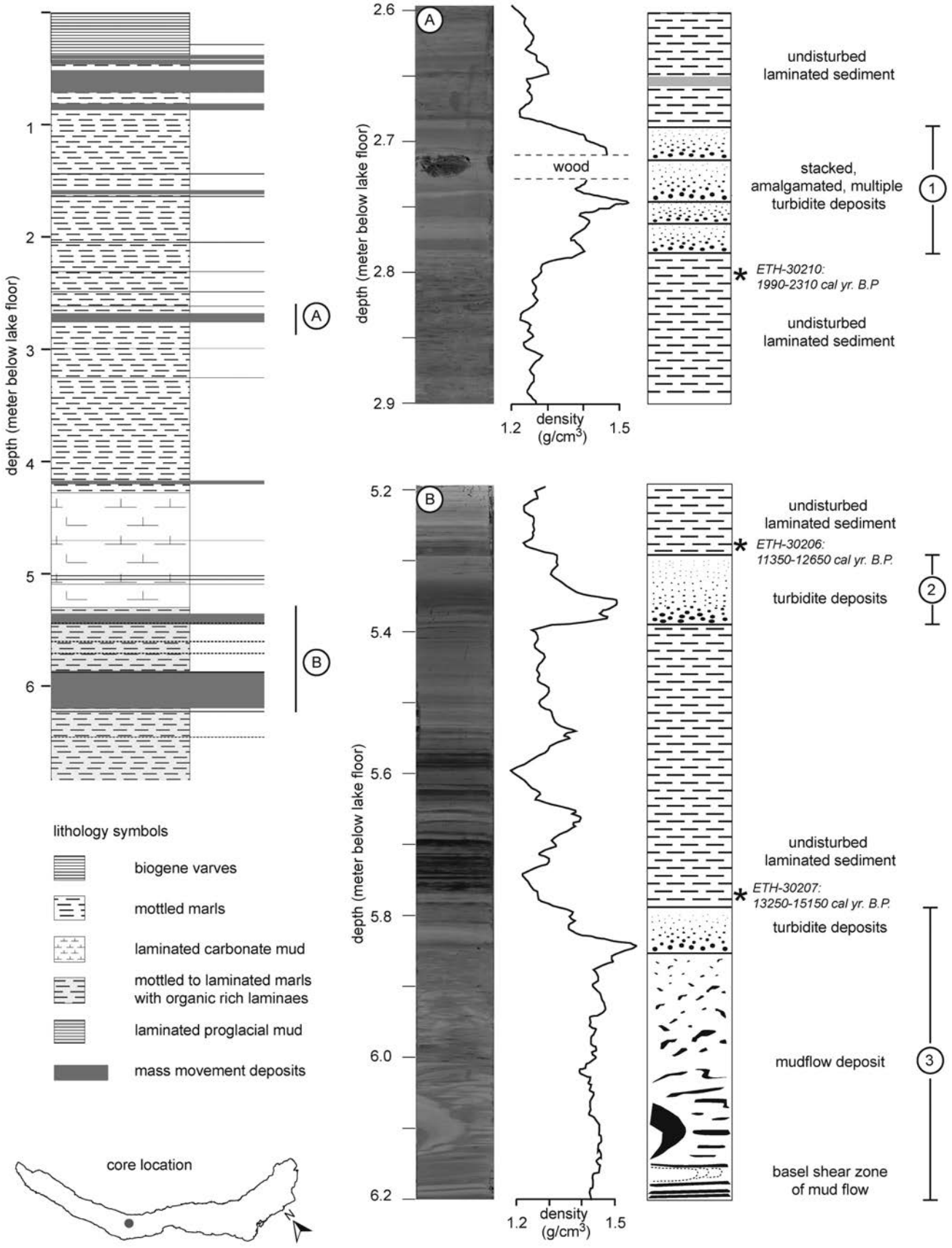

Figure 4.4: Lithologic profile, bulk density log and grayscale core photos (by Urs Gerber) at two specific sections (A and B) from gravity piston core ZHK04-7 retrieved from the deepest central part of Lake Zurich. It shows the distinct sedimentologic «fingerprint» (i.e. mass flow deposits and turbidite deposits) of sublacustrine slope failures triggered by the three major paleo-earthquakes (numbered from 1 to 3). indicate position of AMS 14C sample (see Table 4.1).*

Table 4.1: ^{14}C ages and calibration of samples used to date the prehistoric event horizons.

Core Nr.	Location [1]	Depth in core [m]	Sample Nr.	Sample age[2] [^{14}C yr B.P.]	Sample age[3] [cal. yr B.P.]	$\partial^{13}C$ [‰]	material
ZHK04-7	688526 / 236159	5.32	ETH-30206	10230 ± 85	11350 - 12650	-27.7 ± 1.2	leaf remains
ZHK04-7	688526 / 236159	5.76	ETH-30207	11710 ± 100	13250 - 15150	-26.7 ± 1.2	wood
ZHK04-7	688526 / 236159	2.81	ETH-30210	2135 ± 55	1990 - 2310	-32.2 ± 1.2	leaf remains
ZHK04-5	699687 / 230486	3.78	ETH-30215	8995 ± 80	9750 - 10400	-27.4 ± 1.2	leaf remains
ZHK04-1	685585 / 240583	1.195	ETH-30711	1585 ± 50	1340 - 1570	-26.5 ± 1.2	leaf remains
ZHK04-1	685585 / 240583	2.395	ETH-30712	3230 ± 50	3350 - 3580	-29.2 ± 1.2	leaf remains
ZHK04-5	699687 / 230486	4.12	ETH-30715	11560 ± 90	13150 - 13950	-25.3 ± 1.2	wood
Zübo 1980 [4]	687615 / 237266	5.75	GL8 [8]	9990 ± 150	11058 - 11975	-	wood
Zübo 1980 [4]	687615 / 237266	7.5	GL11[8]	12800 ± 250	14000 - 15595	-	wood
LST [5]	-	-	Tephra	11,230 ± 40	13003 - 13755	-	

[1] Location is given in Swiss Grid (CH1903) Coordinates.

[2] Dating by AMS (accelerator mass spectrometry) with the tandem accelerator at the Institute of Particle Physics at the Swiss Federal Institute of Technology Zurich (ETH).

[3] Calibration (2σ range) was carried out applying the Intercal98-calibration curve (Stuiver and Reimer, 1993).

[4] Dates by Lister (1988).

[5] Laacher See Tephra (LST), radiocarbon dated by Hajdas et al. (1995).

Table 4.2: Dating of prehistoric events.

Sample Nr.	Sample age[1] [^{14}C yr B.P.]	Sample age[2] [cal. yr B.P.]	Offset[3] [cm]	Sed.rate[4] [cm/yr]	Horizon age [cal. yr B.P.]	Horizon age (overlap range) [cal. yr B.P.]	Center of overlap [5] [cal. yr B.P.]
<u>Event horizon 1</u>							
ETH-30711	1585 ± 50	1340 - 1570	-37	0.05	2082 - 2312		
ETH-30712	3230 ± 50	3350 - 3580	60	0.05	2147 - 2377		
ETH-30210	2135 ± 55	1990 - 2310	3	0.06	1937 - 2257	2147 - 2257	2200
<u>Event horizon 2</u>							
ETH-30206	10230 ± 85	11350 - 12650	-	0.02	11350 - 12650		
ETH-30215	8995 ± 80	9750 - 10400	-14	0.01	11109 - 11759		
LST [6]	11230 ± 40	13003 - 13755	21	0.01	10964 - 11716		
GL8 [7]	9990 ± 150	11058 - 11975	-	-	11058 - 11975	11350 - 11716	11530
<u>Event horizon 3</u>							
LST [6]	11230 ± 40	13003 - 13755	-12	0.04	13304 - 14056		
ETH-30207	11710 ± 100	13250 - 15150	-3	0.04	13325 - 15225		
ETH-30715	11560 ± 90	13150 - 13950	-5	0.03	13317 - 14117		
LST [6]	11230 ± 40	13003 - 13755	-7	0.03	13236 - 13988		
GL11[7]	12800 ± 250	14000 - 15595	15	0.05	13700 - 15295	13700 - 13988	13840

[1] Dating by AMS (accelerator mass spectrometry) with the tandem accelerator at the Institute of Particle Physics at the Swiss Federal Institute of Technology Zurich (ETH).

[2] Calibration (2σ range) was carried out applying Intercal98-calibration curve (Stuiver and Reimer, 1993).

[3] Position of the dated sample relative to the event horizon.

[4] Derived from C^{14} data.

[5] Ages are rounded to the decade.

[6] Laacher See Tephra (LST), radiocarbon dated by Hajdas et al. (1995).

[7] Dates by Lister (1988).

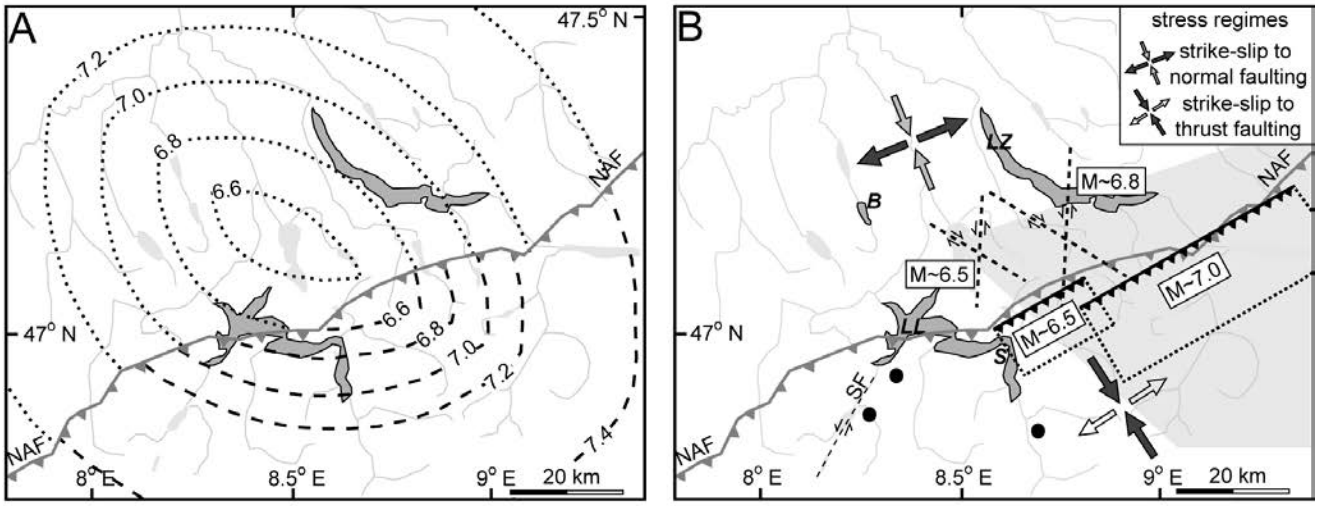

Figure 4.5: A) Zones of earthquake epicenters (dotted and dashed lines for deep foreland and shallow northern Alpine source, respectively) of minimum given magnitude sufficient to produce the observed landslides in Lake Zurich and Lake Lucerne, identified by the grid-search approach (Bakun and Wentworth, 1997). NAF = North-Alpine nappe front. B) Map showing possible epicentral locations (shaded area) satisfying positive and negative paleoseismologic evidences in different lake archives (LZ = Lake Zurich, LL = Lake Lucerne, B = Lake Baldegger, S = Lake Seelisberg). Arrows indicate the two different stress regimes in the foreland and Alpine setting (Kastrup et al., 2004). Superimposed black dashed lines and rectangles conceptually indicate potential Alpine foreland strike-slip fault orientations and projected rupture areas of thrust-type earthquakes, respectively (Wells and Coppersmith, 1994), as expected in the present stress field. Note that exact locations of faults are speculative, because to date, no seismogenic faults are known in the area. Black dots south of Lake Lucerne indicate epicenters of the three historical earthquakes (M ≥ 5.7) and black dashed line south west of Lake Lucerne indicates the known ~20 km long seismically active Sarnen strike-slip fault system (SF) (Gisler et al., 2004).

indicates that three very large earthquakes shook central Switzerland in the past 15000 years, strong enough to trigger multiple mass movements in these two lakes located ~40 km apart. Using the overlap of event-age ranges in both lakes, we date these events at 2220 ±40, 11600 ±120 and 13770 ±70 calendar yr B.P. (Fig. 4.2).

4.4 Source parameter determination

To estimate minimum magnitudes at epicentral locations required to produce mass movements in both lakes, we first assigned EMS98 intensities VII to the sites of lacustrine landslides in Lakes Zurich and Lucerne. This value is the accepted threshold intensity for basinwide landsliding which was calibrated with historic earthquakes in central Switzerland (Monecke et al., 2004). We then calculated magnitudes over a grid of trial source locations (Bakun and Wentworth, 1997) using an empirical intensity-attenuation relation (Fäh et al., 2003), a function of epicentral distance and hypocentral depth*. Based on geologic, structural and seismotectonic information (Fig. 4.1) (Kastrup et al., 2004), we selected a deeper average depth for events in the foreland, and a shallower depth for potential Alpine thrust fault scenarios south of the North-Alpine nappe front. The

*** Source Parameter Determination:**

The calculations of magnitudes over a grid of trial source locations (Bakun and Wentworth, 1997) are based on an empirical intensity attenuation relation (Fäh et al., 2003). The calibration relations are:

For shallow earthquake sources (< ~10 km depth):

$M_i = [I_i - 0.096 + 0.043d_i]/1.27$ (for $d_i < 70$km)

$M_i = [I_i + 1.93 + 0.0064d_i]/1.27$ (for $d_i > 70$km)

For deep earthquake sources (> ~10 km depth):

$M_i = [I_i + 1.73 + 0.030d_i]/1.44$ (for $d_i < 70$km)

$M_i = [I_i + 3.04 + 0.0064d_i]/1.44$ (for $d_i > 70$km)

M_i is the moment magnitude estimates, I_i the EMS98 Intensity value at site i, and d_i the distance (km) from the source location to site i. I_i was set to 7 for all sites of lacustrine landslides in Lakes Zurich and Lucerne, as this is the accepted threshold intensity for basinwide landsliding calibrated with historic earthquakes in Central Switzerland (Monecke et al., 2004). To account for uncertainties of the threshold values of macroseismic intensity for basin wide landsliding and to estimate a lower bound for the calculated magnitude in our study we also applied a more conservative threshold values of 6.5 in the grid search calculations which reduces the resulting magnitude estimates by about 0.3 magnitude units. For high magnitudes (M > 6) the empirical intensity attenuation relation for shallow earthquake sources is not well established because calibration events with M > 5.5 are rare. However, sensitivity analyses of uncertainties related to the hypocenter depth location are relatively small (e.g. applying the attenuation relationship for a deep source south of the NAF rather than a shallow source would only increase magnitude estimates in the near epicentral distance (< 20 km) by ~0.2 magnitude units).

result of this grid-search approach indicates a minimum required magnitude of M = 6.5 if all three events were centrally located between the two lakes, whereas values approaching and exceeding M = 7 are required if the events were located farther away (Fig. 4.5).

To further constrain the potential epicentral area, we considered other well established lacustrine paleoseismic archives within a radius of 60 km from the study area (Monecke et al, 2006) (Fig. 4.5). Lake Baldegger, situated west of the study area, has no earthquake-generated deposits identified in the critical periods for all three events. In the grid-search calculations including these negative evidences we therefore assigned EMS98 intensities <VII to the Lake Baldegger site. Results reveal only valid solutions for a confined sector suggesting that epicentral areas for all three seismic events were located to the east of Lake Lucerne and southeast of Lake Zurich (Fig. 4.5). Lake Seelisberg, a small mountain lake south of Lake Lucerne with specific characteristics not comparable to the other lakes and therefore not considered for grid-search calculations, shows positive evidence for seismically induced deformations dated to 11660 ±590 cal. yr B.P. (Monecke et al, 2006). This further confirms the occurrence of a large paleo-earthquake around 11600 cal. yr B.P.

4.5 Discussion

Due to the absence of known seismogenic faults with surface ruptures and the lack of direct observations in the instrumental and historical catalogue, the location and geometry of faults capable of producing the three large prehistoric earthquakes cannot be identified directly. Nevertheless, plausible earthquake scenarios may be formulated using geologic, structural and seismotectonic information (Fig. 4.1), including the general stress regime for the area NW and SE of the North-Alpine nappe front (Kastrup et al., 2004) and generally accepted relationships between magnitudes and rupture area (Wells and Coppersmith, 1994) (Fig. 4.5). The spatial reconstruction suggests that large prehistoric earthquakes were probably not related to the historically active Sarnen strike-slip fault system south of Lake Lucerne. Furthermore, the calculated magnitude of an event located south of Lake Lucerne would be M ≥ 7.2 and rupture length would be ≥ 60 km (Wells and Coppersmith, 1994), whereas the observed length of the Sarnen fault system is only ~20 km.

A possible scenario involves a deep-seated strike-slip fault below the foreland basin, capable of producing M ≥ 6.5 events. With the present regional stress regime in the northern Alpine foreland (Kastrup et al., 2004), such a seismogenic fault would strike NW-SE (dextral) or N-S (sinistral), which is in agreement with a recently identified, seismically active N-S trending sinistral strike-slip fault in the crystalline basement below the western Swiss molasse basin (Kastrup, 2002).

An Alpine thrust fault system which strikes parallel to the front of the Alpine nappes, is a second and geologically more plausible scenario that could produce the required M 6.5–7.0 event. In the east of the study area, where instrumental earthquake data indicate thrust fault focal-mechanisms close to the North-Alpine nappe front (2nd April, 1989 in Weesen, M = 3, (Fäh et al., 2003)), the calculated minimal magnitude would amount to M ~7. Such earthquakes could be produced by release of accumulated NW-SE compressional stress related to an active basal thrust beneath the Aar massif, along which the central Aar massif is overthrusted onto the autochthonous foreland cover and forms a growing fault-propagation fold (Fig. 4.1). Driving forces for such a major thrust fault might be ongoing Alpine collision (Persaud and Pfiffner, 2004) and/or isostatic plate forces acting on the NW-ward retreating European lithospheric slab (Kissling, 2004). Post-glacial faults in the eastern Swiss Alps (Persaud and Pfiffner, 2004) and strong NW-SE gradients in surface-uplift rates across the northern front of the Aar massif (Schlatter and Marti, 2002) (Fig. 4.1) provide further support for an active basal thust beneath the Aare massif.

4.6 Conclusion

We identify three prehistoric earthquakes more intense than any historically known earthquake in the Alpine area (1601, M = 6.2) and much more intense than those recorded in the foreland (1674, M = 5.4). These prehistoric events are comparable to the largest historically documented earthquake in central Europe (1356, Basel, M = 6.9 (Meghraoui et al., 2001)). Notably, they also affected the location of present-day Zurich, a densely-populated region that was previously believed to be free of major seismic hazards. Furthermore, the occurrence of three strong events along the northern Alpine topographic front within the last 15 000 years indicates active Alpine deformation that potentially will generate rare but destructive events in the future.

We conclude that temporal and spatial correlation of precisely dated paleoseismologic archives, such as the record of sublacustrine landslide deposits, is a valuable tool to constrain chronology, magnitudes and epicenters of prehistoric seismicity. This approach is especially critical in intraplate settings, often characterized by faults that lack surface expression and produce events on timescales much longer than recorded human history.

5 LATE PLEISTOCENE EARTHQUAKE-TRIGGERED MORAINE DAM FAILURE AND OUTBURST OF LAKE ZURICH, SWITZERLAND

In press for publication as: Strasser, M., Schindler, C., and Anselmetti, F.S. (2008): Late Pleistocene earthquake-triggered moraine dam failure and outburst of Lake Zurich, Switzerland. Journal of Geophysical Research-Earth Surface, doi:10.1029/2007JF000802.

Abstract

Lakes impounded by moraines may be considered hazardous in glaciated areas throughout the world because dams can fail suddenly producing destructive floods with peak discharges far in excess of normal flows. This chapter presents a comprehensive case study in the Zurich area (Switzerland) that reveals several independent lines of evidences for the occurrence of a Late Pleistocene (~13760 cal yr. B.P.) moraine breach and subsequent Lake Zurich outburst (discharge volume ~2.5 km^3). Seismic and core data are used in order to track and date the geological fingerprint of this event. Data from areas downstream of the lake show coarse-grained massive (> 25 m-thick) reworked morainic deposits behind 4 breached zones. In Lake Zurich, sedimentary structures recorded in a paleo-water depth of ~36 m indicate strong outburst-induced currents. Hydrodynamic calculations reconstructing the sediment transport capacity explaining the observed bedforms allow estimating averaged outburst discharge to exceed minimum values of ~2400 m^3s^{-1}. The potential maximal magnitude of the outburst is inferred from calculations considering critical flow conditions through the breaches revealing estimated peak discharge of ~20600 m^3s^{-1}. Results further allow for discussion of long-term causes and short-term trigger mechanisms of the dam failure that occurred several thousand years after moraine formation and it is shown that it coincides with a reconstructed strong northern alpine earthquake (Magnitude > 6.5). The study thus suggests that catastrophic drainage of Lake Zurich was initiated as a consequence of the moraine dam failure that either was triggered by primary earthquake shaking or by secondary effects, such as overtopping by landslide-generated waves.

Zusammenfassung

In glazialen Gebieten können Seen, welche durch Moränenwelle aufgestaut sind, ein erhebliches Naturgefahrenpotential beinhalten, da die stauenden Dämme plötzlich versagen können und daraus resultierende Seeausbrüchen zu katastrophalen Fluten mit enormen Abflussraten führen könnten. In dieser Studie werden mehrere, unabhängige Evidenzen in und um den Zürichsee präsentiert, welche auf einen Spät-Pleistozänen (~13760 Jahre vor heute) Durchbruch des Zürcher Moränenwalls und einen darauffolgenden Zürichsee-Ausbruch mit einem rekonstruierten Ausflussvolumen von ca. 2.5 km^3 schliessen lassen. Mit Hilfe von reflexionsseismischen Daten und Bohrkerndaten identifizieren, werden die geologischen Spuren dieses Ereignisses charakterisiert und datiert. Unterhalb des Moränendamms zeigen sich hinter 4 Durchbruchszonen grobkörnige, massive, mehr als 25 m mächtige Ablagerungen von aufgearbeitetem Moränenmaterial. Im Zürichsee existieren Sedimentstrukturen in Paleo-Wassertiefen von ca. 36 m, die auf grosse Wasserströmungen hinweisen. Mit Hilfe von hydrodynamischen Berechnungen können die Strömungen, welche benötigt werden um solche Strukturen zu formen, abgeschätzt werden. Daraus lässt sich auch rekonstruieren, dass durchschnittliche Ausflussraten während des Zürichsee-Seeausbruch mindestens ~2400 m^3s^{-1} erreicht haben müssen. Maximal Spitzenabflussraten dürften in der Grössenordnung von ~20600 m^3s^{-1} gelegen haben, wie sich aus Berechnungen über kritische Fliesseigenschaften durch die Durchbruchszonen herleiten lässt. Im Weiteren wird gezeigt, wie sich langzeitliche klimatische Veränderungen auf die Stabilität des Moränendamms auswirkten, welcher erst mehrere Tausend Jahre nach seiner Entstehung durchbrochen wurde. Es wird gezeigt, dass der Durchbruch zeitlich mit einem starken nordalpinen Erdbeben mit einer Magnitude von > 6.5 auf der Richterskala zusammenfällt. Die Untersuchungen rekonstruieren somit den katastrophalen Abfluss des Zürichsees als Folge des Moränendurchbruchs, welcher entweder primär durch seismische Erschütterungen oder sekundär von überschwappenden Wellen, welche durch die Wasserverdrängung von erdbebeninduzierten Rutschungen im See entstehen können, ausgelöst wurde.

5.1 Introduction

Moraine-dammed lakes are common features in glaciated areas throughout the world. They are considered as a hazard to people and infrastructure in downstream areas because dams may fail suddenly producing destructive floods with peak discharges far in excess of normal flows (e.g. COSTA and SCHUSTER, 1988; CLAGUE and EVANS, 2000; HUGGEL et al., 2004). Such lakes form during phases of glacial retreat behind moraine ridges deposited during an earlier advance. In alpine areas, still existing moraine-dammed lakes were formed after some glacial readvances and subsequent retreats during the Late Pleistocene, or much later, after the maximum advances of the Neoglacial (Little Ice Age) between the mid-19th and early 20th century. Scenarios for the future waning of glaciers in the context of global warming (e.g. OERLEMANS, 2000) anticipate a significant increase in number and extent of potentially hazardous moraine-dammed proglacial lakes.

Historically documented failures of moraine dams, subsequent lake outbursts and their geomorphic effects have been reported from numerous locations, including North America (O'CONNOR and COSTA, 1993; CLAGUE and EVANS, 2000), the Himalayas (WATANABE and ROTHACHER, 1996), the Andes (REYNOLDS, 1992) and the European Alps (HUGGEL, et al., 2002; BLASS et al., 2003). These studies have shown that such events can be caused by different mechanisms including: i) moraine dam overtopping by a wave or a series of waves generated by mass movements into or within the lake or by upstream glacial outbursts, (ii) piping controlled by seepage in mostly silty and sandy diamictic deposits, (iii) ice core or interstitial ice melting within the moraine wall during times of climatic warming, (iv) earthquake shaking or (v) combinations of above mentioned mechanisms (see review in COSTA and SCHUSTER, 1988 and CLAGUE and EVANS, 2000).

Considering longer geologic timescales, many studies document large prehistoric lake outburst floods that resulted from collapses of natural dams (not exclusively moraines but also landslide-, ice- and others dams (e.g. RUDOY, 2002; SCHNEIDER, et al., 2004; CARTER, et al., 2006) (see general considerations in COSTA and SCHUSTER (1988)). Especially in Late Pleistocene and Early Holocene times very large outburst floods occurred during the destabilization of large continental ice sheets after the Last Glacial Maximum (LGM). They include the «Spokane flood» from Lake Missoula (O'CONNOR and BAKER, 1992), Lake Agassiz paleofloods (SMITH and FISHER, 1993) and Lake Bonneville flood (MALDE, 1968). Theses floods are generally interpreted to have had significant impact on landscape evolution in downstream areas, for instance in the context of formation of outburst gorges and changes in river routing systems (e.g. TELLER and THORLEIFSON, 1983; RUDOY, 2002)). Furthermore, they potentially could have triggered short-term climatic excursions due to the large fresh water input into the ocean that temporarily affected the thermohaline circulation pattern (CLARKE, et al., 2004; BROECKER, 2006). Whereas most of these documented mega-floods are related to ice-dam collapses draining both supra- and/or subglacial lakes, detailed case studies on processes, causes and consequences of Late Pleistocene postglacial lake outbursts resulting from moraine-dam failures are rare. Such geologic information is crucial in order to assess the hazard potential of future events, especially in the context of present-day climatic warming and rapid glacier retreat, during which the formation rate of potentially hazardous moraine-dammed lakes is increasing.

Here we present results from a detailed case study in the Zurich area (Central Switzerland, Fig. 5.1) that aims to reconstruct a Late Pleistocene moraine-dam failure and subsequent lake outburst. Occurrence of such an event has been hypothesized by SCHINDLER (1971), but has so far lacked conclusive interpretation of trigger mechanism, accurate timing and consequences. Our new geophysical, sedimentological and geomorphological data of Lake Zurich sediments and of downstream deposits combined with hydrodynamic calculations allow us to reliably support and refine SCHINDLER's outburst hypothesis (1971) and to discuss in detail long-term causes and short-term trigger mechanism(s) and their impact as recorded in geological archives.

5.2 Geological / Geomorphological background

5.2.1 Regional setting

The Linthplain-Lake Zurich-Limmat valley occupies a perialpine, glacially overdeepened, NW-SE trending trough situated in the northern part of the Swiss Plateau (Fig. 5.1). During the last glacial period it was fully occupied by two coalesced alpine glaciers (Linth Glacier and a branch of the Rhine Glacier; Fig 5.1B) with a maximum extent during the LGM reaching ~20 km downstream of today's City of Zurich. During deglaciation, intermediate phases of stagnation and minor glacial readvances resulted in a succession of recessional moraines separating several basins and damming proglacial lakes (PENK and BRÜCKNER, 1909; VON MOOS, 1942; SCHINDLER, 1968; 1974; 2004). The most prominent ice-marginal stages are from NW to SE (from oldest to youngest) (i) Schlieren Moraine (SM in Fig. 5.1) damming the former Schlieren Lake, (ii) Zurich Moraine (ZM) damming Lake Zurich, (iii) Hurden Moraine (HM) separating Lake Zurich from Obersee, (iv) Reichenburg (RM) and (v) Schänis Moraines (SäM) (Fig.5.1). In early Late Glacial times immediately after the glacial retreat back into the alpine valleys, an extended paleolake combining today's Lake Zurich, Walensee and probably also Lake Constance (MÜLLER, 1995) occupied most of the formerly glaciated area. This paleolake was dammed by the Zurich Moraine at a lake level of 416–418 m above sea level (masl) that was significantly higher than today's Lake Zurich level (406 masl). This is indicated by elevated glacio-lacustrine deposits along the shorelines and higher levels of proglacial delta deposits in the vicinity of the Hurden, Reichenburg and Schänis Moraines (SCHINDLER, 1971; 2004). The altitude level of these delta deposits allowed for absolute paleolake level reconstruction after

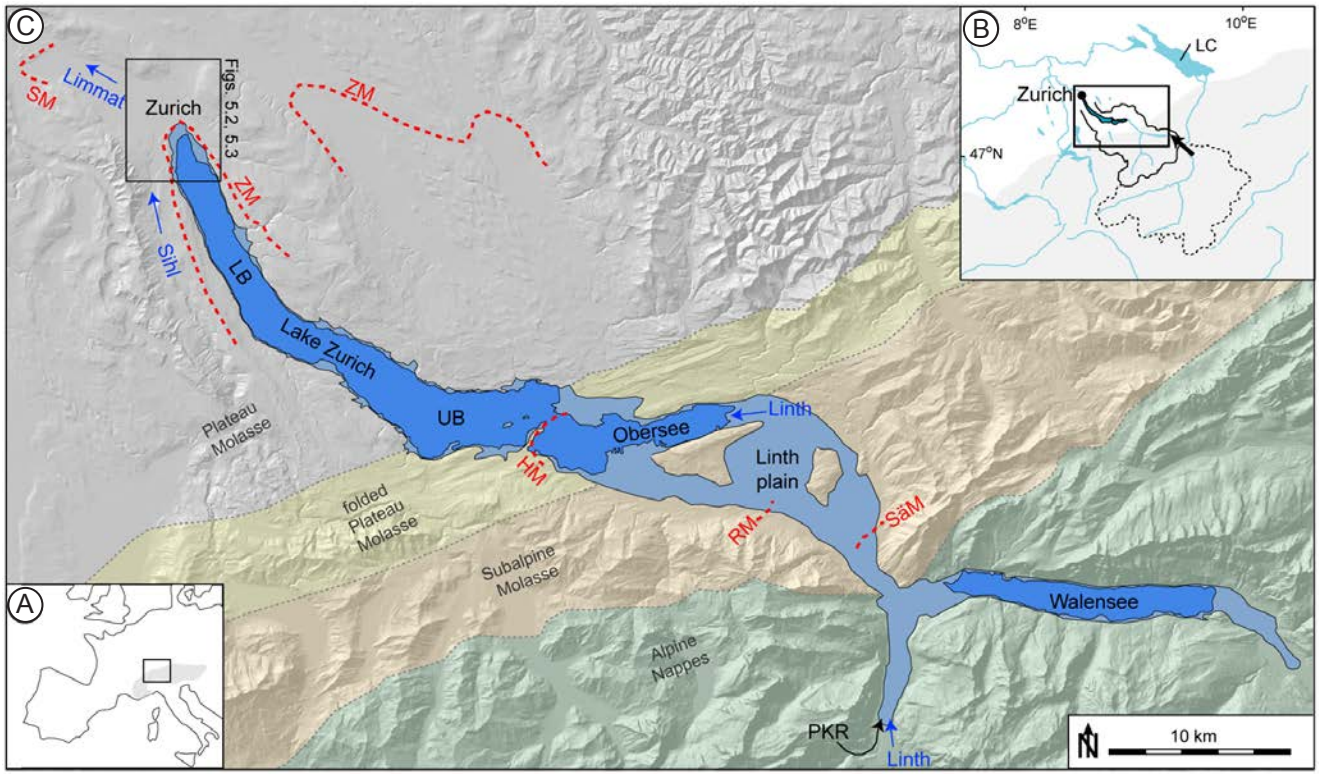

Figure 5.1: Geographic location of the study area embedded in its geomorphic and geological context. A) location with respect to Europe and the Alpine chain (gray shaded area). B) Close up view showing the Alps (gray shaded area) and the northern Swiss Plateau. The catchment area of Lake Zurich (Linth river) is mapped with a solid black line. Dashed line indicates additional glacial catchment area during the Last Glacial Maximum, when a branch of the Rhine glacier coalesced with the Linth glacier (indicated by black arrow). LC = Lake Constance. C) Outlines of today's Lake Zurich (LB = Lower Basin; UB = Upper Basin), Obersee and Walensee (blue) and reconstructed extent (light blue) of the paleolake at ~14000 cal yr. B.P. (see section 5.5.3). Blue arrows and annotations indicate flow direction and major rivers, respectively. Dashed red lines show prominent geomorphic features resulting from moraines that were formed during overall glacier retreat. From oldest to youngest: SM = Schlieren Moraine, ZM = Zurich Moraine, HM = Hurden Moraine, RM = Reichenburg Moraine, SäM = Schänis Moraine. Black arrow (PKR) marks location of Planggen-Klöntal Rockslide [Schindler, 2004]. Background: Shaded relief of digital elevation model (dhm25, Swisstopo) overlain by the general tectonic setting. Rectangle in the northwestern part of figure C indicates location of subsequent figures.

correcting for differential surface uplift between the Zurich and Walensee area (measured uplift rates today, are ~0.1 and 0.6 mm/yr, respectively (Kahle et al., 1997)). Constant altitude levels of paleodelta deposits in the whole study area indicate that a general lake level highstand prevailed during all recessional deglaciation phases after the glacier retreated from the lower Lake Zurich basin at ~17600 cal yr. B.P. (Lister, 1988; calibrated using InterCal04 calibration curve by Reimer, et al., 2004).

In the eastern part of the study area, the paleolake size successively was reduced by the progradation of the Linth delta (Fig. 5.1). This resulted in the separation between Lake Zurich and Walensee ~11500 cal yr. B.P and in the infilling of the Linthplain during Holocene times (Schindler, 2004). Paleolake level since ~Bølling/Allerød and throughout Holocene times, as reconstructed from altitude information of delta deposits, shore terraces and lake shore dwellings, respectively, was significantly lower than the 416–418 masl during the deglaciation phase. These lower lake levels only slightly oscillated between min. 403 and max. 407 masl corresponding to climatic variations, precipitation pattern and Sihl river sediment discharge that partially may have influenced the Limmat river outflow situation (Schindler, 1971; Magny, 2004; Riesen and Naef, 2007)

5.2.2 City of Zurich area

In the Zurich area, the Zurich Moraine (maximal age ~23700 cal yr. B.P (Schlüchter and Röthlisberger, 1995; calibrated using InterCal04 calibration curve by Reimer, et al., 2004)) reaches a height of ~20 m above the present valley floor. The moraine wall itself is composed of up to

three amalgamated structurally complex frontal recessional moraines (Fig. 5.2A). They are partly covered with basal tills from a glacier oscillating back and forth several times during the Zurich Stage (SCHINDLER, 1968). In the north the Schlieren Lake (estimated paleolake level ~405 masl (SCHINDLER, 1968)) initially occupied most of the Limmat valley. High sediment supply from the Sihl river and subsequent Sihl delta progradation continuously reduced the size of the Schlieren Lake so that since early Holocene times the basin has been completely filled (Fig. 5.2B).
Today, there are only isolated remnant hills from the frontal part of the Zurich Moraine, which are separated from each other by four ~200–400 m-wide eroded zones (Fig. 5.2B). In all of these four areas data from drill cores and open constructions pits reveal the top of the indurated moraine deposits to be systematically at a similar topographic level of 402–405 masl. These moraine surfaces occur below ~4–7 m of alluvial, lacustrine and artificial infill deposits (e.g. SCHINDLER, 1968; 1971; JÄCKLI, 1989; and references therein). This indicates that at these locations the uppermost ~20–30 meter of the moraine dam has been eroded sometimes in the past and that the breaches afterwards have been infilled to the present-day level. Several studies (e.g. HUBER, 1938; JÄCKLI, 1989) have reported that the Sihl river temporarily discharged into Lake Zurich backwards through the eroded breaches as indicated by Sihl delta deposits accumulated in Lake Zurich during Bølling/Allerød to Early Holocene times.

5.2.3 Moraine breach hypothesis (SCHINDLER, 1971)

Due to the fact that the level of Lake Zurich was initially higher than the base level of the Sihl river (Fig. 5.2A), and because of observations that all four proposed breach locations are eroded down to a similar topographic level (402–405 masl), SCHINDLER (1971) postulated that the erosion of the moraine wall was mainly caused by an instantaneous moraine failure sometime during Late Glacial times. As a consequence, the level of Lake Zurich must have been lowered within a very short time by ~12 m (i.e. the difference between paleolake level and lake level at the beginning of Sihl delta sedimentation in Lake Zurich).
SCHINDLER's hypothesis (1971) was partly supported by observations from drill cores and open construction pits immediately north of the former moraine wall that showed thick reworked morainic deposits (hereafter termed RM-deposits) intercalated between normally consolidated lake sediments assigned to the Schlieren Lake below, and alluvial gravels assigned to the Sihl fan and Limmat river above.
Since the early 1970's, however, only very few studies tested this hypothesis (FURGER, 1991; SCHINDLER, 2004), and it has not been shown so far whether these RM-deposits conclusively reveal the occurrence of a moraine-dam failure and subsequent lake outburst. Furthermore, the effects that such an event would have had on Lake Zurich and on downstream parts of the Limmat valley, as well as the exact timing and triggering mechanism, remain unknown.

5.2.4 Lake Zurich

Lake Zurich can be divided into two basins: (i) a northwestern, elongated deep basin (max depth 135 m) with steep lateral slopes and a flat basin plain, and (ii) a flat and shallow (~20 m water depth) upper basin, which is separated from the lower basin by a subaqueous rock barrier showing a complex, step-like morphology descending towards the NW (HSÜ and KELTS, 1970; SCHINDLER, 1976). A mostly sub aerial sill formed by the Hurden Moraine with only 2 m deep lake passages separates Lake Zurich from Obersee in the E.
Several previous studies in the 1970's and 1980's described Lake Zurich's geology and its sedimentary and environmental evolution since the LGM (HSÜ and KELTS, 1970; 1984; SCHINDLER, 1974; 1976; KELTS, 1978; GIOVANOLI, 1979; PIKA, 1983; LISTER, 1985; 1988; SIDLER, 1988). These studies are mainly based on data from the deep northwestern basin comprising some seismic lines and piston cores, and one deep drill hole termed «Zübo» (see HSÜ and KELTS, (1984) and references therein). These data reveal that in the lower Lake Zurich basin, the molasse bedrock is covered with an up to 140 m-thick, mainly glacial and glacio-lacustrine infill. The majority of these sediments were accumulated in a subglacial environment. Only the uppermost ~30 m were deposited after the glacier retreated from the lower Lake Zurich basin (see lithostratigraphical description in section 5.4.2.2). In this upper sedimentary succession, none of the previous studies specifically addressed the correlation of characteristic event layers throughout the lake in order to test the moraine-dam failure and lake outburst hypothesis.

5.3 Methods

With the objective to identify and date traces of the proposed lake outburst, we refined the existing sedimentary model of the postglacial infill of the lower Lake Zurich basin and extended it to the upper basin by acquiring new high-resolution seismic reflection data and four new long sediment piston cores. A dense grid of ~300 km of single channel 3.5 kHz seismic profiles (pinger source) was acquired and allowed for imaging the subsurface in a quasi 3-D fashion. The source/receiver was mounted on a cataraft that was pushed in front of a small vessel. DGPS-positioning with a maximum error of ±2 m guaranteed accurate navigation. The digitally-recorded data were processed using both a flat gain and band-pass filtering. Two-way travel time was converted to water depth and sediment thickness using a constant velocity of 1450 ms^{-1}.
Four Kullenberg-type gravity piston cores (KELTS et al., 1986), each 8–10 m in length, were recovered at key positions identified in the seismic data to ground truth the seismic data, for detailed sedimentological analyses and dating. The cores were scanned with a GEOTEK multisensor core logger, which measures bulk density by gamma ray attenuation, p-wave velocity and volumetric low field magnetic susceptibility. Afterwards, cores were

split, photographed and sedimentologically described. One core section that recorded a conspicuous sedimentary succession was imaged with a medical fluoroscope X-ray instrument in order to visualize sedimentary structures that were not visible in the cores macroscopically. The same distinctive interval was analyzed for grain size distribution of bulk sediment using laser diffraction techniques (Malvern Mastersizer Hydro 2000S) at ~0.5 cm intervals along the split core. Accelerator mass spectrometry ^{14}C analysis on terrestrial organic matter (mainly leaf fragments) sampled at different stratigraphic levels in three cores were performed at the Particle Physics Laboratory of ETH Zurich to date the sedimentary succession. Radiocarbon ^{14}C-ages were calibrated using the InterCal04 calibration curve (Reimer et al., 2004). Non-calibrated ages given in previous studies were also calibrated (Reimer et al., 2004), so that all ages in this study refer to the same time scale.

In order to evaluate whether the described RM-deposits (Schindler, 1971) downstream of the Zurich Moraine can be related to the proposed moraine-dam failure, published as well as unpublished core information from the Zurich City area were collected and compiled (Kempf and Walter, 1985; Kempf, et al., 1986; unpublished data provided by geo-consulting companies Jäckli AG, Dr. von Moos AG, Sieber Cassina + Partner AG) (Auxiliary Material, Table A 5.1). Here, we only considered interpreted log information from cores reaching deep enough to clearly identify the RM-facies (see section 5.4.1). Visual spatial core-to-core correlation then allowed reconstructing the relative stratigraphic position, extent and distribution of thickness of these target deposits.

5.4 Data and Results

5.4.1 Reworked morainic deposits (RM-deposits)

Several boreholes drilled in the urban area of Zurich during the last ~40 years recovered a characteristic lithological unit composed of massive diamictic deposits containing subangular, sometimes striated cobbles and boulders, suggesting a glacial origin or glacial deposits as source material (Kempf and Walter, 1985; Kempf et al., 1986; unpublished data provided by geo-consulting companies Jäckli AG, Dr. von Moos AG, Sieber Cassina + Partner AG) (Auxiliary Material, Table A 5.1). This unit is normally consolidated and overlies either laminated lacustrine silt and fine sand or well-sorted alluvial sand and gravel deposits that also are normally consolidated and lack any evidences of being formed or affected by glacial processes. In core logs, the diamictic deposits were described and interpreted as «moränen-artig» (morainic), «verschwemmte Moräne» (flushed till deposits), «verschleppte Moräne» (remobilized till deposits) or «moränenartige Murgang Ablagerungen» (morainic debris flow deposits). From its sedimentary facies, absent evidence of glacial compaction and its peculiar stratigraphic position within a normally consolidated postglacial sedimentary succession, these deposits (here summarized as RM-deposits) are interpreted to indicate a postglacial remobilization of moraine material.

Systematic mapping of thickness, stratigraphic position and elevation of the RM-deposits base and top reveal distinctive spatial depositional features (Fig. 5.3). In the western moraine-proximal part, the deposits form two small well-pronounced lobes with maximum thickness of ~15 to 20 m at their apex points that coincide with the positions of two eroded breach locations through the Zurich Moraine. These two lobes have a length of ~200–600 m. Their stratigraphic position implies that they were deposited above Sihl fan deposits with a contact at an elevation level of ~395 to 400 masl. In the eastern proximal part, the RM-deposits are up to 30 m-thick and stratigraphically overly mostly proglacial lake deposits at ~370–380 masl. Only in the easternmost part the unit is thinner and overlies alluvial fan deposits assigned to a small local creek draining the eastern flank of the Limmat valley (Wolfbach; Fig. 5.3) at ~395 masl. At ~3 km distance from the Zurich Moraine the unit is 5 to 10 m-thick, and a fining and thinning towards more distal parts can be observed in the bore log data. Further downstream, core logs lack any descriptions of the RM-facies but a conspicuous, up to 5 m-thick sand layer was recovered at the stratigraphic position between the lacustrine sediments of Schlieren Lake below and coarse alluvial deposits assigned to the Limmat river above.

5.4.2 Lake Zurich data

5.4.2.1 Seismic stratigraphy

Seismic penetration of the 3.5 kHz signal amounts to ~50 and ~75 ms, corresponding to ~35 and ~60 m in the lower and upper basin, respectively (Fig. 5.4). The imaged succession can be divided into two main seismostratigraphic units:

(i) The lower seismic Unit A comprises a thick (~15–25 m and up to 55 m in the lower and upper basin, respectively) succession of acoustically stratified sediments characterized by parallel, widely-spaced reflections showing alternating high and low seismic amplitudes. Towards the basin margins, these reflections are more closely spaced and often onlap onto the acoustic basement, indicating a dominant ponding-style of sedimentation.

(ii) The upper seismic Unit B (~5–7 m thick) is characterized by closely-spaced, parallel reflections (medium-to-high and low-to-medium amplitudes in the lower and the upper basin, respectively). Unit B forms a drape across the entire basin, which also generally covers the steep slopes and the bedrock high.

In the deep basin the two seismic units are separated by a thin package (0.5–1 m thick) of coherent, high-amplitude reflections. Sedimentary bodies with a horizontal extent

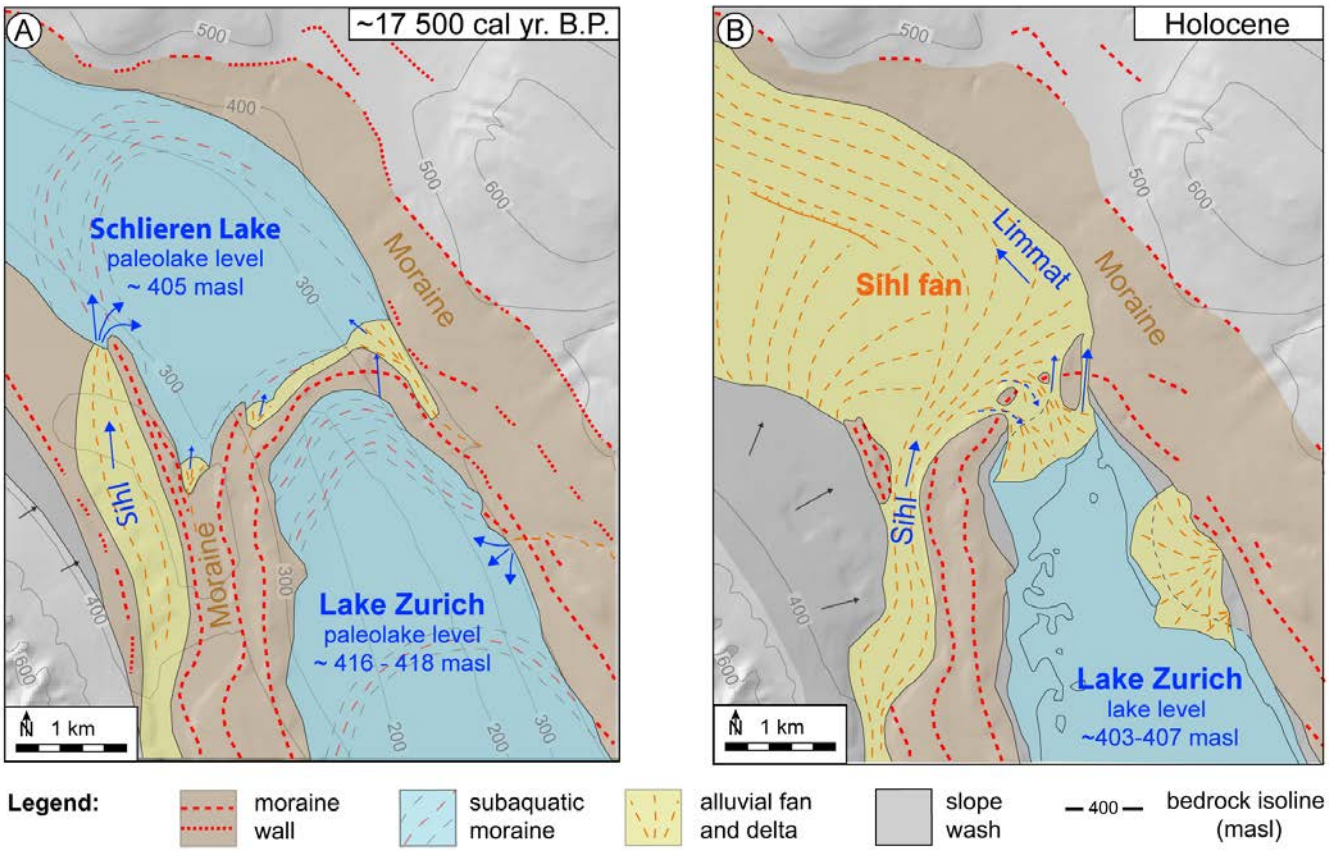

Figure 5.2: Maps showing the reconstructed geomorphologic situation in the area of the City of Zurich based on unpublished reports and core information from geo-consulting companies Jäckli AG, Dr. von Moos AG, Sieber Cassina + Partner AG and publications by Schindler (1968), Kempf et al. (1986) and Jäckli (1989): A) Situation during early Late Glacial times after the Linth Glacier left the Lake Zurich basin (~17500 cal yr. B.P). B) Situation during Holocene times. Background: Shaded relief of digital elevation model (dhm25, Swisstopo) and isohypse of molassic bedrock after Jäckli (1989).

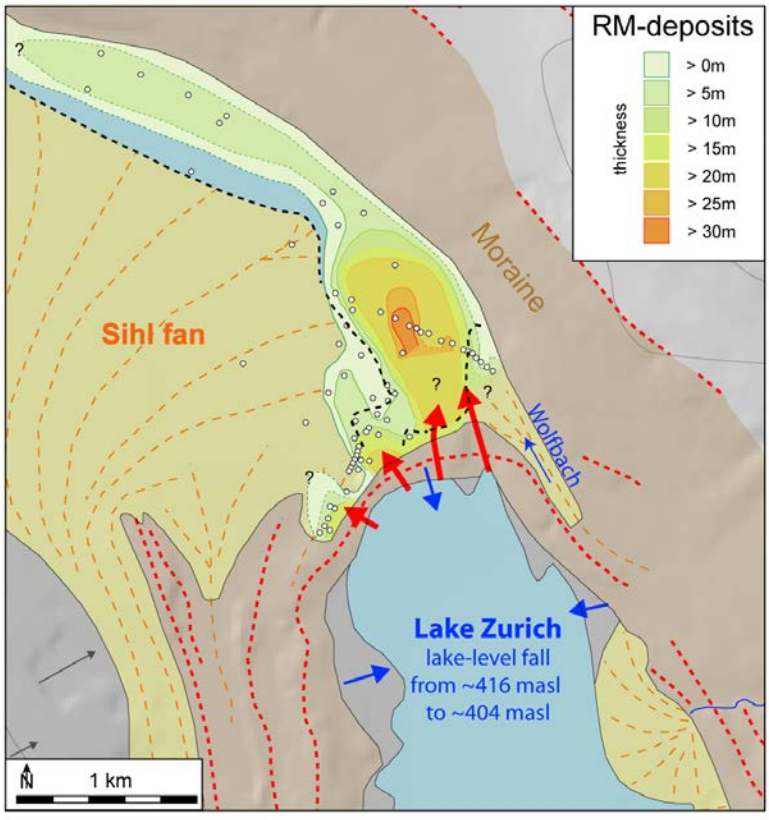

Figure 5.3: Map showing reconstructed thickness distribution of reworked morainic deposits (RM-deposits). The reconstruction is based on core logs from unpublished reports and core information from geo-consulting companies Jäckli AG, Dr. von Moos AG, Sieber Cassina + Partner AG and publications by Kempf and Walter (1985) and Kempf, et al. (1986). Open circles indicate locations, where core information was available. Question marks indicate areas, where data coverage was not sufficient enough to reconstruct exact extent and thickness of the RM-deposits. Red arrows indicate positions of four breaches eroded through the frontal ring of the Zurich Moraine. Black dashed lines indicate boundaries between areas, where the RM-deposits stratigraphically overlay Sihl fan (western part), Schlieren Lakes deposits (central part), and local alluvial fan deposits (eastern part), respectively.

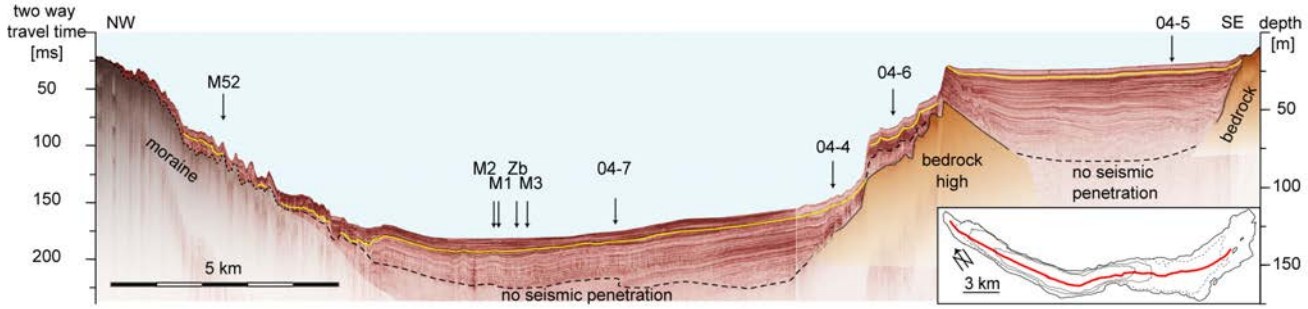

Figure 5.4: 3.5 kHz reflection seismic profile (pinger source) imaging the subsurface of Lake Zurich along the whole longitudinal lake axis and locations of cores shown in Figure 5.5. Yellow line in the seismic data marks the characteristic E-layer showing multiple mass-movement deposits (Figs. 5.7A and B) and wavy seismic features (Fig. 5.7D) in the lower deep and upper flat basin, respectively. It also corresponds approximately to the boundary between seismostratigraphic Unit A below and Unit B above. Inlet in the lower right corner shows location of the seismic line (solid red line). Contour interval is 50 m. Dotted contour line marks 20 m-depth contour line and aims to clarify basin morphology in the upper flat basin.

of a few 10's–100's of meters with internal chaotic-to-transparent seismic facies and clear lateral pinch-out geometries can be identified throughout the sedimentary succession. They indicate that slumping and landsliding along the relatively steep lateral slopes occasionally punctuated the otherwise continuous postglacial sedimentation in Lake Zurich.

5.4.2.2 Lithostratigraphy

All four acquired sediment cores recovered the characteristic postglacial stratigraphic succession that reflects the sedimentary and environmental evolution of Lake Zurich as already described in previous studies from cores in the central part of the deep basin (Giovanoli, 1979; Hsü and Kelts, 1984; Kelts, 1978; Lister, 1985; Pika, 1983; Sidler, 1988). Figure 5.5 shows a compilation of available core information and physical property data from Lake Zurich along the longitudinal lake axis. The general sedimentary succession comprises three lithologic units (from bottom to top):

- Lithologic Unit 1 «glaziale Seebodenlehme» - plastic mud

Sticky, medium-gray, plastic clays to silty clays with high bulk densities showing distinct up to 5 cm-thick laminations in the lower part (laminated plastic mud), thin mm-scale laminations intercalated with yellowish, mm-scale silt to fine sand layers in the middle part (faintly laminated plastic mud) and homogenous to mottled textures in the upper part (mottled plastic mud). This lithologic unit corresponds to the lower seismic Unit A described above. Thicker clastic laminae in deep-water cores contrast thinner laminae in shallow-water cores and thus confirm the ponding depositional style of this sedimentary unit. The lithology and infill pattern indicate glacio-lacustrine sedimentation by underflows in a proglacial environment (Kelts, 1978; Hsü and Kelts, 1984; Lister, 1985).

- Lithologic Unit 2 «Basaler Faulschlamm» - iron sulfide mud

Dark greenish-gray, fine-grained mud with low carbonate content and low bulk densities showing a distinct appearance of several highly FeS-pigmented black laminations and intercalated cm-thick sandy and muddy turbidites. From its stratigraphic position, this unit corresponds to the seismic high-amplitude reflections in the transition zone between seismic Units A and B. It is interpreted that, with postglacial climatic amelioration and the final retreat of the glaciers back into the Alps, sediment supply into the lake was reduced and the lake became stratified. Lacustrine biota increased and oxygen content in the bottom-water dropped occasionally to anoxic levels, resulting in characteristic FeS-pigmented black laminations of the lithological unit (Kelts, 1978; Pika, 1983).

- Lithologic Unit 3 «Seekreide» and «Seekreide-Mergel»- lacustrine chalk and marls

Light gray (lower part) to greenish gray (upper part), faintly layered lacustrine chalk (lower part) and marls (upper part) composed of terrigenous mud rich in authigenic carbonate, intercalated with cm-thick sandy and muddy turbidites. These deposits correspond to the upper seismic Unit B and were deposited when bio-induced calcite precipitation and minor clastic input from small local creeks were the dominant sediment sources in the mesotrophic holomictic lake. The uppermost 50–70 cm show distinct rhythmically layered calcite/organic couplets (varves) representing sedimentation during the last ~100 year of human-induced lake eutrophication (Kelts, 1978; Pika, 1983).

Sixteen ^{14}C ages derived from samples in four different cores footnote: Auxiliary Material, Table A 5.2 provide a high-resolution age control for the cored sedimentary succession. The resulting age model of the composite

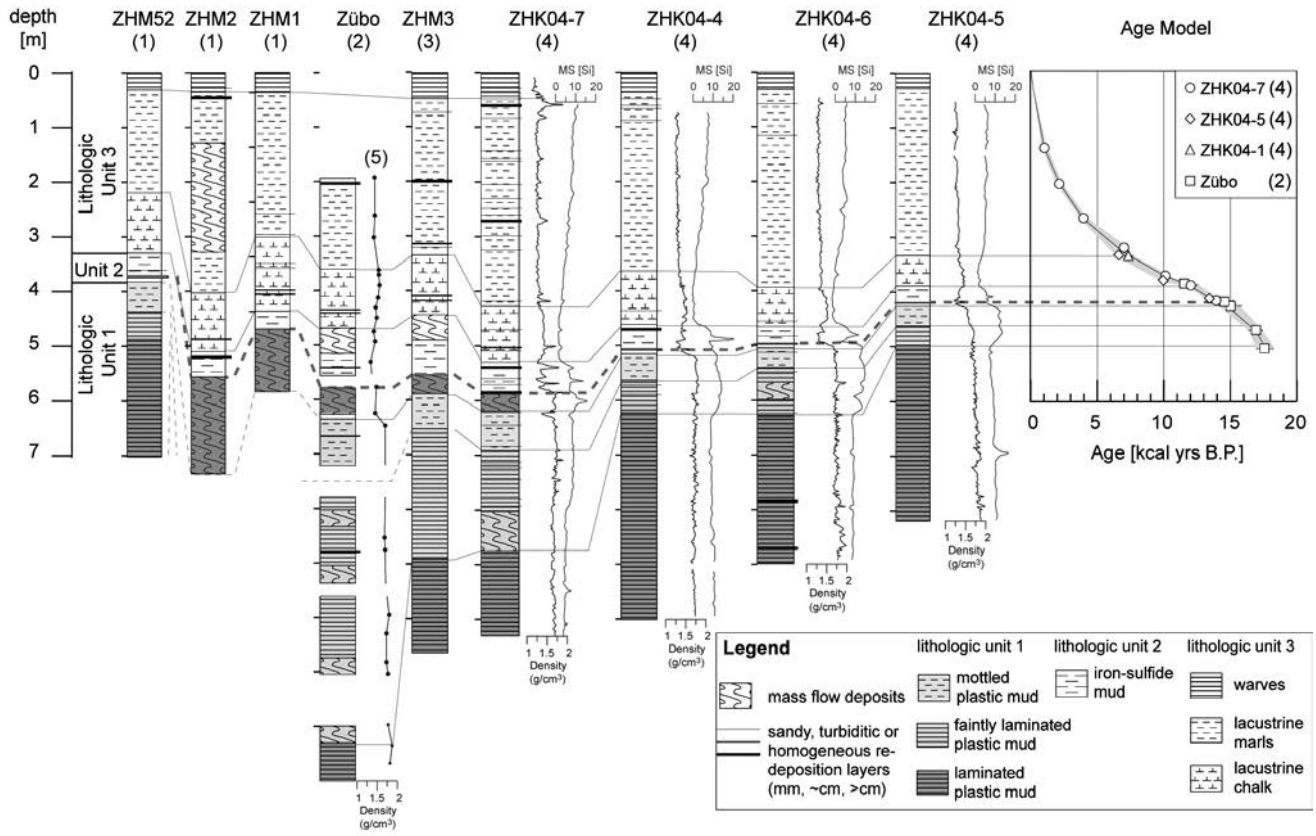

Figure 5.5: Core transect compiling available core information and physical property data from Lake Zurich along the longitudinal lake axis ((1) Giovanoli, 1979, (2) Lister, 1988, (3) Pika, 1983, (4) this study, (5) bulk density data by Eberli, 1984) and age model of the composite stratigraphic section. See Fig. 5.4 for core locations. Red colored deposits and dashed line show the E-layer mass-movement deposits and core-to-core correlation, respectively.

stratigraphic section (Fig. 5.5) reveals Holocene ages for the lithologic Unit 3 (seismic Unit B), Younger Dryas to Bølling ages for lithologic Unit 2 and Oldest Dryas and older ages for the lower lithologic Unit 1 (seismic Unit A).

5.4.2.3 An outstanding event layer

The newly acquired basin-wide quasi-3D stratigraphy allows identifying a conspicuous event layer that was recorded throughout Lake Zurich (hereafter termed E-layer). It occurs in the lowermost part of lithologic Unit 2, a few cm above the boundary to the underlying Unit 1 and is dated to 13760 ±45 cal yr. B.P. (i.e. overlap age of independently dated ages in three different cores, Table 5.1). In all cores (including shallow-water cores ZHM52 and ZHK04-5) this E-layer is characterized by the occurrence of a prominent 1–5 cm-thick turbidite or by 0.5–2 m-thick mass-flow deposits (Fig. 5.5). In the seismic data the E-layer corresponds to a distinct seismostratigraphic horizon at the base of the transition zone between seismic Units A and B. Along this horizon, a total of 23 individual mass-movement bodies with internal chaotic-to-transparent seismic facies and clear lateral pinch-out geometries have been mapped in the seismic data all over Lake Zurich (Figs. 5.6, 5.7A and 5.7B; see Schnellmann et al., (2006) and Strasser and Anselmetti (2008) for detailed description of the used seismic stratigraphic mapping procedure). The occurrence of multiple mass-movement deposits within one isochronous seismostratigraphic horizon suggests simultaneous landsliding throughout the lake and implies a regional trigger mechanism for mass-movement initiation, such as earthquake shaking or lake level change (cf. Shilts and Clague, 1992; Hampton et al., 1996; Schnellmann, et al., 2002).

In the upper basin the E-layer seismically stands out as a remarkably high-amplitude reflection in ~4 m depth (Figs. 5.7C and D). This reflection is immediately overlain by a distinctive seismic facies showing wavy layering formed by one to maximal four seismic reflections with limited lateral continuity (Figs. 5.6B and 5.7D). These features form long-wavelength (50–100 m), low-amplitude (< 50 cm) structures that can be observed throughout the entire upper basin. The resulting undulating upper surface of these features is smoothed out by few overlying reflections, so that the uppermost ~3.5 m of seismic Unit B show the same parallel «layer-cake» reflection pattern as the entire underlying > 55 m-thick sedimentary infill (Unit A; Fig. 5.7C).

In order to sedimentologically characterize these seismically imaged wavy features, core ZHK04-5 was recovered through such a bed form (Fig. 5.7D) and the correlative

Table 5.1: Dating of outburst event.

Sample Nr.	*Sample age[1] [^{14}C yr B.P.]*	*Sample age[2] [cal. yr B.P.]*	*Offset[3] [cm]*	*Sed.rate[4] [cm/yr]*	*Horizon age [cal. yr B.P.]*	*Horizon age (overlap range) [cal. yr B.P.]*	*Center of overlap[5] [cal. yr B.P.]*
ETH-30207	*11710 ± 100*	*13340 - 13770*	*-3*	*0.04*	*13425 - 13855*		
ETH-30715	*11560 ± 90*	*13240 - 13640*	*-5*	*0.03*	*13407 - 13807*		
GL11[6]	*12400 ± 250*	*13750 - 15250*	*5*	*0.04*	*13607 - 15107*		
GL15[6]	*12800 ± 250*	*14150 - 15850*	*15*	*0.04*	*13721 - 15421*	*13721 - 13807*	*13760*

[1]Dating by AMS (accelerator mass spectrometry) with the tandem accelerator at the Institute of Particle Physics at the Swiss Federal Institute of Technology Zurich (ETH).

[2] Calibration (2s range) was carried out applying the IntCal04-calibration curve (Reimer et al., 2004).

[3]Position of the dated sample relative to the event horizon.

[4]Derived from C^{14} data.

[5]Ages are rounded to the decade.

[6]Dates by Lister (1988).

core interval was analyzed in detail. Figure 5.8 shows the compiled data of the target section. In both, core photo and X-ray image, a clear ~2 cm-thick, light gray layer with a fine-sand base can be identified at 4.13 m below lake floor (mblf). It is characterized by an upward decrease in both bulk density and mean grain size and clearly shows a graded textural character. From its sedimentary facies, stratigraphic position and its high impedance contrast compared to the surrounding sediment, as indicated by high bulk density and high p-wave velocity values, this layer correlates to the high-amplitude reflection observed in the seismic data at ~4 m depth (Fig. 5.7D) that corresponds to the basin-wide mass-movement event layer. Above this sand layer, no sedimentary features can be visually

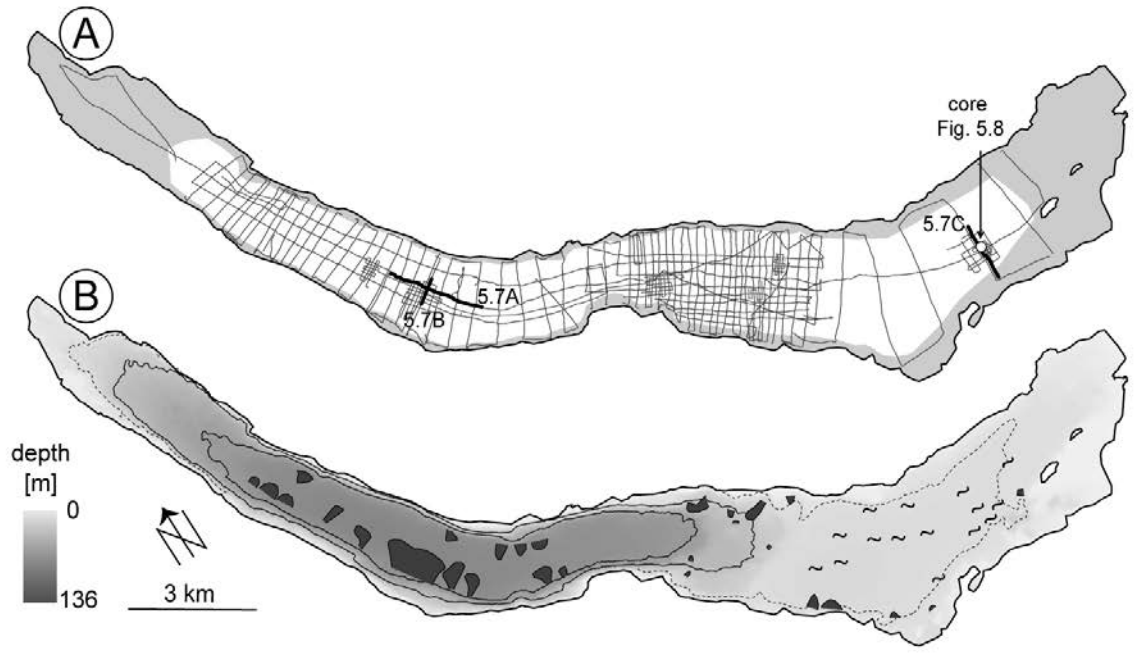

Figure 5.6: A) 3.5 kHz seismic survey grid in Lake Zurich and location of profiles (solid black line) and core ZHK04-5 (open circle) shown in subsequent figures 5.7 and 5.8. Gray shaded areas indicate marginal areas where acoustic signals did not penetrate into the subsurface. B) Distribution of coeval subaquatic landslide deposits (dark grey areas) and bed form structures (~ wiggles) as mapped along the characteristic E-layer in the seismic data from the lower and upper flat basin. Background shows grayscale bathymetry with 50 m contours intervals (black lines). Dotted line marks 20 m-depth contour line and aims to clarify basin morphology in the upper flat basin.

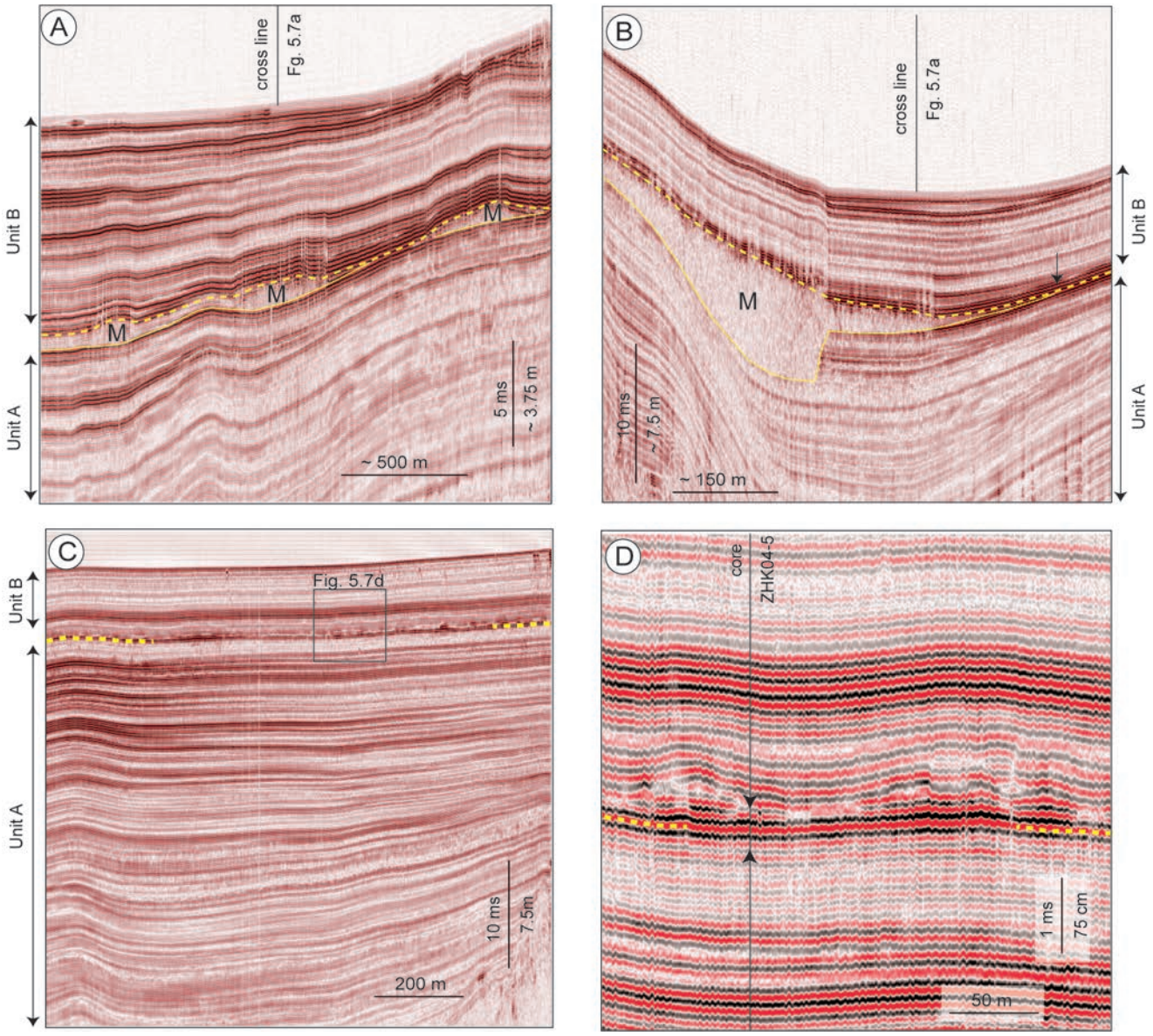

Figure 5.7: 3.5 kHz reflection seismic profiles (pinger source) showing the characteristic seismic features that occur along the E-layer marked by yellow dashed lines in all four panels. See figure 5.6A for location of seismic lines: A) Longitudinal profile along the lake axis in the lower deep basin showing three coeval mass-movement deposits (M). B) Perpendicular cross profile showing the distinct transparent seismic facies of one mass-flow deposit with well-defined lateral pinch out geometry (black arrow). C) Seismic section showing the monotonous parallel-laminated reflection pattern in the sediment-filled upper basin. Rectangle shows approximate location of Figure 5.7D. D) Close up view of wavy seismic features immediately overlying the E-layer in the upper basin. Vertical line gives the position of core ZHK04-5 and arrows indicate the core interval shown in Figure 5.8.

identified within the dark greenish-gray iron sulfide mud. Grain size analysis, however, reveal values of ~30 µm mean grain size within this specific interval indicating slightly coarser material than in the sediment above and below. Furthermore, grain size data suggest inverse grading within a small interval between 4.09 and 4.11 mblf. This interval is overlain by a ~3 cm-thick succession that clearly shows a fining-upward trend. In this section, a ~8° inclining, faint high-density layering can be observed in the X-ray image providing evidence for cross-bedding structures. From its stratigraphic position, this few cm-thick succession characterized by a sequence of reversed and normal grading and cross-bedding, correlates to the observed wavy structures in the seismic data.

Our seismic grid spacing of ~50–100 m does not allow for 3D spatial reconstruction of crest and trough orientations of these wavy structures, nor do 2D seismic lines indicate any consistent symmetries or asymmetries. Nevertheless, these structures clearly appear to be long-wavelength (50–100 m), low-amplitude (< 50 cm) bed forms formed under flowing water conditions that only prevailed during a very short time period. Lacking higher-resolution

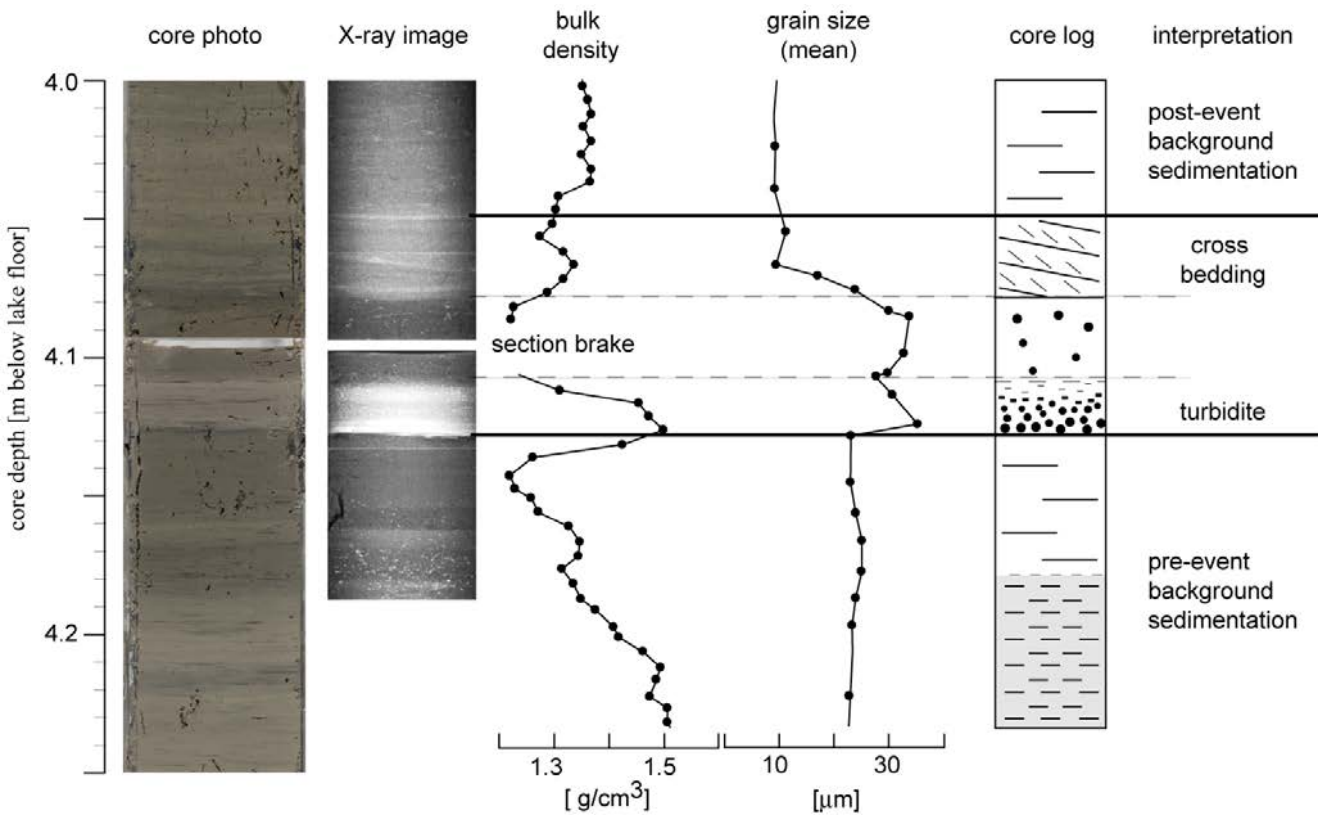

Figure 5.8: Compilation of sedimentological data and observations characterizing the E-layer as cored in core ZHK04-5. See figures 5.6A and 5.7D for core location and depth position of shown interval, respectively. See legend in Figure 5.5 for lithological symbols used in the core log.

spatial information, reconstruction of flow direction and interpretation of formation processes remain inconclusive. Nonetheless, the occurrence of these conspicuous current-induced sedimentary structures immediately overlying the prominent basin-wide mass-movement layer is unique within the entire sedimentary succession and suggests an exceptional event during the Late Pleistocene basin evolution.

5.5 Discussion

Our data from the subsurface of Lake Zurich recorded the fingerprint of an outstanding event (E-layer) affecting both the lower deep as well as the upper flat basin at ~13760 cal yr. B.P. This E-layer thus is a valuable candidate to be related to the proposed catastrophic drainage of the moraine-dammed Lake Zurich (SCHINDLER, 1971). In the following section we will first discuss the relationship between RM-deposits and the proposed moraine breaches and then discuss arguments supporting that the observed bed forms in Lake Zurich can be related to the sudden lake drainage in the aftermath of the moraine dam failure. In the subsequent section we will dwell on possible causes and trigger mechanisms and place our findings in a more general context of natural hazards related to outbursts from moraine-dammed lakes.

5.5.1 Zurich Moraine dam breaches

The sedimentary facies, reconstructed thickness and spatial distribution of the RM-deposits downstream of the moraine suggests that these deposits are related to the four eroded zones of the moraine dam as indicated by thick lobes deposited below the breached dam (Fig. 5.3). It further attests that the Sihl river, which temporarily discharged backwards into Lake Zurich, could not have been the dominant eroding agent, because in this case, one would expect the erosion products to be deposited in the S of the moraine dam and not in the N of it, as observed. Therefore, the four gateways through the moraine must have been formed by erosion from outflowing Lake Zurich water prior to the period, during which the Sihl river discharged southwards into the lake. The lack of quantitative information on the former moraine dam geometry and on the exact location of the lowest points on the initial dam does not allow to conclusively explaining number, location and occurrence of the four breaches. However, as these four gateways are all eroded down to the same topographic level, it is likely that breaching occurred in a single event, because one would expect that continuous erosion of the moraine rather results in one single Lake Zurich outlet channel, which – once started to incise – abandons the other outflow gateways due to lower base level in the incised outflow channel.

The spatial depositional pattern of the RM-deposits and its sedimentary facies with boulder-sized clasts in proximal areas and cobbles and pebbles also > 3 km downstream of the moraine, indicate very high energy transport conditions. Such conditions appear less likely to be related to continuous remobilization in successively eroding lake outlet channels, because an initial Lake Zurich outflow prior to the erosion of the dam may have had a topographic gradient of only ~2–3° (i.e. calculated from the ~12 m height difference between Lake Zurich and Schlieren Lake paleolake levels and reconstructed width of the moraine dam (200–400 m)). Further information on erosion rates and processes comes from our results reconstructing the stratigraphic position of the RM-facies relative to the lacustrine sediments of the Schlieren Lake and the alluvial gravel deposits of the Sihl and Limmat rivers. The two western lobes clearly overlie alluvial gravels assigned to the Sihl fan and thus indicate RM-deposition after the Sihl river already filled in the western parts of the Schlieren Lake basin. There are no evidences in core logs that RM-deposits interfinger with alluvial Sihl fan deposits, but they are described as a massive single unit. These observations point towards discrete remobilization within a short time long after the formation of the moraine dam. In the eastern moraine-proximal area and also in more distal areas further downstream, RM-deposits overlie Schlieren Lake sediments. The resulting boundary separating Sihl fan gravels in the W and Schlieren Lake deposits in the E as RM-deposit substratum (black dashed line in Fig. 5.3), is interpreted to correspond to the paleodelta front of the Sihl river within the Schlieren Lake during the time of RM-deposition. Alternatively, it may mark the boundary of a ~500 m-wide and ~20 m-deep zone where an exceptional flood, potentially resulting from a lake outburst, was channelized incising into formerly deposited alluvial gravels and lacustrine deposits along a former river bed of the Limmat river (Fig. 5.2B).
Combining all arguments, our findings support SCHINDLER's hypothesis (1971) of a sudden Zurich Moraine failure that consequently resulted in catastrophic drainage of Lake Zurich.

5.5.2 Timing

In order to conclusively assign the E-layer observed in Lake Zurich to the moraine dam failure and outburst event, an independent age control is required. The timing of the breaches can be relatively constrained by evaluating the stratigraphic position of Sihl delta deposits in Lake Zurich. The Sihl river temporarily discharged into Lake Zurich after the moraine was breached and the lake level was lowered, so that the partly emptied lake acted as the local base level for the Sihl river. Previous studies (HUBER, 1938; SCHINDLER, 1968; 1971; 1974; 1976) revealed that Sihl delta deposits are intercalated with lacustrine sediments of lithologic Unit 2 and the lower part of lithologic Unit 3. They are never associated with Unit 1 deposits. Thus, the stratigraphic position of the Sihl delta deposits provides a rough age estimate suggesting that the moraine breaches occurred immediately before the onset or during the deposition of lithologic Unit 2.
This independent age estimate is within the same range as the date obtained for the outstanding E-layer (~13760 cal yr. B.P.) that records a remarkable event of simultaneous basin-wide subaquatic landsliding and subsequent formation of peculiar current-induced bed forms in the upper flat basin. We therefore interpret these features to be the fingerprint of the moraine dam failure and subsequent lake outburst.

5.5.3 Lake Zurich outburst

The peculiar bed forms in the upper flat basin suggest that they were formed under flow conditions that allowed for entrainment and transport of sediment particles. Also, the observed sedimentary succession in our core data showing a normally graded turbidite overlain by a sequence of reversed and normal grading with cross-bedding structures indicates peculiar transient sediment transport and flow conditions. The basal turbidite is interpreted to be related to the basin-wide mass-movement event (see subsection 5.4.2.3). The overlying succession of reversed and normal grading may be interpreted as the sedimentary deposits following a hyperpycnal flow (e.g. MULDER et al., 2003). However, a hyperpycnal flow alone may not fully explain the occurrence of cross-bedding structures and the high-wavelength, low-amplitude bed forms throughout the upper flat basin. These structures are rather interpreted to have originated from water movements within the whole water column. We hypothesize that such hydrodynamic conditions may have been induced by far-field drawdown effects related to the sudden lake drainage following the moraine-dam failure.
In order to test this hypothesis, we quantitatively analyzed theoretical discharge scenarios induced by the lake outburst. By performing simple calculations of flow velocities and sediment transport threshold criteria, we evaluate, whether the modeled flow conditions allow for the formation of the observed bed forms. In this first-order approach, we assume that the formation of sedimentary structures is controlled by the capacity of the drainage-induced flow to entrain and transport particles along the bed of the upper flat basin. In cohesive fine-grained material the sediment transport capacity can be approximately evaluated by quantitatively comparing the shear velocity (u^*) of a flow, which tends to move particles, and the grain settling velocity (w), which counteracts movement (e.g. MIDDLETON and SOUTHARD, 1984). The critical threshold condition for full suspension then is given as $w = u^*$ and we can formulate that our hypothesis is a reasonable scenario if:

$$w < u^* \qquad (1)$$

with,

$$w = 1/18 * D^2\gamma'/\mu \qquad \text{Stokes'law} \qquad (2)$$

$$u^* = u/[(1/k) \ln (y/y_o)] \qquad \text{Logarithmic velocity law} \qquad (3)$$

where D is the grain size, γ` is the submerged specific weight (i.e. the difference between solid grain and water density times gravitational acceleration), μ is the water viscosity (equal to 0.001567 kg s^{-1} m^{-1} at 4°C), u is the flow velocity (i.e. discharge volume divided by the cross sectional area divided by time), *k* is Von Karman's constant (equal to a value about 0.4 in clear flows), *y* is the flow depth and y_o is the roughness length (equal to a value of about 1/30 of the mean grain size *D* (Allen, 1997)).

To calculate the settling velocity we used a mean grain size of 30 ±2.5 μm as measured in core ZHK04-5, and a solid grain density of 2.71 ±0.02 g cm^{-3} (Giovanoli, 1979).

To calculate the shear velocity, we first have to estimate the discharge volume, paleowater depth, and duration of the outflow. Standard GIS software is able to reconstruct the surface area of the paleolake prior to the lake-level fall using reconstructions in the Linthplain and Walensee area (Müller, 1995; Schindler, 2004) and extrapolating the paleolake level to ~417 masl in a digital elevation model (DEM) after correction for differential surface uplift between Lake Zurich and Walensee over the last ~14000 years (estimated to be in the order of ~7 m (Kahle et al., 1997)). This reconstructed outline of the paleolake (Fig. 5.1) has an area of ~210 km^2 ±10 km^2 (uncertainties are mainly due to slight discrepancies in the different paleolake outline reconstructions in the eastern part). Assuming a lake-level drop of ~12 m ±2 m (i.e. difference between reconstructed paleolake level and lake level at the beginning of Sihl delta sedimentation in Lake Zurich) the outburst drainage volume then is estimated to be ~2.5 ±0.5 km^3. Note that this estimate does not account for the different slope geometries along the shoreline, which may add another, but negligible small error (< 1 %). Water depth at the sites of observed bedforms were reconstructed based on paleobathymetry reconstructions from the seismic data that recorded the sedimentary structures today at a depth of ~24 ±2 m below lake level corresponding to a paleowater depth of ~36 ±4 m. The discharge cross section was defined perpendicular to the E-W trending axis of the upper Lake Zurich basin because flow directions induced due to far-field drawdown effects of the lake outburst must have been oriented in an axis-parallel fashion. As a representative discharge cross section we calculated an area through the location of site ZHK04-5 using paleobathymetry reconstructions and DEM-data. There, the discharge cross section is ~1.06 ±0.06 km^2 (uncertainties mainly due to inaccurate knowledge of paleoshore line position and value of slope inclinations).

Having constrained estimates of all input parameters and their uncertainties (Tab. 5.2), the shear velocity now mainly depends on the unknown duration of the flow. Our hypothesis can now be tested by plotting w/u* as function of different outflow durations (Fig. 5.9), for which the criterion $w/u^* = 1$ can be used as the critical threshold for the formation of the bed forms. The results of our calculations show that particle entrainment and thus the potential to form the observed bed form structures can be related to Lake Zurich outburst scenarios if the reconstructed outflow volume of ~2.5 ±0.5 km^3 drains within maximal 12 days (range of uncertainties ~7–19 days) or faster (Fig. 5.9).

Assuming a most conservative scenario of draining the whole drainage volume V within the maximal duration of 12 day at constant discharge rates, estimated minimal discharge values would be ~2400 m^3s^{-1} (range of uncertainties ~ 1200–5000 m^3s^{-1}). However, effective peak discharge values may have been significantly higher because the lake outflow may not have lasted as long as the estimated maximal duration. Also, the assumption of constant discharge rates over the entire drainage duration represents a simplified assumption because discharge is likely to have decreased significantly as the lake level dropped. Furthermore, reconstructions considering drainage volume and duration of outflow alone do not account for the complex physical, hydraulic and hydrological processes involved in flowing water through the moraine breaches. Walder and O'Conner (1997) argue that for large outbursts (where the volume of the lake is large relative to the lake level drop as in the Lake Zurich situation) the volume does not exert primary control on peak discharge and maximum values rather are controlled by critical flow conditions defined by the breach geometry and amplitude of lake level drop.

Table 5.2: Parameters used for flow calculations.

input parameter			*mean value*	*lower uncertainty limit*	*upper uncertainty limit*	*references*
grain size	*D*	*[μm]*	*30*	*27.5*	*32.5*	*this study*
discharge volume	*V*	*[km^3]*	*2.5*	*2*	*3*	*this study*
cross sectional area	*A*	*[km^2]*	*1.06*	*1*	*1.12*	*this study*
flow depth	*y*	*[m]*	*36*	*32*	*40*	*this study*
solid grain density	ϱ_s	*[g/cm^3]*	*2.71*	*2.69*	*2.73*	*Giovanoli(1979)*
Karman's constant	*k*	*[ ]*	*0.4*			*Allen(1997)*
roughness length	y_0	*[μm]*	*1/30 D*			*Allen(1997)*
water density	ϱ_w	*[g/cm^3]*	*1*			*at 4°C*
water viscosity	*μ*	*[g s^{-1} m^{-1}]*	*1.567*			*at 4°C*
gravitational acceleration	*g*	*[m/s^2]*	*9.81*			

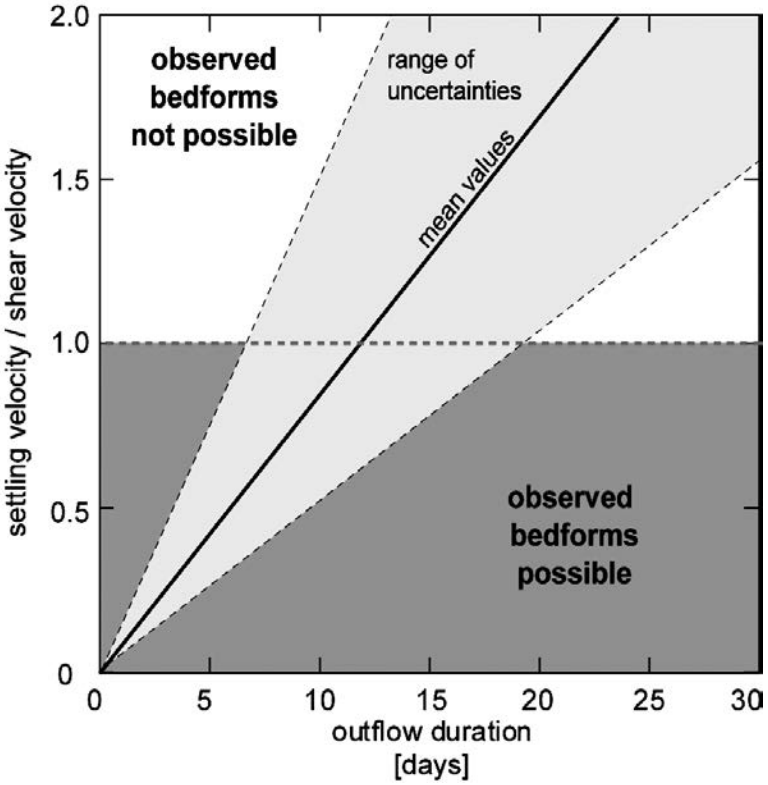

Figure 5.9: Results from calculations evaluating hydrodynamic conditions for different Lake Zurich outburst scenarios (i.e. time of outflow duration) in order to test whether the observed sedimentary structures in the upper flat basin can reasonably be related to the proposed sudden drainage event. We used a threshold criteria (marked as red dashed line) where settling velocity (w) equals shear velocity (u) (see section 5.5.3). Bold line indicates solutions with reconstructed mean values (Table 5.2) and gray area marks range of uncertainties.*

In order to obtain a first-order estimate of potential maximal magnitude of the Lake Zurich outburst we here use a simple, empirically calibrated model-based equation assuming rectangular breach geometry as proposed by Fread (1996):

$$Qp' = 3\ H'\ W'\ (H')\ 0.5 \quad \text{(Fread, 1996)} \quad (4)$$

where Qp' is peak discharge, and H' and W' are the breach height and width, respectively (note that the equation uses non-SI units; Qp' is given in cubic feet per second with 1 m^3s^{-1} = 35.3147 ft^3s^{-1}, and H' and W' are given in feet with 1 m = 3.2808 ft). Using representative mean values as inferred from our study (i.e. H' = lake level drop = 12 ±2 m and W' = mean width of the four breaches = 300 m ±100 m) peak discharge values for the Lake Zurich outburst are estimated to ~20600 m^3s^{-1} (range of uncertainties ~ 10500–34700 m^3s^{-1}).

These results provide a first-order estimate on the potential magnitude of the Lake Zurich outburst event and can be compared to published studies of catastrophic drainages of moraine-dammed lakes that occurred during historic times (Costa and Schuster, 1988; Clague and Evans, 2000 and references therein). Although most of the reported historic events are mostly smaller in terms of discharge volume and thus also in terms of outflow duration, they are in a comparable order of magnitude related to peak discharge rates (~10^3–10^4 m^3s^{-1}). Our simple approach thus supports the interpretation that a moraine-breach-triggered sudden drainage of Lake Zurich induced a current flow in the lake that was strong enough to form the observed sediment structures. Furthermore, the high estimated peak discharge values are in agreement with our interpretation that the RM-deposits downstream the Zurich Moraine were transported under high energy conditions.

5.5.4 Trigger mechanism of the moraine dam failure

The E-layer associated with the moraine dam failure and subsequent catastrophic drainage of Lake Zurich comprises a series of sublacustrine landslides and turbidite deposits that have been recorded throughout the Lake Zurich basin. In core ZHK04-5 retrieved in the upper flat basin, the 2 cm-thick turbidite assigned to the basin-wide mass-movement event stratigraphically underlies the current-induced sediment structures (Fig. 5.8). This observation suggests that landsliding and remobilization of sediment from the slopes predates the occurrence of strong currents induced by the lake drainage. Therefore, we interpret that landsliding was not caused as a consequence of the lake level drop (e.g. shore collapses due to the lake level lowering along freshly emerged water-saturated lake deposits). This is in line with observations from the lower Lake Zurich basin, where seismic data along the slopes show landslide scars in > 30 m water depth. Furthermore, none of the cored mass-flow deposits contains sediments pointing towards remobilization of shore material. Therefore, our data suggest that basin-wide landsliding resulted from sublacustrine slope failures that are related to a process that eventually initiated the catastrophic lake drainage.

It has been reported in many studies that synchronous subaquatic landslide and turbidite deposits can be related to earthquakes that triggered slope failures on a regional scale (e.g., SHILTS and CLAGUE, 1992; SCHNELLMANN, et al., 2002; GOLDFINGER, et al., 2003). STRASSER et al., (2006) showed that the discussed E-layer characterized by 23 individual slides in Lake Zurich is the oldest of three events, during which earthquake shaking led to multiple sliding along the slopes of Lake Zurich. In fact, by temporal and spatial correlation of multiple subaquatic landslide deposits in Lake Zurich and Lake Lucerne, STRASSER et al. (2006) reconstructed the occurrence of three major northern alpine earthquakes (Magnitude M > 6.5) that hit the area of Central Switzerland, with one of them occurring around ~13770 ±70 cal yr. B.P. Hence, we interpret that the moraine-dam failure and subsequent Lake Zurich outburst is related to this large northern alpine earthquake.

It remains unknown, however, whether the primary effects of strong ground motions during the earthquake directly triggered the moraine dam to fail (e.g. NEWMARK, 1965). We further consider the possibility that the earthquake-induced subaquatic landslides have the potential to trigger tsunamis in the lake that may eventually overtop the moraine and initiate incision into the moraine dam. It has been shown that lacustrine landslides that failed during a M ~6.2 earthquake in 1601 A.D. triggered up to 4 m-high tsunami in Lake Lucerne (SCHNELLMANN, et al., 2002). Considering that the Lake Lucerne landslides are comparable in terms of volume, slope angle and mode of failure initiation to the landslides observed in Lake Zurich (STRASSER et al., 2007; STRASSER & ANSELMETTI, 2008), the potential of landslide-triggered wave generation in Lake Zurich has to be taken into account. Furthermore, the earthquake may also have triggered rockfalls and landslides in the eastern part of the paleolake (e.g. Planggen-Klöntal Rockslide (SCHINDLER, 2004); Fig.5.1) and/or instabilities along the steep slopes of today's Walensee) that might have caused impulse waves and thus could have contributed to wave generation.

Our findings imply that the Zurich Moraine dam was stable over several thousands of years before it eventually failed ~13760 cal yr. B.P. We therefore interpret that the internal moraine structure and geometry generally provided favorable moraine dam stability conditions. From a climatic perspective, the Zurich Moraine breach occurred during the Bølling stage, a time period that represents the onset of mid-European climatic amelioration after the end of the LGM (e.g. DENTON, et al., 2005). Interstitial ice and permafrost within the moraine dam could potentially have sustained prior to climatic warming and added to the moraine stability for several thousand of years. Ice and/or permafrost thawing in the core of the moraine as well as increasing amount of water discharge from rapidly melting alpine glaciers in the catchment area of Lake Zurich during climate warming at the beginning of the Bølling stage then may have contributed to decreasing moraine stability conditions.

Given that our findings suggest four simultaneously breached zones, ice core melting or piping as the ultimate trigger is anticipated to be unlikely because it would rather result in one single breach, as has been often reported from historic events (COSTA and SCHUSTER, 1988; CLAGUE and EVANS, 2000 and references therein). This therefore supports our interpretation that a strong northern alpine earthquake was the critical process to eventually cause the moraine to fail at ~13760 cal yr. B.P. The breach was either triggered by primary seismic ground shaking or by secondary earthquake effects such as subaquatic landslide-generated tsunami or rockslide-generated impulse waves, which might have overtopped the moraine dam and initiated failure and subsequent lake outburst.

5.6 Summary and conclusions

Results from our comprehensive case study in the Zurich area (Central Switzerland) provide several independent evidences for the occurrence of a Late Pleistocene (~13760 cal yr. B.P.) moraine dam failure and subsequent Lake Zurich outburst, and thus confirm and refine the Lake Zurich outburst-hypothesis proposed by SCHINDLER (1971). Our geophysical, sedimentological and geomorphological data combined with fluid dynamic calculations reveal a first-order lower-limit estimate on averaged outburst discharge (exceeding minimum values of ~2400 m^3s^{-1}) as well as a estimate on the potential maximal magnitude of the outburst event (peak discharge values ~20600 m^3s^{-1}). We conclude that the catastrophic drainage of Lake Zurich was initiated after the moraine dam failed as a consequence of a strong northern alpine earthquake due to either primary earthquake shaking or secondary effects, such as overtopping by landslide-generated waves. Long-term causes, i.e. destabilization due to potential ice and/or permafrost thawing in the core of the moraine, as well as increasing amount of water discharge from rapidly melting glaciers in the catchment during a phase of climate warming, may have partially contributed to enhance the susceptibility of failure initiation prior to the occurrence of the eventual earthquake trigger.

In general, our findings reveal that moraines damming lakes can be stable over several thousands of years, but also that stability conditions may decrease during periods of climate warming and that failure can be initiated suddenly during a strong seismic shaking event. To assess long-term future hazard scenarios resulting from lake outbursts, especially in the context of present-day climatic warming and rapid glacier retreat, during which the formation rate of potentially hazardous moraine-dammed lakes is increasing, the interplay of neotectonic activities and climate change thus needs to be considered. Both factors, together with moraine-specific internal strength characteristics (e.g. width-to-height ratio, material properties and consolidation stage (cf. CLAGUE and EVANS, 2000)) define threshold stabilities of natural dams and control occurrence and timing of hazardous future lake outburst.

6 CONCLUSION AND OUTLOOK

6.1 Conclusion

This study aimed to better determine and quantify causes and effects of natural hazards related to subaquatic landslides. Using the perialpine, fjord-type Lake Zurich and Lake Lucerne in central Switzerland as natural laboratories, threshold parameters for slope failure initiation along submerged slopes were quantitatively assessed combining sedimentological, geophysical, in situ geotechnical and numerical modeling techniques. This allows evaluating the effects of long-term causes vs. short-term trigger mechanism and provides the basis for deciphering seismic vs. aseismic triggers of subaqautic landslides. Furthermore, systematic investigation of the spatial and temporal distribution of mass-movement deposits in both lakes allows, for the first time, to estimate lower limit magnitudes of prehistoric geological impacts such as earthquakes and lake outbursts that affected the study area over the last ~15000 years. This study thus demonstrates the multi-methodological approach studying the subaquatic-landslide record in different basins to be a successful and promising strategy to tackle the reconstruction of frequency and intensity of past natural impacts. This eventually may yield the means for assessing the geo-hazard potential arising from such rare but pontentially-destructive events.

On the basis of the results from this study, the following major conclusions can be drawn:

6.1.1 Subaqueous slope stability

Lake Lucerne

- Slope stability conditions along non-deltaic lateral slopes of Lake Lucerne are, apart from the slope inclination predefined by the bedrock topography, mainly controlled by the distribution of physical and geotechnical properties of the slope-covering sedimentary succession. The controlling key boundary condition resulted from the glacial-to-postglacial evolution in sedimentation processes and post-depositional consolidation mechanisms.
- Holocene sedimentation rate is a key parameter in «charging» subaqueous slopes. As a consequence, stability conditions thus change over relative short geological time scales.
- Non-deltaic lateral slopes are stable under static loading conditions and an external trigger is required to initiate failure.
- During past earthquake shaking slope failures systematically initiated along glide planes that developed at the lithological boundary between overconsolidated glacio-lacustrine deposits with overpressured formation pore pressures and overlying slightly underconsolidated laminated Late Glacial clays characterized by low shear strength values at their base.

Lake Zurich

- Subaquatic landslides along lateral non-deltaic slopes in Lake Zurich show similar characteristics as in Lake Lucerne and thus imply comparable slope stability conditions and a seismic trigger mechanism. In addition, slope failures occurring along small lateral deltas suggest the influence of climate-controlled increase of sediment supply from small creeks as the cause for subaqueous delta slope failures.
- Two major rotational slide events that occurred during the transition from the Pleniglacial to the Late Glacial period suggest glacial processes, such as rapid glacier destabilization phases and/or episodic glacier outbursts resulting in high sedimentation rate, to be the cause for theses instabilities of glacio-lacustrine deposits in Lake Zurich.

6.1.2 Paleoseismology

- Limit equilibrium slope stability back-analysis of past earthquake-triggered slope failures in Lake Lucerne reveal site-specific minimum horizontal seismic peak ground accelerations of ~0.08 g and ~0.14 g for the historic 1601 A.D. M_W ~6.2 earthquake and a prehistoric, 2220 cal yr. B.P., earthquake, respectively. The result for the 1601 A.D. event lies in the range of calculated values deduced from predictive ground motion models (Bay et al., 2005) and suggests comparable macroseismic threshold intensities (correlation function by Murphy and O'Brien (1977)) as estimated from historic data (I = VII; Schwarz-Zanetti et al., 2003). These findings thus pinpoint the potential of detailed subaqueous slope stability analysis as paleoseismological tool that allows for site specific quantitative reconstruction of prehistoric earthquake shaking.
- The temporal coincidence of three basin-wide coeval multiple slope failure events recorded in Lake Zurich with paleo-earthquakes reconstructed in the Lake Lu-

cerne record imply that three very large earthquakes shook central Switzerland in the past 15000 years, strong enough to trigger multiple mass movements in these two lakes located ~40 km apart. They are dated to 2220 ±40, 11600 ±120 and 13770 ±70 calendar yr B.P. They reached minimum earthquake moment magnitudes of $M_W \geq 6.5$ with epicentres located east of Lake Lucerne and southeast of Lake Zurich, as reconstructed by spatial calculations using an empirical seismic attenuation model. These results indicate ongoing Alpine deformation that generated and potentially will generate again rare but destructive events in heavily-populated regions that are unaccustomed to seismic activity during historic time.

6.1.3 Lake Outburst

The Lake Zurich data acquired for this study, combined with geomorphological and core information from downstream areas, allowed to identify and to reconstruct a Late Pleistocene earthquake-triggered moraine dam failure and subsequent outburst of Lake Zurich. Fluid dynamic calculations reveal that averaged outburst discharge exceeded minimum values of ~2400 m^3s^{-1} and estimated peak discharge of ~20600 m^3s^{-1}. General findings reveal that (i) moraines damming lakes can be stable over several thousands of years, that (ii) stability conditions may decrease during periods of climate warming and that (iii) failure can be initiated suddenly during a strong seismic shaking event.

6.2 Outlook

Although this study contributed to a better understanding of causes and effects of natural hazards related to subaquatic landslides and provided, for the first time, quantitative information on magnitudes and source areas of prehistoric earthquake in central Switzerland, some problems remain unsolved and a lot of new questions arose. In the following sections, some major challenges and possible research approaches to solve open questions are briefly outlined.

6.2.1 Subaqueous landslide initiation and slope stability assessment

Pore pressure is a fundamental parameter for the understanding of the stability of saturated sediments (e.g. THERZAGHI, 1925; HUBBERT and RUBEY, 1959). Results from the in situ geotechnical site characterization in Lake Lucerne suggest that the pore pressure conditions in the glacial deposits are in excess of hydrostatic conditions. The process of overpressuring, however, remains uncertain and, to date, we lack precise quantitative information on in situ pore pressures. Future campaigns monitoring pore pressure in critical depths over longer periods will yield important information to elucidate mechanisms of overpressuring, to evaluate its fluctuation as a function of time and to quantify the excess formation pore pressure and its effect on stability and landslide initiation.

STEGMANN et al. (2007) conceptually showed that during past earthquake shaking transient pore pressure pulses migrated upwards from the overconsolidated section to the weak overlying postglacial section and exhibited an important role in landslide initiation. This effect of pore pressure transients was so far not taken into account in the quantitative slope stability calculations presented in this study. Also, the here used pseudostatic slope stability analysis approach does not consider the dynamic behavior of the sediment during cyclic loading, and therefore does not account for potential failure mechanisms in addition to the load generated by horizontal seismic acceleration. These effects include degradation of soft clays, accumulation of plastic strains, shear-induced excess pore water pressure with increasing number of seismic cycles (e.g. SULTAN et al., 2004, BISCONTIN, 2002). Geotechnical laboratory tests studying the dynamic behavior of the sediment and absolute pore pressure values to estimate effective stresses are needed to better understand landslide initiation and to refine input parameters for future slope stability assessments.

The comprehensive Lake Lucerne data set provides an ideal basis to address these challenges in future studies. Understanding in more detail the interplay between seismic shaking, (transient) pore pressure evolution and subaquatic landslide initiation in Lake Lucerne may also yield important conceptual ideas to improve our understanding of larger submarine landslide occurring at active and passive continental margins.

Detailed in situ geotechnical site characterizations are also needed in Lake Zurich to quantify slope stability condition both along lateral non-deltaic and deltaic slopes. This will yield the means for more in depth evaluation of causes and effects of different processes (e.g. climatic vs. seismic trigger mechanism) affecting slope stability in Lake Zurich. It will also provide quantitative lower limit thresholds needed for reliable back-analysis and quantitative assessments of future scenarios.

6.2.2 Paleoseismology

In this study, minimal earthquake magnitudes and potential epicentre location of three major paleo-earthquakes were estimated using a historically calibrated macroseismic threshold intensity of VII as input parameter for macroseismic reconstructions. These reconstructions could be refined by using reconstructed critical seismic accelerations rather than macroseismic threshold intensities. Data sets of both Lakes Zurich and Lake Lucerne provide the basis for such quantitative reconstruction of critical seismic accelerations during past earthquakes. Past subaquatic slope stability conditions during specific earthquake events may be back-analyzed in future studies on a basin-wide

scale and compared with the known distribution of past earthquake-triggered mass-movement deposits in the basins. This would allow for more quantitative paleoseismologic investigations assessing regional minimal and maximal ground shaking accelerations during past earthquake events that eventually may be incorporated into regional models back-analyzing more reliably magnitudes and epicentre locations.

An important open question that arose from the result of this study is the exact location, focal mechanism and tectonic driving forces of the identified large northern Alpine earthquakes. In order to achieve advancements in our understanding of the underlying geological/tectonic processes capable of producing the observed events, further paleoseismological archives are needed. Positive and/or negative evidences in such additional archives will better constrain epicenter locations, which will allow for a more detailed process-oriented seismotectonic discussion. Additionally, theoretical considerations of strain accumulation during seismic cycles in potentially capable source areas or even along potentially capable fault zones may further reveal arguments for identifying or excluding areas/faults that may produce rare but destructive seismic events.

6.2.3 Tsunami hazard

Schnellmann et al. (2002) showed that the subaquatic landslides in Lake Lucerne are capable of triggering tsunami waves of up to 4 m in height matching historic descriptions (Cysat, 1601). Although lateral, non-deltaic landslides in Lake Zurich show similar characteristics as in Lake Lucerne and thus are likely to also have triggered tsunami waves in Lake Zurich, it remains to be proven whether or not Lake Zurich indeed experienced waves during past earthquake events. This could be addressed by evaluating the tsunamigenic potential of subaquatic landslides using numerical tsunami models and by investigating coastal archives not affected by human settlements (e.g. pond south of peninsula Au) for tsunami deposits.

In order to assess tsunami hazard in Swiss lakes, a basin-wide slope stability assessment modeling potential future seismic shaking events is required to identify areas susceptible for future slope instabilities. Critical slopes then can be analyzed for there tsunamigenic potential (e.g. volume of potentially unstable strata, rigidity of slope-covering sediment, etc.). Further improvement in the current knowledge of regional variability of slope characteristics and hence also in assessing the tsunamigenic-landslide susceptibility is expected to be gained from spatial bathymetric mapping using multibeam techniques. High-resolution bathymetric maps nowadays are key requirements for reliable slope stability analysis and subaquatic natural hazard assessments (e.g. Locat ant Lee, 2002; Solheim, 2006 and references therein). Multibeam bathymetry maps further may allow for identifying creep structures and incipient scars in areas that have been identified in the slope stability model to be susceptible for future (tsunamigenic) landsliding. In combination, such quantitative information eventually can be implemented into numerical tsunami models that will reveal estimates on potential wave height and inundation scenarios. These data then may yield important information for assessing the risk of tsunami impacts on coastal infrastructure and communities along the shore lines of Lake Lucerne, Lake Zurich and eventually other Swiss lakes.

REFERENCES

Aeschbach-Hertig, W., 1994, Helium und Tritium als Tracer für physikalische Prozesse in Seen [PhD thesis]: Zurich, ETH Zurich.

Allen, P.A., 1997, Earth Surface Processes: Oxford, Blackwell Science, 404 p.

Andrews, D.C.A., and Martin, G.R., 2000, Criteria for liquefaction of silty soils, 12th World Conference on Eartqhuake Engineering Auckland, New Zealand.

Anselmetti, F., S., Bühler, R., Finger, D., Girardclos, S., Lancini, A., Rellstab, C., and Sturm, M., 2007, Effects of Alpine hydropower dams on particle transport and lacustrine sedimentation: Aquatic Sciences, v. 69, p. 179–198.

Azizian, A., and Popescu, R., 2006, Three-dimensional seismic analysis of submarine slopes: Soil Dynamics and Earthquake Engineering, v. 26, p. 870–887.

Bakun, W.H., and Wentworth, C.M., 1997, Estimating earthquake location and magnitude from seismic intensity data: Bulletin of the Seismological Society of America, v. 87, p. 1502–1521.

Baster, I., 2002, Holocene delta in western Lake Geneva and its peleoenvironmental implications: seismic and sedimentological approach [PhD thesis]: Genève, Université de Genéve.

Bay, F., Wiemer, S., Fäh, D., and Giardini, D., 2005, Predictive ground motion scaling in Switzerland: Best estimates and uncertainties: Journal of Seismology, v. 9, p. 223–240.

Beck, C., Van Rensbergen, P., De Batist, M., Berthier, F., Lallier, S., and Manalt, F., 2001, The Late Quaternary sedimentary infill of Lake Annecy (northwestern Alps): an overview from two seismic-reflection surveys: Journal of Paleolimnology, v. 25, p. 149–161.

Becker, A., Davenport, C.A., and Giardini, D., 2002, Palaeoseismicity studies on end-Pleistocene and Holocene lake deposits around Basle, Switzerland: Geophysical Journal International, v. 149, p. 659–678.

Biscontin, G., Pestana, J.M., and Nadim, F., 2004, Seismic triggering of submarine slides in soft cohesive soil deposits: Marine Geology, v. 203, p. 341–354.

Blass, A., Anselmetti, F.S., and Ariztegui, D., 2003, 60 years of glaciolacustrine sedimentation in Steinsee (Sustenpass, Switzerland) compared with historic events and instrumental meteorological data: Eclogae Geologicae Helvetiae, v. 96, p. S59–S71.

Boe, R., Hovland, M., Instanes, A., Rise, L., and Vasshus, S., 2000, Submarine slide scars and mass movements in Karmsundet and Skudenesfjorden, southwestern Norway: morphology and evolution: Marine Geology, v. 167, p. 147–165.

Boe, R., Longva, O., Lepland, A., Blikra, L.H., Sonstegaard, E., Haflidason, H., Bryn, P., and Lien, R., 2004, Postglacial mass movements and their causes in fjords and lakes in western Norway: Norwegian Journal of Geology, v. 84, p. 35–55.

Boner, M., Gebhardt, A.C., and Pabst, B., 1999, Are Late Glacial Deposits Exposed in Lake Zürich?, Abstract at COL Symposium 1999; Looking into the sediment subsurface of lakes: Zürich.

Bouma, A.H., 1987, Megaturbidite - an Acceptable Term: Geo-Marine Letters, v. 7, p. 63–67.

Broecker, W.S., 2006, Was the younger dryas triggered by a flood?: Science, v. 312, p. 1146–1148.

Bührer, H., and Ambühl, H., 1996, Der Vierwaldstättersee 1961–1992 - Eine Dokumentation: Schriftenreihe der EAWAG, v. 10, p. 54 pp.

Camerlenghi, A., Urgeles, R., Ercilla, G., and Brückmann, W., 2007, Scietific Ocean Drilling Behind the Assessment of geo-hazards from submarine slides: Scientific Drilling, v. 4, p. 45–47.

Carter, D.T., Ely, L.L., O'Connor, J.E., and Fenton, C.R., 2006, Late Pleistocene outburst flooding from pluvial Lake Alvord into the Owyhee River, Oregon: Geomorphology, v. 75, p. 346–367.

Chapron, E., Beck, C., Pourchet, M., and Deconinck, J.F., 1999, 1822 earthquake-triggered homogenite in Lake Le Bourget (NW Alps): Terra Nova, v. 11, p. 86–92.

Clague, J.J., and Evans, S.G., 2000, A review of catastrophic drainage of moraine-dammed lakes in British Columbia: Quaternary Science Reviews, v. 19, p. 1763–1783.

Clarke, G.K.C., Leverington, D.W., Teller, J.T., and Dyke, A.S., 2004, Paleohydraulics of the last outburst flood from glacial Lake Agassiz and the 8200 BP cold event: Quaternary Science Reviews, v. 23, p. 389–407.

Coleman, J.M., and Prior, D.B., 1988, Mass-Wasting on Continental Margins: Annual Review of Earth and Planetary Sciences, v. 16, p. 101–119.

Costa, J.E., and Schuster, R.L., 1988, The Formation and Failure of Natural Dams: Geological Society of America Bulletin, v. 100, p. 1054–1068.

Cysat, R., 1601, Collectanea Chronica und denkwürdige Sachen pro Chronica Lucernensi et Helvetiae, in Schmid, J., ed., Quellen und Forschungen zur Kulturgeschichte von Luzern und der Innerschweiz, Volume 1: Luzern, Diebold Schilling Verlag, p. 882–888.

Daut, G., 1988, Subaquatische Massenbewegungen im Starnberger See und im Tegernsee [PhD thesis]: München, Technische Universität München.

Deichmann, N., Baer, M., Braunmiller, J., Dolfin, D.B., Bay, F., Delouis, B., Fah, D., Giardini, D., Kastrup, U., Kind, F., Kradolfer, U., Kunzle, W., Rothlisberger, S., Schler, T., Salichon, J., Sellami, S., Spuhler, E., and Wiemer, S., 2000, Earthquakes in Switzerland and surrounding regions during 1999: Eclogae Geologicae Helvetiae, v. 93, p. 395–406.

Denton, G.H., Alley, R.B., Comer, G.C., and Broecker, W.S., 2005, The role of seasonality in abrupt climate change: Quaternary Science Reviews, v. 24, p. 1159–1182.

Deplazes, G., Anselmetti, F.S., and Hajdas, I., 2007, Lake sediments deposited on the Flims rockslide mass: the key to date the largest mass movement of the Alps, v. 19, p. 252–258.

Duncan, J.M., 1996, State of the Art: Limit Equilibrium and Finite-Element Analysis of Slopes: Journal of Geotechnical Engineering, v. 122, p. 577–596.

Eberli, G.P., Hsü, K.J., and Kelts, K.R., 1984, Water content and bulk density of Zuebo sediments in Hsü, K.J., and Kelts, K.R., eds., Quaternary geology of Lake Zurich; an interdisciplinary investigation by deep-lake drilling, Stuttgart, Schweizerbart, p. 115–124.

Evans, J., Dowdeswell, J.A., Grobe, H., Niessen, F., Stein, R., Hubberten, H.W., and Whittington, R.J., 2002, Later Quaternary sedimentation in Kejser Franz Joseph Fjjord and the continental margin of East Greenland, in Dowdeswell, J.A., and O Cofaigh, C., eds., Glacier-Influenced Sedimentation on High-Latitude Continental Margins, Volume 203: Geological Society, London, Special Publications: London, The Geologcial Society of London, p. 149–179.

Eyles, N., Boyce, J.I., Halfman, J.D., and Koseoglu, B., 2000, Seismic stratigraphy of Waterton Lake, a sediment-starved glaciated basin in the Rocky Mountains of Alberta, Canada and Montana, USA: Sedimentary Geology, v. 130, p. 283–311.

Fäh, D., Giardini, D., Bay, F., Bernardi, F., Braunmiller, J., Deichmann, N., Furrer, M., Gantner, L., Gisler, M., Isenegger, D., Jimenez, M.J., Kastli, P., Koglin, R., Masciadri, V., Rutz, M., Scheidegger, C., Schibler, R., Schorlemmer, D., Schwarz-Zanetti, G., Steimen, S., Sellami, S., Wiemer, S., and Wossner, J., 2003, Earthquake Catalogue Of Switzerland (ECOS) and the related macroseismic database: Eclogae Geologicae Helvetiae, v. 96, p. 219–236.

Fäh, D., Gisler, M., Jaggi, B., Kästli, P., Lutz, T., Masciadri, V., Matt, C., Mayer-Rosa, D., Rippmann, D., Schwarz-Zanetti, G., Tauber, J., and T., W., submitted, An interdisciplinary Revision of the 1356 Basel Earthquake.: submitted to Geophysical Journal International.

Ferry, M., Meghraoui, M., Delouis, B., and Giardini, D., 2005, Evidence for Holocene palaeoseismicity along the Basel-Reinach active normal fault (Switzerland): a seismic source for the 1356 earthquake in the Upper Rhine graben: Geophysical Journal International, v. 160, p. 554–572.

Finckh, P., Kelts, K., and Lambert, A., 1984, Seismic Stratigraphy and Bedrock Forms in Perialpine Lakes: Geological Society of America Bulletin, v. 95, p. 1118–1128.

Florineth, D., and Schluchter, C., 1998, Reconstructing the Last Glacial Maximum (LGM) ice surface geometry and flowlines in the central Swiss Alps: Eclogae Geologicae Helvetiae, v. 91, p. 391–407.

Fread, 1996, Dam-breach floods, in Singh, V.P., ed., Hydrology of disasters Volume 24: Water Science and Technology Library: Dordrecht, Kluwer Academic Publishing, p. 85–126.

Fredlund, D.G., and Krahn, J., 1977, Comparison of Slope Stability Methods of Analysis: Canadian Geotechnical Journal, v. 14, p. 429–439.

Furger, G., 1991, Von der Geologie zum Stofftransportmittel sic [PhD thesis]: Zürich, ETH Zurich.

Giardini, D., Wiemer, S., Fäh, D., and Deichmann, N., 2004, Seismic Hazard Assessment of Switzerland: Swiss Seismological Service, ETH Zürich.

Giovanoli, F., 1979, Die remanente magnetisierung von Seesedimenten [PhD thesis]: Zürich, ETH Zürich.

Girardclos, S., Fiore, J., Rachoud-Schneider, A.M., Baster, I., and Wildi, W., 2005, Petit-Lac (western Lake Geneva) environment and climate history from deglaciation to the present: a synthesis: Boreas, v. 34, p. 417–433.

Girardclos, S., Schmidt, O.T., Sturm, M., Ariztegui, D., Pugin, A., and Anselmetti, F.S., 2007, The 1996 AD delta collapse and large turbidite in Lake Brienz: Marine Geology, v. 241, p. 137–154.

Gisler, M., Fäh, D., and Kästli, P., 2004, Historical seismicity in Central Switzerland: Eclogae-Geologicae-Helvetiae, v. 97, p. 221–236.

Goldfinger, C., Nelson, C.H., and Johnson, J.E., 2003, Holocene earthquake records from the Cascadia subduction zone and northern San Andreas Fault on precise dating of offshore turbidites: Annual Review of Earth and Planetary Sciences, v. 31, p. 555–577.

Gyger, M., Mueller Vonmoos, M., and Schindler, C., 1976, Untersuchungen zur Klassifikation spaet- und nacheiszeitlicher Sedimente aus dem Zuerichsee: Schweizerische Mineralogische und Petrographische Mitteilungen, v. 56, p. 387–406.

Haeberli, W., and Schlüchter, C., 1987, Geological evidence to constrain modelling of the Late Pleistocene Rhonegletscher, Swiss Alps. The Physical Basis of Ice Sheet Modelling., Proceedings of the Vancouver Symposium, Volume IAHS, 170: Vancouver, p. 333–346.

Hajdas, I., IvyOchs, S.D., Bonani, G., Lotter, A.F., Zolitschka, B., and Schluchter, C., 1995, Radiocarbon age of the Laacher See Tephra: 11,230+/-40 BP: Radiocarbon, v. 37, p. 149–154.

Hampton, M.A., Lee, H.J., and Locat, J., 1996, Submarine landslides: Reviews of Geophysics, v. 34, p. 33–59.

Hantke, R., 2003, Unterseeische Moränen im Vierwald-

stätter See, in Lienert, S., ed., Geologie und Geotope im Kanton Schwyz, Volume 14: Einsiedeln, Schwyzerische Naturforschende Gesellschaft, p. 106–109.

Heim, A., 1876, Bericht und Expertengutachten über die im Februar und September 1875 in Horgen vorgekommenen Rutschungen, in Expertenkommission, ed., Hofer und Burgen, p. 22.

Heim, A., 1908, Über rezente und fossile subaquatische Tuschungen und deren lithologischen Bedeutung, Neues Jahrbuch für Mineralogie, Geoglogie und Paläontologie, Volume Band II, p. 136–157.

Hsü, K.J., and Kelts, K., 1985, Swiss Lakes as a Geological Laboratory .1. Turbidity Currents: Naturwissenschaften, v. 72, p. 315–321.

Hsü, K.J., and Kelts, K.R., 1970, Seismic investigation of Lake Zurich; part II, Geology: Eclogae Geologicae Helvetiae, v. 63, p. 525–538.

Hsü, K.J., and Kelts, K.R., 1984, Quaternary geology of Lake Zurich an interdisciplinary investigation by Deep-Lake drilling, Contribution to Sedimentology: Stuttgart, Schweizerbart, p. 210.

Hubbert, K.M., and Rubey, W.W., 1959, Role of fluid pressure in mechanics of overthrust faulting: Geological Society of America Bulletin, v. 70, p. 115–166.

Huber, R., 1938, Der Schuttkegel der Sihl im Gebiete der Stadt Zürich und das prähistorische Delta am See: Vierteljahresschrift der Naturforschendengesellschaft in Zürich, v. 83, p. 131–214.

Huggel, C., Haeberli, W., Kaab, A., Bieri, D., and Richardson, S., 2004, An assessment procedure for glacial hazards in the Swiss Alps: Canadian Geotechnical Journal, v. 41, p. 1068–1083.

Huggel, C., Kaab, A., Haeberli, W., Teysseire, P., and Paul, F., 2002, Remote sensing based assessment of hazards from glacier lake outbursts: a case study in the Swiss Alps: Canadian Geotechnical Journal, v. 39, p. 316–330.

Institute, B.S., 1977, Methods of testing soild for civil engineering purposes, BS 1377. BSI, London: London, BSI.

Ivy Ochs, S., Schafer, J., Kubik, P.W., Synal, H.A., and Schluchter, C., 2004, Timing of deglaciation on the northern Alpine foreland (Switzerland): Eclogae-Geologicae-Helvetiae, v. 97, p. 47–55.

Jäckli, H., 1989, Geologie von Zürich: Zürich, Orell Füssli.

Kahle, H.G., Geiger, A., Bürki, B., Gubler, E., Marti, U., Wirth, B., Rothacher, M., Gurtner, W., Beutler, B., Bauersima, I., and Pfiffner, O.A., 1997, Recent curstal movements, geoid, and density distribution: contribution from integrated satellite and terrestrail measurments, in Pfiffner, O.A., Lehner, P., Heitzmann, P., Mueller, S., and Steck, A., eds., NRP 20 - Deept Strucutre of the Swiss Alps: Basel, Birkhäuser, p. 251–259.

Kastrup, U., 2002, Seismotectonics and stress field variations in Switzerland [PhD thesis]: Zurich, ETH Zurich.

Kastrup, U., Zoback, M.L., Deichmann, N., Evans, K.F., Giardini, D., and Michael, A.J., 2004, Stress field variations in the Swiss Alps and the northern Alpine foreland derived from inversion of fault plane solutions: Journal of Geophysical Research-Solid Earth, v. 109, p. B01402.

Keefer, D.K., 2002, Investigating landslides caused by earthquakes - A historical review: Surveys in Geophysics, v. 23, p. 473–510.

Kelts, K., 1978, Geological and Sedimentary Evolution of Lake Zurich and Zug, Switzerland [PhD thesis]: Zurich, ETH Zurich.

Kelts, K., 1998, Components in lake sediments: Smear slide identificaction., p. http://lrc.geo.umn.edu/smears/smsl.html.

Kelts, K., Briegel, U., Ghilardi, K., and Hsu, K., 1986, The Limnogeology-EtH Coring System: Schweizerische Zeitschrift für Hydrologie-Swiss Journal of Hydrology, v. 48, p. 104–115.

Kelts, K., and Hsu, K.J., 1980, Resedimented facies of 1875 Horgen slumps in Lake Zurich and a process model of longitudinal transport of turbidity currents: Eclogae Geologicae Helvetiae, p. 73; 1, Pages 271–281.

Kempf, T., Freimoser, M., Haldimann, P., Longo, V., Müller, E., Schindler, C., Styger, G., and Wyssling, L., 1986, Die Grundwasser Vorkommen im Kanton Zürich: Bern, Schweizerische Geotechnische Kommision, 211 p.

Kempf, T., and Walter, U., 1985, Wärmegewinnung aus dem Grundwasser im Infiltrationsbereich der Limmat in Zürich: Wasser Energie Luft, v. 77, p. 343.

Kissling, E., 2004, Alpine orogeny and Seismictiy in Switzerland: 2nd Swiss Geoscience Meeting, Lausanne, v. Abstracts, p. 210.

Kopp, J., 1938, Der Einfluss des Krienbaches auf die Gestatlung des Luzernesees und die Hebung des Seespiegels des Viervaldstättersees: Eclogae Geologicae Helvetiae, v. 31, p. 376–378.

Kramer, S.L., 1996, Geotechnical earthquake engineering: New Jersey, Prentice Hall, 653 p.

Kuen, E., 1999, Der Uferabbruch im Kusen: Küsnachter Jahrheft, v. 39, p. 44–50.

Lambe, T.W., and Whitmann, R.V., 1979, Soil Mechanics: Singapore, John Wiley & Sons, 553 p.

Lee, H.J., 2005, Undersea landslides: extent and significance in the Pacific Ocean, an update: Natural Hazards and Earth System Sciences, v. 5, p. 877–892.

Lee, H.J., and Edwards Brian, D., 1986, Regional method to assess offshore slope stability: Journal of Geotechnical Engineering, v. 112, p. 486–509.

Lemcke, G., 1992, Ablagerungen aus Extremereignissen als Zeitmarker der Sedimentationsgeschichte im Becken von Vitznau/Weggis (Vierwaldstättersee, Schwiz) [MSc thesis]: Götting, Georg-August-Universtität Götting.

Leroueil, S., Vaunat, J., Picarelli, L., Locat, J., Lee Homa, J., and Faure, R., 1996, Geotechnical characterization of slope movements, Proceeding of International Symposium on Landslides, Volume 1: Trondheim, p. 53–74.

Leynaud, D., Mienert, J., and Nadim, F., 2004, Slope stability assessment of the Helland Hansen area offshore the mid-Norwegian margin: Marine Geology, v. 213, p. 457–480.

Lister, G.S., 1985, Late Pleistoncene Alpine Degalciation and Post-Glacial Climatic Developments in Switzerland: the record from sediments in a peri-alpine lake basin. [PhD thesis]: Zürich, ETH Zürich.

Lister, G.S., 1988, A 15,000-year isotopic record from Lake Zuerich of deglaciation and climatic change in Switzerland: Quaternary Research, v. 29, p. 129–141.

Lister, G.S., Giovanoli, F., Eberli, G., Finckh, P., Finger, W., He, Q., Heim, C., Hsu, K.J., Kelts, K., Peng, C., Sidler, C., and Zhao, X., 1984, Late Quaternary Sediments in Lake Zurich, Switzerland: Environmental Geology, v. 5, p. 191–205.

Locat, J., and Lee, H.J., 2002, Submarine landslides: advances and challenges: Canadian Geotechnical Journal, v. 39, p. 193–212.

Locat, P., Leroueil, S., Locat, J., and Duchesne, M.J., 2003, Characterisation of submarine flow-slide at Pointe-Du-Fort, Saguenay Fjord, Quebec, Canada, in Locat, J., and Mienert, J., eds., Submarine Mass Movements and their consequences: 1st international Symposium, p. 521–529.

Longva, O., Janbu, N., Blikra, L.H., and Boe, R., 2003, The 1996 Finneidfjord slide; seafloor failure and slide dynamics, in Locat, J., and Mienert, J., eds., Submarine Mass Movements and their consequences: 1st international Symposium, p. 531–538.

Lu, T.S., and Bryant, W.R., 1997, Comparison of vane shear and fall cone strengths of soft marine clay: Marine Georesources & Geotechnology, v. 15, p. 67–82.

Lunne, T., Robertson, P.K., and Powell, J.J.M., 1997, Cone Penetration Testing in Geotechnical Practice, Spon Press, 312 p.

Lysa, A., Sejrup, H.P., and Aarseth, I., 2004, The late glacial-Holocene seismic stratigraphy and sedimentary environment in Ranafjorden, northern Norway: Marine Geology, v. 211, p. 45–78.

Mackiewicz, N.E., Powell, R.D., Carlson, P.R., and Molnia, B.F., 1984, Interlaminated ice-proximal glacimarine sediments in Muir Inlet, Alaska: Marine Geology, v. 57, p. 113–147.

Magny, M., 2004, Holocene climate variability as reflected by mid-European lake-level fluctuations and its probable impact on prehistoric human settlements: Quaternary International, v. 113, p. 65–79.

Malde, H.E., 1968, The catastrophic late Pleistocene Bonneville flood in the Snake River plain, Idaho: U.S. Geological Survey Professional Paper, v. 596, p. 52 p.

Mayer-Rosa, D., and Cadiot, B., 1979, Review of the 1356 Basel Earthquake - Basic Data: Tectonophysics, v. 53, p. 325–333.

Meghraoui, M., Delouis, B., Ferry, M., Giardini, D., Huggenberger, P., Spottke, I., and Granet, M., 2001, Active normal faulting in the upper Rhine graben and paleoseismic identification of the 1356 Basel earthquake: Science, v. 293, p. 2070–2073.

Michetti, A.M., Audemard, F.A., and Marco, S., 2005, Future trends in paleoseismology: Integrated study of the seismic landscape as a vital tool in seismic hazard analyses: Tectonophysics, v. 408, p. 3–21.

Middleton, G.V., and Southard., J.B., 1984, Mechanic of Sediment Movement: Tulsa, S.E.P.M., 401 p.

Mienert, J., 2004, COSTA-continental slope stability: major aims and topics: Marine Geology, v. 213, p. 1–7.

Moernaut, J., De Batist, M., Charlet, F., Heirman, K., Chapron, E., Pino, M., Brummer, R., and Urrutia, R., 2007, Giant earthquakes in South-Central Chile revealed by Holocene mass-wasting events in Lake Puyehue: Sedimentary Geology, v. 195, p. 239–256.

Mohrig, D., and Marr, J.G., 2003, Constraining the efficiency of turbidity current generation from submarine debris flows and slides using laboratory experiments: Marine and Petroleum Geology, v. 20, p. 883–899.

Monecke, K., Anselmetti, F., Becker, A., Schnellmann, M., Sturm, M., and Giardini, D., 2006, Earthquake-induced deformation structures in lake deposits: A Late Pleistocene to Holocene paleoseismic record for Central Switzerland: Eclogae Geologicae Helvetiae, v. 99, p. 343–362.

Monecke, K., Anselmetti, F.S., Becker, A., Sturm, M., and Giardini, D., 2004, The record of historic earthquakes in lake sediments of Central Switzerland: Tectonophysics, v. 394, p. 21–40.

Morgenstern, N.R., 1967, Submarine slumping and initiation of turbidity currents, in Richards, A.F., ed., Marine Geotechnique UP: Urbana, IL, p. 189–220.

Morgenstern, N.R., and Price, V.E., 1965, Analysis of Stability of General Slip Surfaces: Geotechnique, v. 15, p. 79.

Mulder, T., and Cochonat, P., 1996, Classification of offshore mass movements: Journal of Sedimentary Research, v. 66, p. 43–57.

Mulder, T., Syvitski, J.P.M., Migeon, S., Faugeres, J.C., and Savoye, B., 2003, Marine hyperpycnal flows: initiation, behavior and related deposits. A review: Marine and Petroleum Geology, v. 20, p. 861–882.

Müller, B.U., 1995, Das Walensee-/Seeztal - eine Typusregion alpiner Talgenese: Von Entstehung und Vergehen des grossen Rheintal-/Zürichsee [PhD thesis]: Bern, Universität Bern.

Murphy, J.R., and O'Brien, L.J., 1977, The correlation of peak ground acceleration amplitude with seismic intensity and other physical parameters, Volume 67, p. 877–915.

Newmark, N.M., 1965, Effects of Earthquakes on Dams and Embankments: Geotechnique, v. 15, p. 139–160.

Niessen, F., Lister, G.S., and Giovanoli, F., 1992, Dust transport and palaeoclimate during the Oldest Dryas in Central Europe: implications from varves (Lake Constance): Climate Dynamics, v. 8, p. 71–81.

Nipkow, 1920, Vorläufige Mitteilungen über Untersuchungen des Schlammabsatzes im Zürichsee: Zeischrift für Hydrologie, v. 1, p. 1–28.

Nittrouer, C.A., 1999, STRATAFORM: overview of its design and synthesis of its results: Marine Geology, v. 154, p. 3–12.

Nomade, J., Chapron, E., Desmet, M., Reyss, J.L., Arnaud, F., and Lignier, V., 2005, Reconstructing historical seismicity from lake sediments (Lake Laffrey, western Alps, France): Terra Nova, v. 17, p. 350–357.

O'Connor, J.E., and Baker, V.R., 1992, Magnitudes and Implications of Peak Discharges from Glacial Lake Missoula: Geological Society of America Bulletin, v. 104, p. 267–279.

O'Connor, J.E., and Costa, J.E., 1993, Geologic and hydrologic hazards in glacierized basins in North America resulting from 19th and 20th century global warming: Natural Hazards, v. 8, p. 121–140.

Oerlemans, J., 2000, Holocene glacier fluctuations: is the current rate of retreat exceptional?: Annals of Glaciology, v. 31, p. 39–44.

Owen, M., Day, S., and Maslin, M., 2007, Late Pleistocene submarine mass movements: occurrence and causes: Quaternary Science Reviews, v. 26, p. 958–978.

Penk, A., and Brückner, E., 1909, Die Alpen im Eiszeitalter: Leipzig, Tauchnitz.

Persaud, M., and Pfiffner, O.A., 2004, Active deformation in the eastern Swiss Alps: post-glacial faults, seismicity and surface uplift: Tectonophysics, v. 385, p. 59–84.

Pfiffner, O.A., and Heitzmann, P., 1997, Titel, in Pfiffner, O.A., Lehner, P., Heitzmann, P., Mueller, S., and Steck, A., eds., NRP 20-Deep Structure of the Swiss Alps.: Basel, Birkhäuser, p. 115–122.

Pfiffner, O.A., and Kühni, A., 2001, Geological and Hydrological Profiles, Part1: Geology, in Geology, F.o.o.W.a., ed., Hydrological atlas of Switzerland: Basel, Birkhäuser.

Pika, J., 1983, Zur Isotopengeochemie und Mineralogie der lacustrinen Ablagerungen im Zürichsee und im Schwarzen Meer [PhD thesis]: Zürich, ETH Zürich.

Plötze, M., Giudici Trausch, J., Messerklinger, S., and Springman, S.M., 2003, Swiss Lacustrine Clay: Mineralogical and mechanical characteristics, in Cudny, K.a., ed., Int. Workshop on Geotechnics of Soft Soils - Theory and Practice: Noordwijkerhout, p. 473–478.

Prior, D.B., Bornhold, B.D., and Johns, M.W., 1984, Depositional Characteristics of a Submarine Debris Flow: Journal of Geology, v. 92, p. 707–727.

Quigley, R.M., and Ogunbadejo, T.A., 1972, Clay Layer Fabric and Oedometer Consoidation of Soft varved clay: Canadian Geotechnical Journal, v. 9, p. 165–175.

Reimer, P.J., Baillie, M.G.L., Bard, E., Bayliss, A., Beck, J.W., Bertrand, C.J.H., Blackwell, P.G., Buck, C.E., Burr, G.S., Cutler, K.B., Damon, P.E., Edwards, R.L., Fairbanks, R.G., Friedrich, M., Guilderson, T.P., Hogg, A.G., Hughen, K.A., Kromer, B., McCormac, G., Manning, S., Ramsey, C.B., Reimer, R.W., Remmele, S., Southon, J.R., Stuiver, M., Talamo, S., Taylor, F.W., van der Plicht, J., and Weyhenmeyer, C.E., 2004, IntCal04 terrestrial radiocarbon age calibration, 0–26 cal kyr BP: Radiocarbon, v. 46, p. 1029–1058.

Reynolds, J.M., 1992, The identification and mitigation of glacier-related hazards: examples from the Cordillera Blanca, Peru, in McCall G.J.H., Laming, D.J.C., and Scott, S.C., eds., Geohazards: London, Chapman and Hall, p. 143–157.

Riesen, K., and Naef, F., 2007, What can Neolithic and Bronze Age lake dwellings tell us about former Climate Change?, Abstract at EGU: Vienna.

Rothwell, R.G., 1989, Minerals and mineraloids in marine sediments an optical identification guide: London etc., Elsevier Applied Science, XIV, 279 p.

Rudoy, A.N., 2002, Glacier-dammed lakes and geological work of glacial superfloods in the Late Pleistocene, Southern Siberia, Altai Mountains: Quaternary International, v. 87, p. 119–140.

Schindler, C., 1968, Zur Quartaergeologie zwischen dem untersten Zuerichsee und Baden: Eclogae Geologicae Helvetiae, p. 61; 2, Pages 395–433.

Schindler, C., 1971, Geologie von Zürich und ihre Beziehung zu Seespiegelschwankungen.: Vierteljahresschrift der Naturforschendengesellschaft in Zürich, v. 116, p. 285–315.

Schindler, C., 1974, Zur Geologie des Zuerichsees: Eclogae Geologicae Helvetiae. 67; 1, Pages 163–196. 1974. 0012-9402.

Schindler, C., 1976, Eine geologische Karte des Zuerichsees und ihre Deutung: Eclogae Geologicae Helvetiae, v. 69, p. 125–138.

Schindler, C., 2004, Zum Quartär des Linthgebietes zwischen Luchsingen , dem Walensee und dem Züricher Obersee, Landesgeologie, BWG.

Schlatter, A., and Marti, U., 2002, Neues Landeshöhennetz der Schweiz LHN95: Vermessung, Photogrammetrie, Kulturtechnik, v. 1, p. 13–17.

Schlüchter, C., and Röthlisberger, C., 1995, 100 000 Jahr Gletschergeschicht, in (SANW), S.A.d.N., ed., Gletscher im ständigen Wandel, Volume 6: Zürich, vdf Hochschulverlag AG, p. 47–64.

Schneider, J.-L., Pollet, N., Chapron, E., Wessels, M., and Wassmer, P., 2004, Signature of Rhine Valley sturzstrom dam failures in Holocene sediments of Lake Constance, Germany: Sedimentary Geology, v. 169, p. 75–91.

Schnellmann, M., 2004, Late Quaternary Mass-Movements in a Perialpine Lake (Lake Lucerne, Switzerland) - Sedimentary Processes, Natural Hazards, and Paleoseismic Reconstructions [PhD thesis]: Zurich, ETH Zurich.

Schnellmann, M., Anselmetti Flavio, S., Giardini, D., McKenzie Judith, A., and Ward Steven, N., 2002, Prehistoric earthquake history revealed by lacustrine slump deposits: Geology, v. 30, p. 1131–1134.

Schnellmann, M., Anselmetti, F.S., Giardini, D., and McKenzie, J.A., 2005, Mass movement-induced fold-and-thrust belt structures in unconsolidated sediments in Lake Lucerne (Switzerland): Sedimentology, v. 52, p. 271-289.

Schnellmann, M., Anselmetti, F.S., Giardini, D., and McKenzie, J.A., 2006, 15,000 Years of mass-movement history in Lake Lucerne: Implications for seismic and tsunami hazards: Eclogae Geologicae Helvetiae, v. 99, p. 409–428.

Schwarz-Zanetti, G., 1998, Grundzüge der Klima- und Umweltgeschichte des Hoch- und Spätmittelalters in Mitteleuropa [PhD thesis]: Zurich, University of Zurich.

Schwarz-Zanetti, G., Deichmann, N., Fäh, D., Giardini, D., Jimenez, M.J., Masciadri, V., Schibler, R., and Schnellman, M., 2003, The earthquake in Unterwalden on September 18, 1601: A historico-critical macroseismic evaluation: Eclogae Geologicae Helvetiae, v. 96, p. 441–450.

Shilts, W.W., and Claque, J.J., 1992, Documentation of earthquake-induced disturbance of lake sediments using subbottom acoustic profiling: Canadian Journal of Earth Science, v. 29, p. 1018–1042

Sidler, C., 1988, Signification de la palynologie appliquée aux sédiments détritique et organiogène du Pléistocène supérieur: Eam-Terdiglaciaire vürmien et de l'Holocène entre Zoug, Zurich et Baden (Suisse) [PhD thesis]: Zurich, L'Ecole polytechnique fédérale Zurich.

Siegenthaler, C., Finger, W., Kelts, K., and Wang, S., 1987, Earthquake and Seiche Deposits in Lake Lucerne, Switzerland: Eclogae Geologicae Helvetiae, v. 80, p. 241–260.

Siegenthaler, C., Hsu, K.J., and Kleboth, P., 1984, Longitudinal Transport of Turbidity Currents - a Model Study of Horgen Events: Sedimentology, v. 31, p. 187–193.

Siegenthaler, C., and Sturm, M., 1991, Slump induced surges and seiment transport in Lake Uri, Switzerland, International Association of Theoretical and Applied Limnology, Volume 24, p. 955–958.

Sieh, K.E., 1978, Prehistoric Large Earthquakes Produced by Slip on San Andreas Fault at Pallett Creek, California: Journal of Geophysical Research, v. 83, p. 3907–3939.

Sims, J.D., 1973, Earthquake-Induced Structures in Sediments of Van Norman Lake, San Fernando, California: Science, v. 182, p. 161–163.

Sims, J.D., 1975, Determining Earthquake Recurrence Intervals from Deformational Structures in Young Lacustrine Sediments: Tectonophysics, v. 29, p. 141–152.

Sletten, K., Blikra, L.H., Ballantyne, C.K., Nesje, A., and Dahl, S.O., 2003, Holocene debris flows recognized in a lacustrine sedimentary succession: sedimentology, chronostratigraphy and cause of triggering: Holocene, v. 13, p. 907–920.

Smith, D.G., and Fisher, T.G., 1993, Glacial Lake Agassiz - the Northwestern Outlet and Paleoflood: Geology, v. 21, p. 9–12.

Solheim, A., 2006, Submarine mass movements and their consequences, 2nd international symposium: Summary: Norwegian Journal of Geology, v. 86, p. 151–154.

Stegmann, S., Strasser, M., Kopf, A., and Anselmetti, F.S., 2007, Geotechnical in situ characterisation of subaquatic slopes: The role of pore pressure transients versus frictional strength in landslide initiation: Geophysical Research Letter, p. L07607.

Stegmann, S., Villinger, H., and Kopf, A., 2006, Design of a modular, marine free-fall cone penetrometer: Sea Technology, v. 47, p. 27-+.

Strasser, M., and Anselmetti, F.S., 2008, Mass-movement event stratigraphy in Lake Zurich; A record of varying seismic and environmental impacts.: Beiträge zur Geologie der Schweiz, Geotechnische Serie, No. 95, p. 23–41.

Strasser, M., Anselmetti, F.S., Fah, D., Giardini, D., and Schnellmann, M., 2006, Magnitudes and source areas of large prehistoric northern Alpine earthquakes revealed by slope failures in lakes: Geology, v. 34, p. 1005–1008.

Strasser, M., Schindler, C., and Anselmetti, F.S., 2008, Late Pleistocene eartqhuake-triggered moraine dam failure and ouburst of Lake Zurich, Switzerland: Journal of Geophysical Research - Earth Surface, doi:10.1029/2007JF000802.

Strasser, M., Stegmann, S., Bussmann, F., Anselmetti, F.S., Rick, B., and Kopf, A., 2007, Quantifying subaqueous slope stability during seismic shaking: Lake Lucerne as model for ocean margins: Marine Geology, v. 240, p. 77–97.

Stuiver, M., and Reimer, P.J., 1993, Extended C-14 Data-Base and Revised Calib 3.0 C-14 Age Calibration Program: Radiocarbon, v. 35, p. 215–230.

Sturm, M., and Lotter, A.F., 1995, Lake sediments as environmental archives: EAWAG news, v. 38, p. 6–9.

Sturm, M., and Matter, A., 1978, Turbidites and varves in Lake Brienz (Switzerland); deposition of clastic detritus by density currents, in Matter, A., and Tucker, M.E., eds., Modern and ancient lake sediments; proceedings of a symposium, Volume Special Publication of the International Association of Sedimentologists. 2, Blackwell. Oxford International. 1978., p. 147–168.

Sultan, N., Cochonat, P., Canals, M., Cattaneo, A., Dennielou, B., Haflidason, H., Laberg, J.S., Long, D., Mienert, J., and Trincardi, F., 2004, Triggering mechanisms of slope instability processes and sediment failures on continental margins: a geotechnical approach: Marine Geology, v. 213, p. 291–321.

Teller, J.T., and Thorleifson, L.H., 1983, Galcial Lake Agassiz, in Teller, J.T., and Clayton, L., eds., Glacial Lake Agassiz: St. John's, Newfoundland, Geological Association of Canada, p. 261–290.

Terzaghi, K., 1925, Erdbaumechanik: Wien, Deuticke, 339 p.

Terzaghi, K., Peck, R.B., and Mesri, G., 1996, Compressibility of confined layers of soil, Soil Mechniscs in Engineering practice, Volume Third edition: New York.

Thevenon, F., and Anselmetti, F.S., 2007, 7200 years of human impact evidenced by automated image analysis of pyrogenic products from Lake Lucerne sediments

(Central Switzerland): Quaternary Science Reviews, v. 26, p. 2631–2643

URGELES, R., LEYNAUD, D., LASTRAS, G., CANALS, M., and MIENERT, J., 2006, Back-analysis and failure mechanisms of a large submarine slide on the ebro slope, NW Mediterranean: Marine Geology, v. 226, p. 185–206.

VAN RENSBERGEN, P., DE BATIST, M., BECK, C., and CHAPRON, E., 1999, High-resolution seismic stratigraphy of glacial to interglacial fill of a deep glacigenic lake: Lake Le Bourget, Northwestern Alps, France: Sedimentary Geology, v. 128, p. 99–129.

VITTORI, E., LABINI, S.S., and SERVA, L., 1991, Palaeoseismology - Review of the State-of-the-Art: Tectonophysics, v. 193, p. 9–32.

VON MOOS, A., 1942, Zur Quartärgeologie von Hurden-Rapperswil (Zürichsee): Eclogae Geologicae Helvetiae, v. 36.

WALDER, J.S., and O'CONNOR, J.E., 1997, Methods for predicting peak discharges of floods caused by failure of natural and constructed earthen dams, : Water Resource Research, v. 33, p. 2337–2348.

WALDMANN, N., ARIZTEGUI, D., ANSELMETTI, F.S., AUSTIN Jr., J.A., DUNBAR, R., MOY, C.M., and RECASENS, C., 2008, Seismic stratigraphy of Lago Fagnano sediments (Tierre del Fuego, Argentina) - A potential achrive of paleoclimatic change and tectonic activitiy since the Late Glacial: Geologica Acta, v. 6. 101–110

WATANABE, T., and ROTHACHER, D., 1996, The 1994 Lugge Tsho glacial lake outburst flood, Bhutan Himalaya: Mountain Research and Development, v. 16, p. 77–81.

WELLS, D.L., and COPPERSMITH, K.J., 1994, New Empirical Relationships among Magnitude, Rupture Length, Rupture Width, Rupture Area, and Surface Displacement: Bulletin of the Seismological Society of America, v. 84, p. 974–1002.

WESSELS, M., 1998, Natural environmental changes indicated by Late Glacial and Holocene sediments from Lake Constance, Germany: Palaeogeography, Palaeoclimatology, Palaeoecology, v. 140, p. 421–432.

ZHAO, X.F., HSUE, K.J., KELTS, K., and KELTS, K.R., 1984, Varves and other laminated sediments of Zuebo, in Hsü, K.J., and Kelts, K.R., eds., Quaternary geology of Lake Zurich; an interdisciplinary investigation by deep-lake drilling: Stuttgart, Schweizerbart, p. 161–176.

APPENDIX A

Table A 5.1: Compiled core information on remobilized morainic deposits (RM-deposits).

Stratigraphic succession	core ID	X [1] coordinate	Y [1] coordinate	Base of RM-deposit [masl]	Thickness of RM-deposits [m]	references
lake deposit -> reworked morainic deposits (RM) -> alluvial gravel deposits	9	681841	249454	387	7	JG[2] (GW Limmattal, 1969)
	23	682820	248585	377	21	JG[2] (GW Limmattal, 1969)
	83-6	682720	247712	377	2	JG[2] (SZU)
	83-8	682652	247609	378	12	JG[2] (SZU)
	-	682863	248069	380	25	JG[2] 71.251
	-	682494	248821	377	1	JG[2] 79/126
	1	682474	248424	381	9	Kempf et al., 1986
	3	682823	248277	381	30	Kempf et al., 1986
	4	682911	248228	364	31	Kempf et al., 1986
	5	682951	248211	378	24	Kempf et al., 1986
	6	682972	248196	380	20	Kempf et al., 1986
	7	683016	248184	382	20	Kempf et al., 1986
	8	683087	248152	376	24	Kempf et al., 1986
	9	683099	248147	375	25	Kempf et al., 1986
	10	683221	248093	382	19	Kempf et al., 1986
	11	683252	248079	389	11	Kempf et al., 1986
	12	683274	248065	392	6	Kempf et al., 1986
	13	683298	248043	394	4	Kempf et al., 1986
	14	683325	248021	395	4	Kempf et al., 1986
	15	683354	247991	396	4	Kempf et al., 1986
	16	683395	247970	394	7	Kempf et al., 1986
	-	679751	250394	386	2	S+C[3]
	-	682770	247887	370	10	VM[4]
	-	683153	248129	380	25	VM[4] 2018-5
	-	682638	248892	395	5	VM[4] 4067
	32/126	682906	247583	385	10	VM[4] 7007
alluvial gravel deposits -> reworked morainic deposits (RM) -> alluvial gravel deposits	2	682617	247442	393	10	JG[2] (SZU)
	4	682585	247450	401	2	JG[2] (SZU)
	423	682595	247671	370	6	JG[2] (SZU)
	426	682467	247166	398	10	JG[2] (SZU)
	433	682586	247567	395	4	JG[2] (SZU)
	83-11	682431	247105	400	7	JG[2] (SZU)
	83-7	682611	247524	385	16	JG[2] (SZU)
	84-51	682409	247060	405	4	JG[2] (SZU)
	84-51	682443	247036	398	15	JG[2] (SZU)
	84-53	682378	247021	406	3	JG[2] (SZU)
	84-63	682601	247492	391	11	JG[2] (SZU)
	84-65	682593	247472	392	7	JG[2] (SZU)
	B1-23	682605	247387	397	5	JG[2] (SZU)
	104	682401	248948	390	2	Kempf & Walter, 1985
	202-25	682524	247938	396	9	Kempf et al., 1986
	501-24	682628	248056	399	1	Kempf et al., 1986
	503-26	682429	247840	399	5	Kempf et al., 1986
	-	682695	247809	400	5	VM[4]
reworked morainic deposits (RM) -> alluvial gravel deposits	8	681105	249827	<383	> 7	JG[2] (GW Limmattal, 1969)
	11	681795	249415	<400	> 5	JG[2] (GW Limmattal, 1969)
	D4	681025	249617	<385	> 7	JG[2] (GW Limmattal, 1969)
	421	682670	247441	<381	> 19	JG[2] (SZU)
	422	682724	247593	<385	> 3	JG[2] (SZU)
	84-B	682671	247632	<384	> 2	JG[2] (SZU)
	2	682737	248311	<384	> 16	Kempf et al., 1986
	21	682540	248234	<387	> 19	Kempf et al., 1986
	22	682571	248321	<380	> 12	Kempf et al., 1986
	-	682569	248383	<485	> 20	VM[4] 2018-5

[1] *Location is given in Swiss Grid (CH1903) Coordinates.*

[2] *unpublished data provided by Jäckli Geologie Zürich*

[3] *unpublished data provided by Sieber & Cassina, Zürich*

[4] *unpublished data provided by Geo Von Moos AG, Zürich*

Table A 5.2: ^{14}C ages and calibration of samples from Lake Zurich.

Core Nr.	Location [1]	Depth in core [m]	Composite depth[2] [m]	Sample Nr.	Sample age[3] [^{14}C yr B.P.]	Sample age[4] [cal. yr B.P.]	material
ZHK04-7	688526 / 236159	2.07	1.41	ETH-30212	1095 ± 50	920 - 1150	leaf remains
ZHK04-7	688526 / 236159	2.81	2.05	ETH-30210	2135 ± 55	1990 - 2320	leaf remains
ZHK04-7	688526 / 236159	3.52	2.68	ETH-30213	3615 ± 55	3820 - 4090	leaf remains
ZHK04-7	688526 / 236159	4.13	3.21	ETH-30209	6105 ± 70	6790 - 7170	leaf remains
ZHK04-7	688526 / 236159	5.03	3.71	ETH-30208	8895 ± 80	9700 - 10250	leaf remains
ZHK04-7	688526 / 236159	5.32	3.9	ETH-30206	10230 ± 85	11600 - 12400	leaf remains
ZHK04-7	688526 / 236159	5.76	4.17	ETH-30207	11710 ± 100	13340 - 13770	wood
ZHK04-5	699687 / 230486	3.38	3.38	ETH-30216	5740 ± 70	6390 - 6730	leaf remains
ZHK04-5	699687 / 230486	3.78	3.78	ETH-30215	8995 ± 80	9750 - 10300	leaf remains
ZHK04-5	699687 / 230486	4.12	4.12	ETH-30715	11560 ± 90	13240 - 13640	wood
ZHK04-1	685585 / 240583	6.62	3.35	ETH-30762	6505 ± 65	7270 - 7520	leaf remains
Zübo 1980 [5]	687615 / 237266	5.75	3.86	GL8	9990 ± 150	11150 - 12100	wood
Zübo 1980 [5]	687615 / 237266	7.4	4.2	GL11	12400 ± 250	13750 - 15250	wood
Zübo 1980 [5]	687615 / 237266	7.5	4.27	GL15	12800 ± 250	14150 - 15850	wood
Zübo 1980 [5]	687615 / 237266	9.5	4.71	GL10	14150 ± 250	16500 - 17300	wood
Zübo 1980 [5]	687615 / 237266	13.8	5.05	GL 2	14600 ± 250	17100 - 18050	wood

[1] *Location is given in Swiss Grid (CH1903) coordinates.*

[2] *Projection to composite depth (i.e. relative to ZHK04-5) based on lithostratigraphic (visual core description, bulk density and magnetic susceptibility logs) and seismostratigraphic correlation*

[3] *Dating by AMS (accelerator mass spectrometry) with the tandem accelerator at the Institute of Particle Physics at the Swiss Federal Institute of Technology Zurich (ETH).*

[4] *Calibration (2s range) was carried out applying the IntCal04-calibration curve (Reimer et al., 2004).*

[5] *Dates by Lister (1988).*

APPENDIX B

***Figure B 1**: Bathymetry of the Lake Zurich study area (50 m contour interval and 20 m-depth contour (dottet line) in the upper flat basin), and location of sediment cores and seismic profiles shown in appendix.*

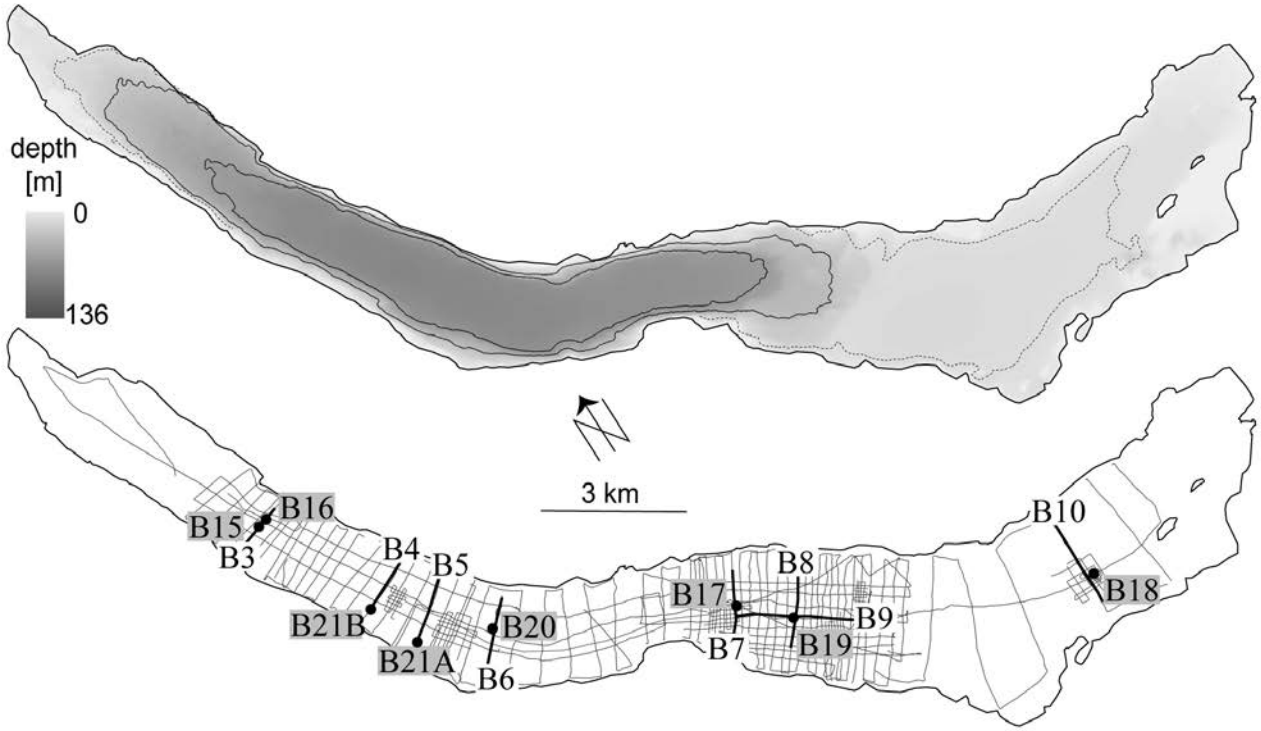

***Figure B 2**: Bathymetry of the Lake Lucerne study area (10 m contour interval) and location of sediment cores shown in appendix.*

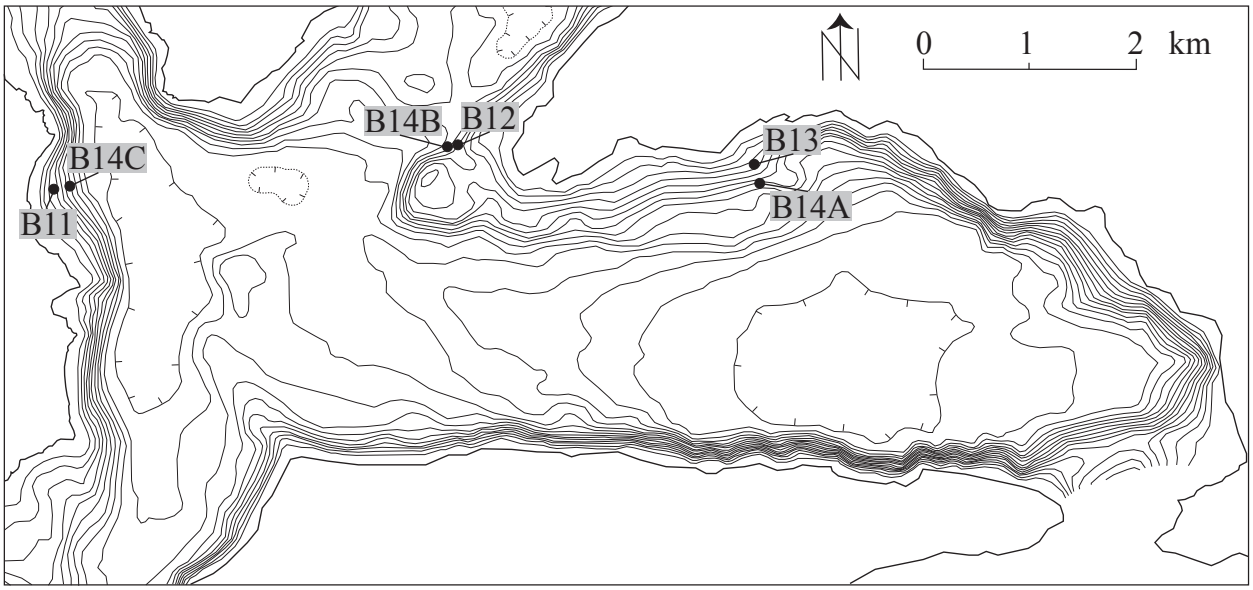

***Figure B 3**: Seismic Profile Z21-4Q*

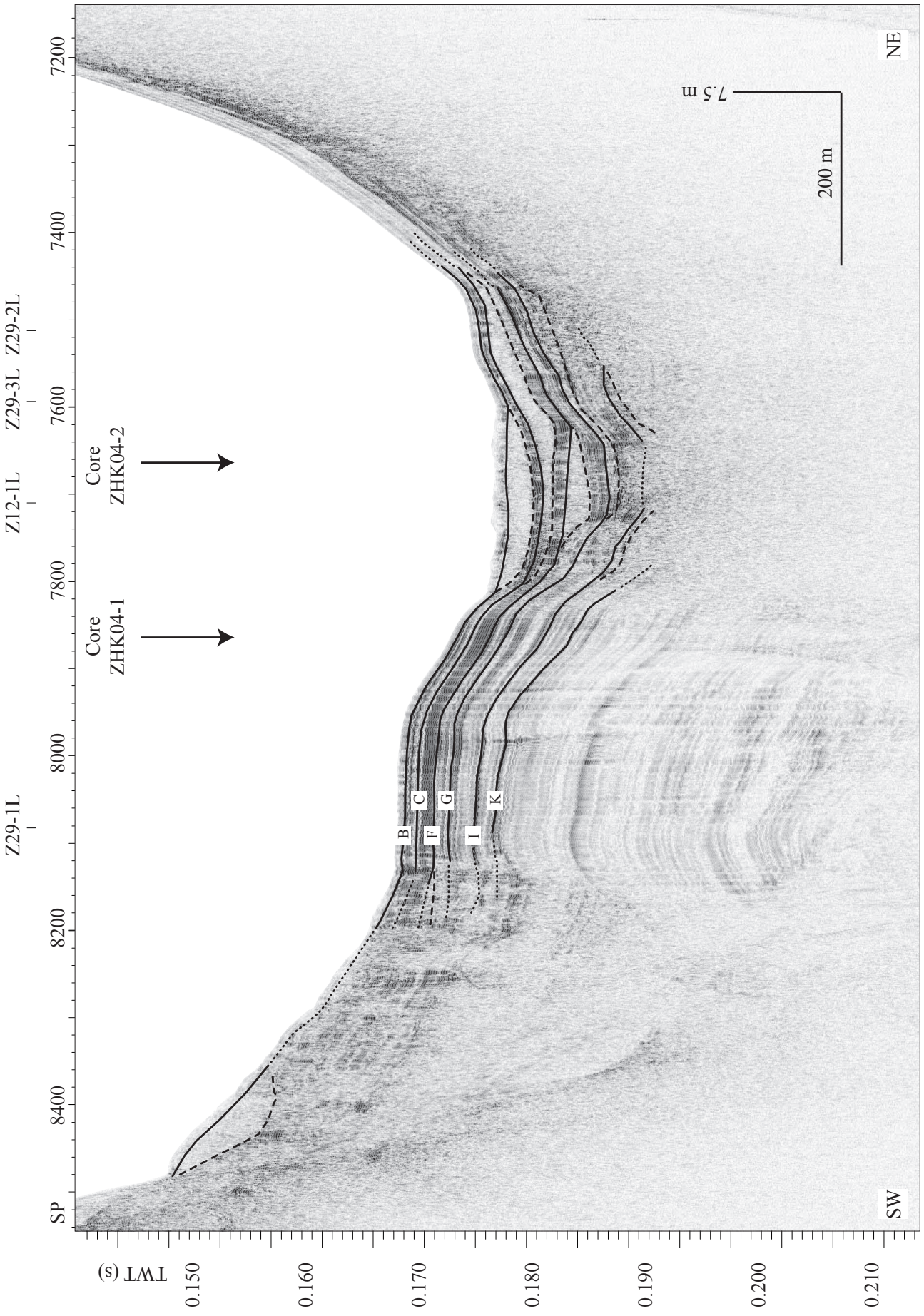

***Figure B 4**: Seismic Profile Z15-5Q*

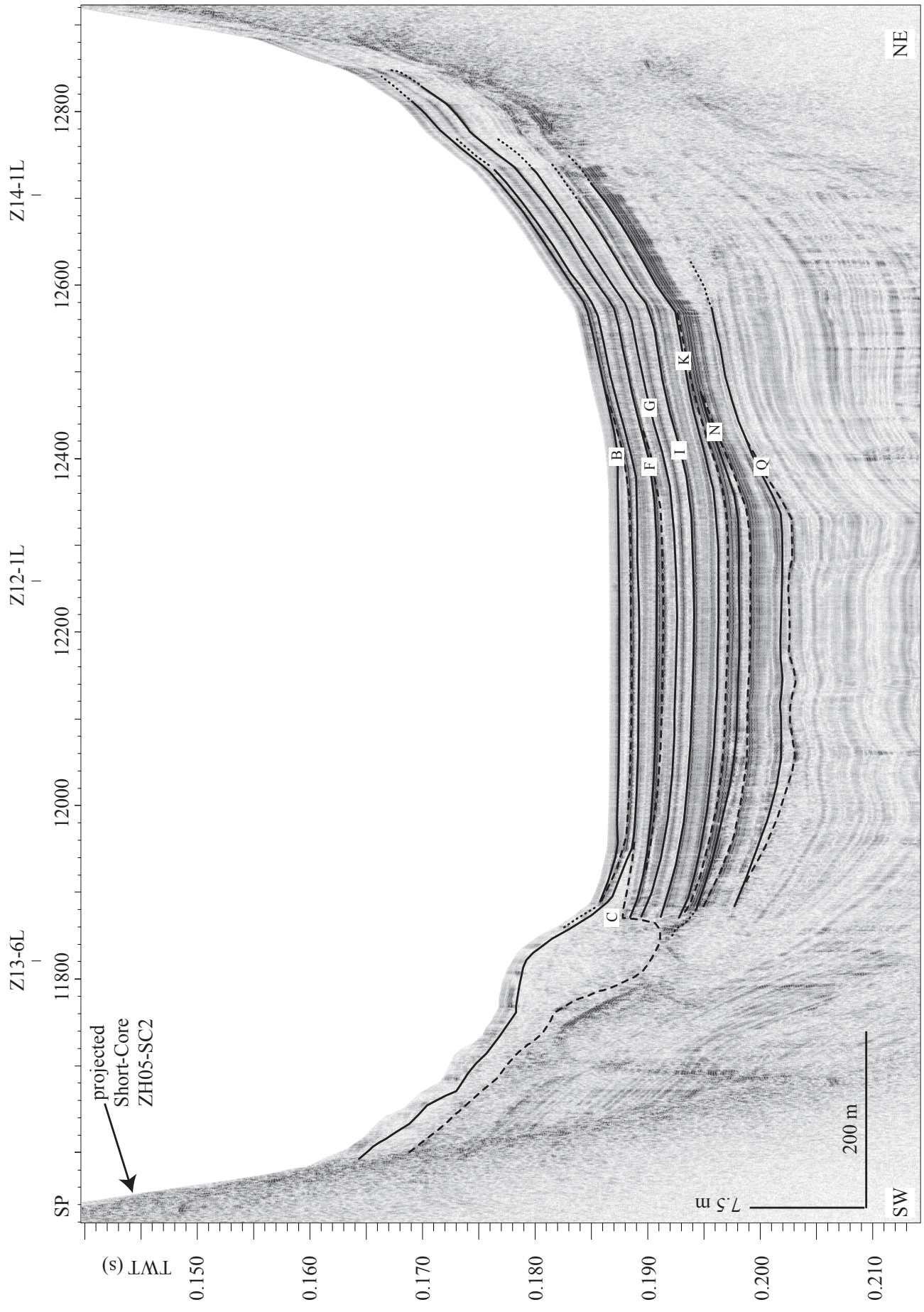

***Figure B 5**: Seismic Profile Z1-2Q*

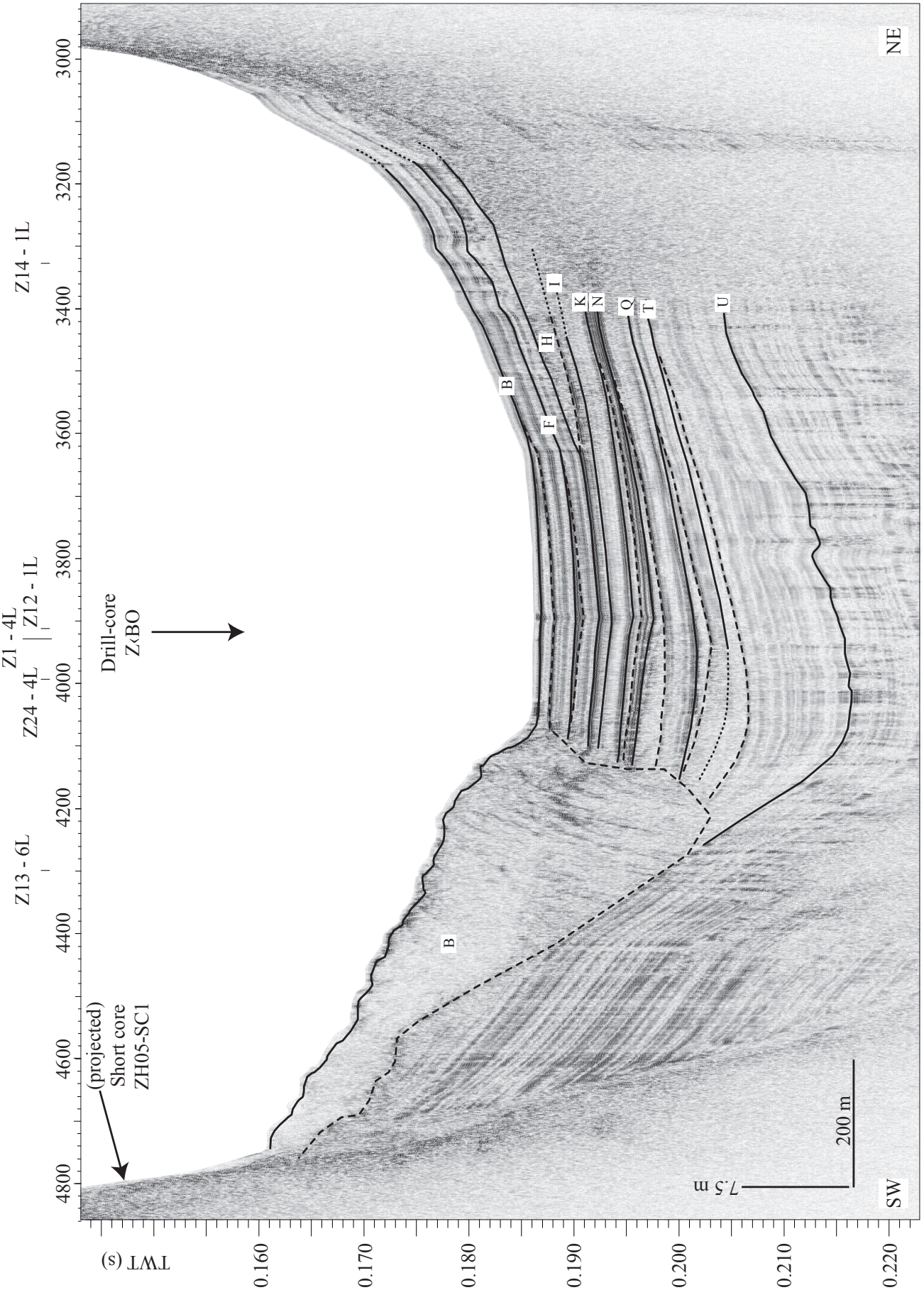

***Figure B 6**: Seismic Profile Z0-1Q*

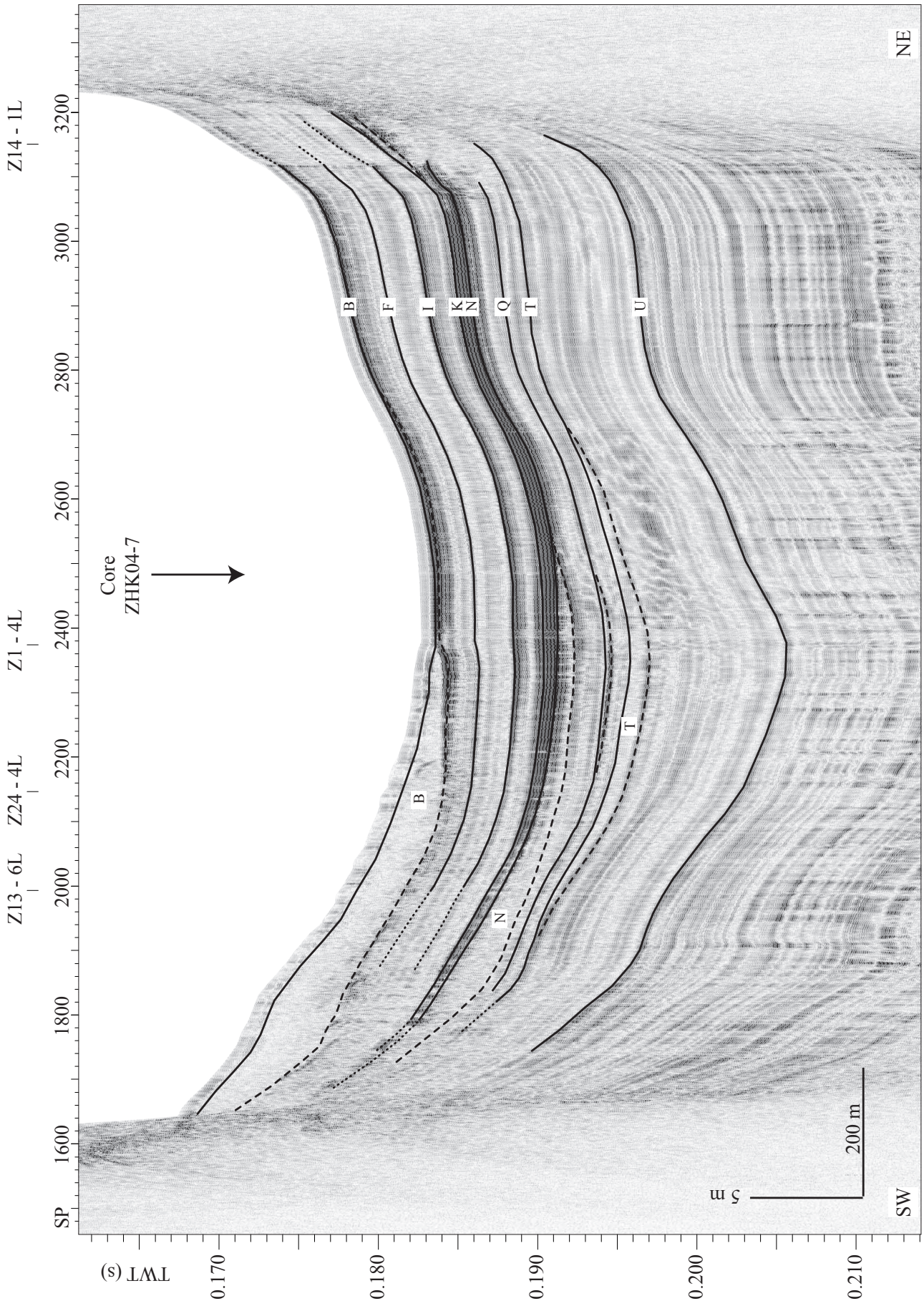

***Figure B 7**: Seismic Profile Z6-6Q*

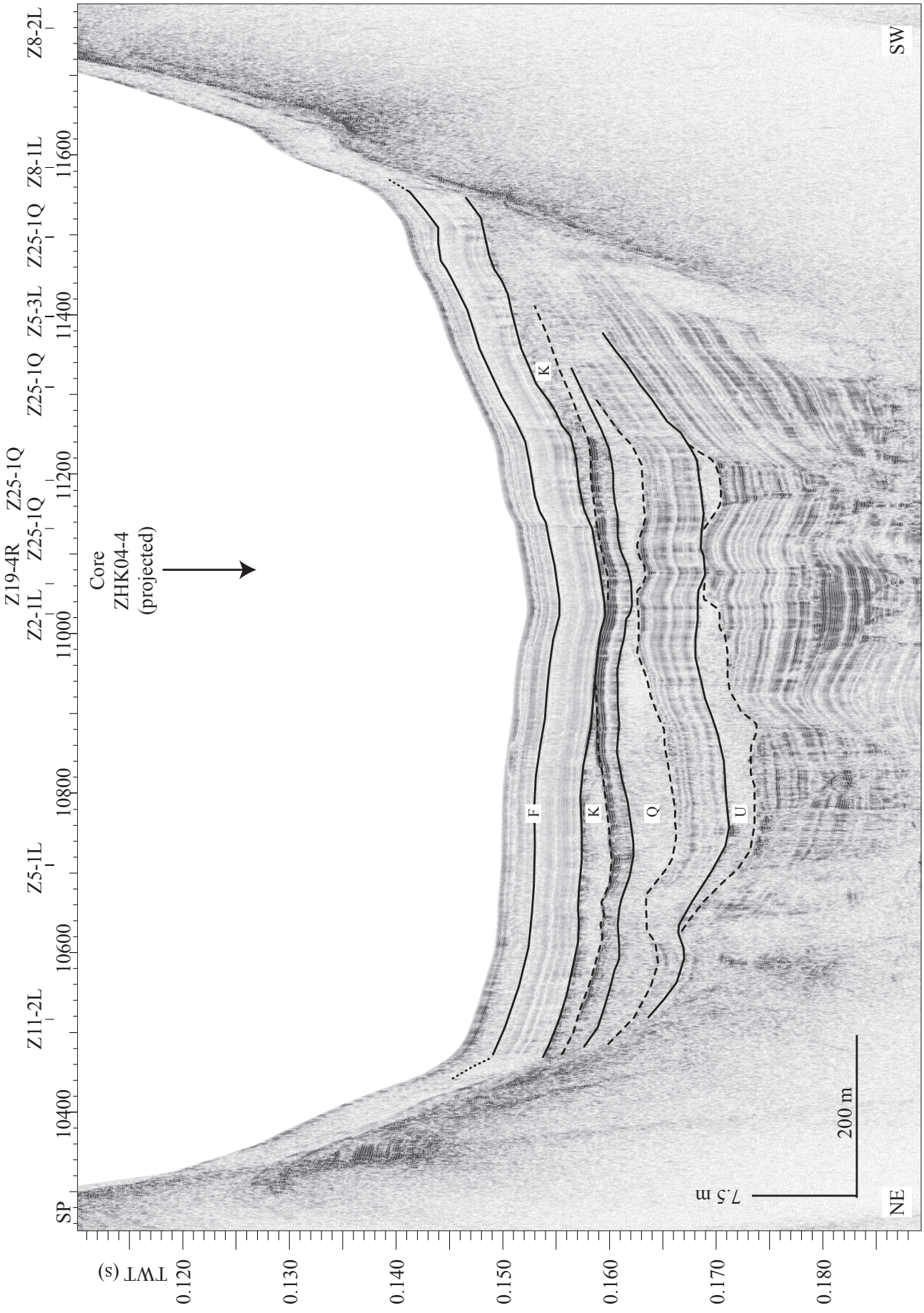

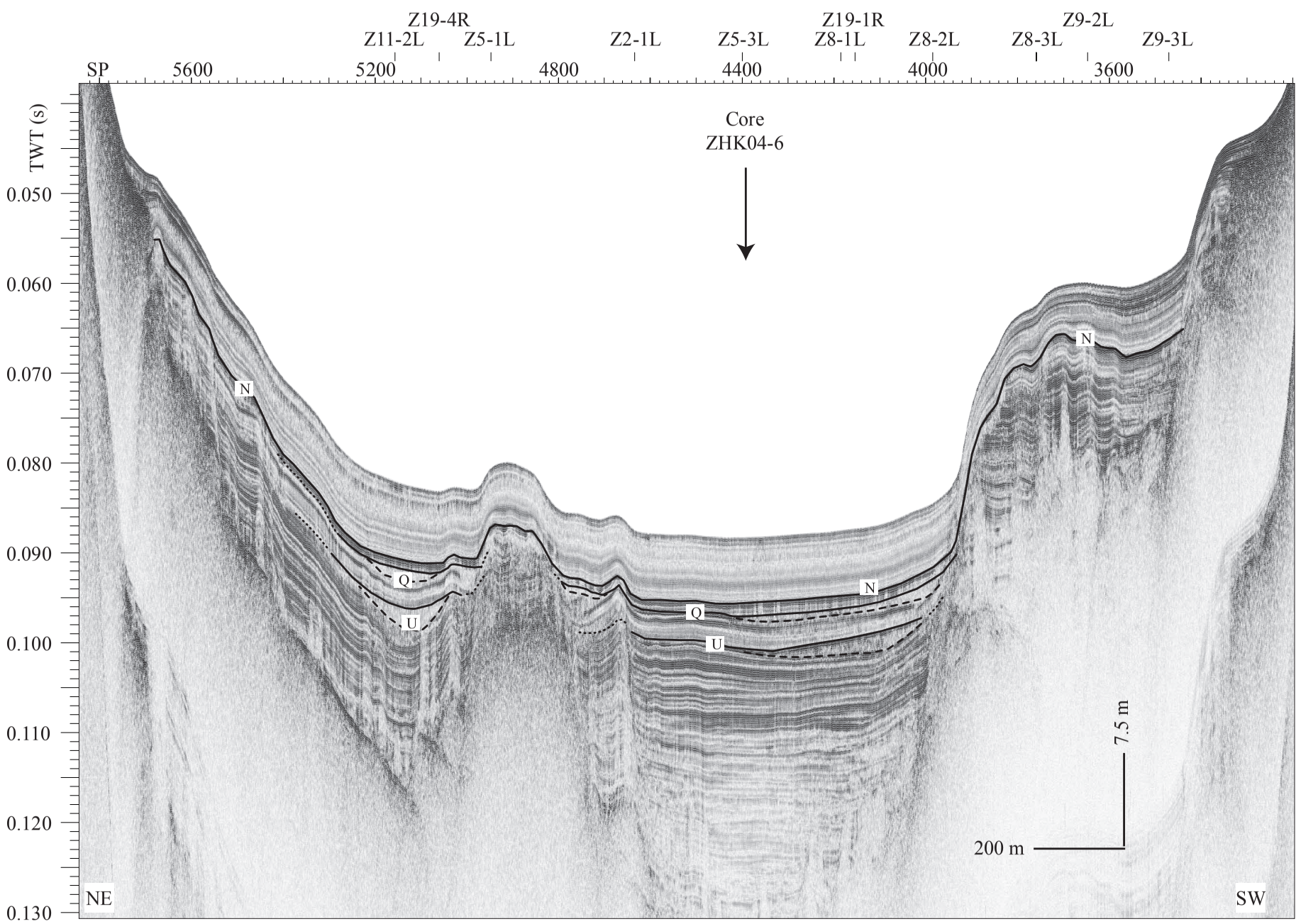

Figure B 8: *Seismic Profile Z7-2Q*

***Figure B 9**: Seismic Profile Z5-3L*

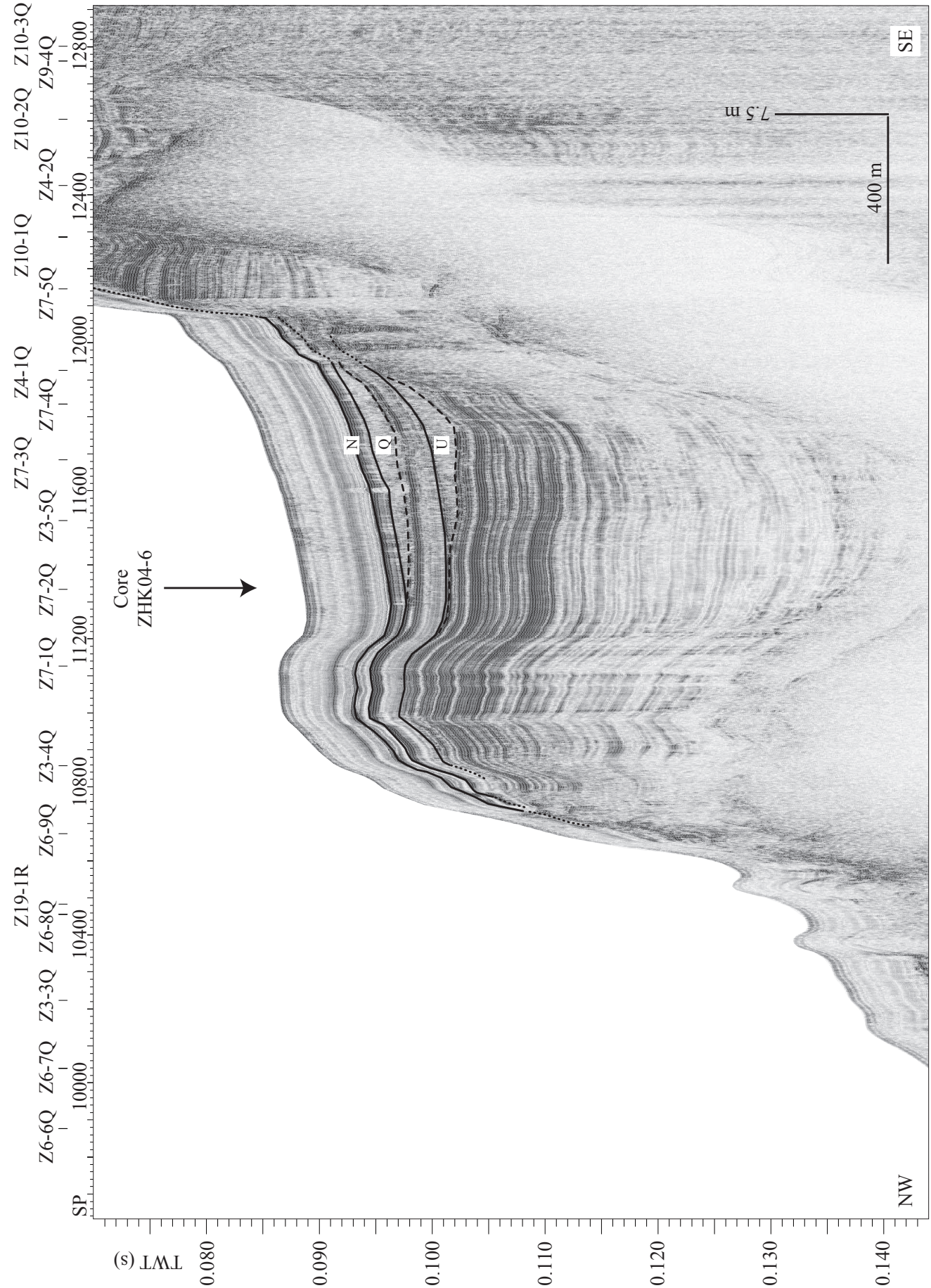

***Figure B 10**: Seismic Profile Z18-4Q*

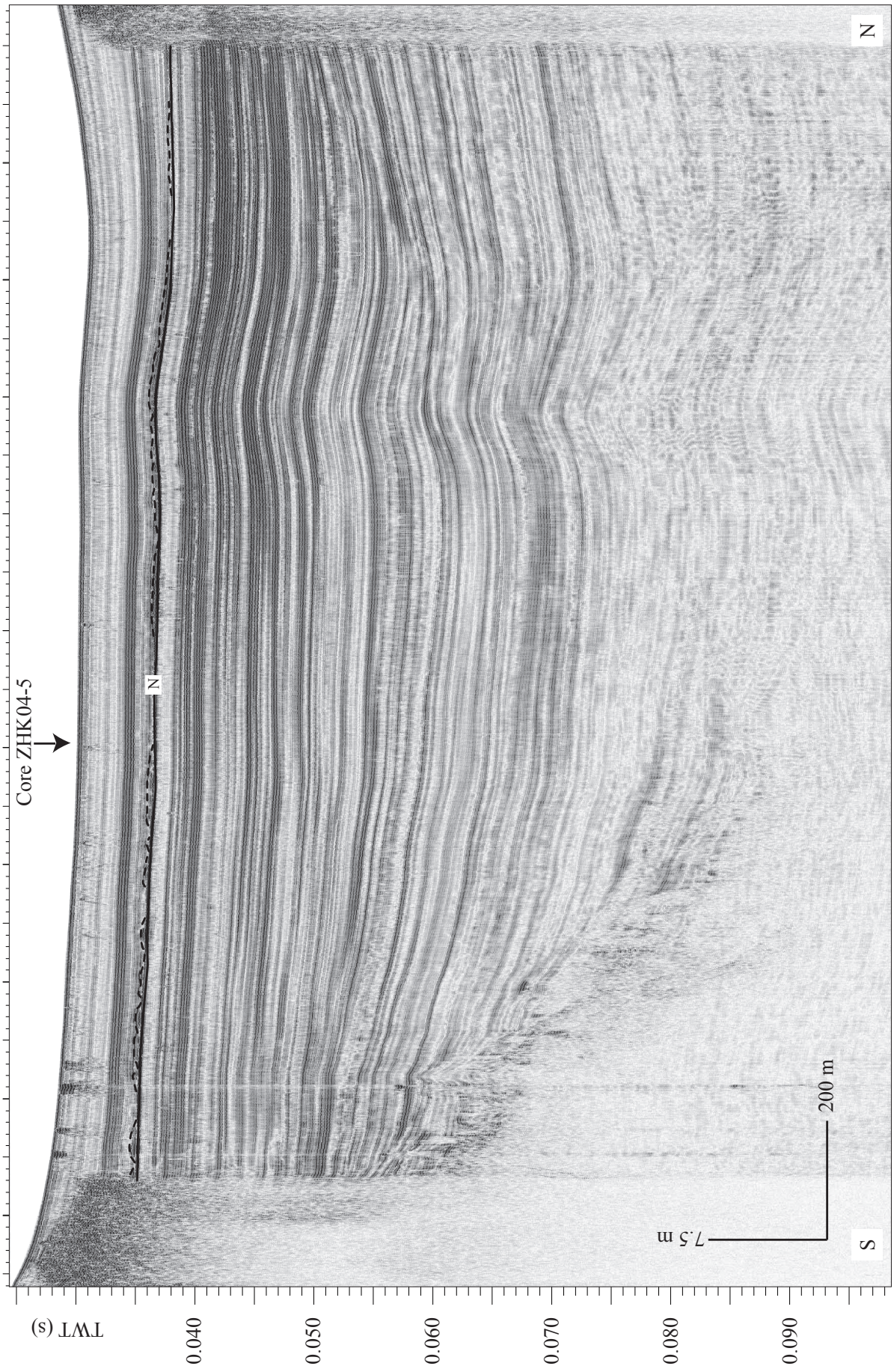

***Figure B 11**: Core 4WS05-1K (Kullenberg coring system)*

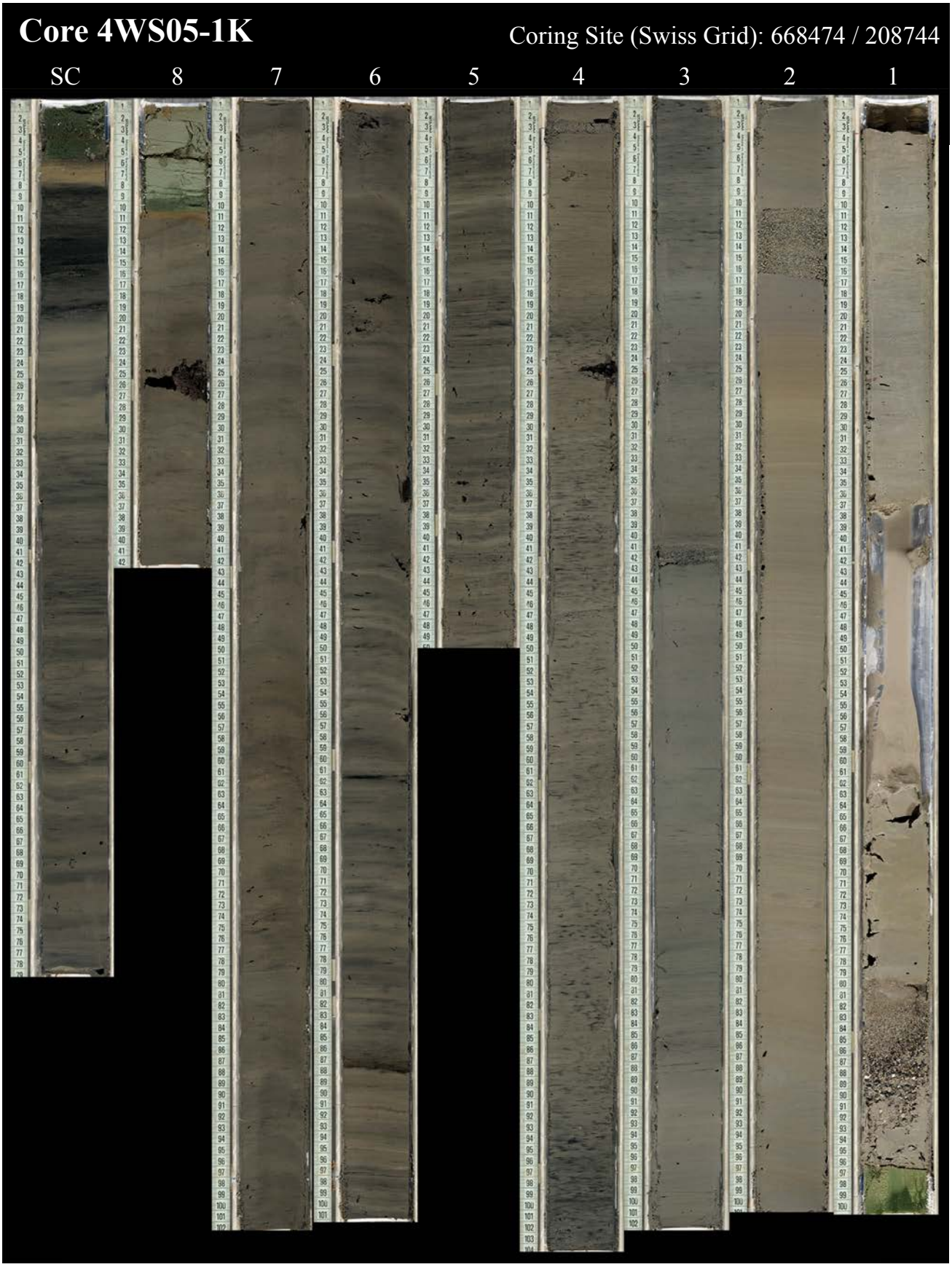

***Figure B 12**: Core 4WS05-4K (Kullenberg coring system)*

***Figure B 13**: Core 4WS05-6K (Kullenberg coring system)*

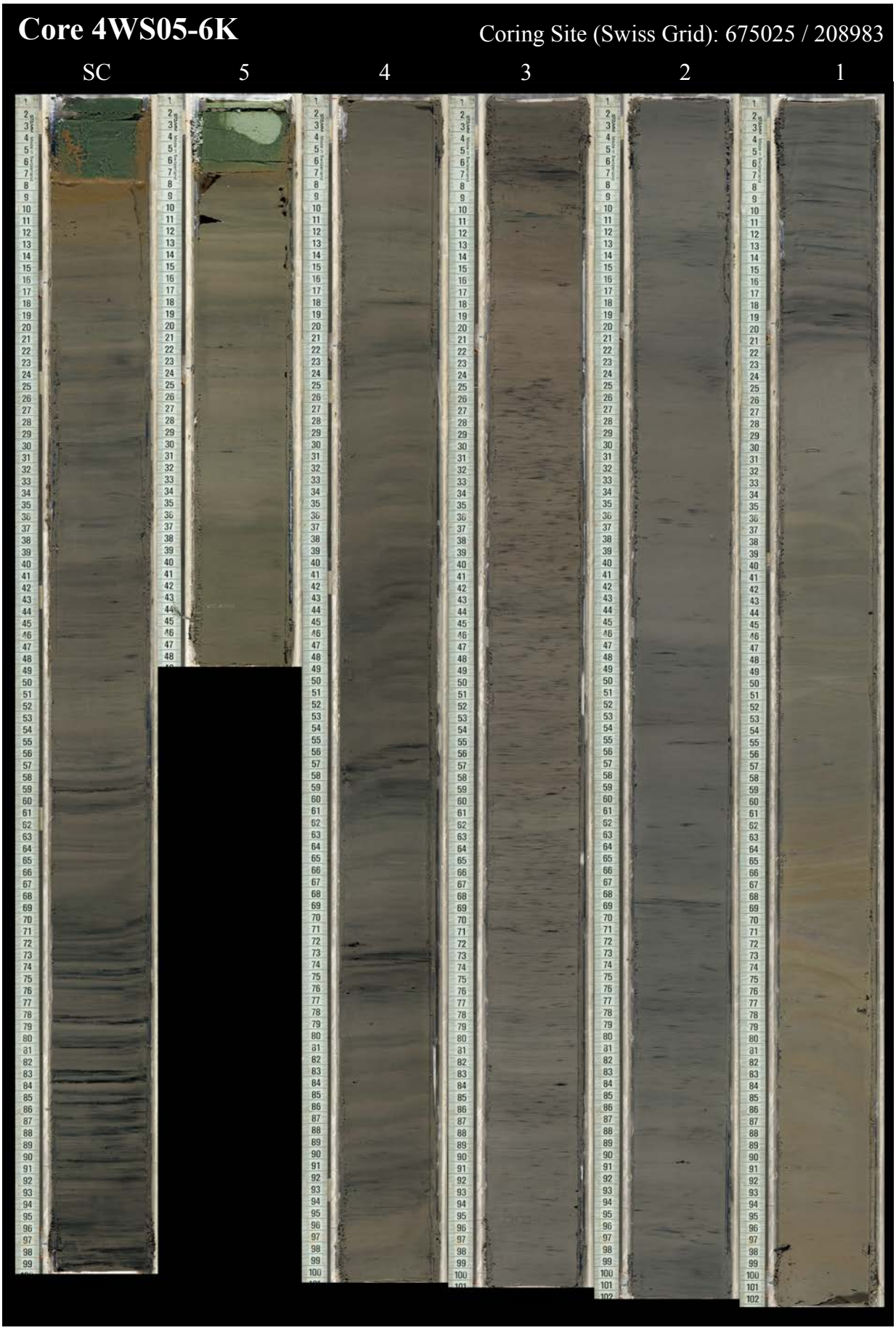

***Figure B 14**: Cores 4WS05-SC, 04-7 and 06-1 (gravity short core system)*

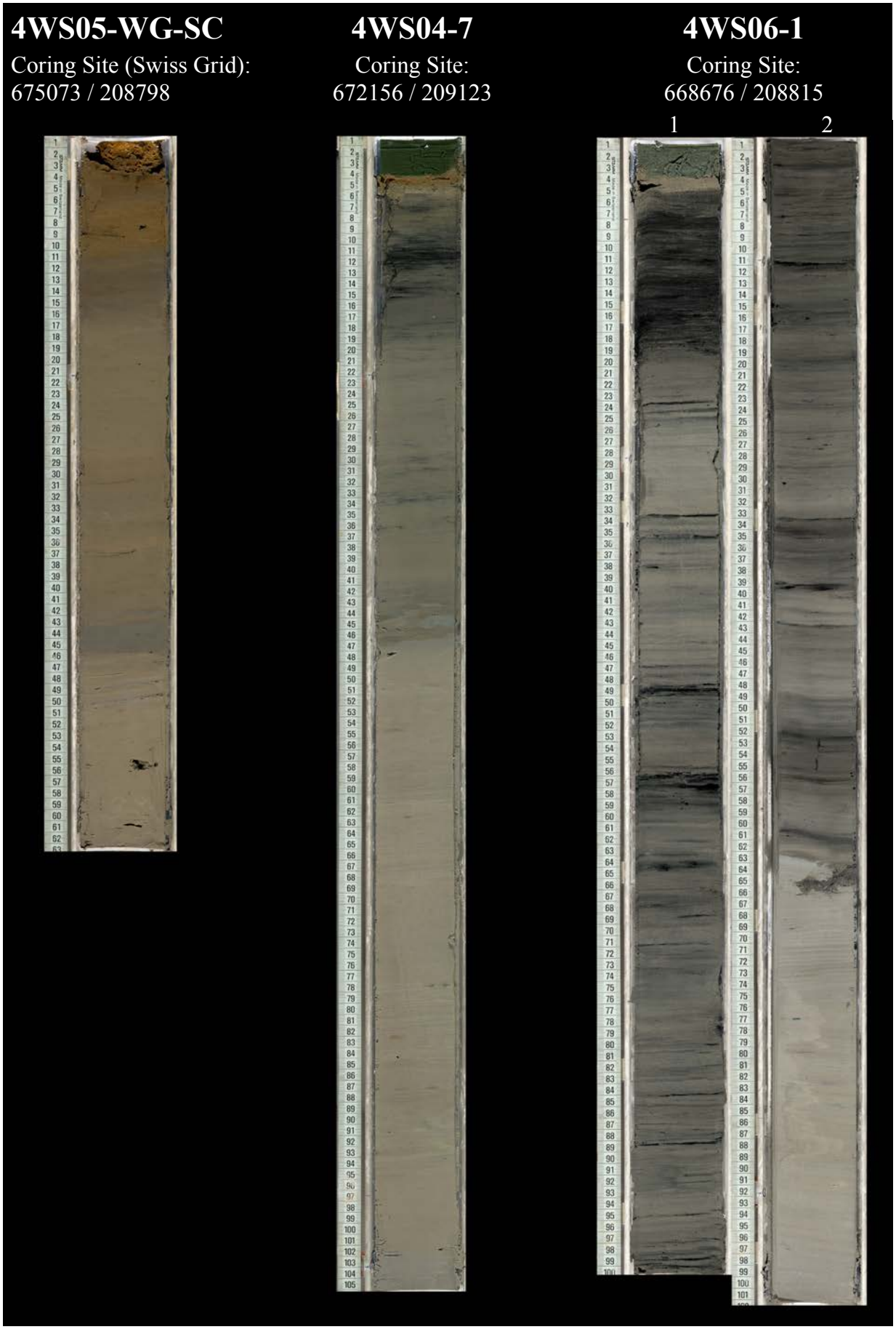

***Figure B 15**: Core ZHK04-1 (Kullenberg coring system)*

***Figure B 16**: Core ZHK04-2 (Kullenberg coring system)*

***Figure B 17**: Core ZHK04-4 (Kullenberg coring system)*

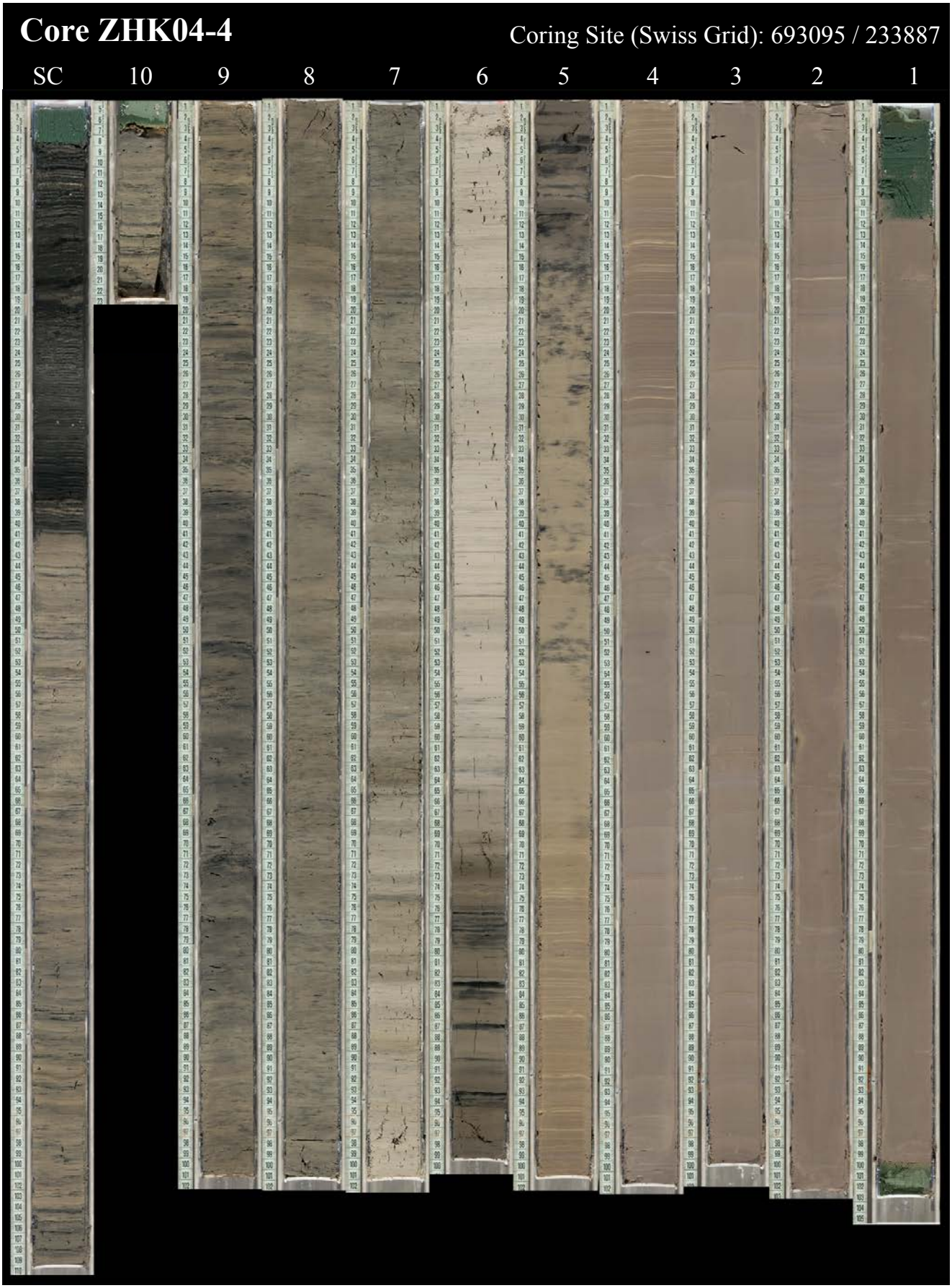

***Figure B 18**: Core ZHK04-5 (Kullenberg coring system)*

***Figure B 19**: Core ZHK04-6 (Kullenberg coring system)*

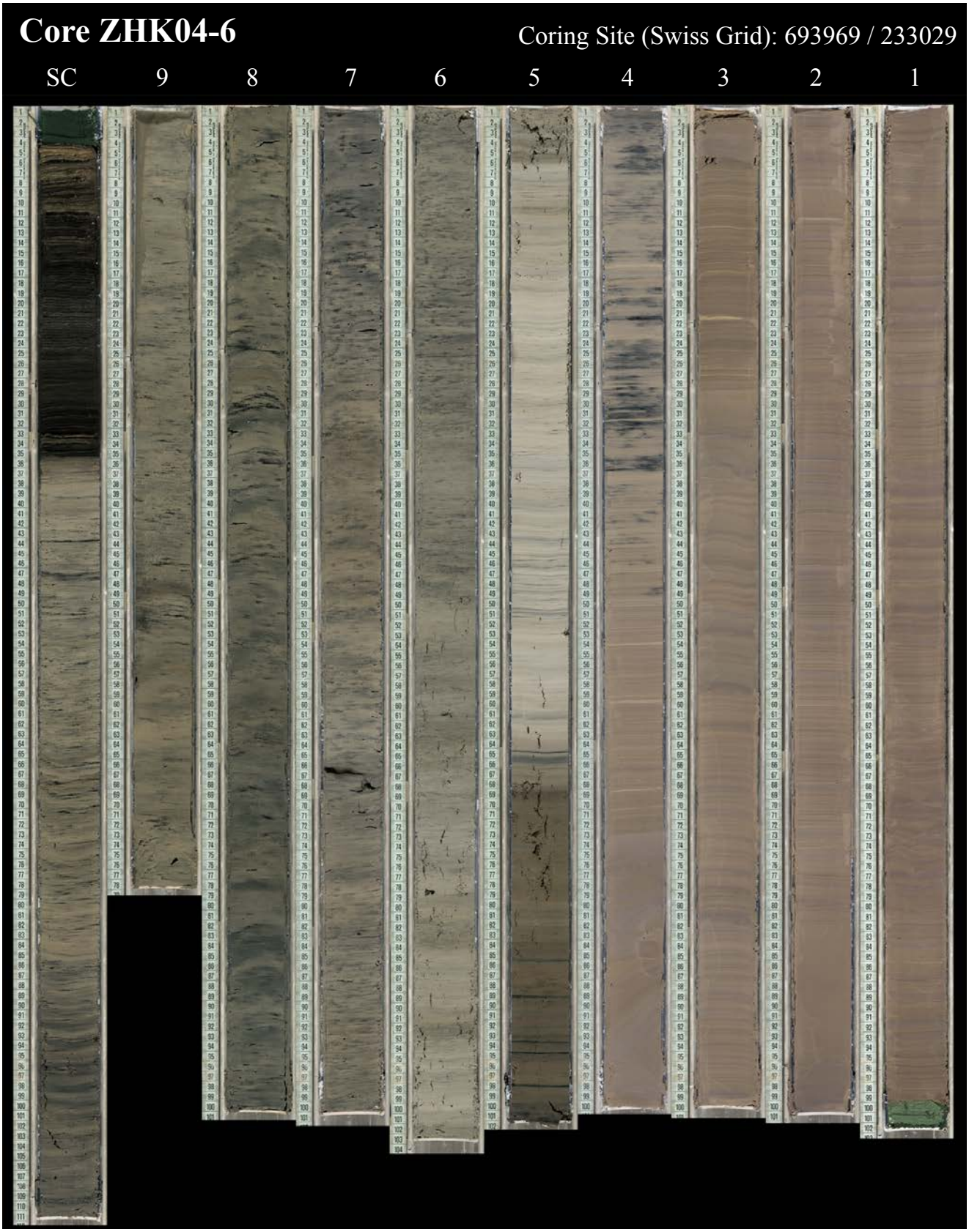

***Figure B 20**: Core ZHK04-7 (Kullenberg coring system)*

***Figure B 21**: Cores ZH05-SC1 and SC2 (gravity short core system)*

ZH05-SC1

Coring Site (Swiss Grid):
686859 / 236740

ZH05-SC2

Coring Site (Swiss Grid):
686556 / 237933

CURRICULUM VITAE OF MICHAEL STRASSER

Date of Birth:	September 19, 1977
Place of Birth:	Kilchberg (ZH), Switzerland
Citizenship:	Swiss

Education:

2003–2007	Doctoral studies at the Geological Institute, ETH Zurich, Switzerland Title of PhD dissertation: Quantifying Late Quaternary natural hazards in Swiss Lakes: subaquatic landslides, slope stability assessments, paleoseismic reconstructions and lake outbursts Supervisor: Prof. F. S. Anselmetti
2000–2003	Graduate studies at the Department of Earth Science, ETH Zurich Title of Diploma thesis: Erosion Processes and geomorphologic landscape evolution in arid climatic environments; 'Lluta collapse', northern Chile Supervisor: Prof F. Schlunegger
1998–2000	Undergraduate studies at the Department of Earth Science, ETH Zurich, Switzerland
1990–1997	Kantonsschule Chur, Switzerland
1984–1990	Primarschule Chur, Switzerland